UILU-ENG-98-2003

CIVIL ENGINEERING STUDIES
Transportation Engineering Series No. 96
Illinois Cooperative Highway and Transportation
Series No. 262

ISSN-0197-9191

MECHANISTIC-EMPIRICAL EVALUATION OF THE Mn/ROAD LOW VOLUME ROAD TEST SECTIONS

Report Preparation by

N. Garg
M.R. Thompson

Cooperative Evaluation of
Mn/Road Test Results to
Illinois Conditions

Project IHR-535
ILLINOIS COOPERATIVE HIGHWAY AND TRANSPORTATION RESEARCH PROGRAM

A cooperative investigation
conducted by the

TRANSPORTATION RESEARCH LABORATORY
DEPARTMENT OF CIVIL ENGINEERING
ENGINEERING EXPERIMENT STATION
UNIVERSITY OF ILLINOIS AT URBANA-CHAMPAIGN

in cooperation with the

STATE OF ILLINOIS
DEPARTMENT OF TRANSPORTATION
and the
MINNESOTA DEPARTMENT OF TRANSPORTATION
Mn/ROAD RESEARCH PROJECT
and the
U.S. DEPARTMENT OF TRANSPORTATION
FEDERAL HIGHWAY ADMINISTRATION

UNIVERSITY OF ILLINOIS
URBANA, ILLINOIS

MAY 1998

ACKNOWLEDGMENTS/DISCLAIMERS

This study was sponsored by the Illinois Department of Transportation (IDOT) - Division of Highways as part of IHR-535 (COOPERATIVE EVALUATION OF Mn/ROAD TEST RESULTS TO ILLINOIS CONDITIONS). IHR-535 is a cooperative effort between the Minnesota Department of Transportation (Mn/DOT), the Illinois Department of Transportation (IDOT), and the Department of Civil Engineering - University of Illinois @ Urbana-Champaign to provide broad utilization of the data obtained from the Minnesota Road Research Project (Mn/ROAD). The cooperation is facilitated through a **MEMORANDUM OF UNDERSTANDING** between Mn/DOT and IDOT. The generous cooperation and help of the MnROAD staff is acknowledged.

Technical Report Documentation Page

1. Report No,	2. Government Accession No.	3. Recipient's Catalog No.
FHWA-IL-UI-262		

4. Title and Subtitle	5. Report Date
MECHANISTIC-EMPIRICAL EVALUATION OF THE MN/ROAD LOW VOLUME ROAD TEST SECTIONS	May, 1998
	6. Performing Organization Code
7. Author(s) NAVNEET GARG - MARSHALL THOMPSON	8. Performing Organization Report No. UILU-ENG-98-2003
9. Performing Organization Name and Address Department of Civil Engineering Engineering Experiment Station University of Illinois at Urbana-Champaign Urbana, IL 61801-2352	10. Work Unit (TRAIS)
	11. Contract or Grant No. IHR - 535
12. Sponsoring Agency Name and Address Illinois Department of Transportation Bureau of Materials & Physical Research 126 East Ash Street Springfield, IL 62706	13. Type of Report and Period Covered Project Report
	14. Sponsoring Agency Code

15. Supplementary Notes

The cooperation and help of the Minnesota Department of Transportation and the Mn/ROAD project staff are acknowledged.

16. Abstract

This study utilized IDOT mechanistic-empirical (M-E) procedures and Mn/ROAD low-volume road (LVR) data and information to verify/refine/modify analysis and design concepts and procedures for LVR flexible pavements. The Mn/ROAD LVR flexible pavements include conventional flexible, full-depth asphalt, surface-treatment and aggregate-surface sections. Laboratory test results, field distress measurements, and FWD test data were used to study the affect of granular material quality on pavement performance and deflection response. The results from the rapid shear tests, permanent deformation tests and field rutting measurements show that granular material rutting potential can be characterized by a rapid shear triaxial test at 15-psi confining pressure. For conventional flexible pavements, granular material quality did not affect the pavement deflection response, but material quality effects were significant for aggregate-surface and surface-treatment pavements. ILLI-PAVE predicted pavement responses were fairly accurate for sections with thicker asphalt concrete surfaces. The FWD deflection basin parameter AUPP (Area Under Pavement Profile) can be used to predict the strains at the bottom of AC layer. Effect of subgrade type on pavement response and performance was studied. Sandy subgrades showed little or no change in pavement structural response due to spring-thaw effects. For the cohesive subgrade sections, moisture changes and spring-thaw effects increased surface deflections. The study showed that the IDOT LVR flexible pavement mechanistic-empirical design concepts and procedures are valid and adequate.

17. Key Words	18. Distribution Statement
Flexible Pavements Granular Base Test Roads	No restrictions. This document is available to the public through the National Technical Information Service, Springfield, VA 22161

19. Security Classif. (of this report)	20. Security Classif. (of this page)	21. No. of Pages	22. Price
Unclassified	Unclassified	304	

SUMMARY

The objective of this study was to utilize IDOT mechanistic-empirical procedures and Mn/ROAD low-volume road (LVR) data and information to verify/refine/modify analysis and design concepts and procedures for LVR flexible pavements. Laboratory test results, field distress measurements, and FWD test data were used to study the affect of granular material quality on pavement performance and deflection response. The results from the rapid shear tests and permanent deformation tests show that the rutting potential of a granular material can be characterized from rapid shear test at 15-psi confining pressure. The rapid shear test results at 15-psi confining pressure reflect the rutting trends observed in the field. For conventional flexible pavements, granular material quality did not affect the pavement deflection response. Granular material quality effects on pavement deflection response were significant in the case of aggregate-surface/surface treated pavements. The field measured pavement responses were compared to the ILLI-PAVE (finite element program) predicted pavement responses. Estimate of pavement responses is fairly accurate in the case of test sections where the asphalt concrete (AC) surface behaves like a structural layer (AC thickness higher than 5-inch). The analyses of field FWD data showed that Area Under Pavement Profile can be used to predict the strains at the bottom of AC layer. The 'Design Time' concept was utilized to consider temperature effects on AC fatigue computations. The analysis showed that the 'Design Time' is primarily effected by AC thickness. The granular layer thickness and subgrade type (sand or cohesive) do not have any effect on 'Design Time'. Effect of subgrade type on pavement response and performance was studied. The test sections with sandy subgrade showed little or no change in pavement structural response due to changes in moisture conditions in the subgrade (during spring-thaw). For test sections with cohesive subgrade, the effects of moisture changes during spring-thaw on the pavement structural response were significant. In the IDOT mechanistic-empirical design procedure, the design criteria for conventional flexible pavements are AC fatigue and subgrade stress. In the Mn/ROAD LVR test sections, no AC fatigue was observed, and the subgrade stress ratios were in the desirable range (0.2-0.4). However, some of the conventional flexible test sections experienced severe rutting which was attributed to the granular layer. The aggregate layer in pavement must posses sufficient shear strength/rutting resistance (for a given asphalt concrete thickness) to minimize rutting within the granular layer.

TABLE OF CONTENTS

LIST OF TABLES

LIST OF FIGURES

CHAPTER - I
INTRODUCTION

1.1 Introduction

There is a demand for the construction of new and/or improved low-volume roads (LVR). It is therefore very important to be able to design and construct economical and structurally adequate LVR pavements. A LVR pavement may be defined as any type of roadway which carries low volumes of traffic. In Illinois, LVR pavements are referred to as Class III and Class IV roads. Roads and streets with structural design traffic between 400 and 2000 average daily traffic (ADT) are referred to as Class III roads, and those with structural design traffic less than 400 ADT are referred to as Class IV roads.

The Illinois Department of Transportation (IDOT) Bureau of Local Roads and Streets mechanistic-empirical design procedure is based on relating pertinent pavement responses (stresses, strains, and deflections) to the occurrence of pavement distress (cracking, rutting, etc.) through the use of transfer functions. The design criteria for conventional flexible pavements are asphalt concrete fatigue and subgrade stress ratio. A subgrade stress ratio (SSR) criterion is used to consider subgrade rutting. The governing design criteria for full-depth asphalt concrete pavements is the tensile strain at the bottom of asphalt concrete layer. Reduced strain corresponds to increased fatigue life. A "Design Time" concept is used to consider the effect of climate on pavement structure. The fatigue life of an asphalt concrete layer estimated based on design time asphalt concrete modulus is equal to the fatigue life calculated based on the 12-monthly asphalt concrete modulus inputs. The "Critical Period" for a fine-grained cohesive subgrade occurs during spring thaw. Subgrade rutting is controlled by limiting the subgrade stress ratio (deviator stress/unconfined compressive strength) at the asphalt concrete-subgrade interface to an acceptable level during the "Critical Period".

The objective of this study is to utilize Mn/ROAD data and information to further verify/refine/modify mechanistic-empirical based flexible pavement analysis and design concepts and procedures.

1.2 Minnesota Road Research Project (Mn/ROAD)

Mn/ROAD is the largest and most technologically advanced roadway research facility in the world. Developed by Minnesota Department of Transportation (MnDOT) and the University of Minnesota, the project is a veritable outdoor laboratory that measures the effects of real traffic and weather on a variety of different pavement designs. Nearly 4500 state-of-the-art electronic sensors are embedded within 40 test sections (cells) of differing pavement composition. These buried sensors trigger millions of bytes of data daily, tracking the causes of pavement distress - heavy trucks and seasonal environmental changes. The combination of electronic data generation, live and calibrated traffic, and the extensive array of pavement structures makes Mn/ROAD unique among road research facilities. The Mn/ROAD facility is located parallel to Interstate 94 (I-94) in Otsego, Minnesota, which is approximately 40-miles northwest of the Minneapolis-St. Paul metropolitan area. Figures 1.1 and 1.2 show the aerial views of the test facility. Mn/ROAD's 40 test sections, each 500-feet in length, are paved with different thicknesses of portland cement concrete, asphalt concrete, and aggregate.

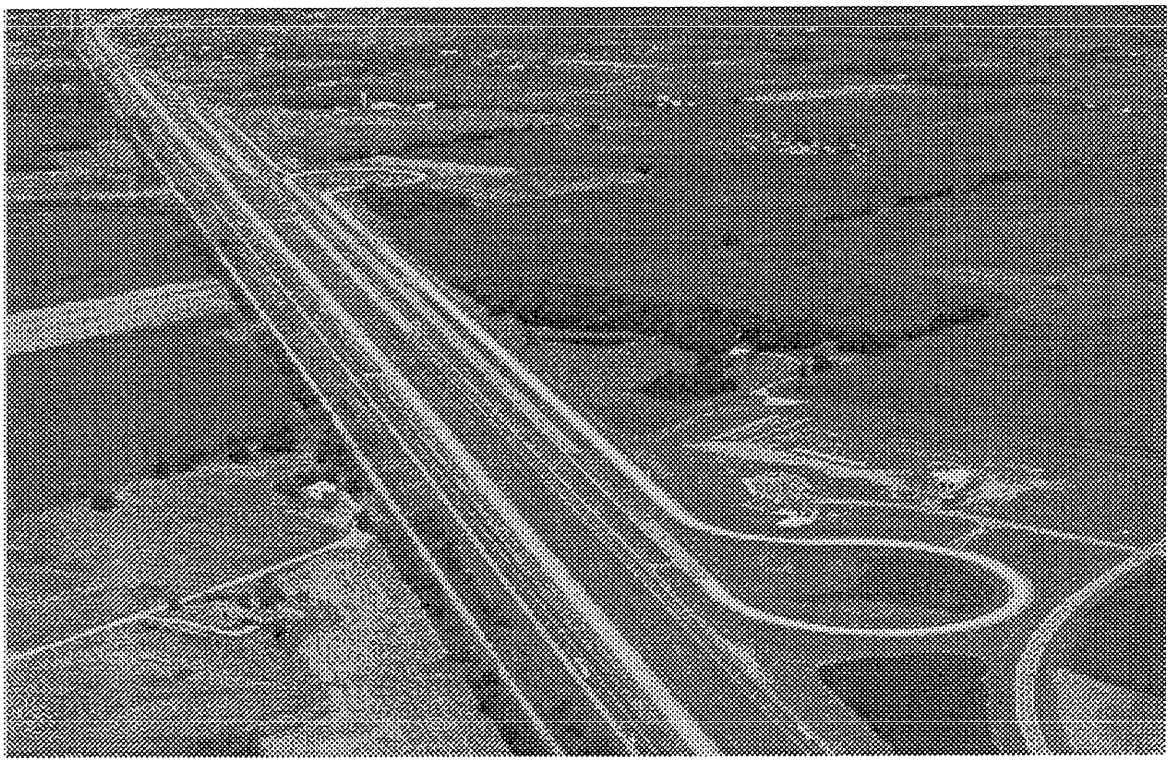

Figure 1.1. Aerial View of Mn/ROAD Test Facility Parallel to Interstate I-94 in Otsego, Minnesota

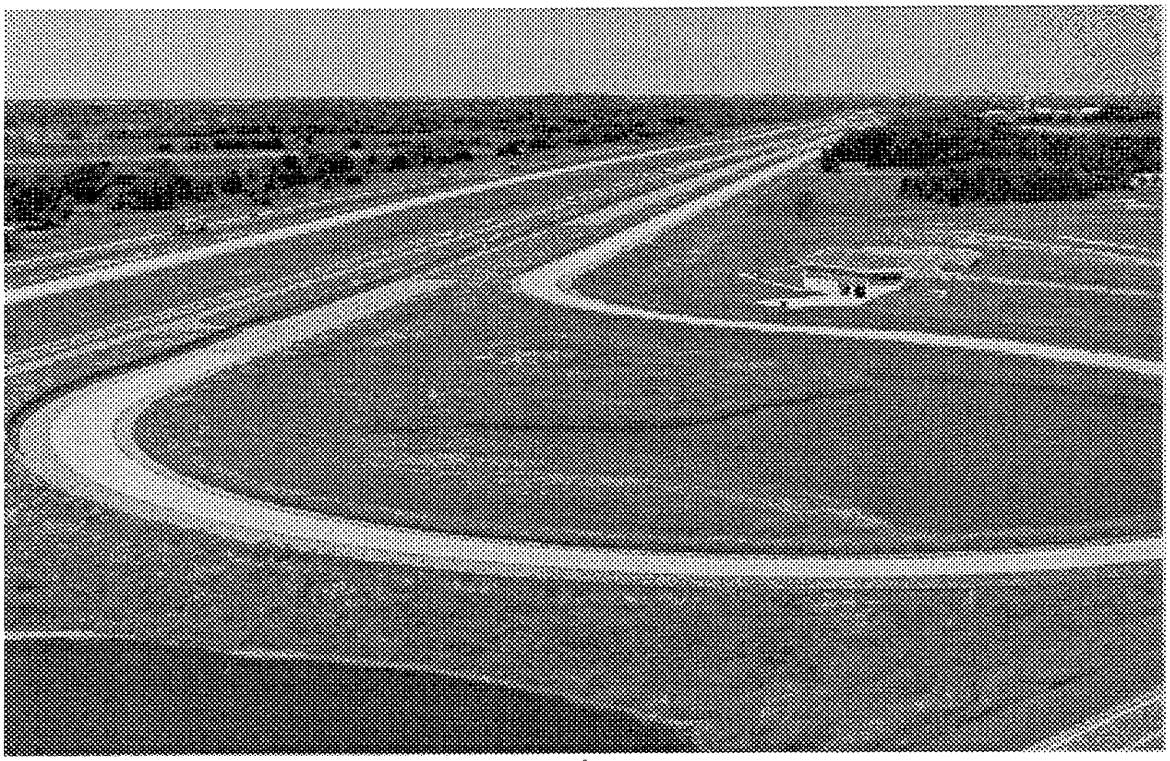

Figure 1.2. Aerial View of Low-Volume Road Loop at Mn/ROAD Test Facility

The facility consists of 3-miles of two-lane interstate and 2.5-miles of closed loop low-volume test track. The cells are distributed over the two roadways to represent a wide range of pavement types, with varying combinations of surface, base, subbase, drainage, and compaction. The interstate portion of the test facility consists of 5-year and 10-year mainline test sections. Both the 5-year and 10-year mainline sections have portland cement concrete pavements (9 test sections) and asphalt concrete pavements (14 test sections). The low-volume facility consists of 17 test sections, including 6 conventional flexible pavements, 2 full-depth asphalt concrete pavements, 2 aggregate surface pavements, 2 surface treated pavements and 5 portland cement concrete pavements. The pavement sections are designed so that different combinations of materials, layer thicknesses and design details can be evaluated. Only flexible pavement test sections (conventional flexible pavements, full-depth asphalt concrete pavements, surface-treated/aggregate surface pavements) were evaluated in this study. The LVR design configurations of 6 conventional flexible pavements, 2 full-depth asphalt concrete pavements, and 4 aggregate surface/surface treated pavements are shown in Figure 1.3. Six different types of granular materials are used as base and subbase materials. Mn/ROAD includes two different type of subgrade soils - cohesive subgrade (R=12) and

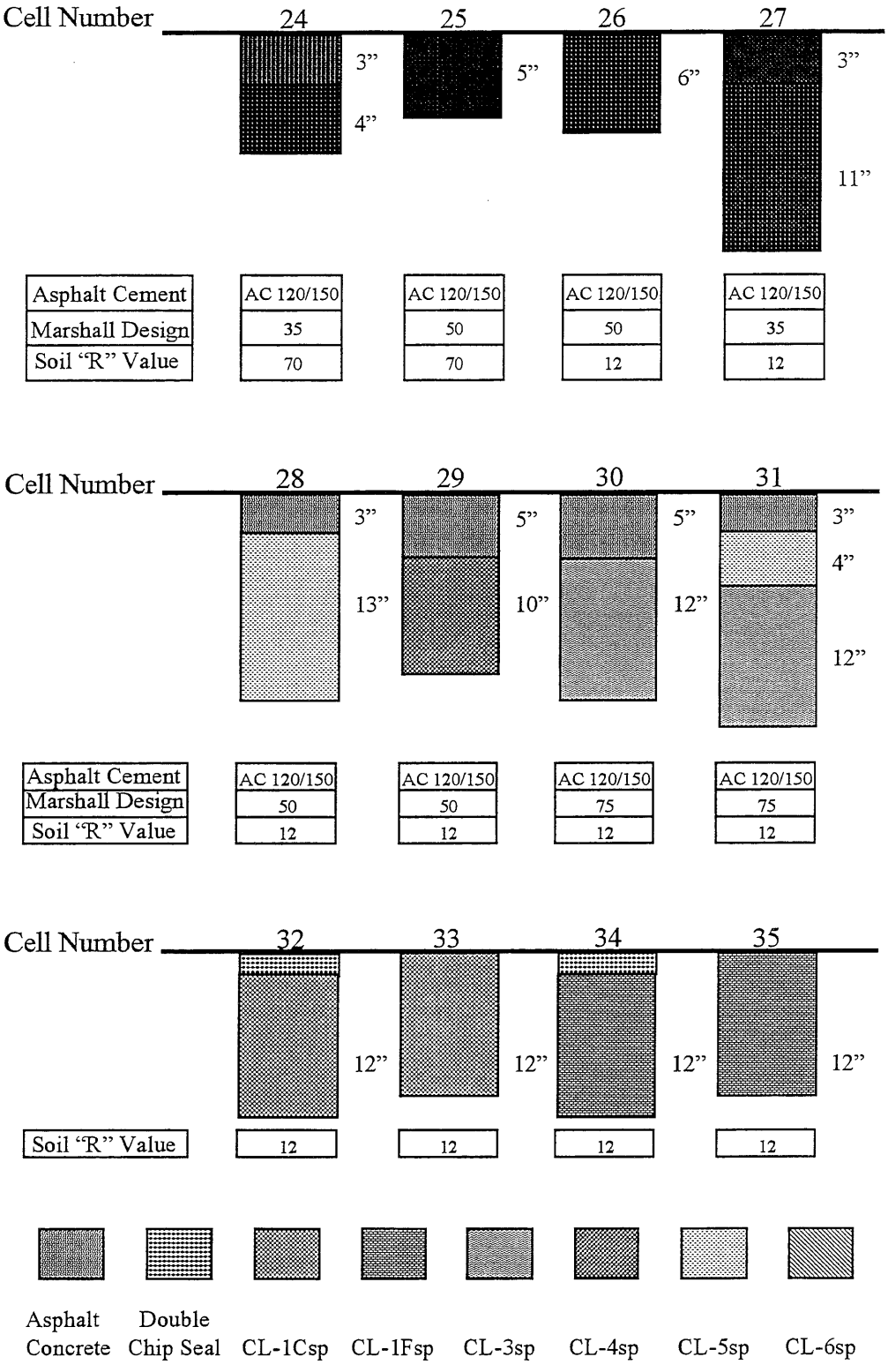

Figure 1.3. Low-Volume Road Test Sections at Mn/ROAD Project

sandy subgrade (R=70). These sections are loaded by a 5-axle tractor-trailer (Figure 1.4). In the inner lane the tractor-trailer is loaded to 80,000-pounds. In the outer lane the tractor-trailer travels the loop in the opposite direction, loaded to 102,500- pounds. Each pass of tractor-trailer accumulates 2.45 and 9.15 flexible ESAL's in the respective lanes. In an attempt to balance the deterioration of the lanes, the lower load level lane receives four times as many passes of the tractor-trailer as the overloaded lane. The tractor-trailer travels in the low-volume road loop at 30-40 mph. The tractor has an air suspension system and the trailer has a leaf spring suspension system. The tandem axles are equipped with dual 11R24.5 tires inflated to 100-psi pressure. Figure 1.5 shows the wheel configuration for the tractor-trailer.

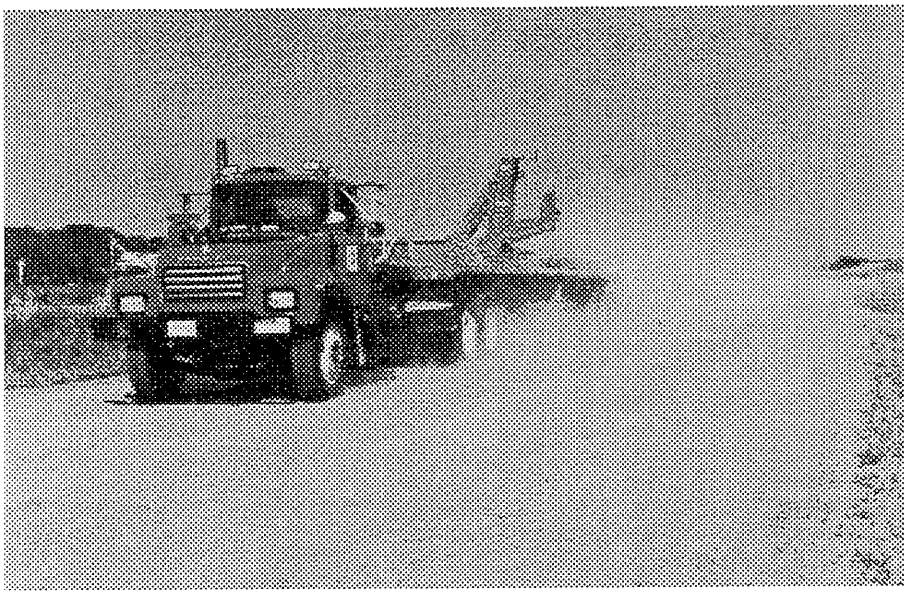

Figure 1.4. Low-Volume Road Traffic Loading Test Vehicle

Nearly 4500 electronic sensors were placed in the various pavement layers. They are cabled directly to 26 roadside cabinets where information is collected and sent to the Minnesota Materials Research and Engineering Laboratory. More than twenty miles of conduit and cable connect the sensors to the roadside cabinets. About ten miles of fiber optic cable then sends the data from the cabinets to the central computer system at the site. Data are collected from the Mn/ROAD database using ORACLE queries.

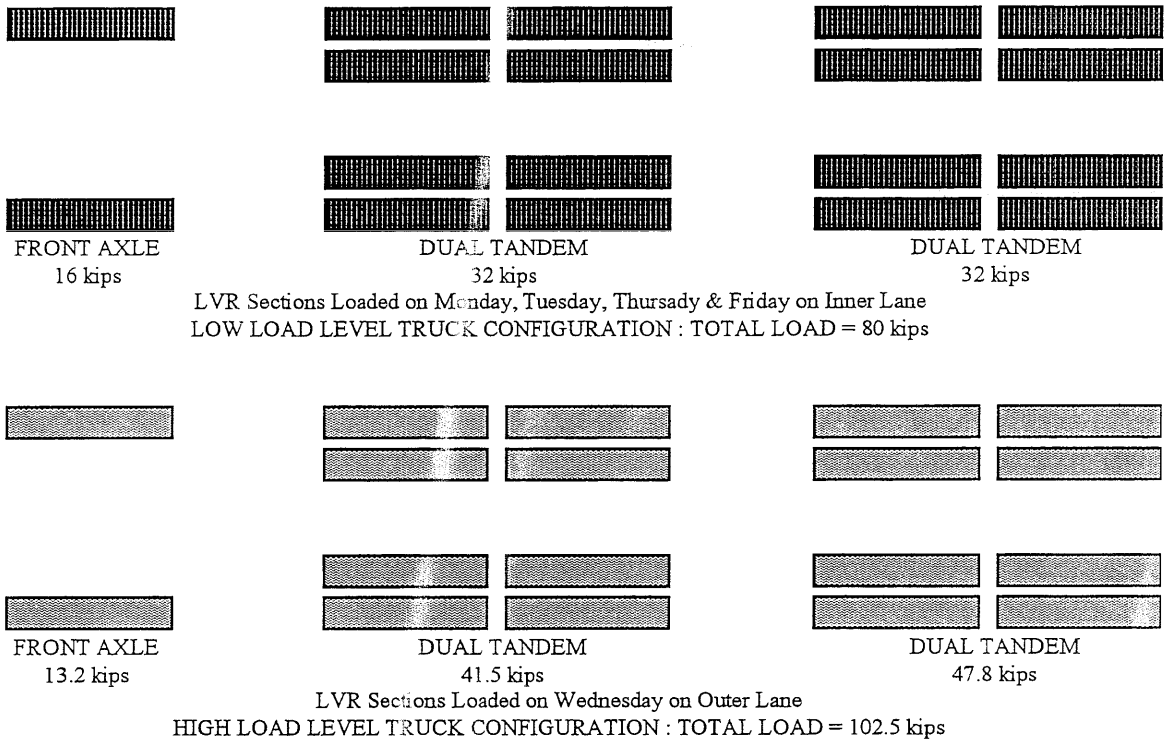

Figure 1.5. Low-Volume Road Traffic Loading Test Vehicle

1.3 Problem Statement

The primary objective of this study was to utilize IDOT mechanistic-empirical procedures and Mn/ROAD low-volume road data and information to further verify/refine/modify IDOT's analysis and design concepts and procedures for low-volume road flexible pavements.

1.4 Research Objectives

The mechanistic-empirical approach to the design of pavement considers three main factors. The first factor is the proper characterization and evaluation of the paving materials and subgrade soils. This is accomplished through the laboratory simulation (moisture, density, loading conditions, etc.) of the field conditions and the proper selection of the material models. The second factor is a suitable structural model for accurately calculating the critical deflections, stresses, and strains in the pavement structure. The third factor is the consideration of performance characteristics of the materials and their likely modes of failure. Using the material properties obtained from laboratory testing (at University of Illinois, Mn/ROAD, and University of Minnesota) as inputs, the pavement

responses (stress, strain, displacement) under different loading conditions were predicted using advanced structural model (ILLI-PAVE). The predicted behavior was confirmed with the observed pavement response at the Mn/ROAD test sections. The research goals and objectives were achieved through a systematic study as described below:

- In conventional flexible pavements with thin asphalt concrete surfaces, the granular base is an important component. Therefore, characterization of granular materials is very important. The first objective of this research was to study the effect of granular material quality on the flexible pavement response and performance.

  ◊ Characterize granular material based on gradation, percent crushed particles, and moisture sensitivity.
  ◊ Perform rapid shear tests, and Dynamic Cone Penetrometer (DCP) test to evaluate the shear strength of materials.
  ◊ Perform dynamic triaxial tests on granular materials to study the resilient response and permanent deformation behavior.
  ◊ Utilize University of Illinois backcalculation procedures to analyze the Mn/ROAD Falling Weight Deflectometer (FWD) data.

- Common modes of distress in asphalt concrete layer are rutting, fatigue cracking, and thermal cracking. Rutting and thermal cracking are mix related problems and can be eliminated or controlled by proper mix design. Fatigue cracking is related to the strain at the bottom of asphalt concrete layer. The objective was to evaluate the "Design Time" concept for considering temperature effects on asphalt concrete fatigue computations and study the effects of asphalt concrete thickness, granular base thickness, and subgrade type on "Design Time".

- Evaluate the "Critical Period" concept for subgrade characterization in conventional flexible pavements and surface treated pavements. Study the effects of subgrade type on pavement structural response and performance. The laboratory tests on cohesive subgrade soils were performed by Mn/ROAD personnel.

- Evaluate criteria for design.
  - ◊ Rutting.
  - ◊ Subgrade stress ratio.
  - ◊ Asphalt concrete fatigue.

- Evaluate the transfer functions.

- Validate/confirm the design algorithms.

1.5 Report Outline

This report is a written summary of above mentioned study. The second chapter presents a summary of pertinent literature in the field of flexible pavement analysis and design. Material characterization through comprehensive laboratory testing was a major part of this study. Chapters III, IV, and V discuss the material characterization phase of this study. Chapter-III describes the Mn/ROAD granular materials and the laboratory testing procedures. The results from laboratory testing of granular materials are presented and discussed in Chapter-IV. Testing on cohesive subgrade was performed by Mn/ROAD staff. Chapter-V discusses the results from laboratory testing on cohesive subgrade.

Six different granular materials were used in Mn/ROAD project low-volume road flexible pavement test sections. The effect of granular material quality on pavement structural response and performance is discussed in Chapter-VI. ILLI-PAVE was used to estimate the structural responses (stress, strain, deflection) of the test section. The estimated responses were compared to the field measured responses (from FWD tests) in Chapter-VII. Chapter-VIII discusses the "Design Time" concept for considering asphalt concrete fatigue. This chapter includes the results from climatic modeling of Mn/ROAD test sections. "Critical Period" concept for subgrade characterization is presented in Chapter-IX. Effect of subgrade type on pavement response and performance is discussed in this chapter. The conclusions from the study and recommendations for future research are given in Chapter-X.

1.6 Summary

The design of low-volume roads requires special consideration for the granular base layer and the subgrade because of the lack of or very thin asphalt concrete surfaces. The Illinois Department of Transportation (IDOT) Bureau of Local Roads and Streets utilizes a flexible pavement design procedure that is based on mechanistic-empirical concepts. In this study, the data and information from Mn/ROAD low-volume road test sections are used to verify/refine/modify the IDOT mechanistic-empirical design procedure for low-volume roads. In this chapter, the problem statement and the research approach are described and a brief outline of report is presented.

CHAPTER - II
LITERATURE REVIEW

2.1 Introduction

A pavement is a complex engineering structure. Pavement analysis and design involves the interaction of three equally important components: i) the subgrade; ii) the paving materials; iii) the characteristics of applied loads; and iv) climate. Three approaches that are or could be employed for analysis and design of pavement structures are as follows:

1. Empirical Approach -Relying upon or derived from observations or experiments. Guided by experience and not theory.
2. Mechanistic Approach - Tending to explain a phenomena by reference to physical causes.
3. Mechanistic-Empirical Approach - Combination of empirical and mechanistic approach.

The AASHTO Guide [1] states that mechanistic method or procedures refer to the ability to translate the analytical calculations of pavement response (stress, strain, deflection) to performance (fatigue cracking, rutting).

Failure in pavements is not a phenomena of chance, but a phenomena that has a definite mechanical cause. In recent times, there has been a thrust to move towards mechanistic approach. Figure 2.1 shows the components of mechanistic design procedure. In mechanistic-empirical approach, the mechanistic structural responses are passed on to statistical/empirical "transfer functions" predicting distress as a function of load repetitions. The pavement structural responses obtained from the structural model are for given time, climate, pavement structure, material properties, and loading conditions. Pavement responses will vary as any of the above mentioned inputs vary. Pavement performance is generally a long term consideration. Therefore, the mechanistic design procedures must account for the effect of the varying inputs to the structural model. Transfer functions relate pavement responses obtained from structural models to pavement performance as measured by the type and degree of distress (fatigue cracking, rutting, roughness, etc.). Generally, the predicted and actual pavement distress/performance do not compare favorably. Shift factors are utilized in various transfer functions to adjust structural model calculated

responses/lab based material testing predicted performance to more realistically reflect field observed pavement distress/performance.

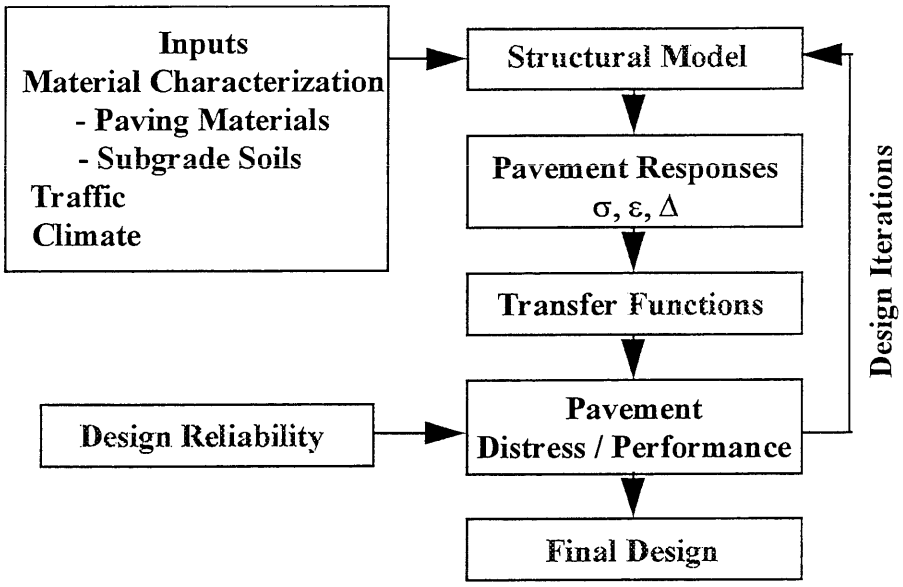

Figure 2.1. Components of a Mechanistic Design Procedure

The following sections present the summary of studies that have significantly contributed to the mechanistic-empirical analysis and design of flexible pavements.

2.2 Traffic Classification for Low Volume Roads (LVR)

The characteristics of vehicles using a road depend on the type of road and the level of service being provided. The type of vehicles using LVR are similar to those using other roads in the highway system with the possible exception being the extremely heavy multiple unit trucks. Vehicles types are commonly classified as passenger vehicles (P.V), single-units (S.U), and multiple-unit (M.U) vehicles [2]. The passenger vehicle classification includes all 4-wheeled vehicles whose major function is passenger service. The single unit classification includes all other single unit vehicles such as 4-wheeled pickup and panel trucks, 6-wheeled (dual wheel rear axle) trucks such as dump and heavier delivery trucks and buses, and 10-wheeled (tandem rear axle) trucks. The multiple unit classification includes all vehicles consisting of more than one unit such as tractor-trailer combinations.

In the Illinois Department of Transportation (IDOT) mechanistic-empirical design procedure for low-volume roads [2], the structural design traffic is the estimated average daily traffic (ADT) for the year representing one-half of the design period. In Illinois, Class III and Class IV roads are classified as low-volume roads. Roads and streets with structural design traffic between 400 and 2000 ADT are classified as Class III roads. Class IV roads have structural design traffic less than 400 ADT. For Class III and Class IV roads, a minimum design period of 15 years is allowed. The structural design traffic is estimated from current traffic count data obtained either by manual counts or from traffic maps published by IDOT. If P.V, S.U, and M.U counts are not available for Class III and IV roads and streets, an estimate of those counts are made from the following component percentages of the total traffic :

Class of	Percentage of Structural Design Traffic		
Road or Street	P.V	S.U	M.U
III	88	7	5
IV	88	9	3

For Class III roads and streets, the design traffic factor (T.F) is determined for various design periods (D.P) from the 73,280-pound and 80,000-pound load limit formulae as follows :

Traffic Factor equation for 73,280-pound load limit

$$T.F = D.P * [0.073*P.V + 44.350*S.U + 154.943*M.U] / 1{,}000{,}000 \quad \text{.....[2.1]}$$

Traffic Factor equation for 80,000-pound load limit

$$T.F = D.P * [0.073*P.V + 54.57*S.U + 192.175*M.U] / 1{,}000{,}000 \quad \text{.....[2.2]}$$

The formulae given above are based on the statewide average distribution of vehicle types and axle loadings, which are directly applicable to most roads and streets. For Class IV roads and streets, thicknesses are provided based on the daily volume of heavy commercial vehicles (HCV). Thus, a design traffic factor is not necessary.

2.3 Material Characterization

Material characterization is one of the most important steps in the mechanistic design procedure. The material properties of the layers forming the pavement structure have a significant effect on the behavior of pavement.

2.3.1 Surface Layer

The surface layer is directly affected by the horizontal and vertical forces imposed by the traffic. In addition, the surface layer is directly exposed to various destructive effects of the environment such as temperature, frost action, moisture, and chemicals. The surface layer must posses sufficient strength or stability such that horizontal and vertical forces of the traffic can be resisted. Sufficient internal stability is required in order to limit rutting, shoving, and raveling to acceptable values. The internal stability must be maintained over the range of temperatures to which the surface is subjected. In the case of low-volume roads, the surface is generally thin asphalt concrete (AC) layer or aggregate surface (with or without surface treatment).

The AC layer is characterized as a constant modulus material. AC temperatures are considered in selecting modulus values. AC mean monthly pavement temperatures (MMPT) are estimated based on mean monthly air temperatures (MMPT). MMPT's are then used to estimate AC modulus from an appropriate AC modulus-temperature relation. Thompson and LaGrow [3] proposed a Design Time concept to consider the effect of climate on pavement structure. It is used in the current IDOT design procedures for conventional flexible pavements and full-depth asphalt concrete pavements. The fatigue life of an AC pavement estimated based on design time AC modulus is equal to the fatigue life calculated based on the 12-monthly AC modulus inputs. SHELL air-mix temperature procedure was used. The SHELL method relates mean monthly air temperature to mean monthly pavement for various asphalt thicknesses. NCHRP 1-26 phase 1 Final Report [4] stated that Illinois CMS model was adequate for considering climatic effects. Climatic-Materials-Structural (CMS) model [5,6] was used to estimate MMPT's as a function of MMAT. CMS includes a one-dimensional forward finite-difference heat-transfer model and an isothermal model that calculates temperature and moisture profiles as a function of time based on pertinent climatic inputs. Based on the pavement temperatures, the asphalt concrete moduli, can be estimated by using Eac-PT relationship. The results from NCHRP 1-26 Phase 1 Final Report [4] show that the design time is relatively insensitive to AC thickness, pavement section, AC fatigue algorithm, and AC modulus-temperature relation. MMAT was the dominant factor that influenced design time.

The modulus of the asphalt concrete mix (E_{AC}) is a very important material characterization input in the mechanistic-empirical design of flexible pavements. The major factors affecting E_{AC} are

asphalt binder properties, temperature, time of loading, and mixture composition. For a given asphalt concrete mix, the effect of temperature variation on the modulus should be considered. E_{AC} can be estimated based on the asphalt binder properties, mixture composition, time of loading, and temperature. Another approach is to characterize typical AC mixtures for the temperature ranges of interest. The most direct application of this approach is to conduct resilient modulus tests on laboratory prepared specimens or field cores. E_{AC} - split tensile strength relations for typical AC mixtures can also be established which can then be used to predict the modulus. Modulus backcalculation methodology can also be utilized to establish E_{AC} - temperature relationships from Falling Weight Deflectometer (FWD) testing of existing flexible pavements.

Most procedures require asphalt binder stiffness as an input for predicting AC mixture modulus. Several methods [7,8,9] have been developed that predict asphalt binder stiffness as a function of loading time, penetration index, ring and ball softening point, and temperature of asphalt cement. Heukelom et al. [10], Francken et al. [11], and Bonnaure et al. [12] developed procedures for predicting AC mixture stiffness from asphalt binder stiffness and mixture composition data. The Bonnaure et al. [12] procedure is utilized in the Shell Pavement Design Manual [13]. A statistically based algorithm (Table 2.1) for estimating AC modulus is utilized in the Asphalt Institute's DAMA pavement analysis and design computer program [14]. The equation was developed from an extensive laboratory testing data base. Miller et al. [15] indicated that the equation is highly satisfactory for dense graded crushed stone and gravel mixes. Illinois DOT mechanistic-empirical design procedure for full-depth asphalt pavements [16] utilizes the Asphalt Institute procedure for establishing the Design E_{AC} - Design AC Mixture Temperature relationships (Figure 2.2).

ASTM methods ASTM D 4123 (Indirect Tension Test for Resilient Modulus of Bituminous Mixtures) and ASTM D 3497 (Dynamic Modulus of Asphalt Mixtures) are widely used for resilient modulus testing. Hill [17] utilized field cores to establish AC modulus - AC split tensile strength relations for two mixtures. Resilient modulus testing was conducted according to ASTM D4123. The split tensile strength testing was performed at the standard Marshall rate of 2-inches/minute. The following relationship between the resilient modulus (E_{AC}) and the indirect tensile strength (σ_T) of the asphalt concrete mixtures (for a temperature of 77 °F) were developed :

TABLE 2.1
Asphalt Institute Equation for Predicting AC Mixture Stiffness (Ref. 14)

$$\log|E^*| = 5.553833 + 0.028829\left(\frac{P_{200}}{f^{0.17033}}\right) - 0.03476(V_v) + 0.070377\left(\eta_{70^\circ F,10^6}\right) + 0.000005\left[t_p^{(1.3+0.49825\log f)} P_{ac}^{0.5}\right] - 0.00189\left[t_p^{(1.3+0.49825\log f)} \frac{P_{ac}^{0.5}}{f^{1.1}}\right] + 9.931757\left(\frac{1}{f^{0.02774}}\right)$$

where :

$\log|E^*|$ = dynamic modulus (stiffness) of asphalt concrete, psi;

P_{200} = percent aggregate passing No. 200 sieve;

f = frequency, Hz;

V_v = percent air voids;

$\eta_{70F,10^6}$ = absolute viscosity at 70 F, poise x 10^6;

P_{ac} = asphalt content, percent by weight of mix; and

t_p = temperature, F.

This equation has a multiple square correlation coefficient, R^2, equal to 0.939, and a Mean Square Error (MSE) of 0.01525. Therefore, the Root Mean Square Error (RMSE), better known as the Standard Error of Estimate (SEE), is 0.1235.

AC-10 : E_{AC} (ksi) = -183 + 5.87 * σ_T (psi) .....[2.3]

R = 0.976, SEE = 38.2 ksi, n = 20 tests

AC-20 : E_{AC} (ksi) = -173 + 6.07 * σ_T (psi) .....[2.4]

R = 0.801, SEE = 110 ksi, n = 63 tests

All : E_{AC} (ksi) = -176 + 6.06 * σ_T (psi) .....[2.5]

R = 0.857, SEE = 101 ksi, n = 83 tests

where E_{AC} is the resilient modulus (ksi) at 77 °F, and σ_T is the indirect tensile strength (psi) at 77

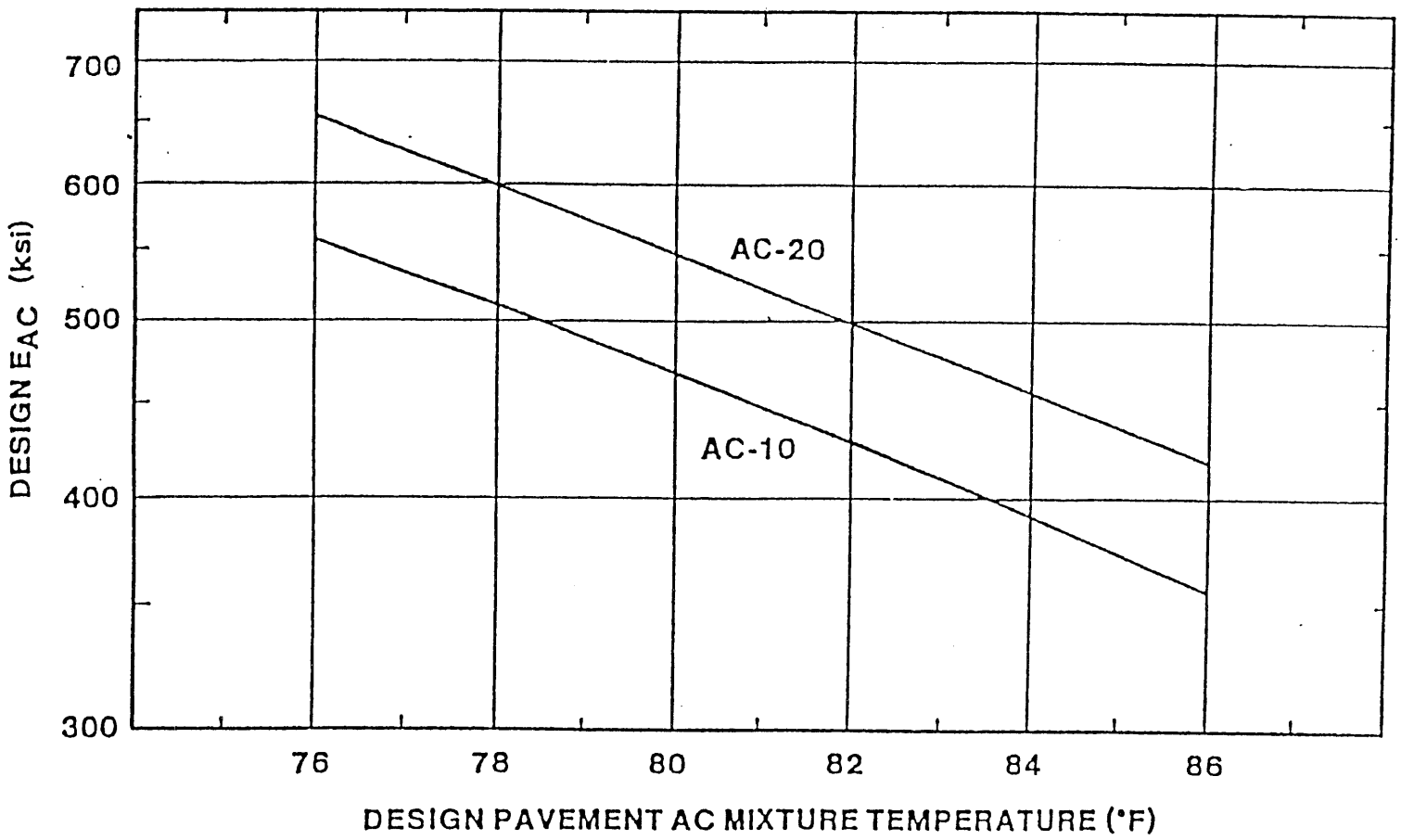

Figure 2.2. Design Asphalt Concrete Modulus Relation [Ref. 16]

°F. Equations 2.3, 2.4, 2.5 illustrate that a good estimate of the AC resilient modulus can be made from the AC indirect tensile strength. The NCHRP Project 1-26 [18] evaluation of AAMAS [19] test data included developing linear regression equations for the resilient modulus as a function of the indirect tensile strength. The results showed that the standard errors of estimate (SEE) were frequently quite large (277-ksi to 1100-ksi). The data spread increased as the value of the indirect tensile strength increased. The largest data scatter was observed at the lower test temperatures (41 °F and 55 °F). At lower temperatures, the AC mixture is very stiff and the damaging effects caused by the traffic loading are minimal. AC mixture properties at higher temperatures are of greater concern. Smaller SEE values were obtained for test results corresponding to 77 °F and 104 °F. The study showed that there is not a unique relationship between E_{AC} and AC split tensile strength. The relationship is influenced by the testing temperature, compaction procedure, and mixture composition.

Fatigue in the asphalt concrete layer is one of the design criterion for the flexible pavement design. The magnitude of the AC flexural strains is dependent on the wheel loading conditions, thickness of paving material layers, and properties of the various paving layers and subgrade soil. Fatigue transfer functions relate the number of load repetitions to reach certain pavement cracking failure conditions (i.e., crack initiation, 10-percent area cracking, etc.,) to the maximum tensile strain in the asphalt concrete layer. Miner's hypothesis is the most commonly used procedure. Fatigue algorithms for the AC mixtures are normally given by the following strain based relation [20]:

$$N = k\,(1/\varepsilon)^{n} \qquad \text{.....[2.6]}$$

In some cases the relation also includes a mixture modulus term and has the form:

$$N = k'\,(1/\varepsilon)^{n'}\,(1/E)^{m'} \qquad \text{.....[2.7]}$$

where N is the number of load repetitions to failure, ε is the AC tensile strain, and E is AC modulus. Several agencies and research groups have developed AC fatigue relations for use in the pavement design procedures. Both strain based and strain/modulus based relations have been developed.

The Asphalt Institute fatigue equation is based on the work done by Finn et al. [21], Pell and Cooper [22], and Epps [23]. The equation is as follows:

$$N = C * 18.4 * (4.32 * 10^{-3}) * (1/\varepsilon)^{3.29} * (1/E)^{0.854} \quad \text{.....[2.8]}$$

where:

N is number of 18-kip equivalent single axle loads for 20 % or greater fatigue cracking,

ε is maximum tensile strain in the asphalt layer, in/in,

E is asphalt mixture dynamic modulus, psi, and

C is a correction factor equal to: $C = 10^{M}$

where $M = 4.84 * [V_b/(V_v+V_b) - 0.69]$

V_b is the volume of asphalt, percent, and

V_v is the volume of air voids, percent.

A strain based fatigue algorithm is utilized in the Illinois DOT thickness design procedure [24, 25] for full-depth AC pavements. For a typical Illinois DOT Class I AC (dense-graded mixture), the fatigue equation is as follows:

$$N = 5 * 10^{-6} * (1/\varepsilon)^{3.0} \quad \text{.....[2.9]}$$

The equation was established based on considerations of mixture composition factors, split strength characteristics, and field calibration studies [24, 26].

Transport and Road Research Laboratory (TRRL) developed AC fatigue cracking criteria based on an analysis of the field performance of several experimental flexible pavements [27]. A multi-layer linear elastic analysis procedure was utilized to calculate dynamic strains. Miner's hypothesis was utilized to accumulate fatigue damage. Mixed traffic loading and pavement temperature conditions were considered. An equivalent temperature was established for the 9-kip standard wheel load. According to TRRL, the use of AC modulus corresponding to the equivalent temperature results in the same damage under repeated 9-kip wheel loads as was generated by the full range of combinations of wheel loads and pavement temperatures. For 85-percent probability of survival and an equivalent temperature at 20°C (68F), the fatigue algorithms are as follows:

Dense Bitumen Macadam Roadbase $N = 4.17 * 10^{-10} * (1/\varepsilon)^{4.16}$ .....[2.10]

Rolled Asphalt Roadbase $N = 1.66 * 10^{-10} * (1/\varepsilon)^{4.32}$ .....[2.11]

Several other algorithms [13, 28, 29, 30] were developed for estimating the fatigue life of AC. It is apparent that there is no unique AC fatigue algorithm that can be utilized in a mechanistic-empirical pavement design procedure. However, the general form of the algorithm is evident.

2.3.2 Base Course Layer & Subgrade Soils

The main function of the base course is to distribute the vertical loads over a greater area in order to reduce the stresses applied to the underlying materials, and to reduce pavement deformation. To perform this function, unbound aggregate base materials must posses adequate shear strength and should be able resist degradation that might be caused by the repeated, dynamic stresses applied by the traffic.

The response of granular material in the laboratory has in recent years usually been obtained by conducting a repeated loading test in a triaxial cell. Both resilient strains and permanent strains resulting from a large number of load applications are measured. Although the repeated load tests has some limitations, the test reasonably and closely simulates the actual field conditions and provides realistic engineering properties of the unbound granular materials. Procedures for repeated load testing have been proposed by several agencies and groups [31, 32, 33]. In 1982, AASHTO [34] adopted a testing procedure (T274-82) for "Resilient Modulus of Subgrade Soils". In the Fall of 1989, the AASHTO Materials Committee withdrew AASHTO T274-82 from their "Standard Tests" [34]. In 1991, AASHTO approved an interim method of resilient modulus testing (AASHTO T292-91 I; "Resilient Modulus Testing of Subgrade Soils and Untreated Base/Subbase Materials") and the method is included in the 1991 AASHTO Interim Test Methods (Part II) publication [35]. A SHRP Testing Protocol (P46-Resilient Modulus of Unbound Granular Base/Subbase Materials and Subgrade Soil) has been developed and is currently in use. SHRP P 46 requires electro-hydraulic equipment for applying repeated loads. The load duration is 0.1-seconds and the cycle duration is 1-second. The specimen is conditioned for 500-1000 load repetitions at a confining pressure of 15-psi and deviator stress of 13.5-psi. SHRP P46 has been

approved as an AASHTO Interim Method of Test (AASHTO T294-92 I; "Resilient Modulus Testing of Subgrade Soils and Untreated Base/Subbase Materials-SHRP Protocol P46"), and now carries the designation T294-94.

Several investigators [36, 37, 38, 39, 40, 41, 42, 43, 44, 45, 46, 47, 48] have conducted comprehensive laboratory studies on the repeated loading behavior of granular materials. Based on these studies, it can be deduced that the following factors have significant influence on the response of granular materials under repeated loads:

1. Stress level (confining and deviator stresses),
2. Degree of saturation and/or moisture content,
3. Dry density,
4. Grain-size distribution,
5. Stress duration or the loading frequency,
6. Particle shape,
7. Particle size, and
8. Specimen size.

The resilient behavior of granular materials and subgrade soils is an important factor in pavement analysis and design. Resilient modulus is defined as:

$$E_R = \sigma_d / \varepsilon_r \qquad \text{.....[2.12]}$$

where

E_R - Resilient Modulus,

σ_d - Repeated deviator stress, and

ε_r - Recoverable axial strain

Several models have been proposed to predict the resilient modulus of granular materials. Some of the commonly used models are described in brief in the following sections.

K-θ Model

The K-θ model [36] is the most widely used model to characterize the stress-hardening modulus behavior of granular materials. The resilient modulus is predicted as:

$$E_R = K * \theta^n \quad \text{.....[2.13]}$$

where θ is the bulk stress (= $\sigma_1 + \sigma_2 + \sigma_3$), K and n are experimentally determined parameters. The characteristic plot of the modulus varying with bulk stress is generally drawn on a log-log scale and represented by a straight line. The K-θ model is frequently used to characterize the nonlinear stress dependent behavior of granular materials.

Some studies [49, 50] have shown that the K-θ model can give inaccurate results since it neglects the effect of shear stress on the resilient modulus. Brown and Pappin [51] observed that the K-θ model can only represent a very limited range of stress paths and thus is likely to lead to erroneous results.

Bulk-Shear Modulus Model

Boyce [52] found that the resilient strain was influenced by mean normal stress (p) and also the ratio of deviator stress to normal stress. He developed a resilient modulus model in terms of secant bulk modulus (K) and the secant shear modulus (G), which are functions of stress level. Boyce developed the following equations for the incremental stress-strain behavior with a power dependence of both moduli on the isotropic mean stress:

$$K = [K_i * p^{(1-\mu)}] / [1 - \beta(q/p)^2] \quad \text{.....[2.14]}$$

$$G = G_i * p^{(1-\mu)} \quad \text{.....[2.15]}$$

where K_i and G_i are initial values of bulk and shear moduli respectively, μ is a model constant less than 1, $\beta = (1 - \mu)K_i / (6 * G_i)$, and q is the deviator stress. Using only three parameters, i.e., μ, K_i, and G_i, the K-G model was found to give reasonably good agreement with measured strains when predicting the resilient modulus of granular materials.

Countour Model

Brown and Pappin [51] extended the three parameter model of Boyce [52] to the five parameter contour model in which a stress path dependency was added in the formulation. The volumetric and shear strains were found to be influenced by the length of the stress path followed. Using a special triaxial apparatus, granular materials were tested for different realistic stress paths varying independently the axial and confining pressures. The contour model is capable of predicting resilient modulus test results very well. However, the required resilient modulus testing is complicated and material constant evaluation is cumbersome when compared to other simpler approaches.

Uzan's Model

Uzan [50] proposed a model that includes the effects of shear stress on resilient modulus. An additional deviator stress term was included in the formulation of the K-θ model. The model is of the form:

$$E_R = K3 * \theta^{K4} * \sigma_d^{K5} \qquad \text{.....[2.16]}$$

where σ_d is deviator stress, θ is the bulk stress ($= \sigma_1 + \sigma_2 + \sigma_3$), K3, K4 and K5 are experimentally determined parameters. The Uzan model, when compared to the more complicated shear and volumetric strain contour model, also gives reasonably good agreement. This is mainly due to the Uzan model's ability to incorporate shear stress and strain effects in a realistic representation of the granular material behavior. Due to its simplicity and ease in material constant evaluation, the Uzan model can be used as an improved nonlinear model in flexible pavement design procedures.

Modified K-G Model

Jouve et. al. [53] developed a modified version of Boyce's [52] equations for the bulk modulus and shear modulus of granular material. The modified K-G model follows the stress paths chosen in the triaxial tests by Brown and Pappin [51], but ignores the dilatancy phenomenon ($K \leq 0$) which is incompatible with the elastic model and the reciprocal theorem. For the modified K-G model, the bulk and shear moduli are defined as follows:

$$K = K_i * p^{(1-\mu)} \{1 + \gamma(q/p)^2\} \quad \text{.....[2.17]}$$

$$G = G_i * p^{(1-\kappa)} \quad \text{.....[2.18]}$$

where p is mean normal stress, q is deviator stress, and K_i, G_i, γ, κ, and μ are constants evaluated from the test data. Jouve et. al. used the modified K-G model to verify the Boyce's relationship concluding that $\mu = \kappa$ is statistically true. The aggregate particle shapes used in the tests were also found to influence the elastic behavior of completely crushed unbound granular material.

Thom Model

Thom [54] proposed a new elastic stress - strain model for dry granular material for the range of stress paths which can be applied using triaxial and hollow cylinder testing apparatus. Thom considered the resilient response separately for volumetric and shear strain components. The proposed model accounted for microtexture, and particle shape and size of the unbound aggregates. As a result, the model required more material constants to relate the volumetric and shear strains to the principal stresses and shear stresses:

$$\varepsilon_V = A * \Delta(\ln p)^B * (\Delta p)^C - D * \{\Delta[\ln(\sigma_1/\sigma_3)]^2\}^E \quad \text{.....[2.19]}$$

$$\varepsilon_q = F * \Delta[\ln(\sigma_1/\sigma_3)]^G * \{\Delta\tau + (\Delta S/3)\}^H \quad \text{.....[2.20]}$$

where σ_1, σ_3 are principal stresses, p is mean normal stress, S is in-plane mean stress, τ is shear stress, Δ means change in, and A, B, C, D, E, F, G, and H are statistically evaluated material constants determined experimentally. Thom concluded that the specimens comprised of aggregates containing large particles had greater elastic stiffness and shear strength compared to those having smaller particles.

Octahedral Shear Stress Model

Witczak and Uzan [55] proposed a modification to the Uzan model by replacing the deviator stress term in Equation 2.16 by an octahedral shear stress term. This model considers the dilation effect

that takes place when a pavement element is subjected to a large principal stress ratio (σ_1/σ_3). The model involves normalized values of the bulk and octahedral shear stress and is given as follows:

$$E_R = K6 * p_a * [\theta/p_a]^{K7} * [\tau_{oct}/p_a]^{K8} \quad \text{.....[2.21]}$$

where θ is the bulk stress ($= \sigma_1 + \sigma_2 + \sigma_3$), τ_{oct} is octahedral shear stress, p_a is atmospheric pressure, and K6, K7 and K8 are multiple regression constants evaluated from resilient modulus test data.

UT-Austin Model

Pezo [56] proposed a model that predicts resilient modulus as a function of deviator stress and confining pressure. The axial strains (measured during laboratory testing) are used as the main response variable and are predicted as a function of the deviator stress and confining pressure. Linear regression was performed to obtain a best fit equation of the form :

$$\text{Log } \varepsilon_a = a + K7 * \text{Log}(\sigma_d) + K8 * \text{Log}(\sigma_3) \quad \text{.....[2.22]}$$

where ε_a is the measured resilient axial strain, σ_d is the deviator stress, and σ_3 is the minor principal stress (confining pressure). The response was transformed into the following model :

$$E_R = N6[\sigma_d^{N7}][\sigma_3^{N8}] \quad \text{.....[2.23]}$$

where $N6 = 10^{-a}$, $N7 = 1 - K7$, and $N8 = -K8$.

The model is statistically sound since the prediction variables are independent from the response variables.

Several other models [57, 58] have been developed to predict resilient modulus of granular materials but are not commonly used.

Fine-grained cohesive soils show decreasing resilient modulus with increasing stress (stress softening behavior). Robnett and Thompson [31] have demonstrated that for practical pavement design and analysis purposes, repeated unconfined ($\sigma 3 = 0$) compression testing is satisfactory for resilient testing of cohesive soils. Figures 2.3 and 2.4 show the arithmetic model and Figure 2.5 shows the semi-log model (for the same data sets)[59]. An arithmetic stress dependent behavior is shown to adequately describe the stress softening behavior of fine-grained soils. Poku and Drumm [60] proposed the hyperbolic model (Figure 2.6) to account for stress-softening behavior. Hyperbolic model and semi-log model are continuos functions, whereas the arithmetic model is bi-linear. Extensive resilient testing data at the University of Illinois [61] were analyzed based on the arithmetic model. The study showed that E_{Ri} (the resilient modulus at the intersection point) is a good indicator of a soil's resilient behavior. E_{Ri} is typically associated with a repeated deviator stress of about 6-psi. The slope values K_1 and K_2, display less variability and influence pavement structural response to a smaller degree than does E_{Ri}.

Many factors influence the resilient behavior of cohesive soils. Several studies [3, 61, 62, 63] have shown that the resilient moduli and moisture sensitivity of fine-grained soils can be estimated from standard soil test data such as clay content, plasticity index, liquid limit, and optimum moisture content. Various resilient modulus-strength (unconfined compressive strength, CBR) correlations are also available but should be used with caution.

Rutting potential of granular materials is a function of their shear strength and the existing stress state. Stress state can be expressed as:

1. Repeated deviator stress, σ_D;
2. Principal stress ratio, σ_1 / σ_3; and
3. Deviator stress ratio, $(\sigma_1 - \sigma_3) / \sigma_3$.

Stress ratio, defined as the ratio of repeated stress to ultimate strength, gives a good indication about the rutting potential. High stress ratios are generally associated with high rutting potentials. Permanent strain-load repetition relations are generally expressed in terms of permanent strain-log N or log permanent strain-log N. The most commonly used model used to describe the laboratory

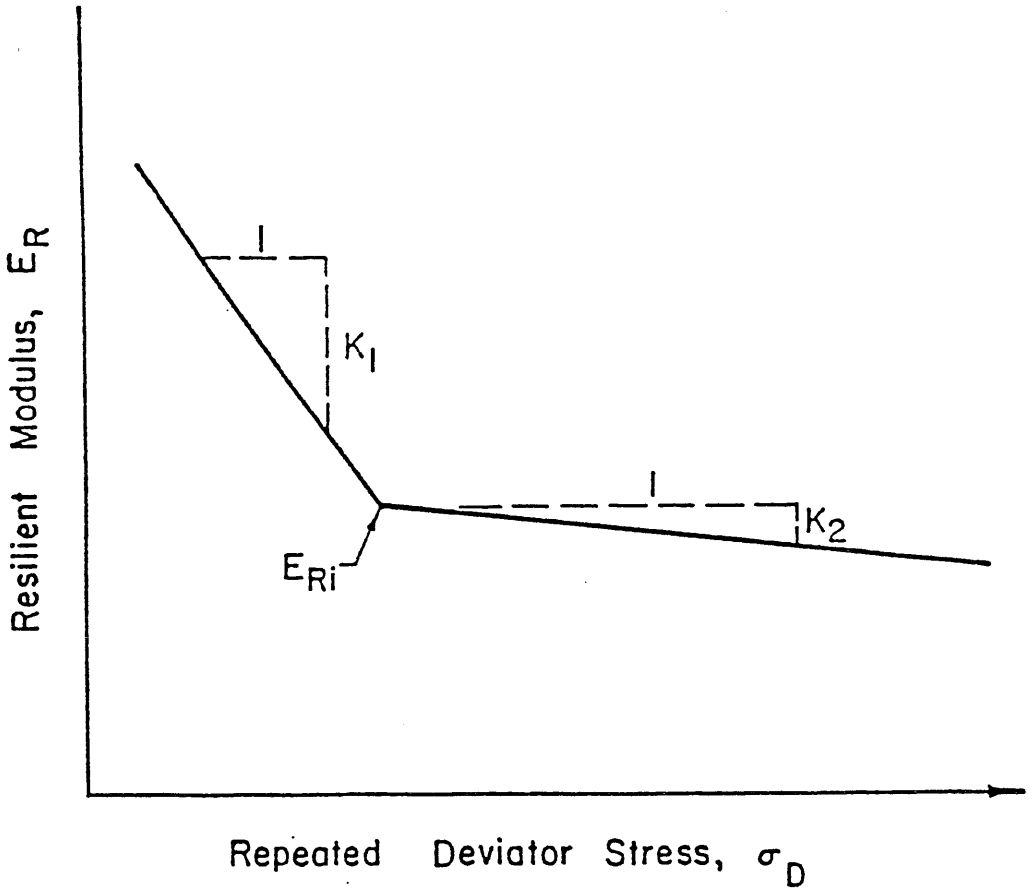

Figure 2.3. Arithmetic Model for Stress Dependent Resilient Behavior of Fine Grained Soils [Ref. 31]

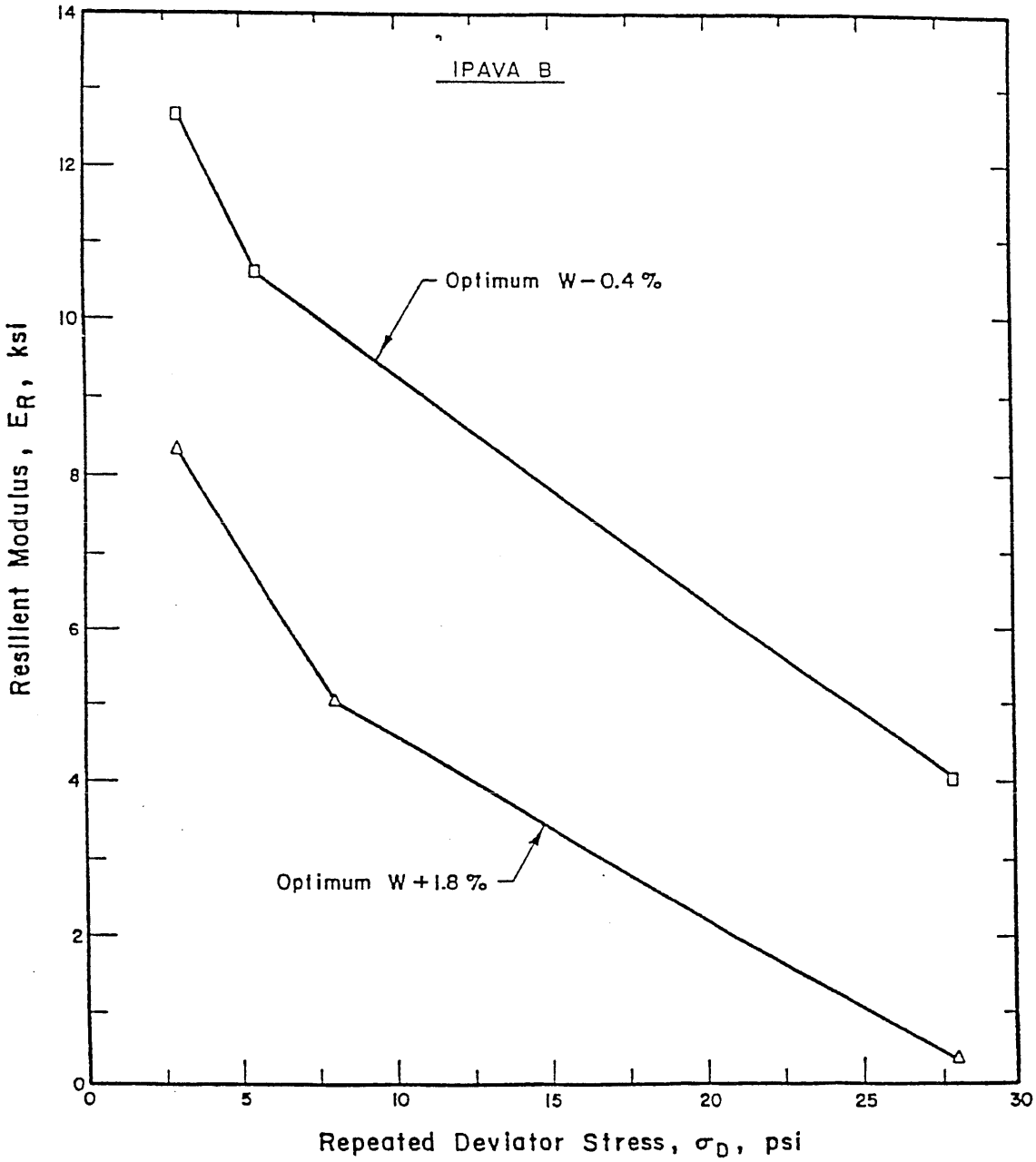

Figure 2.4. Typical Stress Dependent Resilient Behavior of a Fine Grained Soil (AASHTO A-7-6) [Ref. 59]

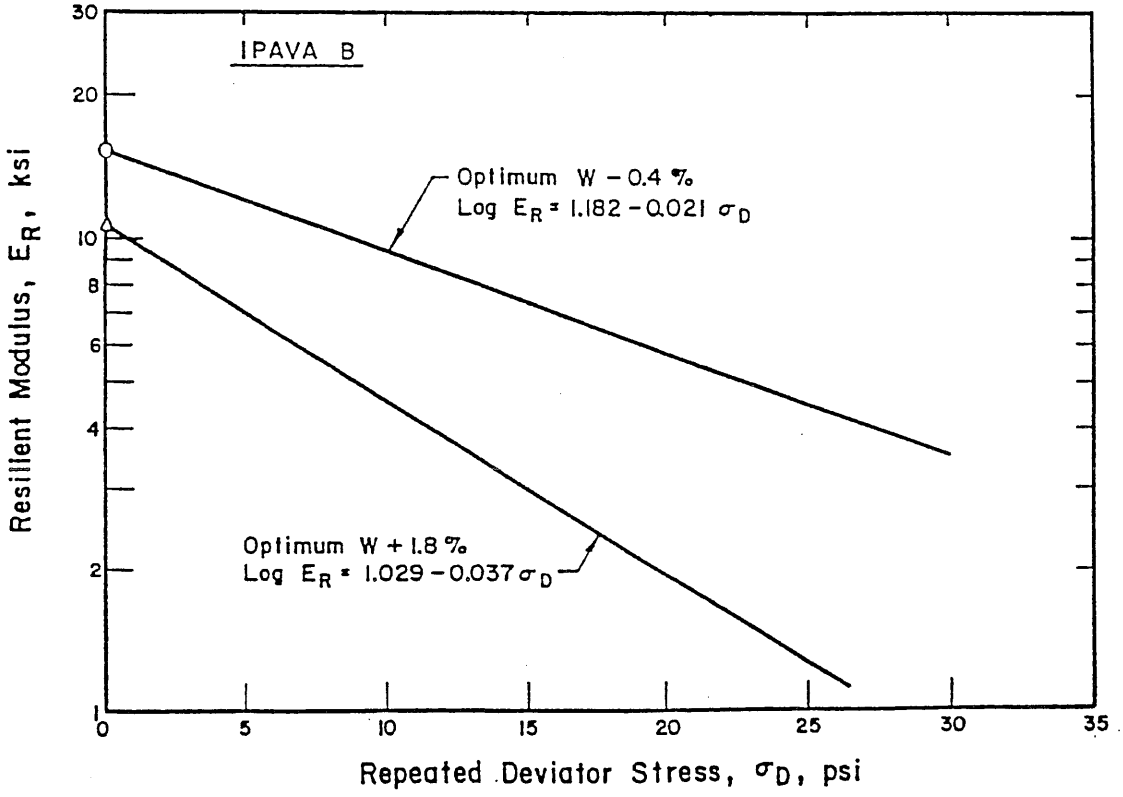

Figure 2.5. Semi-Log Model for Stress Dependent Resilient Behavior of a Fine Grained Soil (AASHTO A-7-6) [Ref. 59]

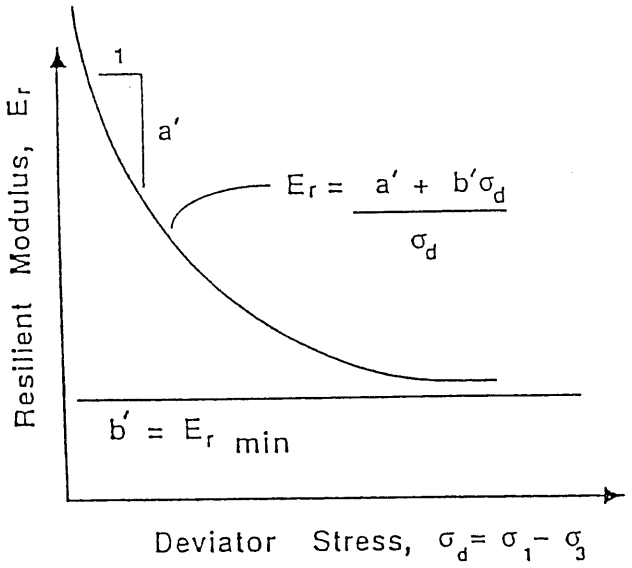

a. Hyperbolic Representation of Resilient Modulus Response

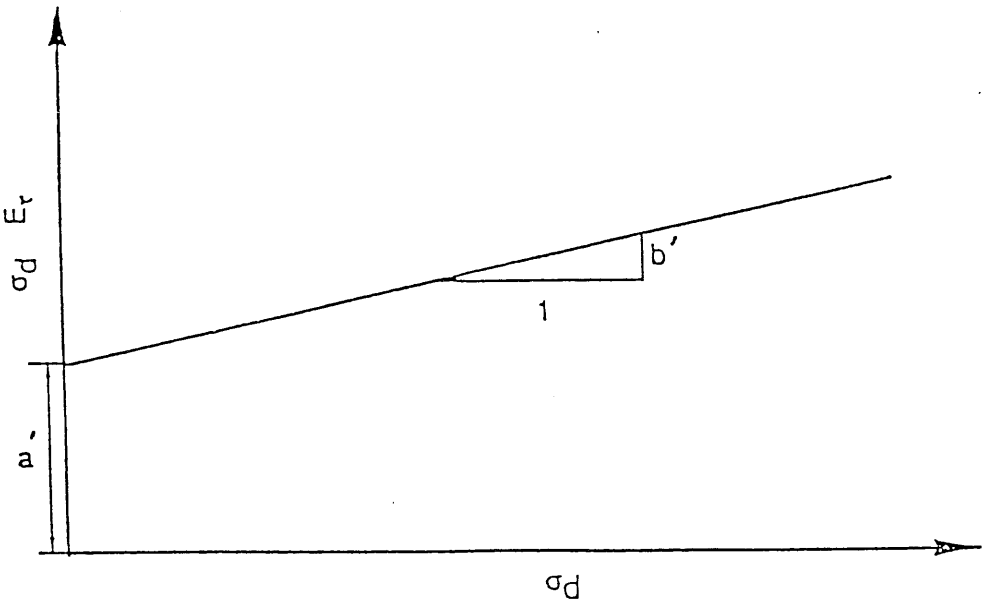

b. Transformed Coordinates for Determination of Hyperbolic Parameters a' and b'

Figure 2.6. The Hyperbolic Model [Ref. 60]

repeated load testing data was developed by Monismith et. al. [64]. The model is described as follows:

$$\varepsilon_P = A * N^b \quad \text{.....[2.24]}$$

where ε_P is the permanent strain, A and b are experimentally determined coefficients, and N is the number of load repetitions. Extensive studies [39, 65, 66, 67, 68, 69] have shown that the "b" term in the model varies between 0.1 to about 0.2 The "A" term is quite variable and is strongly influenced by repeated stress state and material strength.

A permanent strain accumulation prediction model was developed at Ohio state University [67] that is valid for describing progress in all pavement layers - asphalt concrete, granular base course, subbase materials, and subgrade soils. The model is described as follows:

$$\varepsilon_P / N = A * N^m \quad \text{.....[2.25]}$$

where ε_P is the plastic strain at N number of load cycles, N is the number of load cycles, A is the experimental constant depending on the material and state of stress condition, and m is experimental constant depending on material type. Experimental data [67] shows that "m" varies within a narrow range for cohesive soils and granular materials. Typical "m" for the cohesive soils is -0.88 and for granular materials, it is -0.8. The "A" term is quite variable and depends on material, repeated stress state and moisture/density conditions.

Repeated load tests conducted by Raymond and Bathurst [70] on granular materials and the analysis on data collected [18] showed that Log(permanent deformation/N)-LogN for field pavement sections would be useful in calibrating the rutting model, particularly in the situation where pavement deformation in the granular layers can be established.

The problem with predicting rut-depth in pavements is the inadequate knowledge about predicting the magnitude and sequence of load applications on pavement (stress history effects). For mix loading conditions, application of repeated stress states of varying magnitudes affects the

permanent strain accumulation [39, 64]. Thompson and Nauman [71] used a phenomenological pavement surface rutting model to analyze the AASHO Road Test data. The model is of the form:

$$RR = RD/N = A/N^{B} \quad \text{.....[2.26]}$$

where

RR = Rutting Rate,

RD = Rut depth, inch,

N = Number of repeated load applications, and

A & B = Terms developed from field calibration testing data.

The results showed that stable pavement rutting trends were related to estimated pavement structural responses, particularly the subgrade stress ratio (SSR). If the SSR was below a threshold level, low 'A' terms were noted. They concluded that the Rutting Rate model is particularly helpful in analyzing the pavement rutting data for a specific pavement section and estimating future rutting for pavement management system use. The rutting rate approach is a practical and easily used procedure.

2.4 Conventional Flexible Pavement Design Procedure

The current Illinois mechanistic design procedure for conventional flexible pavements is based on resilient soil and material testing procedures, the ILLI-PAVE structural model, and the design algorithms developed from an extensive ILLI-PAVE data base [72]. AC rutting is considered in material selection and AC mixture design procedure. AC fatigue cracking is related to maximum tensile strain at the bottom of AC layer. Granular base rutting is controlled by establishing a minimum thickness of AC surface to limit the stress -state in the granular base to a level that will not produce unacceptable rutting. NCHRP 1-26 [18] reported that subgrade rutting potential can be reasonably assessed by considering the subgrade stress ratio (SSR) at the pavement structure - subgrade interface. The acceptable level is in the range of 0.4 to 0.75 depending on ESAL's.

2.4.1 Modeling Pavement Structural Response

Previous studies [73, 74, 75] have demonstrated that the stress-dependent, finite element pavement model ILLI-PAVE provides reliable and realistic predictions. In ILLI-PAVE, the pavement is

considered an axisymmetric solid of revolution. Non-linear, stress dependent resilient modulus material model and failure criteria for granular materials and fine-grained soils are incorporated into the ILLI-PAVE finite element model. The principal stresses in the granular material and fine-grained soil layers are modified at the end of each iteration so that they do not exceed the shear strength as defined by the Mohr-Coulomb theory of failure.

2.4.2 Design & Response Algorithms

Simplified design and response algorithms have been developed from a comprehensive ILLI-PAVE data base [73] for 18-kip axle loads and representative conventional flexible pavement configurations, materials and subgrades. The algorithms are generally used for a-priori flexible pavement design. The algorithms developed are as follows:

Design Algorithms

$$\text{Log}(\varepsilon_{ac}) = 2.9496 + 0.1289*T_{ac} - 0.5195*\text{Log}(T_g)/T_{ac} - 0.0807*(\text{Log}E_{ac})*T_{ac} - 0.0408*\text{Log}(E_{Ri}) \quad \text{.....[2.27]}$$

$$\text{Log SSR} = 0.3056 + 0.0560*T_{ac} - 0.0222*T_g - 0.0495*(\text{Log}E_{ac})*T_{ac} - 0.4242*\text{Log}E_{Ri} \quad \text{.....[2.28]}$$

Response Algorithms

$$\text{Log DEV} = 1.7694 - 0.0735*T_{ac} - 0.0222*T_g - 0.2539*\text{Log}E_{ac} + 0.0223*E_{ri} \quad \text{.....[2.29]}$$

$$\text{Log D0} = 1.9692 + 0.0465*T_{ac} - 0.5637*(\text{Log}T_g)/T_{ac} - 0.0464*(\text{Log}E_{ac})*T_{ac} - 0.2079*\text{Log}(E_{Ri}) \quad \text{.....[2.30]}$$

where

DEV = Subgrade deviator stress, in psi

SSR = Subgrade stress ratio

D0 = Surface deflection at the point of loading, in mils

ε_{ac} = Tensile strain at the bottom of the AC layer, in micro-in/in

T_{ac} = Thickness of AC layer, in inches

T_g = Thickness of granular base course, in inches

E_{ac} = Resilient modulus of AC layer, in ksi

E_{Ri} = "breakpoint" resilient modulus of the subgrade, in ksi

2.5 Full-Depth Asphalt Concrete Pavement Design Procedure

The current Illinois mechanistic design procedure for full-depth asphalt concrete pavements is based on resilient soil and material testing procedures, the ILLI-PAVE structural model, and the design algorithms developed from an extensive ILLI-PAVE database [25]. The primary modes of failure in full-depth AC pavements are AC rutting, subgrade rutting, and AC fatigue cracking. AC rutting and thermal cracking is considered in material selection and AC mixture design procedure. Subgrade rutting can be controlled by limiting the deviator stress at AC-subgrade interface to an acceptable level. Full-depth AC pavement thickness requirements for design traffic levels are generally sufficient to control subgrade rutting [26]. Thus, the governing design criteria is AC tensile strain. AC fatigue cracking is related to maximum tensile strain at the bottom of AC layer.

2.5.1 Modeling Pavement Structural Response

The tensile strains at the bottom of asphalt concrete layer are determined using ILLI-PAVE. The inputs required are AC thickness, AC dynamic modulus, and subgrade resilient modulus. Seasonal effects are considered through the use of Design Time concept [26].

2.5.2 Design & Response Algorithms

Simplified design and response algorithms have been developed from a comprehensive ILLI-PAVE data base [26]. The algorithms developed are as follows:

Design Algorithms

$$\text{Log}(\varepsilon_{ac}) = 5.746 - 1.589*\text{Log}(T_{ac}) - 0.774*(\text{Log}E_{ac}) - 0.097*\text{Log}(E_{Ri}) \quad \text{.....[2.31]}$$

Response Algorithms

$$\text{Log DEV} = 2.744 - 1.138*\text{Log}(T_{ac}) - 0.515*\text{Log}(E_{ac}) + 0.289*E_{Ri} \quad \text{.....[2.32]}$$

$$\text{Log D0} = 3.135 - 0.895*\text{Log}(T_{ac}) - 0.359*\text{Log}(E_{ac}) - 0.287*\text{Log}(E_{Ri}) \quad \text{.....[2.33]}$$

where

DEV = Subgrade deviator stress, in psi

D0 = Surface deflection at the point of loading, in mils

ε_{ac} = Tensile strain at the bottom of the AC layer, in micro-in/in

T_{ac} = Thickness of AC layer, in inches

E_{ac} = Resilient modulus of AC layer, in ksi

E_{Ri} = "breakpoint" resilient modulus of the subgrade, in ksi

2.6 Surface Treatment Pavement Design Procedure

A surface treatment pavement includes a granular base layer with a surface treatment. The surface treatment is considered as a non-structural layer [76]. Surface treated pavements are typically designed for average (50 %) design reliability. The primary form of distress and the major design consideration is surface rutting. The granular layers and the subgrade contribute to rutting. The granular material rutting potential can be considered by specifying quality, gradation, liquid limit, plastic limit, strength, and construction parameters. The subgrade rutting can be controlled by limiting the subgrade stress ratio.

Simplified design algorithms have been developed from a comprehensive ILLI-PAVE data base [76]. The algorithms developed are as follows:

Subgrade Stress Ratio Algorithms:

$$SSR = 1.31 - 0.051 * T_{GR} - 0.204 * \text{Log } E_{Ri} \quad \text{.....[2.34]}$$

$$R^2 = 0.90, \text{ SEE} = 0.09$$

$$\text{Log SSR} = -0.184 - 0.034 * T_{GR} + 0.178 * \text{Log } \Delta \quad \text{.....[2.35]}$$

$$R^2 = 0.93, \text{ SEE} = 0.06$$

Response Algorithms:

$$\text{Log } \sigma_{DEV} = 1.051 + 0.517 * \text{Log } E_{Ri} - 0.038 * T_{GR} \quad \text{.....[2.36]}$$

$$R^2 = 0.98, \text{ SEE} = 0.06$$

$$\text{Log}\,\Delta = 2.434 - 0.565 * \text{Log}\,T_{GR} - 0.029 * E_{Ri} \quad \text{.....[2.37]}$$

$$R^2 = 0.96,\ SEE = 0.06$$

E_{Ri} Algorithm:

$$E_{Ri} = 24.2 - 5.71 * (\Delta 3) + 0.35 * (\Delta 3)^2 \quad \text{.....[2.38]}$$

$$R^2 = 0.98,\ SEE = 0.57$$

where

- σ_{DEV} - Subgrade deviator stress, psi
- SSR - Subgrade stress ratio (σ_{DEV}/Q_u)
- Q_u - Subgrade unconfined compressive strength, psi
- T_{GR} - Granular base thickness, inch
- E_{Ri} - Subgrade "breakpoint" resilient modulus, ksi
- Δ - Surface deflection @ 0-inch offset, mils, for 9-kip FWD loading
- $\Delta 3$ - Surface deflection @ 36-inch offset, mils, for 9-kip FWD loading

2.7 Summary

A brief background on mechanistic design procedures for conventional flexible pavements, full-depth asphalt pavements, and surface treated pavements has been presented. Laboratory tests and models used to characterize the paving materials have been discussed. Simple algorithms, developed from extensive database, have been presented that can be used for a-priori pavement design. Currently, Illinois is the only state where the DOT has a mechanistic-empirical design procedure for the local roads and streets.

The following sections of this thesis describe the material characterization phase and the results of analysis performed on the data and information obtained from Mn/ROAD project.

CHAPTER - III
LABORATORY TESTING PROCEDURES & MATERIALS

3.1 Introduction

The shear strength, permanent deformation, and resilient modulus of granular materials are quite important relative to the behavior and performance of the material in a pavement layer. Some important factors influencing these properties are gradation, moisture and density, maximum particle size, amount and plasticity of fines, particle geometrical characteristics, and confining pressure. Over the years, University of Illinois (U of I) has developed and successfully used a testing procedure for unbound granular materials. In the first phase, triaxial shear tests are performed at a rapid shearing rate to establish the shear strength parameters (friction angle "ϕ", and cohesion "c"). In the second phase, the specimen is subjected to 1000 load repetitions at 45-psi deviator stress and 15-psi confining pressure and is referred to as the "conditioning stage". The third phase consists of subjecting the "conditioned" specimen to 100 load repetitions at different stress states (described later) for measuring resilient modulus. In the fourth phase, following resilient modulus testing, the specimen is subjected to rapid shear test at 15-psi confining pressure to study the stress history effects on shear strength.

A laboratory testing program was established to determine pertinent engineering properties of the granular bases and subgrade sand used in the various low-volume road test sections at Mn/ROAD. Rapid shear tests and repeated loading tests were conducted to determine the shear strength parameters (friction angle "ϕ", and cohesion "c"), resilient modulus (E_R), rutting potential, stress history effects on shear strength, and moisture susceptibility. Dynamic cone penetrometer (DCP) tests were conducted to get an indication about the shear strength (CBR) of the granular materials and subgrade sand.

This chapter describes the testing equipment, testing procedures, and the materials that were used in the laboratory testing program.

3.2 Specimen Preparation

Six-inch diameter and 12-inch high cylindrical specimens were prepared for conducting rapid shear

tests and repeated load tests. The specimens were prepared using a split aluminum mold (Figure 3.1). A neoprene membrane, 31-mils thick, was attached to the lower platen and high vacuum grease was applied at the contact points. The split mold was assembled and the membrane was folded over the top of the mold and secured with a hose clamp. A vacuum line was attached to the mold to hold the membrane tight against the mold. A nonwoven geofabric was placed at the bottom of the mold to prevent the drainage port from being clogged. The material (aggregate mixed with required amount of water) was placed in the mold in five lifts and each lift was rodded 25 times using a standard rod for concrete testing. The surface of each lift was leveled after rodding, and compaction foot was placed over it. A pneumatic vibratory compactor was used for compaction. Specimen density was calculated by measuring the compacted thickness of each lift, referenced to the top of the mold. Each lift was then scarified upto a depth of approximately 1-inch, and the next lift then placed and compacted. After compaction, the final height and density of specimen were noted. The vacuum was removed and applied to the bottom end of the specimen to create suction through the specimen thereby causing a confinement by the membrane. The loading platen was placed at the top of the specimen. The split aluminum mold was then removed and a 25-mil thick latex membrane was placed on the specimen. The second membrane (latex membrane) was required because the neoprene membrane generally was punctured while compacting the specimen. The triaxial chamber was then assembled and loading piston was placed through the bushings in the top lid. The triaxial assembly was placed into the MTS rig for testing. About 5-psi confining pressure was applied and the vacuum line was removed. The drainage port was left open so that the tests could be performed under drained conditions. A pressure gauge was used at the drainage port to check for any leakage through the membranes. If there were no leaks, specimen was ready for testing. The assembled triaxial chamber along with the specimen is shown in Figure 3.2.

DCP tests were performed on 9-inch diameter and 15-inch high cylindrical specimens. The specimens were compacted using a pneumatic hammer (described above) in a steel mold in six lifts.

3.3 Testing Equipment

The cyclic loading system used in this study was Material Testing System (MTS) Closed-Loop Servo Hydraulic System, Model 407. The main part of the system consists of controller, loading frame, and hydraulic power supply. The system is fitted with a 10-kip ram. The ram is fitted with

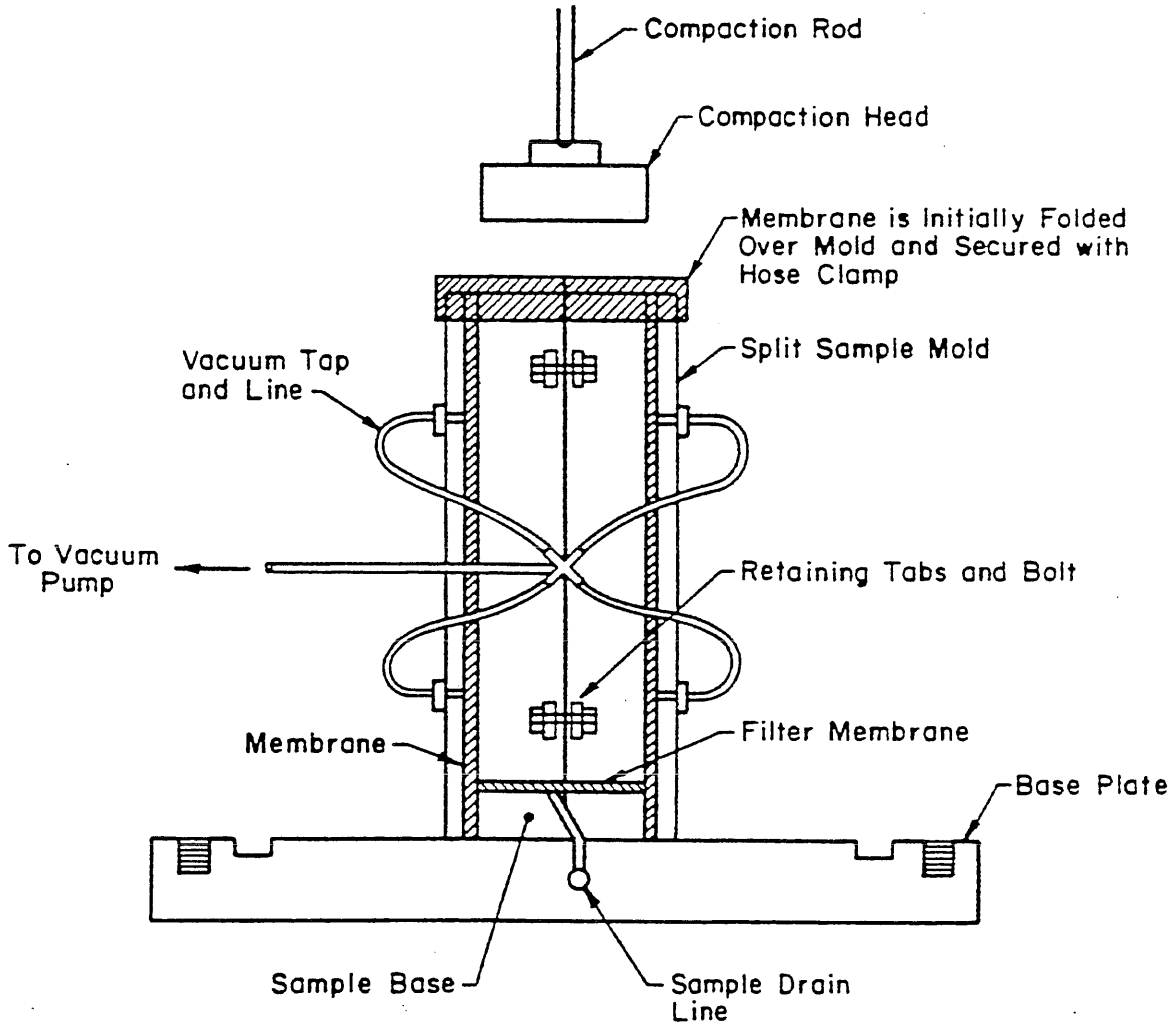

Figure 3.1. Triaxial Sample Mold

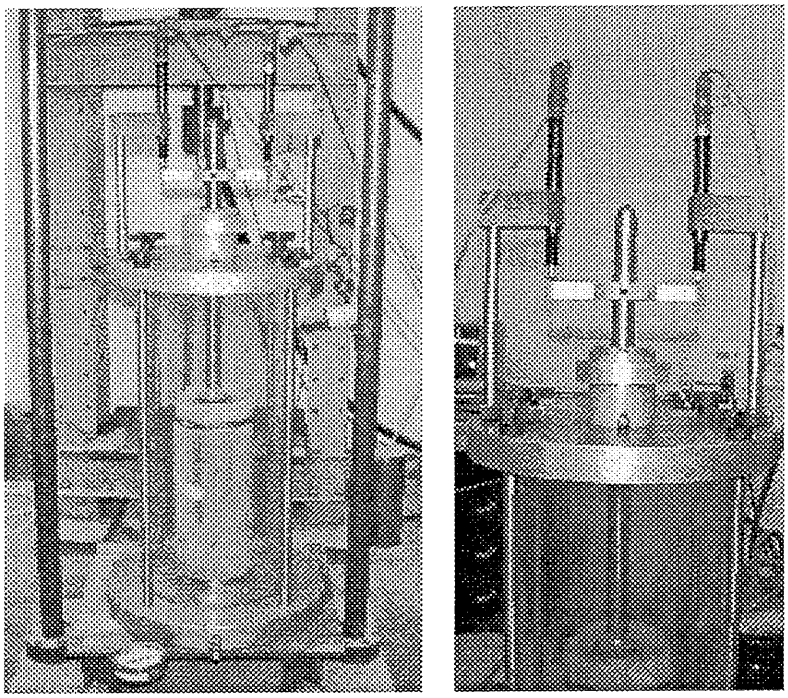

Figure 3.2. Assembled Triaxial Chamber Along with the Specimen

an internal Linear Variable Differential Transducer (LVDT). The MTS-407 controller provides the electronics for closed-loop control and controls the system operation. In a closed-loop system, a control signal such as ramp or cyclic waveform is generated from a program source. The DC (load controller) or AC (displacement controller) takes this signal and converts it into a control signal that generates force, or displacement to occur to the specimen. This force, or displacement is measured by the associated system transducer (a load cell, or LVDT respectively). While the force, or displacement is being applied, the AC or DC controller compares input from the program with the output of the controlling transducer. If there is any difference in the two signals, a servo valve command signal is generated, and the system responds accordingly to keep the feedback equal to the command. Figure 3.3 shows the MTS controller.

An IBM Personal Computer AT, fitted with an 8-channel Data Translation No. 2801-A analog:digital (A/D) board, triggered the MTS and recorded the data. The A/D board has a maximum sampling rate of 27,500 readings per second.

Two external LVDT's, mounted on the top plate of the triaxial chamber, were used to measure the

displacements during the resilient modulus tests. A T-bar was attached to the loading piston which actuated the external LVDT's.

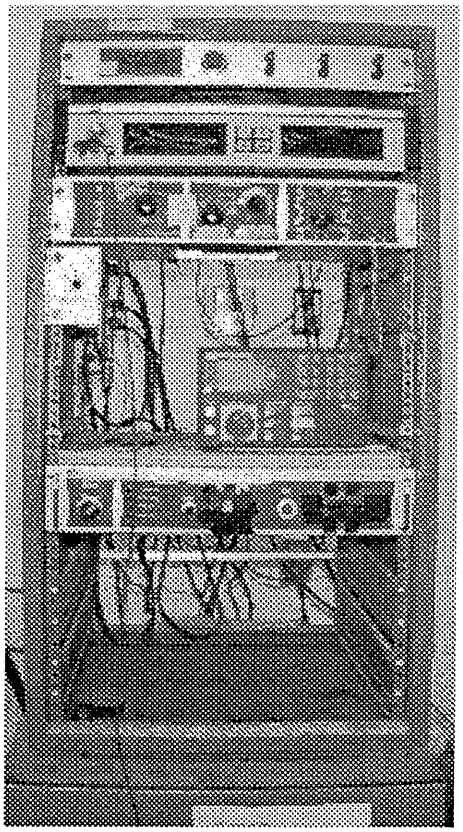

Figure 3.3. MST 407 Controller

3.4 Rapid Shear Testing

A triaxial shear test performed at a rapid shearing rate is more representative of highway loading conditions than the conventional slow triaxial shear test (strain rate of 1-3 percent per minute). Rapid shear tests were performed at confining pressures of 5-psi, 10-psi, 15-psi, 20-psi, and 30-psi to determine the friction angle "ϕ", and cohesion "c" used to define the Mohr-Coulomb failure envelope. Six-inch diameter and 12-inch high cylindrical specimens were tested. Air was used as the confining medium. Deviator stress was applied axially at a constant displacement rate of 1.5 inch/second (strain rate of 12.5 percent per second). This corresponds to 5% strain in 400 milliseconds.

Using the failure deviator stress and confining pressure, the Mohr-Coulomb envelope is determined by regression technique. Linear regression was performed to obtain a best fit equation of the form

$$\sigma_1 = a + b*\sigma_3 \quad \text{.....[3.1]}$$

where σ_1 is major principal stress and σ_3 is minor principal stress. Cohesion (c) and angle of internal friction (ϕ) were evaluated as follows :

$$c = a / [2*\sqrt{b}] \quad \text{.....[3.2]}$$

$$\phi = \sin^{-1}[(b-1)/(b+1)] \quad \text{.....[3.3]}$$

where 'a' and 'b' are regression coefficients.

3.5 Permanent Deformation Testing

The conditioning cycle data indicates rutting potential. Conditioning was performed at a deviator stress of 45-psi and a confining pressure of 15- psi for 1000 load repetitions. The following model was used to characterize the rutting potential :

$$\varepsilon_p \% = A N^b \quad \text{.....[3.4]}$$

where N is the number of load repetitions and A is the antilog of 'a' in :

$$\text{Log } \varepsilon_p \% = a + b \text{ Log } N \quad \text{.....[3.5]}$$

'b' represents the amount of strain (%) accumulated per Log cycle.

3.6 Resilient Modulus Testing

Cylindrical specimens (6-inch diameter; 12-inch height) were subjected to various triaxial stress states that were less than the failure stress states. A haversine load waveform was applied with a load pulse duration of 0.1-seconds (10-Hz), and a rest period of 0.9- seconds. The specimens were initially conditioned for 1000 load repetitions at a deviator stress of 45-psi and a confining pressure of 15-psi (stress state referred to as 45/15). Data recorded were permanent deformation, resilient

deformation, and applied deviator stress. Measurements were made at 1, 10, 50, 100, 500, and 1000 load applications. After conditioning, modulus testing was conducted at various stress states listed below. The deviator stresses ranged from 10-psi to 60-psi and confining pressures ranged from 5-psi to 30-psi. Bulk stress (θ) ranged from 25-psi to 150-psi. One hundred load repetitions were applied at each sequence (stress state). If the difference between the modulus values at 50th and 100th load repetition was more than 5 percent, the sequence was repeated.

Stress States Used in Resilient Modulus Testing:

σ_d psi	σ_3 psi	σ_1 psi	$\theta = \sigma_1+2*\sigma_3$ psi	σ_1/σ_3	**No. of Load Repetitions**
45	15	60	90	4	1000*
10	5	15	25	3	100
15	5	20	30	4	100
20	10	30	50	3	100
30	10	40	60	4	100
30	15	45	75	3	100
45	15	60	90	4	100
45	30	75	135	2.5	100
60	30	90	150	3	100

* sample conditioning

σ_d - Deviator stress, psi

σ_1 - Major principal stress, psi

σ_3 - Minor principal stress, psi

θ - Bulk stress, psi

σ_1/σ_3 - Principal stress ratio

Resilient modulus for each stress state was evaluated as follows :

$$E_R = \sigma_d/\varepsilon_r \quad \text{.....[3.6]}$$

where :

E_R = Resilient Modulus, psi

σ_d = Applied Deviator Stress, psi

ε_r = Resilient (recoverable) strain

3.7 Conditioned Rapid Shear Tests

Conditioned rapid shear tests evaluate the effect of stress history on the shear strength of the material. After the completion of the repeated load resilient modulus sequences, the sample was subjected to a rapid shear test at a confining pressure of 15-psi. A comparison was made between the peak shear strength of the unconditioned sample and the conditioned sample.

3.8 Dynamic Cone Penetrometer Tests

Dynamic Cone Penetrometer (DCP) data are indicative of shear "strength" (CBR) of the granular materials. Cylindrical specimens (9-inch diameter, 15-inch height) were prepared and tested in the laboratory. The calibrated lower rod was driven into the material using the 17.6-pound anvil on the upper rod. The DCP was mounted on a guide frame to maintain vertical alignment. Figure 3.4 and Figure 3.5 show the DCP and DCP mounted on a guide frame respectively. The rod penetration after each anvil blow was recorded as inches/blow. This was recorded as the "penetration rate" (PR). CBR was estimated from PR as follows [77]:

$$\text{Log}_{10}\,\text{CBR} = 0.84 - 1.26 * \text{Log}_{10}\,(\text{PR}) \quad \text{.....[3.7]}$$

3.9 Mn/ROAD Granular Materials & Subgrade Sand

Six different granular materials were used as base and subbase materials in the Mn/ROAD project test sections. The material specifications are given in Table 3.1. In aggregate classes CL-1Fsp, CL-1Csp, CL-3sp, CL-4sp, crushed/fractured particles were not permitted. Ten to fifteen percent crushed/particles were required for CL-5sp. Hundred percent crushed/fractured particles were required for CL-6sp. Laboratory tests showed all the materials to be non-plastic. MnDOT performed gradation tests on field samples. At the University of Illinois, gradation tests were performed on the bulk stockpile samples supplied by MnDOT. The results obtained from field samples and stockpile samples for different aggregate classes are given in Tables 3.2 through 3.8.

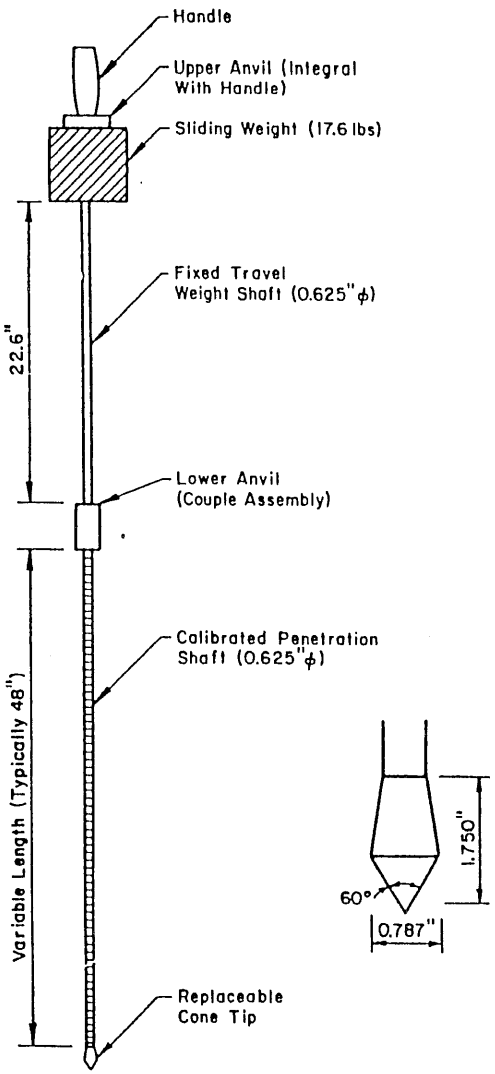

Figure 3.4. Dynamic Cone Penetrometer (DCP)

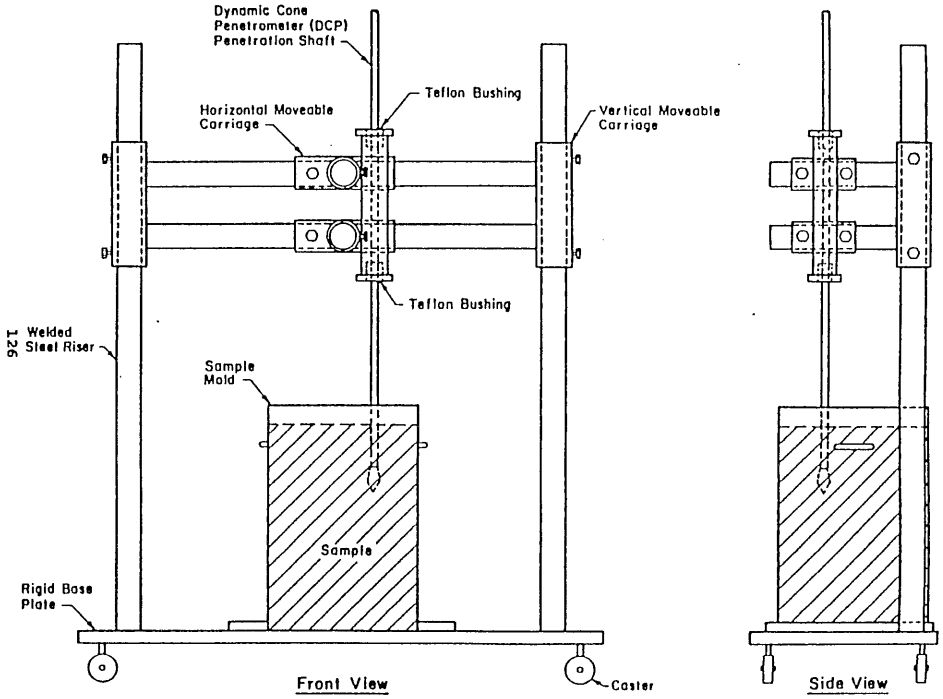

Figure 3.5. Dynamic Cone Penetrometer (DCP) Alignment Device

TABLE 3.1
MRRP Base and Surfacing Aggregate (S.P. 8680-123)

	Percent Passing Sieve Size										Plasticity	
Aggregate Class	1-1/2"	1"	3/4"	1/2"	3/8"	No. 4	No. 10	No. 40	No. 200	LL	PI (min.)	PI (max.)
CL-1C sp	--	--	100	--	65-90	40-70	25-50	10-30	4-12	35 max.	0	6
CL-1F sp	--	--	100	--	80-95	65-85	45-70	25-45	8-16	35 max.	6	12
CL-3 sp	--	--	--	100	95-100	85-100	65-90	30-50	8-15	35 max.	0	12
CL-4 sp	100	95-100	90-100	--	80-95	70-85	55-70	15-30	5-10	35 max.	0	12
CL-5 sp	--	100	90-100	--	70-85	55-70	35-55	15-30	3-8	25 max.	0	6
CL-6 sp	--	100	85-100	--	50-70	30-50	15-30	5-15	0-5	25 max.	0	6

Special Crushing Requirements :
CL-1 sp through CL-4 sp : crushed/fractured particles not allowed
CL-5 sp : 10-15 percent crushed/fractured particles required
CL-6 sp : 100 percent crushed/fractured particles required

TABLE 3.2
Gradation Test Results for CL-1Csp

		Mean		MnDOT Tests	
Sieve Size	Specs.	MnDOT Tests	UIUC Tests	Std.Dv.	COV,%
2"	100	100	100	0	0.00
1"	100	100	100	0.00	0.00
3/4"	100	100	95.9	0.00	0.00
3/8"	65-90	83.2	75.6	5.17	6.22
#4	40-70	63.2	60.6	2.99	4.74
#10	25-50	48.2	51.1	2.96	6.14
#40	10-30	23.7	23.6	3.85	16.24
#200	4-12	7.8	7.9	1.08	13.90

TABLE 3.3
Gradation Test Results for CL-1Fsp

		Mean		MnDOT Tests	
Sieve Size	Specs.	MnDOT Tests	UIUC Tests	Std.Dv.	COV,%
2"	100	100	100	0.00	0.00
1"	100	100	100	0.00	0.00
3/4"	100	100	100.0	0.00	0.00
3/8"	80-95	88	90.0	1.41	1.61
#4	65-85	73.9	76.0	3.33	4.51
#10	45-70	61.8	64.0	3.15	5.11
#40	25-45	30.3	33.0	1.56	5.16
#200	8-16	9.75	10.0	0.41	4.17

TABLE 3.4
Gradation Test Results for CL-3sp

		Mean		MnDOT Tests	
Sieve Size	Specs.	MnDOT Tests	UIUC Tests	Std.Dv.	COV,%
3/4"	100	100.00	100.00	0.00	0.00
3/8"	95-100	99.13	100.00	0.33	0.33
#4	85-100	92.38	93.69	1.58	1.71
#10	65-90	81.25	84.35	1.64	2.02
#40	30-50	39.75	43.14	2.68	6.74
#200	8-15	11.81	11.87	1.30	10.97

TABLE 3.5
Gradation Test Results for CL-4sp

		Mean		MnDOT Tests	
Sieve Size	Specs.	MnDOT Tests	UIUC Tests	Std.Dv.	COV,%
2"	100	100	100	0.00	0.00
1"	95-100	100	100	0.00	0.00
3/4"	90-100	98.6	96.7	0.49	0.50
3/8"	80-95	90.8	89.2	0.40	0.44
#4	70-85	80	78.0	1.10	1.37
#10	55-70	61.8	62.1	2.48	4.02
#40	15-30	25.4	23.5	1.62	6.40
#200	5-10	8.3	7.2	0.89	10.72

TABLE 3.6
Gradation Test Results for CL-5sp

		Mean		MnDOT Tests	
Sieve Size	Specs.	MnDOT Tests	UIUC Tests	Std.Dv.	COV,%
2"	100	100	100	0.00	0.00
1"	100	100	100	0.00	0.00
3/4"	90-100	96	98.2	0.87	0.90
3/8"	70-85	78.25	84.7	2.22	2.84
#4	55-70	66.25	71.1	0.97	1.46
#10	35-55	52.875	54.8	2.71	5.13
#40	15-30	22.125	28.7	3.14	14.19
#200	3-8	6.95	10.8	0.86	12.38

TABLE 3.7
Gradation Test Results for CL-6sp

		Mean		MnDOT Tests	
Sieve Size	Specs.	MnDOT Tests	UIUC Tests	Std.Dv.	COV,%
1"	100	100.00	100.00	0.00	0.00
3/4"	85-100	97.00	96.01	0.71	0.73
3/8"	50-70	66.25	67.20	1.20	1.81
#4	30-50	42.50	40.75	0.87	2.04
#10	15-30	26.88	25.12	0.93	3.45
#40	5-15	12.88	11.88	0.78	6.06
#200	0-5	4.55	4.78	0.80	17.58

TABLE 3.8
Gradation Test Results for R-70 Subgrade Sand (UIUC Tests)

Sieve	% Passing		
	Test #1	Test #2	Mean
3/8"	100.00	100.00	100
#4	99.31	99.44	99.4
#10	88.81	89.74	89.3
#16	76.86	77.94	77.4
#40	33.45	35.04	34.2
#80	3.74	4.00	3.9
#200	0.91	0.94	0.9

AASHTO T-99 compaction tests were performed at MnDOT and University of Illinois to determine the optimum moisture content and maximum dry density of the granular materials and subgrade sand. The results obtained from field measurement are given in Table 3.9.

TABLE 3.9
Moisture Content and Density Results from Field Measurements

Material	Moisture Content, %			Density, pcf		
	Mean	Std. Dev.	COV, %	Mean	Std. Dev.	COV, %
CL-1C sp	7.9	0.27	3.47	134.8	2.11	1.57
CL-1F sp	8.3	0.72	8.68	128.1	1.80	1.41
CL-3 sp	6.8	0.53	7.79	127.8	1.02	0.80
CL-4 sp	7.9	0.4	5.06	129.8	0.89	0.69
CL-5 sp	6.9	0.43	6.26	137.0	1.85	1.35
CL-6 sp	5.3	0.78	14.66	132.1	1.77	1.34

The results obtained from AASHTO T-99 tests are given in Table 3.10. At the University of Illinois, AASHTO T-99 tests were performed only on materials CL-1Fsp, CL-1Csp, CL-4sp, CL-5sp and R70 subgrade sand, because the optimum moisture content and the maximum dry density appeared to be different from the ones obtained by MnDOT.

TABLE 3.10
AASHTO T-99 Test Results

	Optimum Moisture Content, %		Maximum Dry Density, pcf	
Material	MnDOT	UIUC	MnDOT	UIUC
CL-1C sp	9.0	7.0	131.5	140.0
CL-1F sp	10.9	9.5	124.2	131.4
CL-3 sp	8.0	-	125.3	-
CL-4 sp	10.0	9.4	126.0	132.0
CL-5 sp	8.1	7.7	132.7	139.0
CL-6 sp	6.8	-	128.7	-
R-70 Sand	13.5	13.8	117.0	113.0

"-" denotes test not performed

3.10 Summary

The laboratory testing program undertaken to characterize the Mn/ROAD granular materials and subgrade sand has been presented. Target moisture contents and densities were selected based on the field measured values and AASHTO T-99 test results given in Tables 3.9 and 3.10 respectively.

The results obtained from the laboratory tests are presented in Chapter-IV.

CHAPTER - IV

ANALYSES OF RESULTS FROM LABORATORY TESTING ON GRANULAR MATERIALS AND SUBGRADE SAND

4.1 Introduction

Unbound aggregate materials, such as crushed stone, gravel, and sand, are used as surface layers, bases and subbases. The load-deformation response of unbound aggregates is a very important consideration in the pavement design. Both permanent and resilient deformation characteristics are significant. Also of importance is the granular layer shear strength. Since unbound granular materials have little or no tensile strength, shearing resistance of the material is utilized to develop a load-distributing quality which significantly reduces the stresses transmitted to the underlying layers. Some important factors influencing the shear strength of untreated granular materials are gradation, moisture and density, maximum particle size, amount and plasticity of fines, particle geometrical characteristics, and confining pressure. Upon application of vertical load to a granular layer, deformation occurs. The deformation occurring is composed of two components - resilient or recoverable deformation , and permanent or non-recoverable deformation. Permanent deformation is the result of either compaction or lateral shear deformation due to load whereas resilient deformation is the deformation which occurs under transient loading and is recoverable.

The resilient modulus of granular materials is an important input variable for the design of pavement structures. Statistically developed models (from laboratory test results) are used to characterize the resilient behavior of granular materials. The K-θ model has been the most popular model used in granular material characterization.

This chapter summarizes the results obtained from comprehensive laboratory testing of granular materials used as base, subbase, and subgrade (sand) in the Minnesota Road Research Project (Mn/ROAD Project) test sections. The tests were performed at optimum moisture content and maximum dry density as obtained from AASHTO T-99 tests and at moisture and density levels measured in the field. The results from field measurements and AASHTO T-99 tests are given in Table 3.9 and 3.10 respectively. Rapid shear tests and repeated loading tests were conducted to determine the shear strength parameters (friction angle "ϕ", and cohesion "c"), resilient modulus

(E_R), rutting potential, stress history effects on shear strength, and moisture susceptibility. Dynamic cone penetrometer (DCP) tests were conducted to get an indication about the shear strength (CBR) of the granular materials and subgrade sand.

4.2 Rapid Shear Test Results

Axial load-deformation data from rapid shear test performed on a given material at a given confining pressure is reduced to develop a relationship (stress-strain curve) between deviator stress ($\sigma_1 - \sigma_3$) and axial strain. The stress-strain relationship is generally curved. Peak deviator stress at a given confining pressure is referred to as the shear strength of the material at that confining stress. If a clear peak is not observed in the stress-strain curve, the deviator stress corresponding to 5-percent axial strain is defined as the shear strength. Figures 4.1 through 4.11 show the results from rapid shear tests on different materials at different moisture and density levels. An increase in shear strength was observed with increase in confining pressure. Friction angle "ϕ" and cohesion "c" for different materials are summarized in Table 4.1. Materials CL-1C and CL-1F were not tested at higher moisture contents due to the difficulty in preparing specimens.

TABLE 4.1
Results from Rapid Shear Testing on Mn/ROAD Granular Materials

Material	Moisture Content, %	Dry Density pcf	Friction Angle, ϕ degree	Cohesion, c psi
CL-1C sp	9.0	132.0	35	7
CL-1F sp	8.3	131.0	31	14
CL-3 sp	6.8	127.0	44	7
CL-3 sp	8.0	128.0	44	7
CL-4 sp	7.9	130.0	45	7
CL-4 sp	9.4	132.0	31	17
CL-5 sp	7.7	139.0	39	8
CL-5 sp	6.8	137.0	43	11
CL-6 sp	6.3	134.0	47	18
CL-6 sp	5.3	133.0	51	14
R70 Sand	10.5	117.0	41	5

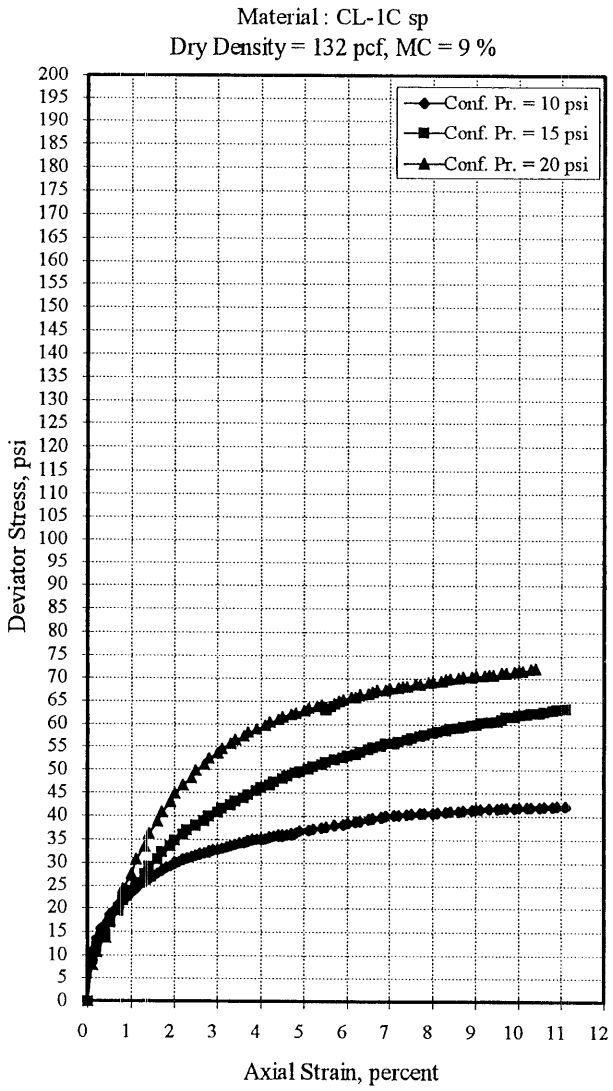

Figure 4.1. Rapid Shear Test Results for CL-1Csp

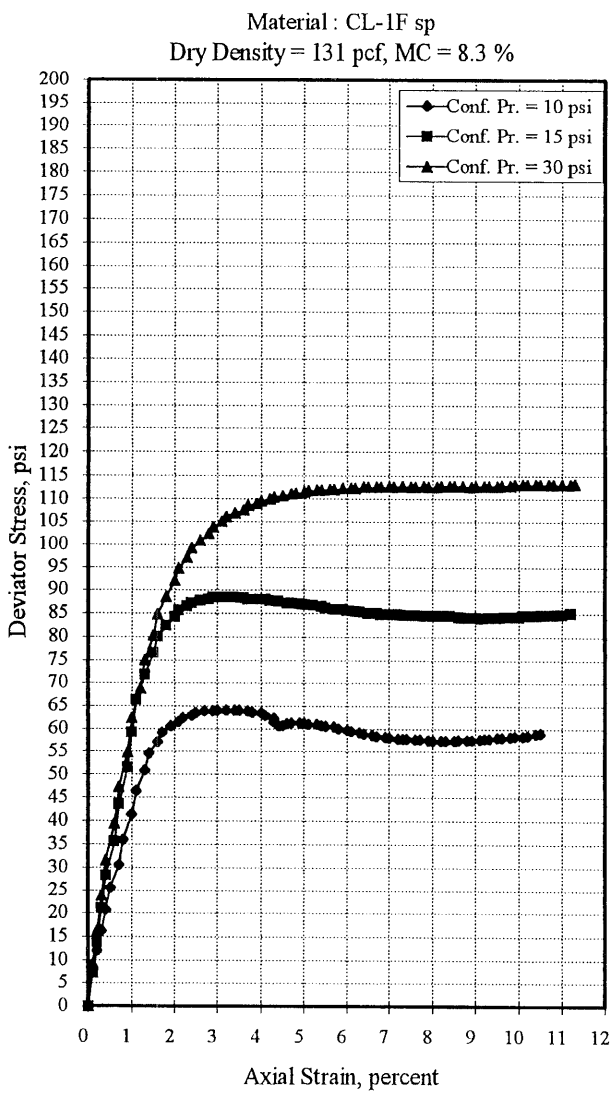

Figure 4.2. Rapid Shear Test Results for CL-1Fsp

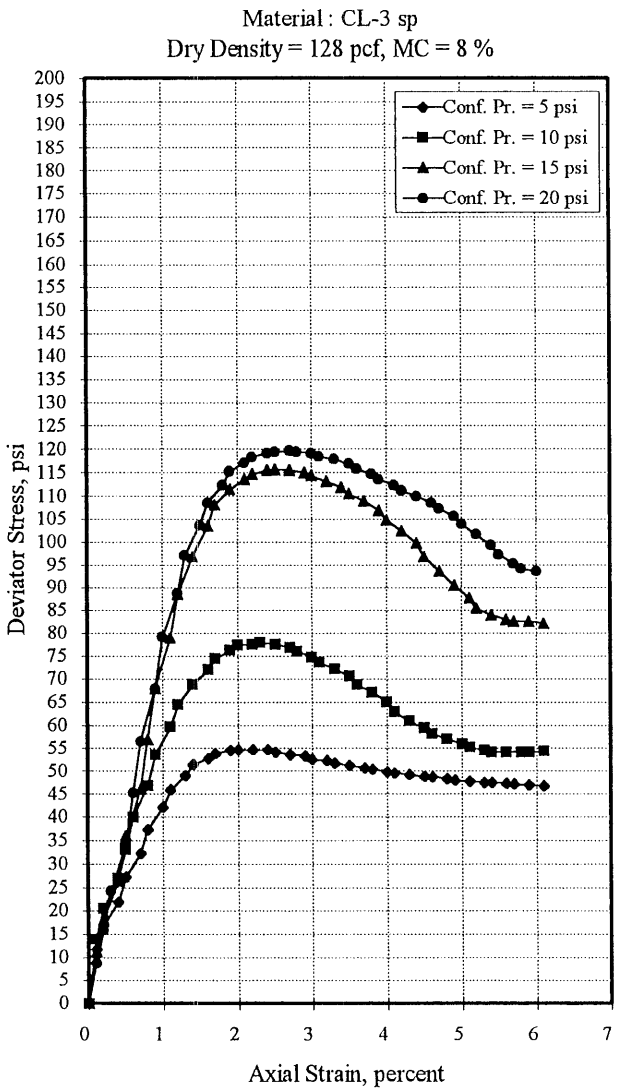

Figure 4.3. Rapid Shear Test Results for CL-3sp

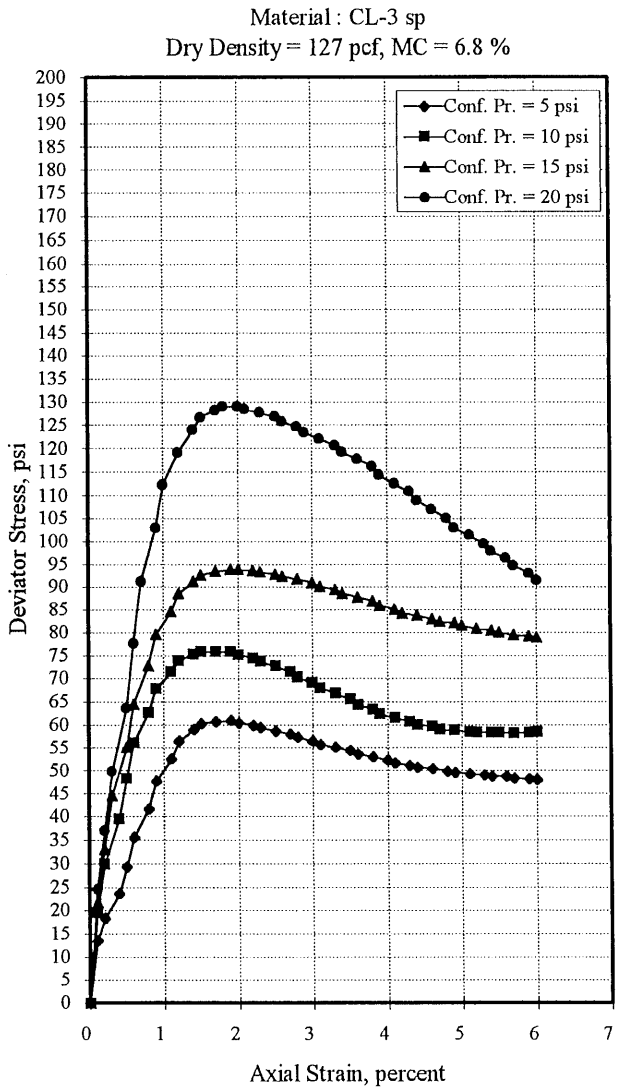

Figure 4.4. Rapid Shear Test Results for CL-3sp

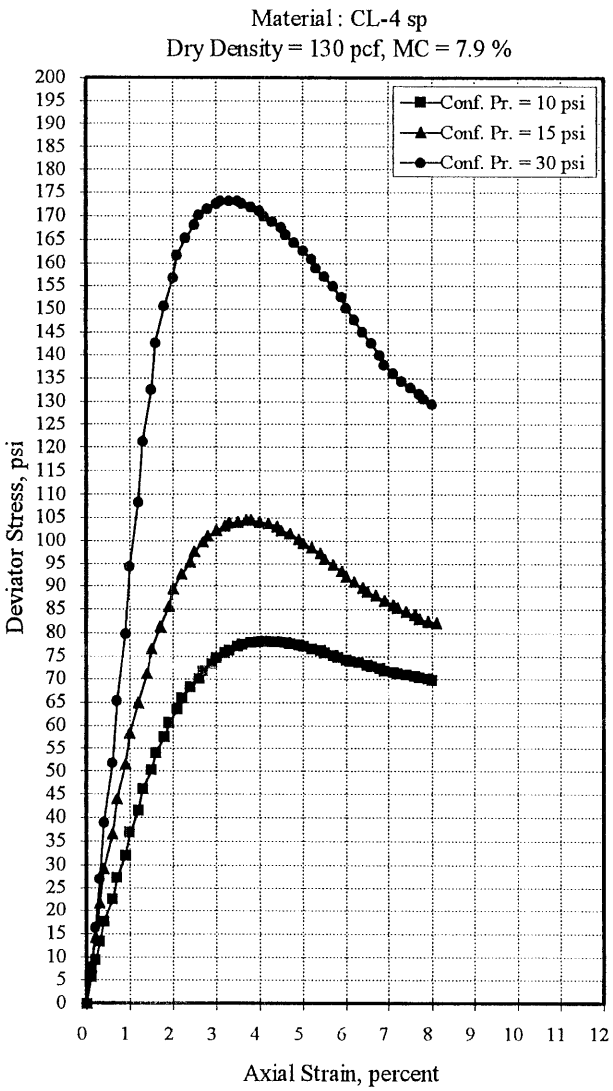

Figure 4.5. Rapid Shear Test Results for CL-4sp

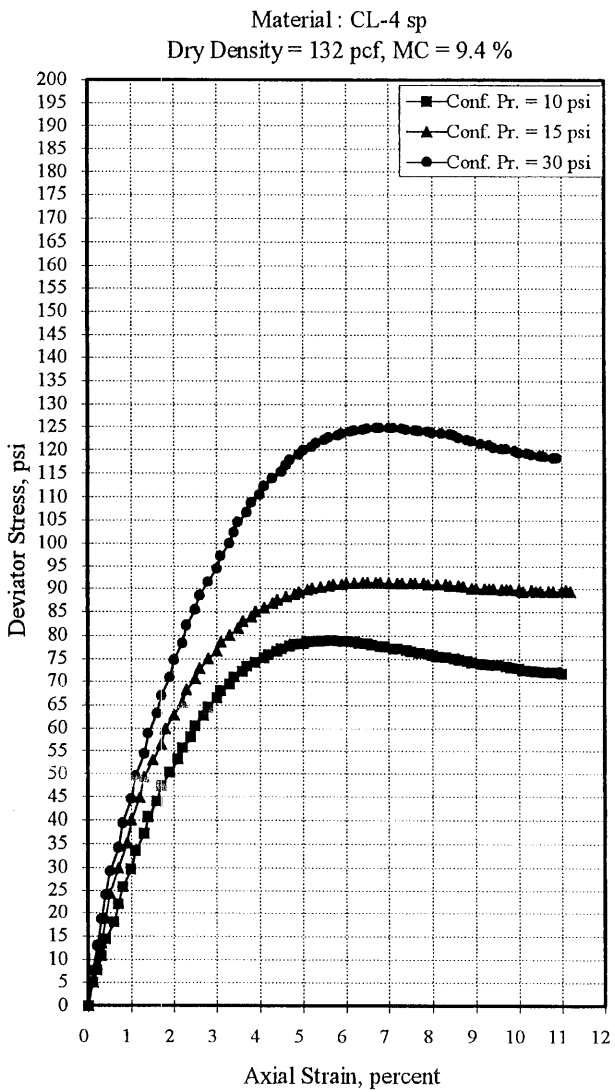

Figure 4.6. Rapid Shear Test Results for CL-4sp

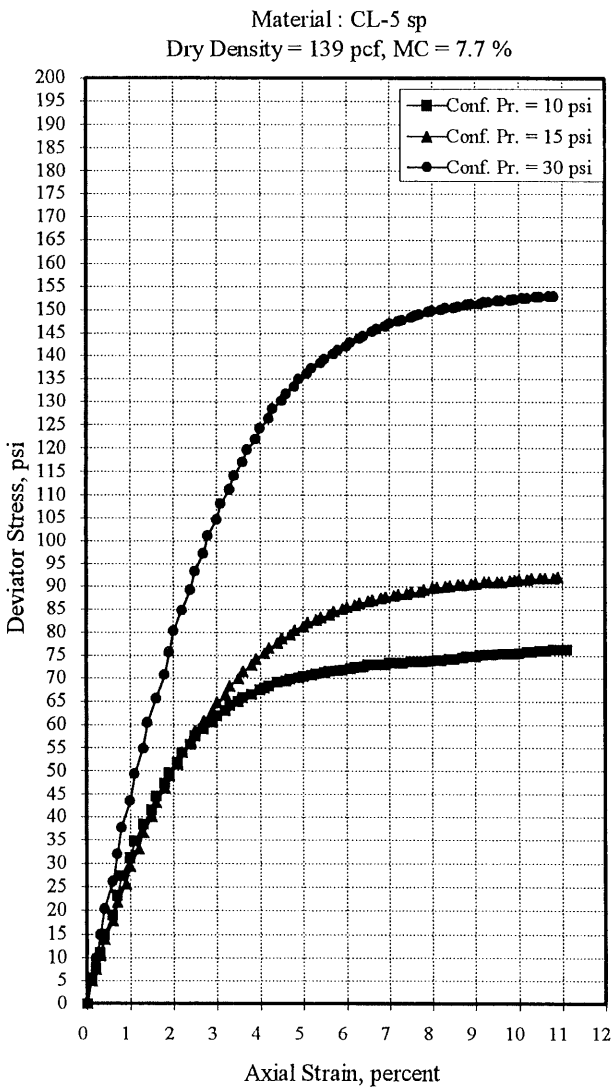

Figure 4.7. Rapid Shear Test Results for CL-5sp

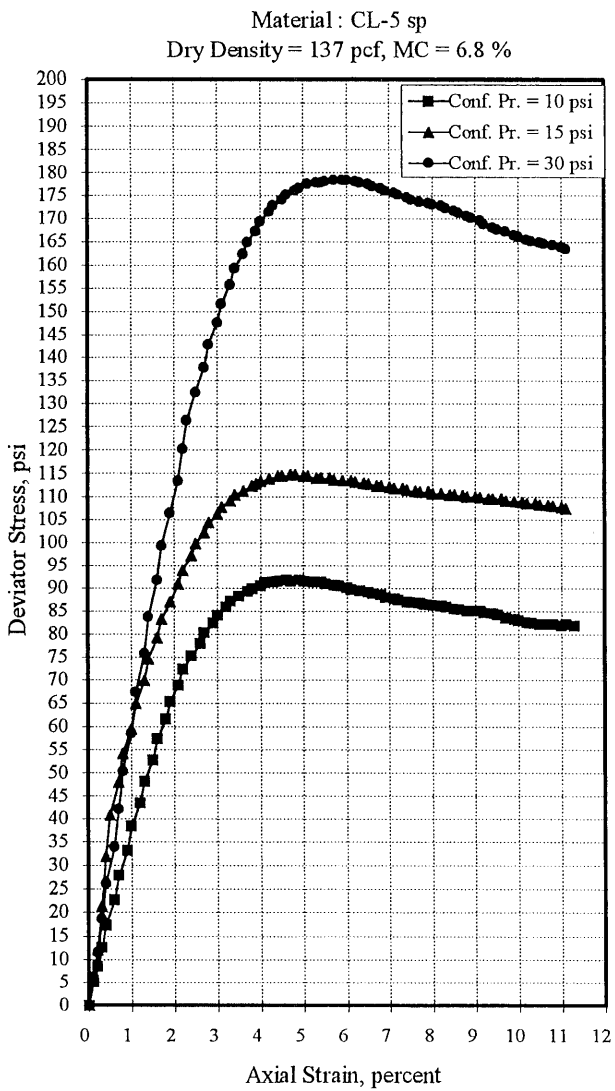

Figure 4.8. Rapid Shear Test Results for CL-5sp

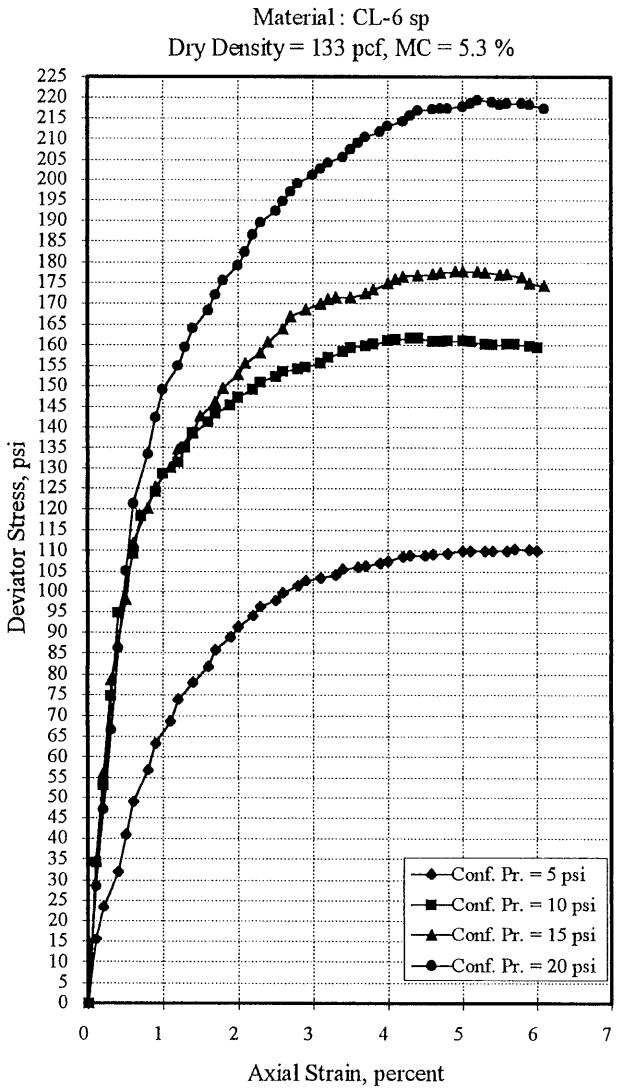

Figure 4.9. Rapid Shear Test Results for CL-6sp

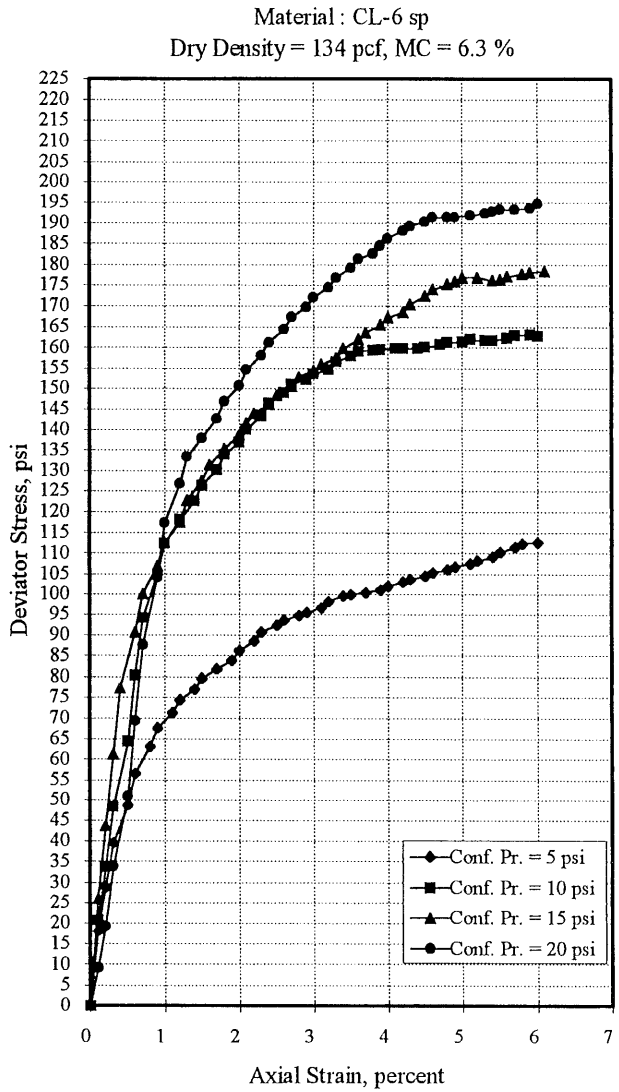

Figure 4.10. Rapid Shear Test Results for CL-6sp

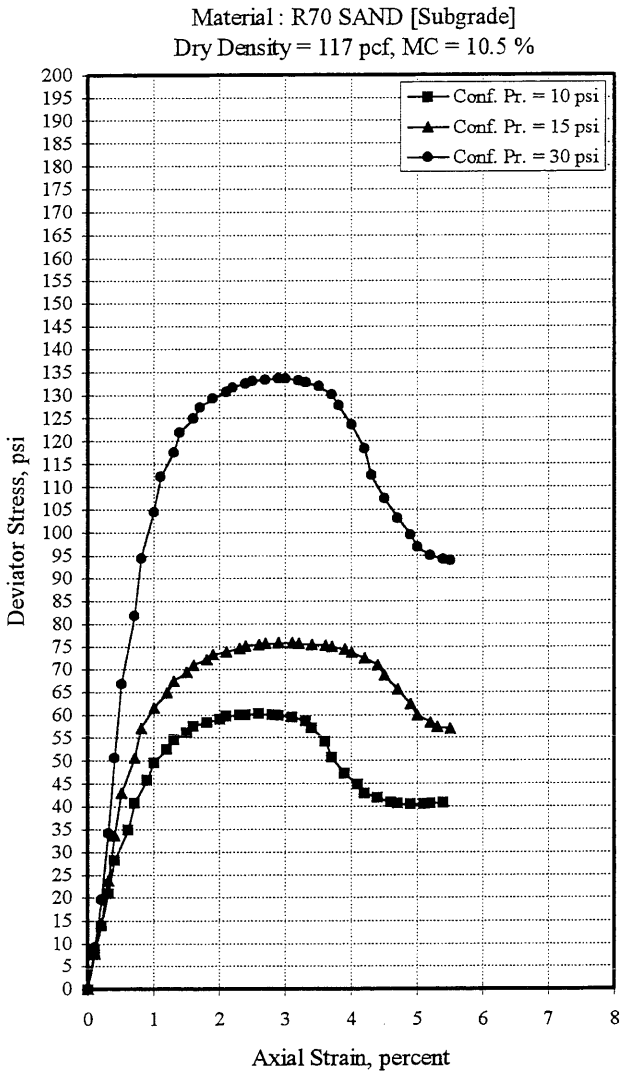

Figure 4.11. Rapid Shear Test Results for Subgrade Sand

Considering the results from rapid shear tests at confining pressure of 15-psi, the materials can be placed into three groups:

Group 3 : Peak σ_d less than 60-psi - CL-1Csp

Group 2 : Peak σ_d between 60-psi and 120-psi - CL-1Fsp, CL-3sp, CL-4sp, CL-5sp

Group 1 : Peak σ_d higher than 120-psi - CL-6sp

where σ_d is deviator stress (σ_1 - σ_3).

Variable moisture sensitivity was observed in the materials tested. Peak deviator stress obtained at

15-psi confining pressure was used to study moisture sensitivity. Materials CL-1Csp and CL-1Fsp were most sensitive. CL-1Csp and CL-1Fsp could not be tested at higher moisture contents because of difficulties encountered during specimen preparation. For material CL-3sp, a change in moisture content from 8-percent to 6.8-percent resulted in no change in the friction angle. However, a reduction in peak deviator stress from 115-psi to 94-psi was observed. For CL-4sp, a reduction in moisture content from 9.4-percent to 7.9-percent resulted in 45-percent increase in the friction angle. The increase in peak deviator stress at 15-psi confining pressure was 17-percent. For CL-5sp, when the moisture content was reduced from 7.7-percent to 6.8-percent, friction angle increased from 39° to 43° (10-percent increase) and peak deviator stress increased by 42-percent. For CL-6sp, an increase in moisture content from 5.3-percent to 6.3-percent resulted in a decrease in friction angle from 51° to 47°. No change was observed in the peak deviator stress at 15-psi confining pressure.

It was observed that in the case of R-70 subgrade sand the specimens attained a moisture content of 10.5 percent after compaction. Water drained off the specimen during the compaction process.

4.3 Permanent Deformation Test Results

Permanent deformation testing was performed by subjecting the specimens to a repeated load deviator stress of 45-psi and a confining pressure of 15-psi (referred to as 45/15), for 1000 load repetitions. This phase of testing was termed as "conditioning cycle". Some specimens did not survive conditioning at 45/15 and had to be conditioned at lower stress state. Material CL-1C showed the highest rutting potential and was conditioned at 15/10. Material CL-1F was conditioned at 30/15. Table 4.2 gives the 'A' and 'b' values (in the model ε_p % = A N^b) for different materials at different moisture and density levels. Higher 'A' and 'b' values represent higher rutting potential.

Materials that developed at least 90-psi deviator stress at 2-percent axial strain, survived the conditioning at 45-psi deviator stress and 15-psi confining pressure. The rutting parameter 'A' is function of deviator stress at 1-percent axial strain obtained from the rapid shear tests conducted at 15-psi confining pressure. The following correlation was established (Figure 4.12):

$$A = 1.10386 - 0.007911 * \sigma_{d1\%} \quad \text{.....[4.1]}$$

R^2 = 0.97

TABLE 4.2
Results from Permanent Deformation Testing on Mn/ROAD Granular Materials

Material	Moisture Content, %	Dry Density pcf	Parameter "A" %	Parameter "b"	Conditioning Stress State, psi/psi	R^2 Value
CL-1C sp	7.0	140.0	0.3526	0.450	15/10	0.99
CL-1F sp	8.3	127.0	0.8164	0.310	30/15	0.99
CL-3 sp	8.0	127.8	0.5163	0.110	45/15	0.99
CL-3 sp	6.8	127.3	0.4429	0.080	45/15	0.98
CL-4 sp	7.9	130.0	0.6257	0.240	45/15	0.99
CL-4 sp	9.4	132.0	1.0010	0.430	30/15	0.99
CL-5 sp	7.7	139.0	0.3341	0.440	30/15	0.99
CL-5 sp	6.8	137.0	0.2918	0.350	30/15	0.99
CL-6 sp	6.3	134.0	0.1511	0.134	45/15	0.98
CL-6 sp	6.3	139.0	0.1720	0.140	45/15	0.96
CL-6 sp	5.4	133.0	0.1070	0.155	45/15	0.99
CL-6 sp	7.3	131.0	0.2760	0.135	45/15	0.99
R70 Sand	10.5	117.0	0.3327	0.120	45/15	0.99

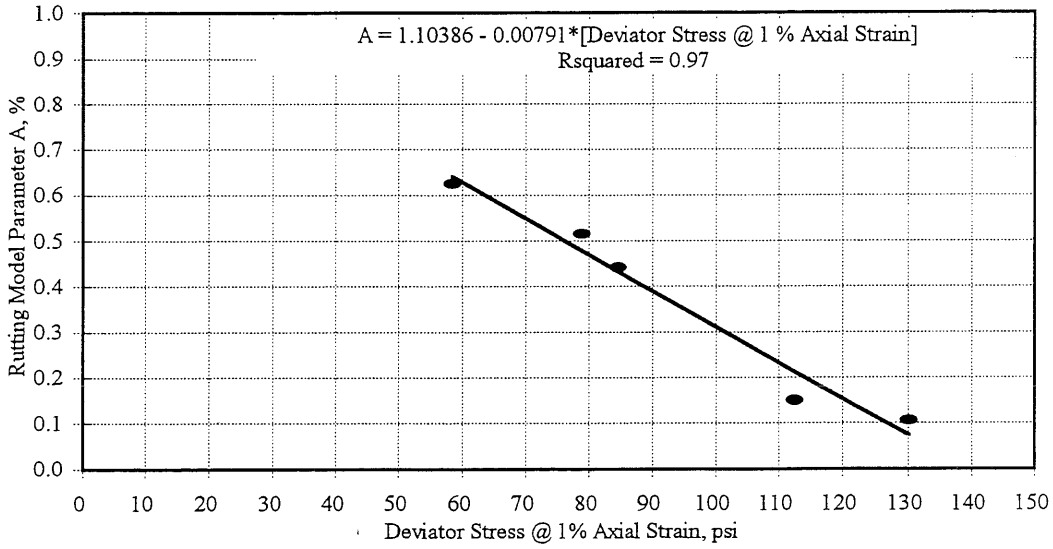

Figure 4.12. Rutting Model Parameter 'A' as a Function of Deviator Stress

where $\sigma_{d1\%}$ is the deviator stress at 1 percent axial strain. Parameter 'b' varied between 0.08 and 0.45 range. For specimens conditioned at 45/15, the 'b' values ranged from 0.08 to 0.24 (Table 4.2). For low shear strength materials (conditioned at 30/15 and 15/10), the 'b' values were in 0.35-0.45 range.

An attempt was made to develop a correlation between 'b' and the shear strength of material. The correlation is :

$$b = 0.6205 - 2.6916 * \text{Log}(\sigma_{d2\%}) + 3.0172 * \text{Log}(\sigma_{d3\%}) - 0.5905 * \text{Log}(\sigma_{d4\%}) \quad \text{.....[4.2]}$$

$$R^2 = 0.996$$

where $\sigma_{d2\%}$, $\sigma_{d3\%}$, $\sigma_{d4\%}$ are deviator stresses in psi at 2-percent, 3-percent, and 4-percent axial strains. Even though the R^2 value for the correlation is very high, the '$3.0172 * \text{Log}(\sigma_{d3\%})$' term defies the engineering logic that rutting potential decreases with increase in shear strength. Several other combinations were tried. There was always some "term" in the regression equation that indicate "increased rutting" with an increase in shear strength.

If only materials CL-3sp and CL-4sp (no crushed/fractured particles) are considered, the following regression equation is obtained:

$$b = 0.5987 - 0.00616 * \sigma_{d1\%} \quad \text{.....[4.3]}$$

$$R^2 = 0.99$$

where $\sigma_{d1\%}$ is the deviator stress in psi at 1-percent axial strain.

A similar relationship could not be developed for materials with crushed/fractured particles (CL-5sp, CL-6sp) as only CL-6sp (100-percent crushed/fractured particles) survived conditioning at 45/15. Material CL-5sp (15-percent crushed/fractured particles) specimens failed during conditioning at 45/15.

It is apparent that there are no clear, overall, and comprehensive relations for estimating the 'b' term. 'A' is the dominant term in the relationship '$\varepsilon_p\ \% = AN^b$' and can be estimated accurately from the rapid shear test results performed at 15-psi confining pressure.

4.4 Resilient Modulus Test Results

The resilient modulus test data were used to develop parameters for three (K-θ [36], UT-Austin [56], and Uzan [50]) resilient modulus models of granular materials. These models are used to estimate the resilient modulus of granular materials as a function of stress state.

K-θ Model [36]

Linear regression was performed to obtain a best fit equation of the form :

$$E_R = a + n \, Log(\theta) \quad \text{.....[4.4]}$$

where θ is the bulk stress ($\sigma_1 + 2*\sigma_3$), σ_1 is major principal stress, and σ_3 is minor principal stress. The response was transformed into the following model :

$$E_R = K*\theta^n \quad \text{.....[4.5]}$$

where K is antilog of 'a'. The stress sensitivity is depicted by 'n'. The K and n parameters for different materials tested are given in Table 4.3.

UT-Austin Model [56]

Linear regression was performed to obtain a best fit equation of the form :

$$Log\,\varepsilon_a = a + K7 * Log(\sigma_d) + K8 * Log(\sigma_3) \quad \text{.....[4.6]}$$

where ε_a is the measured resilient axial strain, σ_d is the deviator stress, and σ_3 is the minor principal stress. The response was transformed into the following model :

$$E_R = N6[\sigma_d^{N7}][\sigma_3^{N8}] \quad \text{.....[4.7]}$$

where $N6 = 10^{-a}$, $N7 = 1 - K7$, and $N8 = -K8$. The values of N6, N7, and N8 for different materials are given in Table 4.3.

TABLE 4.3
Resilient Modulus Testing Results

	Moisture	Dry Density	THETA Model			UZAN's Model				UT-AUSTIN Model			
Material	Content, %	pcf	K	n	R^2	K3	K4	K5	R^2	N6	N7	N8	R^2
CL-1C sp	7.0	140	5719	0.24	0.700	6252	0.14	0.09	0.706	7516	0.1537	0.0781	0.968
CL-1F sp	8.3	127	3917	0.44	0.982	3543	0.62	-0.20	0.991	7942	0.0698	0.3519	0.994
CL-3 sp	8.0	128	2012	0.65	0.989	1774	0.88	-0.25	0.996	5574	0.1322	0.4988	0.984
CL-3 sp	6.8	127	2707	0.60	0.987	2420	0.81	-0.22	0.993	6922	0.1271	0.4586	0.984
CL-4 sp	9.4	132	6490	0.20	0.889	5764	0.42	-0.24	0.943	9925	-0.0534	0.2365	0.995
CL-4 sp	7.9	130	2410	0.60	0.939	2033	0.91	-0.34	0.952	6632	0.0610	0.5137	0.903
CL-5 sp	6.8	137	3827	0.45	0.883	3181	0.79	-0.37	0.909	8842	-0.0232	0.4445	0.934
CL-5 sp	7.7	139	5358	0.32	0.933	4980	0.45	-0.15	0.942	8983	0.0530	0.2565	0.984
CL-6 sp	6.3	134	2583	0.64	0.997	2647	0.59	0.05	0.998	5736	0.3047	0.3380	0.993
CL-6 sp	5.4	133	2807	0.64	0.997	2737	0.68	-0.05	0.997	6707	0.2442	0.3925	0.992
CL-6 sp	7.3	131	3206	0.62	0.996	3225	0.61	0.01	0.996	7121	0.2740	0.3461	0.989
CL-6 sp	6.3	139	4597	0.57	0.998	4478	0.62	-0.05	0.999	10049	0.2168	0.3527	0.997
R70 Sand	10.5	117	2868	0.63	0.985	2428	0.93	-0.33	0.997	8188	0.0723	0.5310	0.993

Uzan's Model [50]

Linear regression was performed to obtain a best fit equation of the form :

$$E_R = a + K4 * Log(\theta) + K5 * Log(\sigma_d) \quad \text{.....[4.8]}$$

where θ is the bulk stress, and σ_d is the deviator stress. The response was transformed into the following model :

$$E_R = K3 * \theta^{K4} * \sigma_d^{K5} \quad \text{.....[4.9]}$$

where K3 is the antilog of 'a'. The values of K3, K4, and K5 for different materials tested are given in Table 4.3.

The R^2 values for UT-Austin model were comparatively higher than the K-θ model and Uzan model. The axial strains were calculated from the estimated modulus values from the three models and were compared to the measured axial strains and resilient modulus values. The objective was to compare the predicted resilient behavior of granular materials by the three models. Figures 4.13 through 4.25 show the comparison between the modulus and axial strain values obtained from different models and the measured values. The axial strain values calculated from the resilient modulus models seem to be in good agreement with the measured axial strain values, except in the case of very low shear strength material CL-1Csp.

4.5 Comparison of MnDOT Results and University of Illinois Results for Resilient Modulus Tests

Resilient modulus tests were performed on Mn/ROAD granular materials by MnDOT and University of Illinois. Similar testing procedures were used except for the conditioning phase. At University of Illinois, sample conditioning was performed at a deviator stress of 45-psi and confining pressure of 15-psi for 1000 load repetitions. At MnDOT, the conditioning was performed at a deviator stress of 15-psi and confining pressure of 15-psi as stated in SHRP Protocol P46 (June 1993).

Figure 4.26 shows the relationship between resilient modulus parameters 'K' and 'n' for the K-θ Model, obtained from the tests conducted at University of Illinois. Following relationship (per Rada & Witczak)

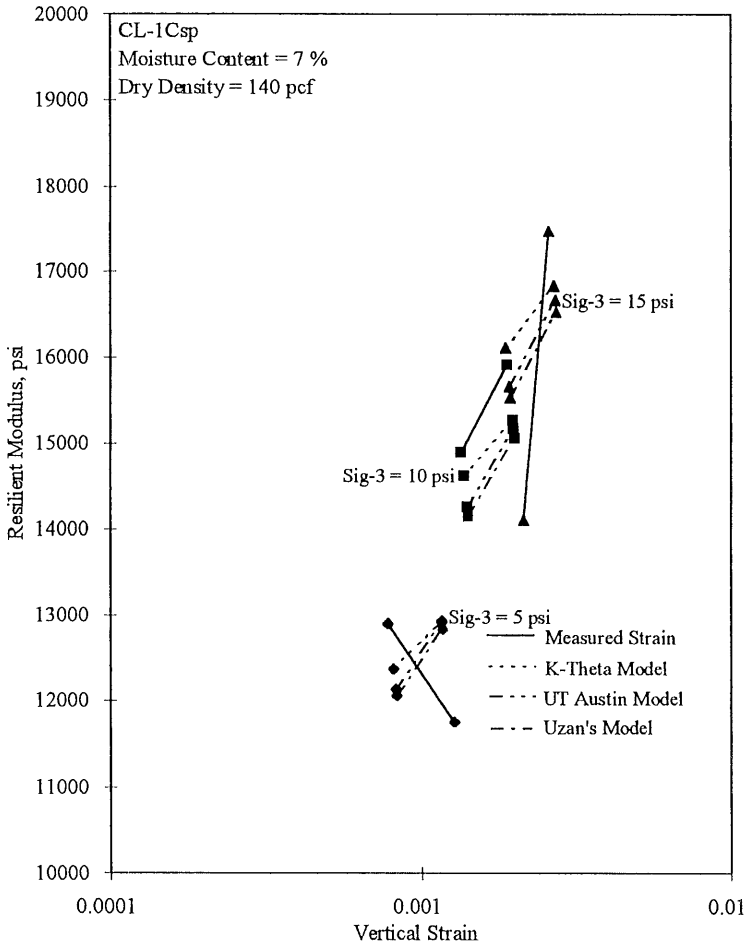

Figure 4.13. Axial Strain - Resilient Modulus Relationship for CL-1Csp

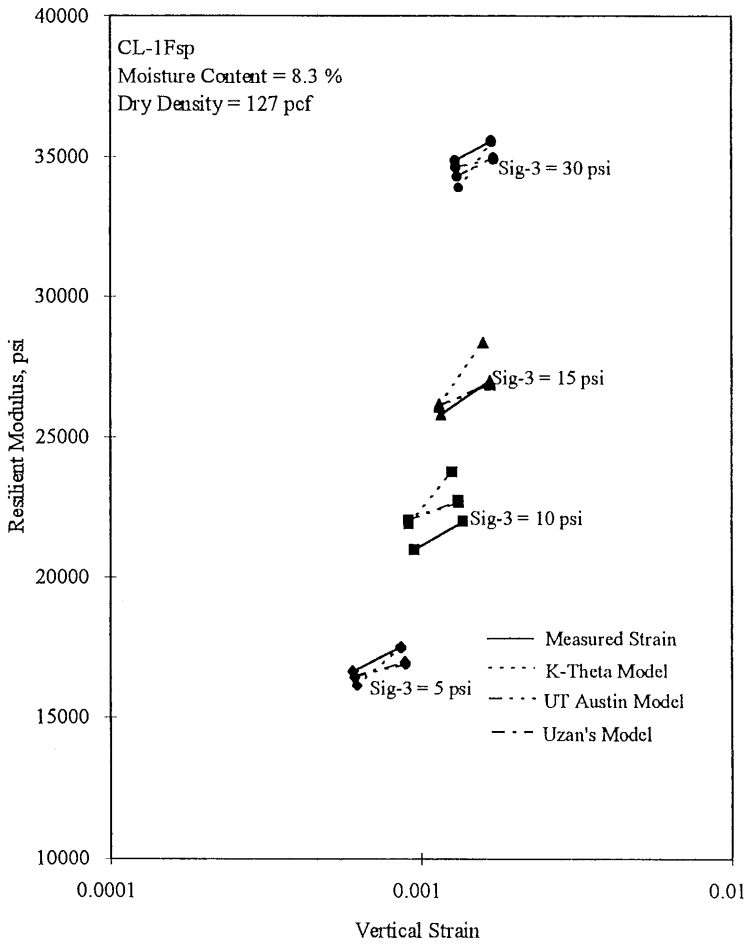

Figure 4.14. Axial Strain - Resilient Modulus Relationship for CL-1Fsp

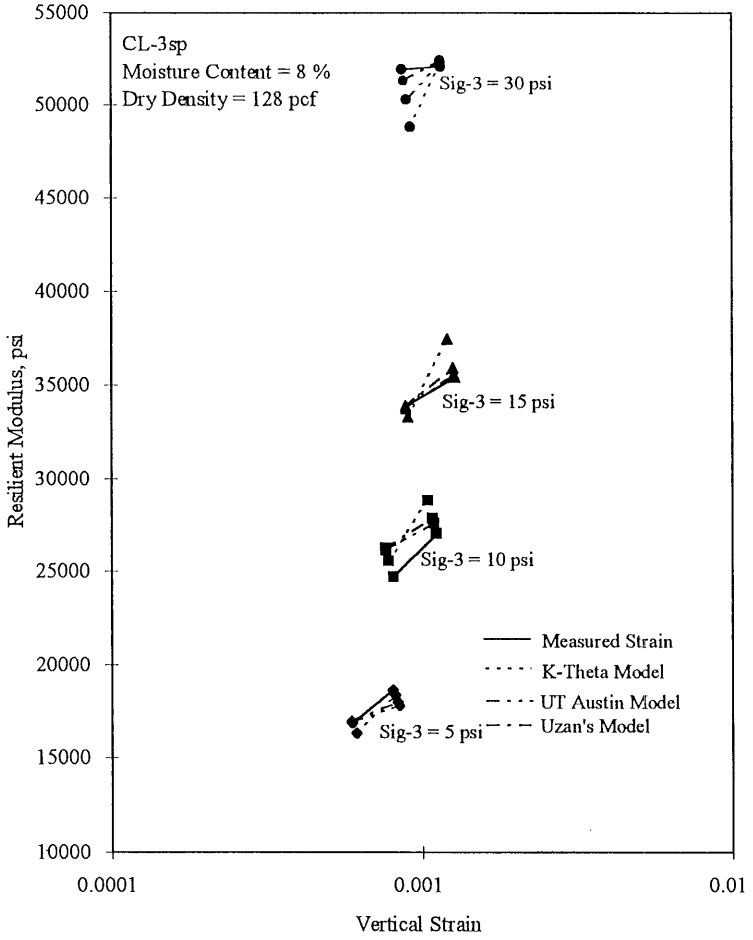

Figure 4.15. Axial Strain - Resilient Modulus Relationship for CL-3sp

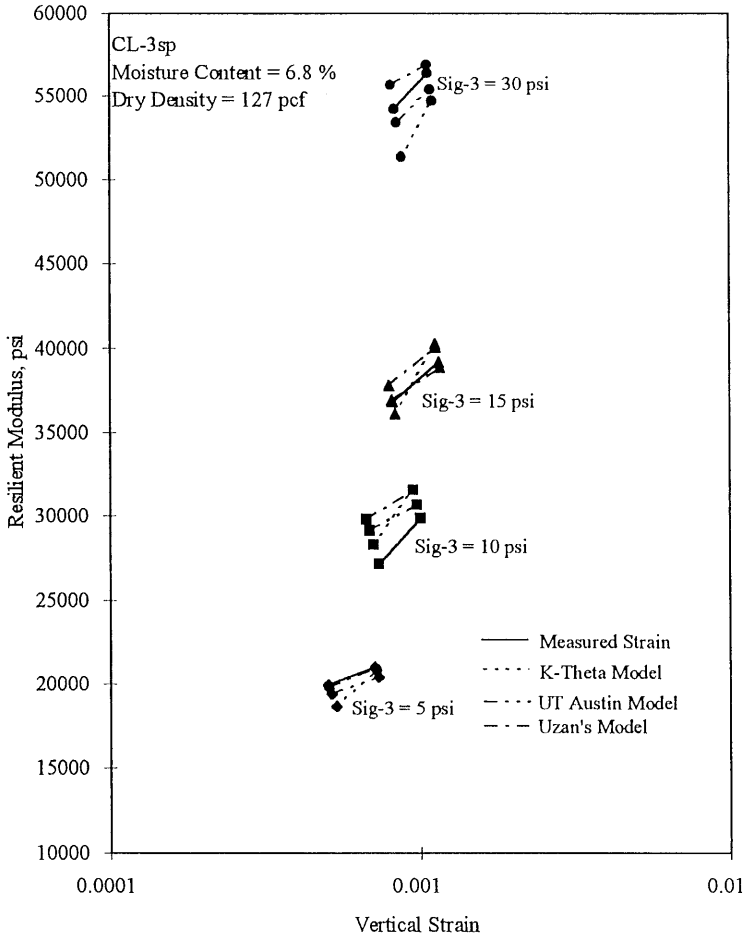

Figure 4.16. Axial Strain - Resilient Modulus Relationship for CL-3sp

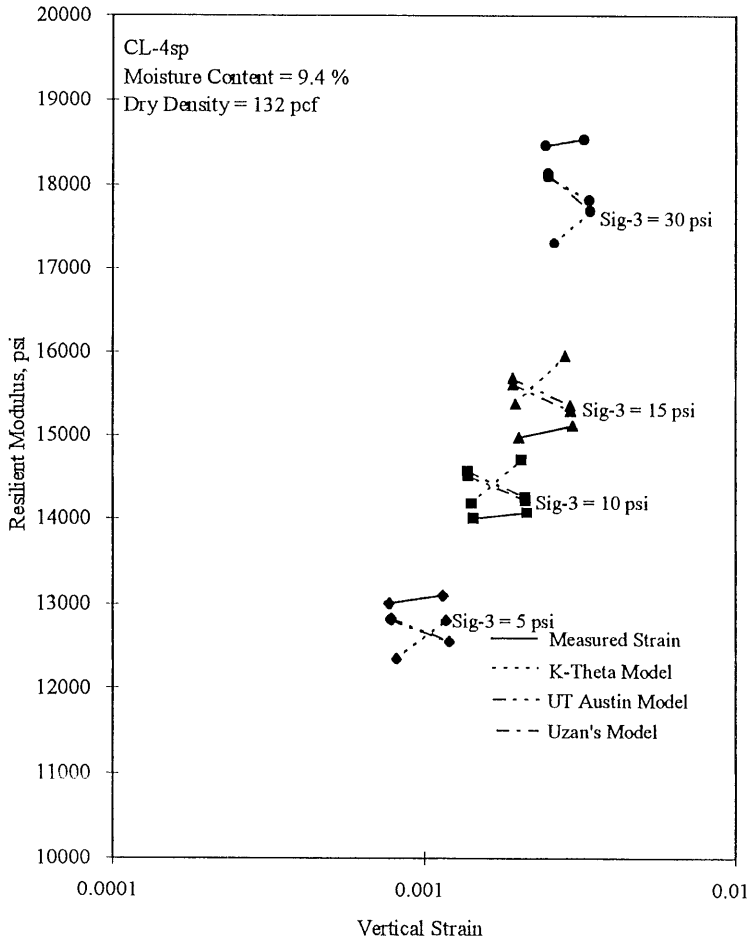

Figure 4.17. Axial Strain - Resilient Modulus Relationship for CL-4sp

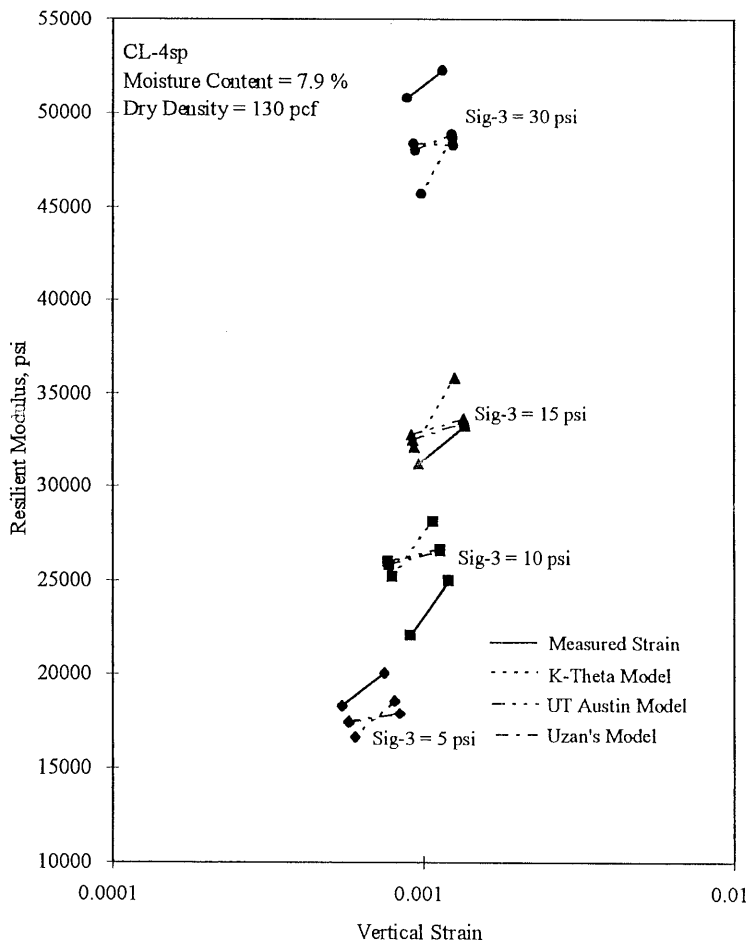

Figure 4.18. Axial Strain - Resilient Modulus Relationship for CL-4sp

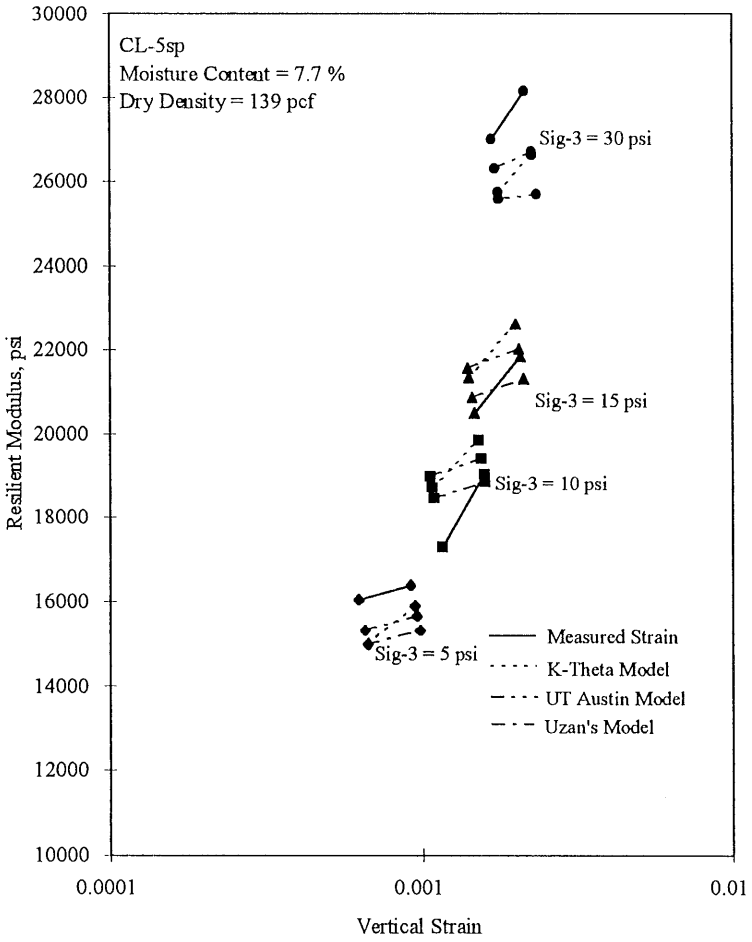

Figure 4.19. Axial Strain - Resilient Modulus Relationship for CL-5sp

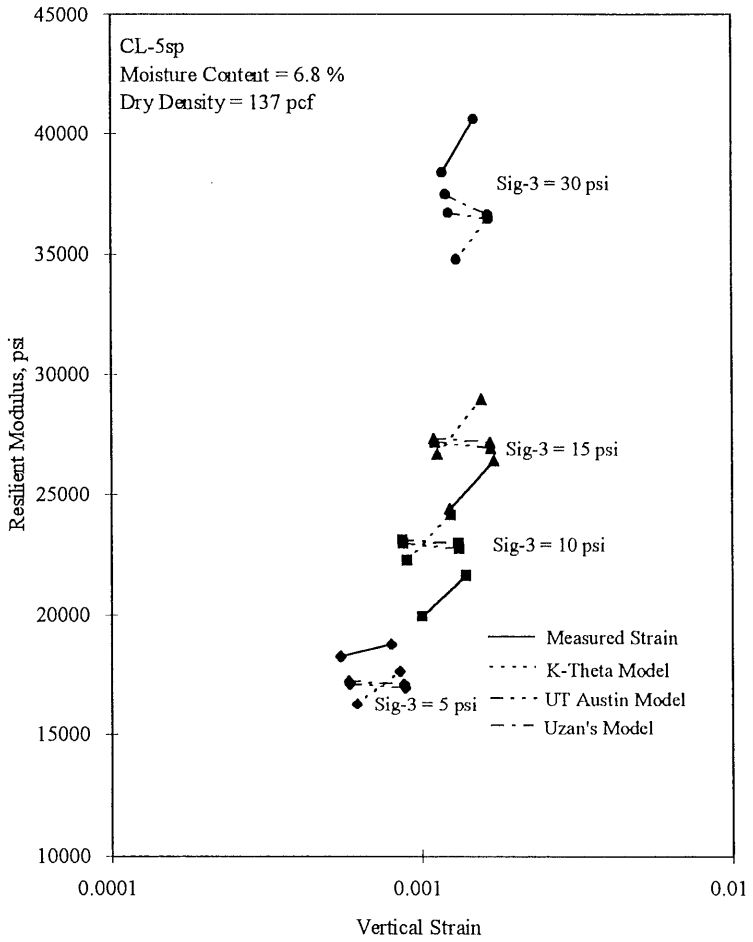

Figure 4.20. Axial Strain - Resilient Modulus Relationship for CL-5sp

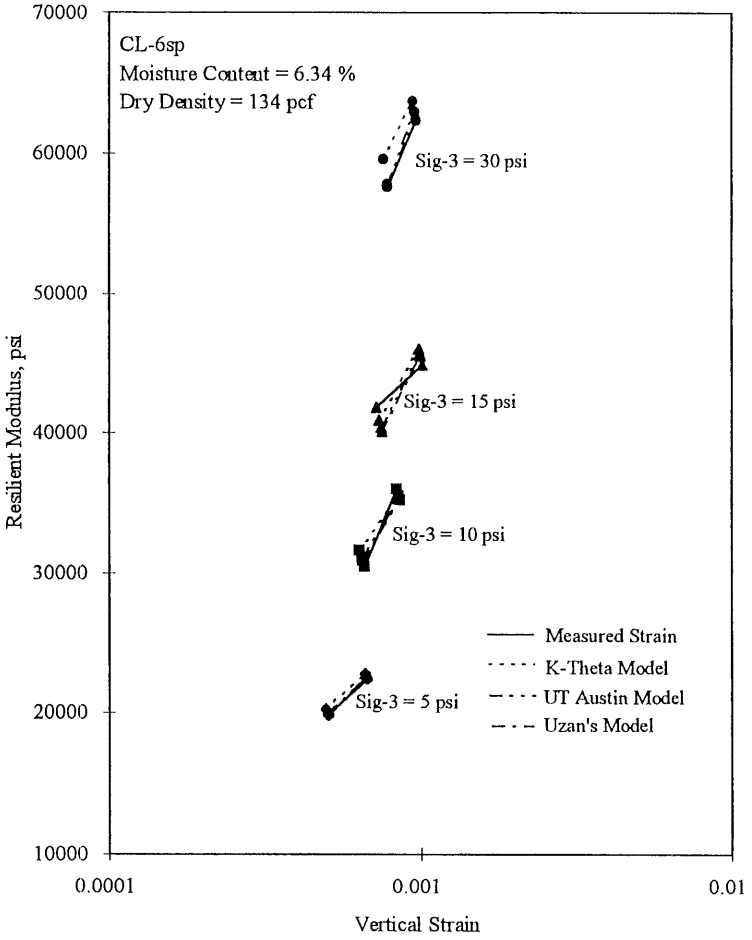

Figure 4.21. Axial Strain - Resilient Modulus Relationship for CL-6sp

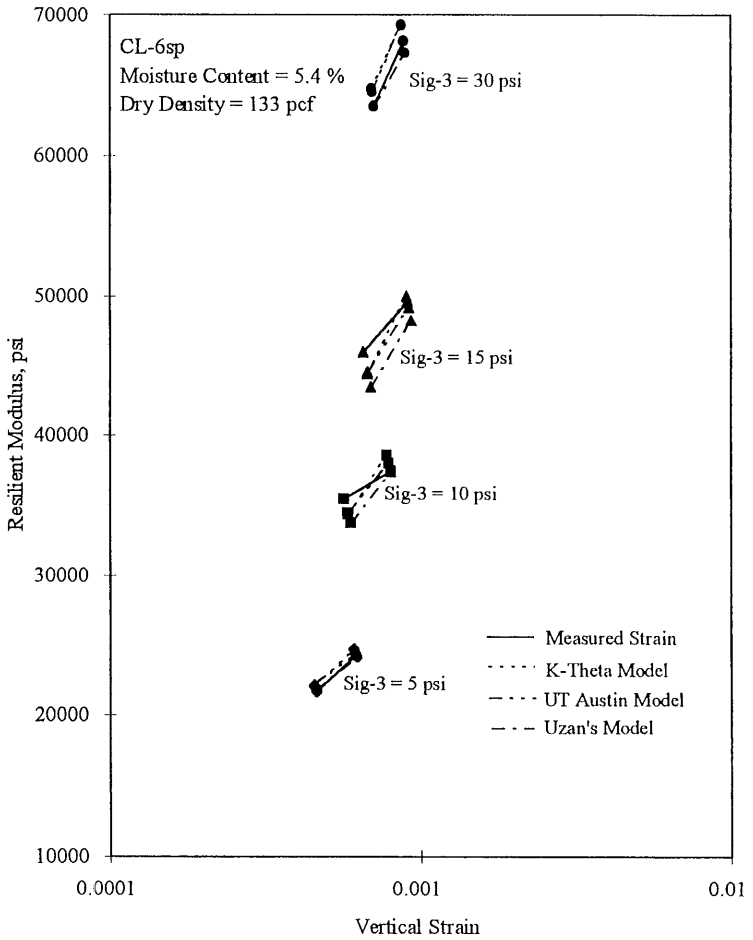

Figure 4.22. Axial Strain - Resilient Modulus Relationship for CL-6sp

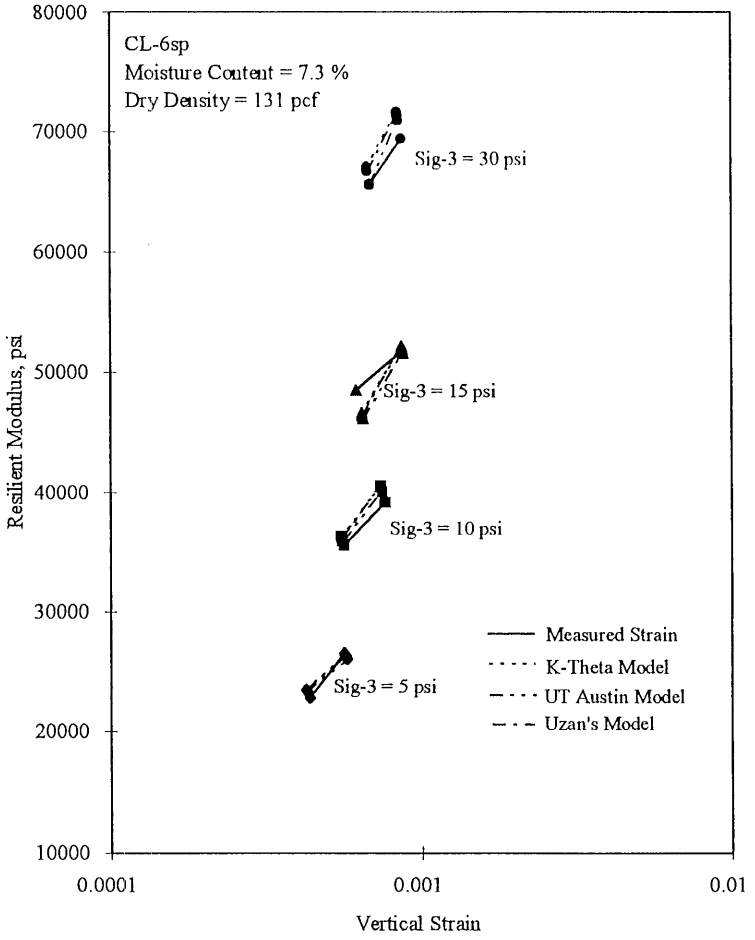

Figure 4.23. Axial Strain - Resilient Modulus Relationship for CL-6sp

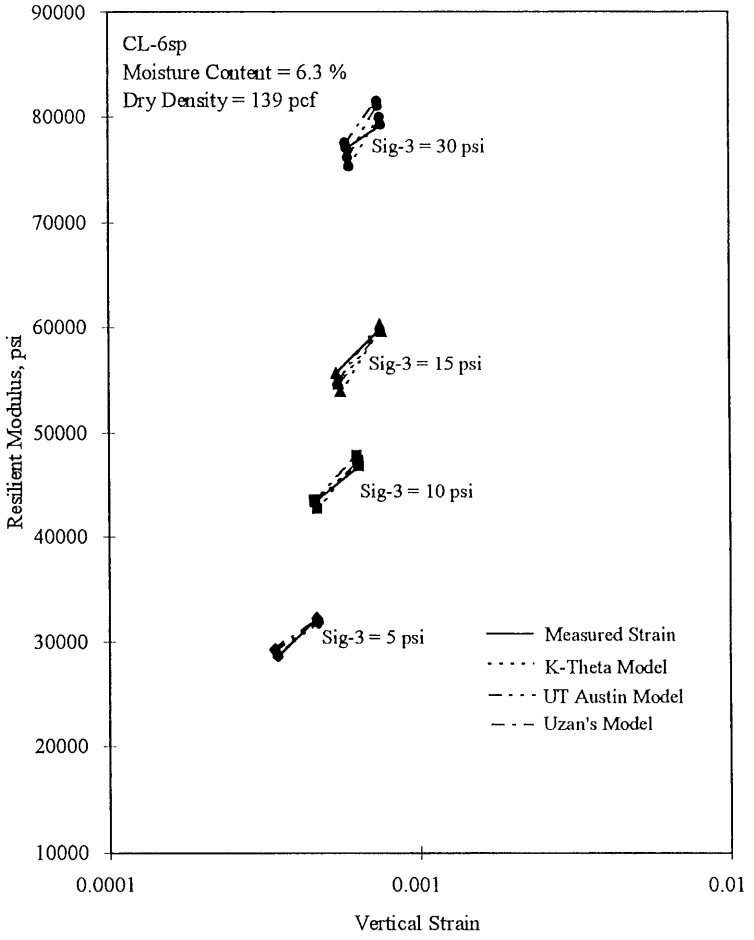

Figure 4.24. Axial Strain - Resilient Modulus Relationship for CL-6sp

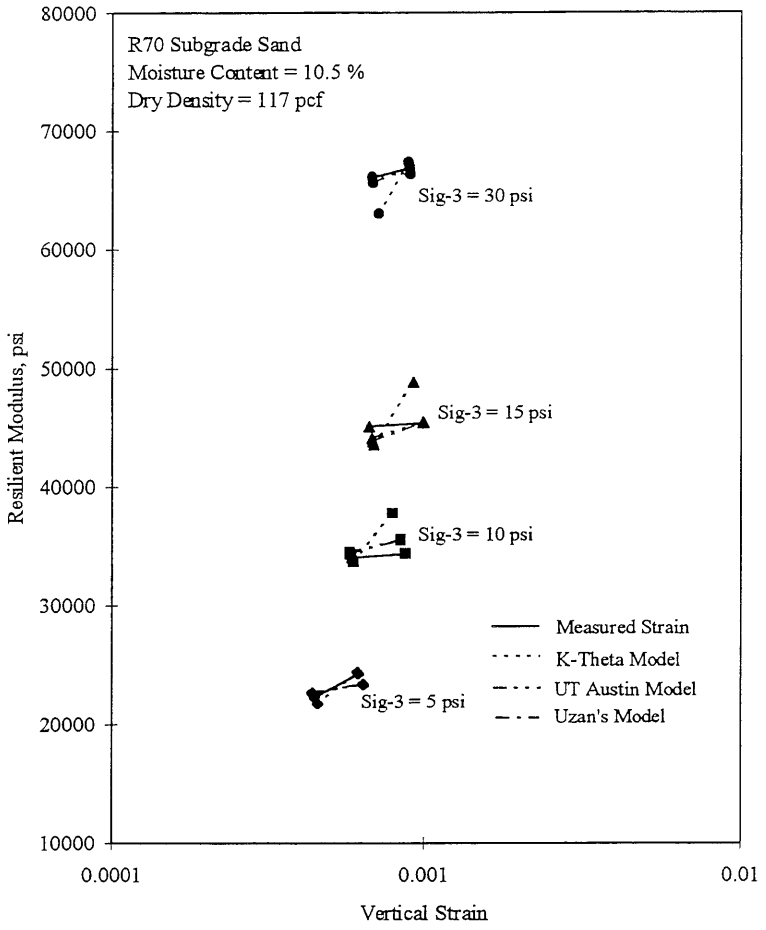

Figure 4.25. Axial Strain - Resilient Modulus Relationship for R70 Subgrade Sand

was established between 'K' and 'n' :

$$\text{Log } K = 3.996 - 0.893*n \quad \text{.....[4.10]}$$

$$R^2 = 0.81$$

Figure 4.27 shows the relationship between resilient modulus parameters 'K' and 'n' for the K-θ Model, obtained from the tests conducted at MnDOT. The relationship established between 'K' and 'n' is:

$$\text{Log } K = 3.939 - 0.94*n \quad \text{.....[4.11]}$$

$$R^2 = 0.36$$

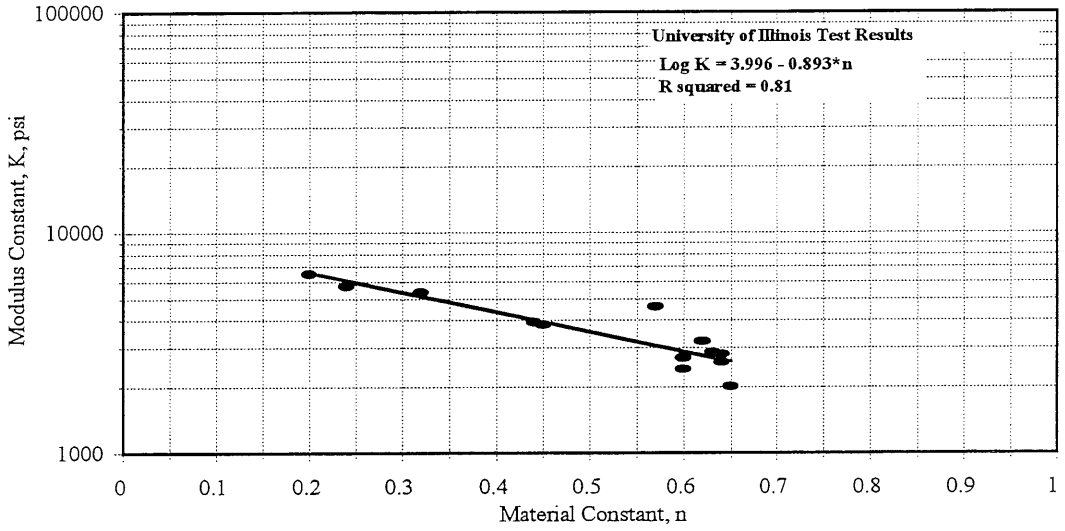

Figure 4.26. Relationship Between Resilient Modulus Parameters K and n

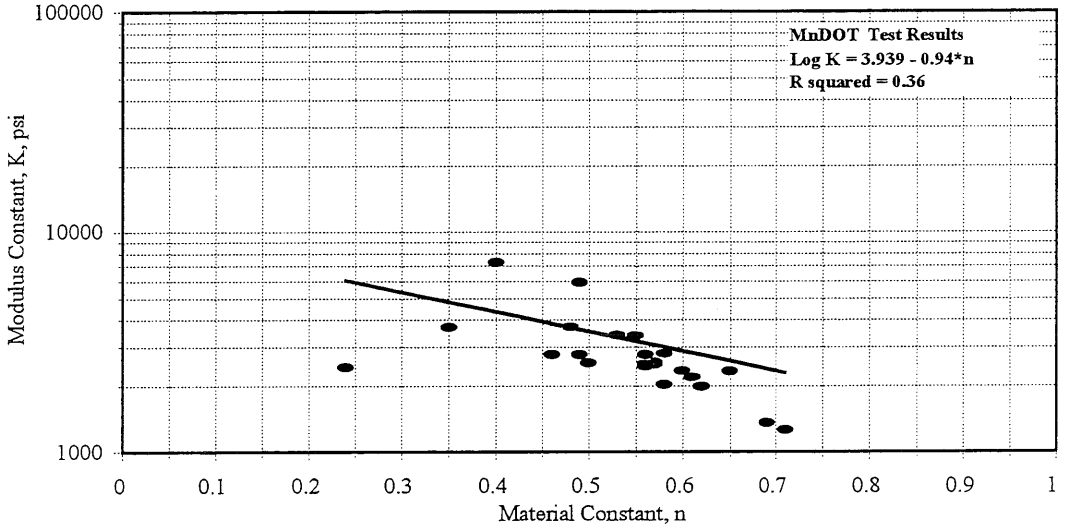

Figure 4.27. Relationship Between Resilient Modulus Parameters K and n

Figure 4.28 shows the comparison between the 'K-n' relationships obtained by Rada & Witczak, University of Illinois, and MnDOT. University of Illinois test results are approximately 17-percent higher than the MnDOT test results.

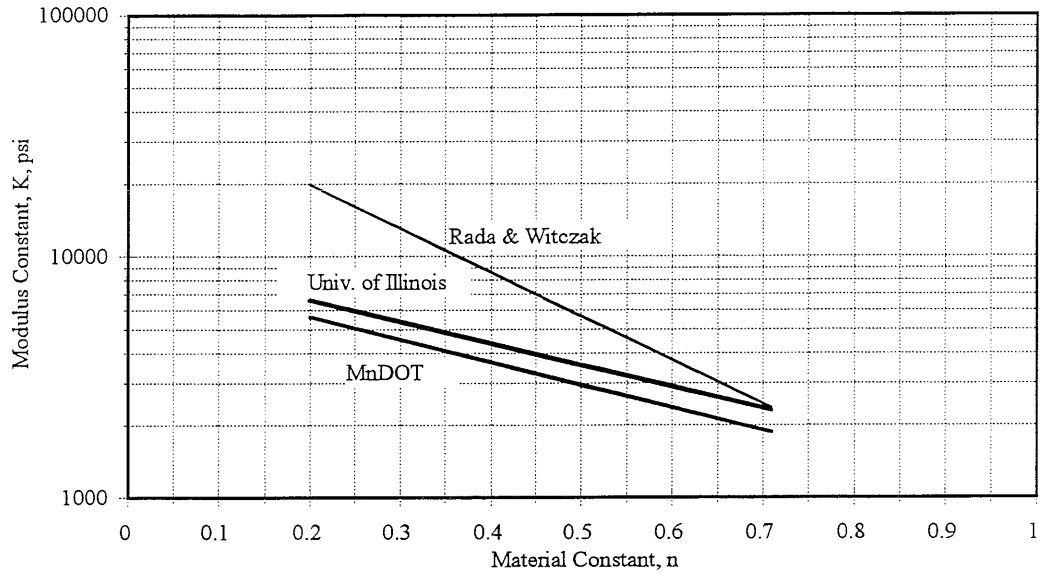

Figure 4.28. Relationship Between Resilient Modulus Parameters K and n

4.6 Conditioned Rapid Shear Test Results

The rapid shear test, performed on the specimen at 15-psi confining pressure after it was subjected to repeated load tests, is termed the conditioned rapid shear test. Results from conditioned rapid shear tests show the effect of repeated loading (stress history) on the shear strength of the material. Figures 4.29 through 4.37 show the comparison between unconditioned shear strength and conditioned shear strength for different materials tested. Conditioned rapid shear tests could not be performed on CL-1C and CL-4sp (9.4 % moisture content) as the specimens failed during the repeated load testing. The general trend is that the shear strength of material increases after it has been subjected to repeated load and peak strength is achieved at a lower strain value. The amount of shear strength increase depends on material properties such as gradation, moisture content, dry density, etc. Table 4.4 shows the conditioned rapid shear test results summary. Material CL-1F experienced a 38-percent increase in the shear strength. In the case of material CL-3sp, an increase in shear strength was observed at lower moisture content. At higher moisture content, no increase was observed in the shear strength, but the peak strength was achieved at a lower strain level. Material CL-5sp experienced a higher increase in strength (44-percent) at higher moisture content, and lower strength increase (16-percent) at lower moisture content. Moisture content did not show any effect on CL-6sp strength increase.

TABLE 4.4
Results from Conditioned Rapid Shear Tests @ 15-psi Confining Pressure on Mn/ROAD Granular Materials

			Unconditioned Rapid Shear Tests		Conditioned Rapid Shear Strength		
Material	Moisture Content, %	Dry Density pcf	Stress @ Failure, psi	Strain @ Failure, %	Stress @ Failure, psi	Strain @ Failure, %	Percent Increase in Shear Strength
CL-1C sp	9.0	132.0	50	5.0	Sample failed during resilient modulus testing.		
CL-1F sp	8.3	131.0	88	3.1	121	1.9	38
CL-3 sp	6.8	127.0	94	1.9	116	1.1	23
CL-3 sp	8.0	128.0	116	2.5	114	1.3	0
CL-4 sp	7.9	130.0	104	3.7	117	2.1	13
CL-4 sp	9.4	132.0	89	5.0	Sample failed during resilient modulus testing.		
CL-5 sp	7.7	139.0	81	5.0	117	4.3	44
CL-5 sp	6.8	137.0	115	4.7	133	3.2	16
CL-6 sp	6.3	134.0	177	5.0	190	3.6	7
CL-6 sp	5.3	133.0	178	5.0	191	4.1	7
R70 Sand	10.5	117.0	76	3.0	84	2.0	11

Material : CL-1F sp
Dry Density = 131 pcf, MC = 8.3 %
Confining Pressure = 15 psi

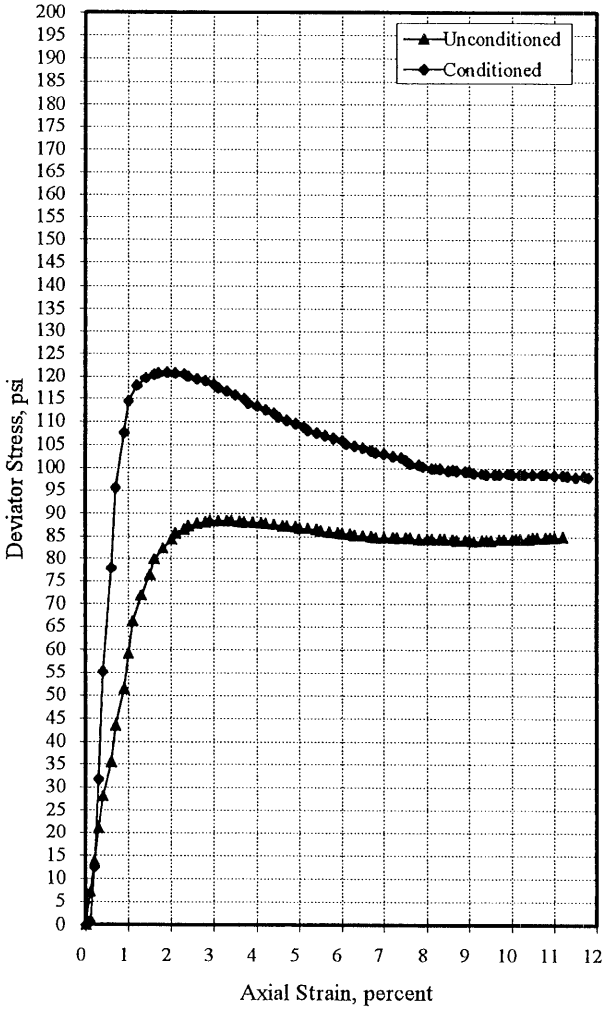

Figure 4.29. Conditioned Rapid Shear Test Results for CL-1Fsp

Material : CL-3 sp
Dry Density = 128 pcf, MC = 8 %
Confining Pressure = 15 psi

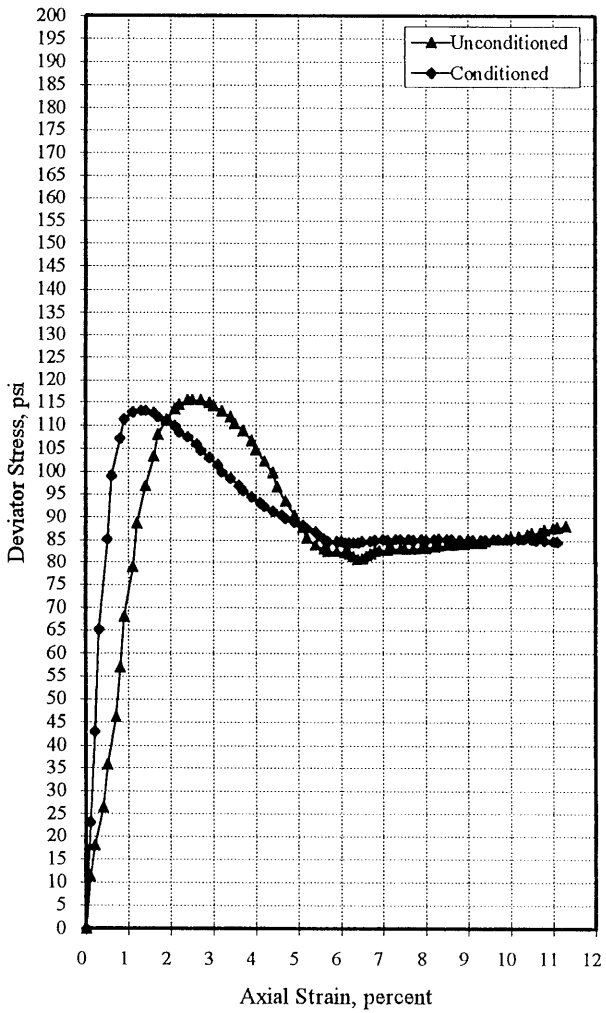

Figure 4.30. Conditioned Rapid Shear Test Results for CL-3sp

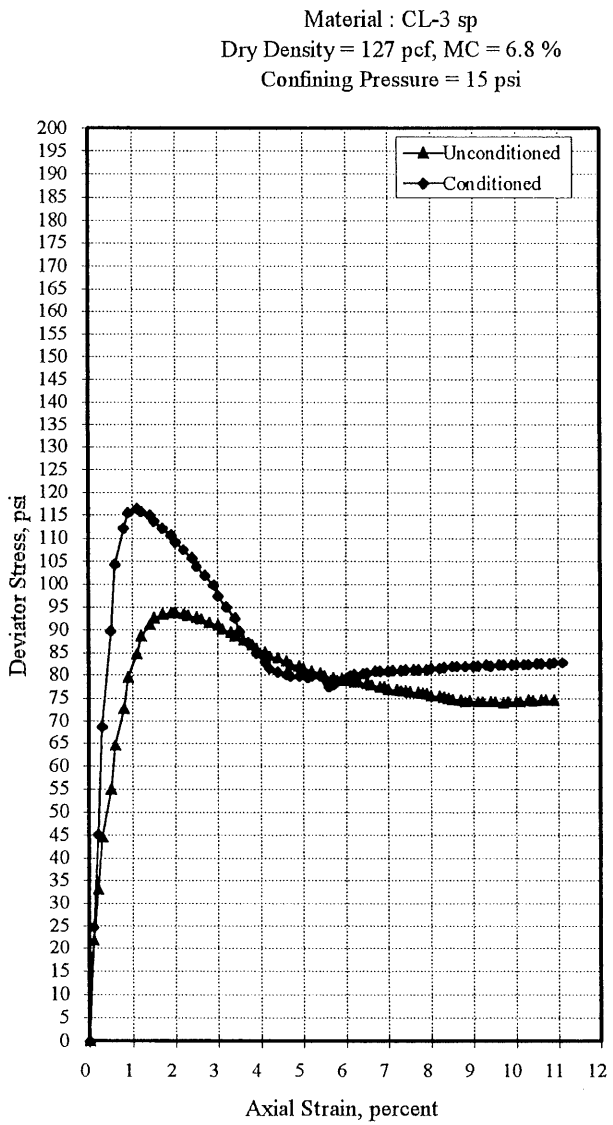

Figure 4.31. Conditioned Rapid Shear Test Results for CL-3sp

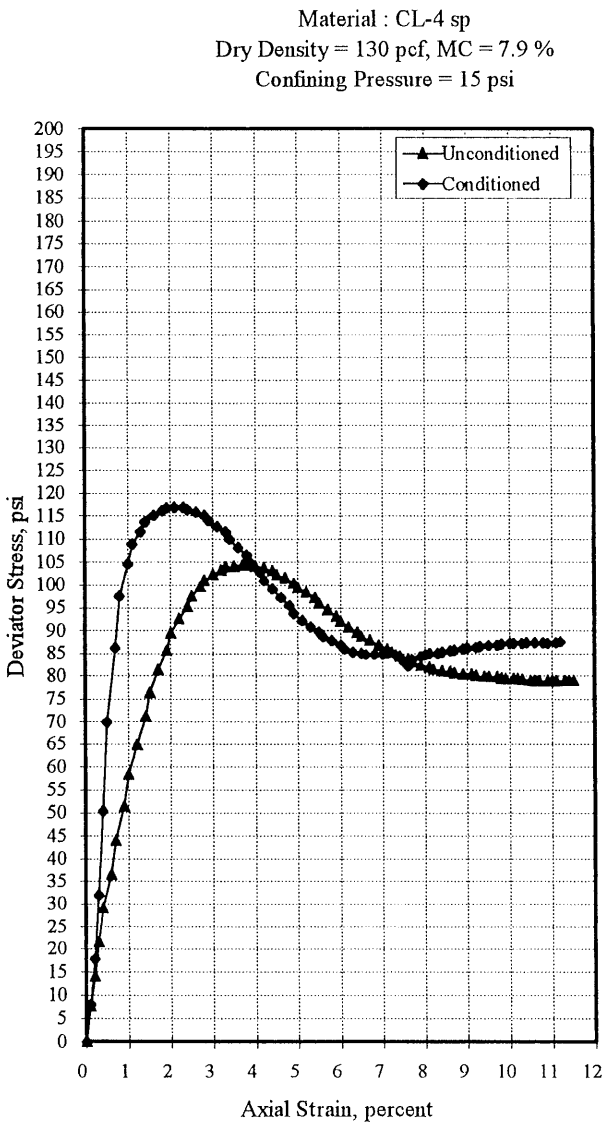

Figure 4.32. Conditioned Rapid Shear Test Results for CL-4sp

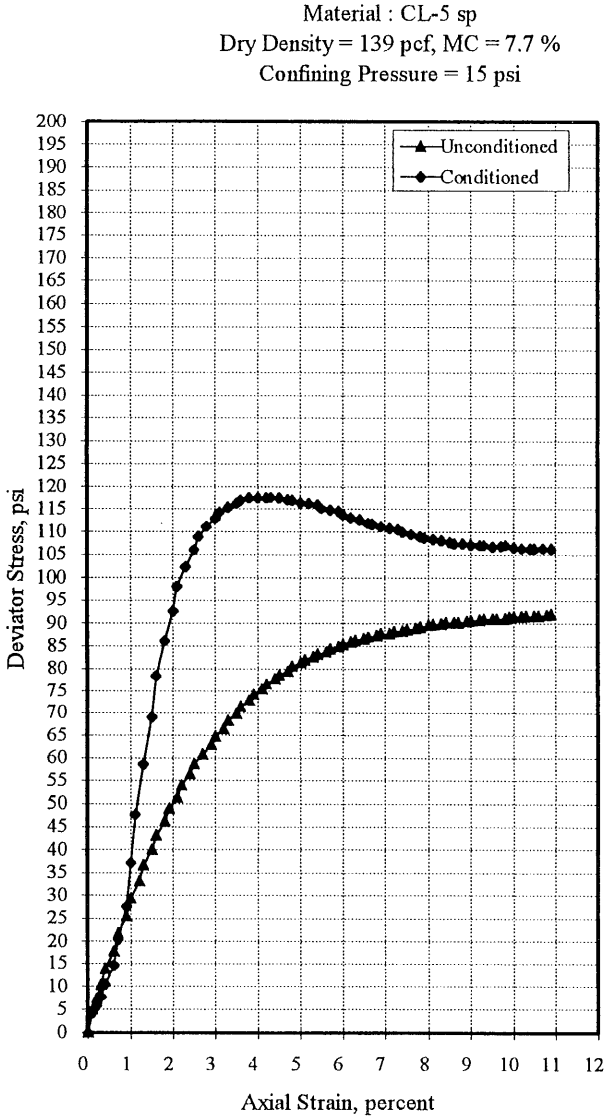

Figure 4.33. Conditioned Rapid Shear Test Results for CL-5sp

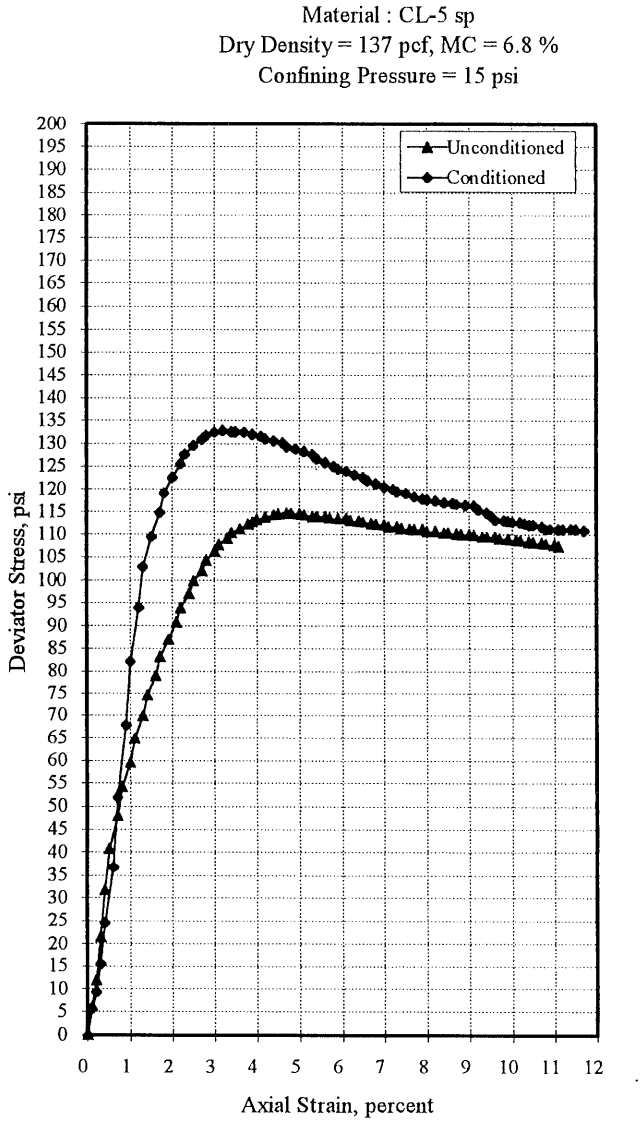

Figure 4.34. Conditioned Rapid Shear Test Results for CL-5sp

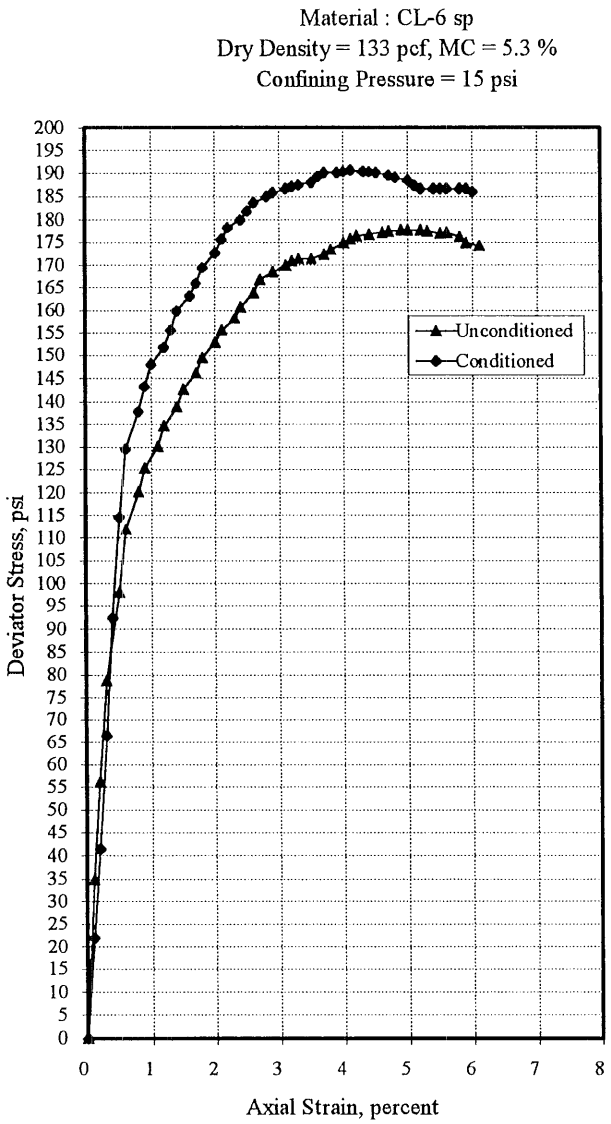

Figure 4.35. Conditioned Rapid Shear Test Results for CL-6sp

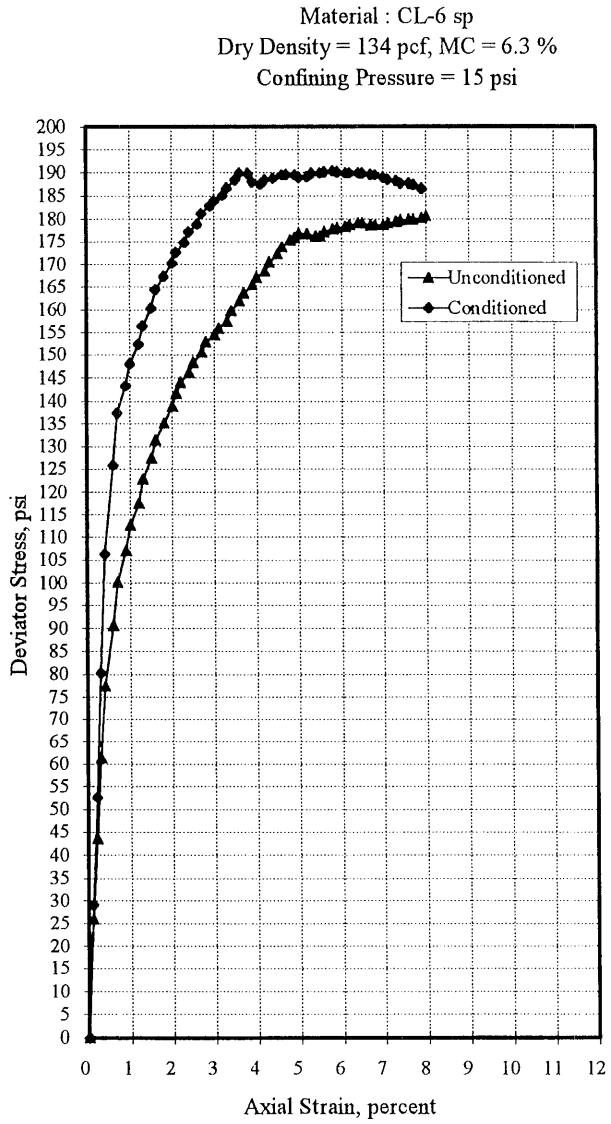

Figure 4.36. Conditioned Rapid Shear Test Results for CL-6sp

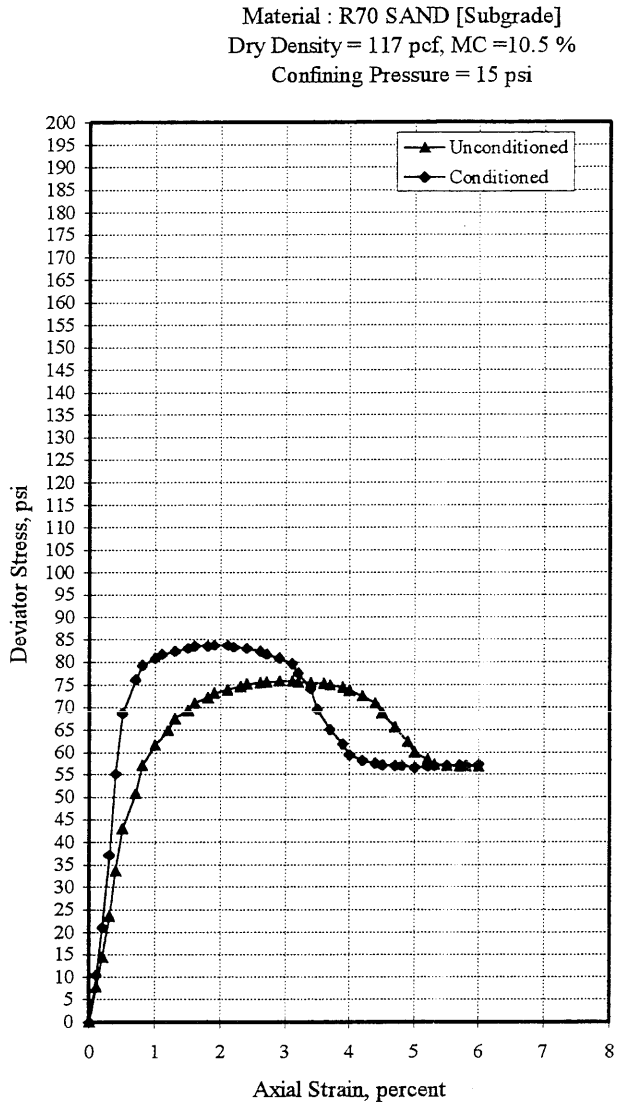

Figure 4.37. Conditioned Rapid Shear Test Results for Subgrade Sand

4.7 Dynamic Cone Penetrometer Test Results

The DCP test results show that, in general, a high penetration rate (PR) value was obtained for the first several inches of penetration. This is due to the lack of overburden or confining stress, and the displacement of material at the surface of the specimen. At greater depths, lower PR values are obtained due to a higher degree of confinement because of overburden. Hence, the PR was evaluated as an average value over the midpoint plus and minus 2-inch range.

Table 4.5 summarizes the results obtained from DCP tests on the granular materials and the subgrade sand at various moisture and density levels. For material CL-1Csp, in the case of

TABLE 4.5
Results from DCP Testing on Mn/ROAD Granular Materials

Material	Moisture Content, %	Dry Density pcf	Penetration Rate inch/blow	CBR, %
CL-1C sp	4.9	143	0.13	90
CL-1C sp	6.8	132	0.54	15
CL-1C sp	7.3	137	0.98	7
CL-1C sp	7.6	139	0.94	7
CL-1C sp	9.3	132	DCP rod penetrated sample under self weight.	
CL-1F sp	7.8	125	0.56	14
CL-1F sp	8.3	127	0.42	20
CL-1F sp	9.0	132	0.76	10
CL-1F sp	9.1	133	0.50	17
CL-1F sp	9.2	125	1.56	4
CL-1F sp	9.5	130	1.10	6
CL-1F sp	11.0	125	2.23	3
CL-3 sp	7.4	126	0.23	45
CL-3 sp	7.9	127	0.29	33
CL-4 sp	6.7	130	0.12	100
CL-4 sp	7.3	126	0.41	21
CL-4 sp	7.5	126	0.57	14
CL-4 sp	7.6	130	0.20	54
CL-4 sp	7.9	126	0.57	14
CL-4 sp	8.7	130	0.29	33
CL-4 sp	9.7	131	0.60	13
CL-4 sp	10.4	126	0.59	14
CL-5 sp	6.4	129	0.78	9
CL-5 sp	7.6	139	0.67	11
CL-5 sp	8.4	138	1.03	7
CL-6 sp	5.6	137	0.26	38
CL-6 sp	6.3	139	0.21	51
CL-6 sp	6.8	136	0.33	28
CL-6 sp	7.3	130	0.56	14
R70 Sand	12.2	116	0.39	22
R70 Sand	13.3	112	0.57	14

specimen prepared at optimum moisture content (OMC) and maximum dry density, the DCP rod penetrated the full height of specimen under its self weight. This case showed that CL-1Csp at OMC and maximum dry density could not develop enough shear strength to counter the penetration

of DCP rod. Figures 4.38 through 4.44 show the moisture/density effects on the PR values for the granular materials and subgrade sand.

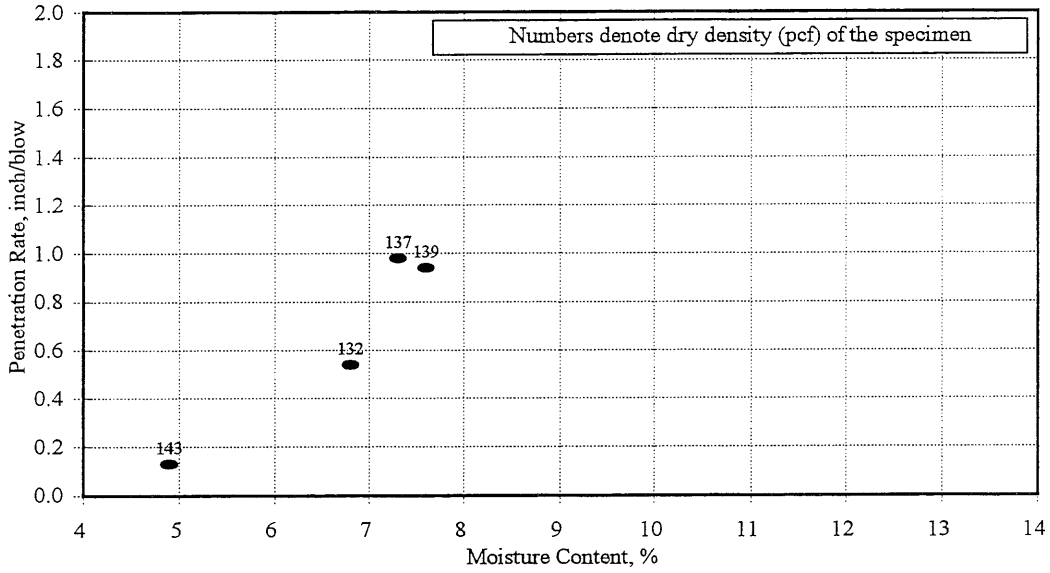

Figure 4.38. Moisture/Density Effects on DCP Test Results for CL-1Csp

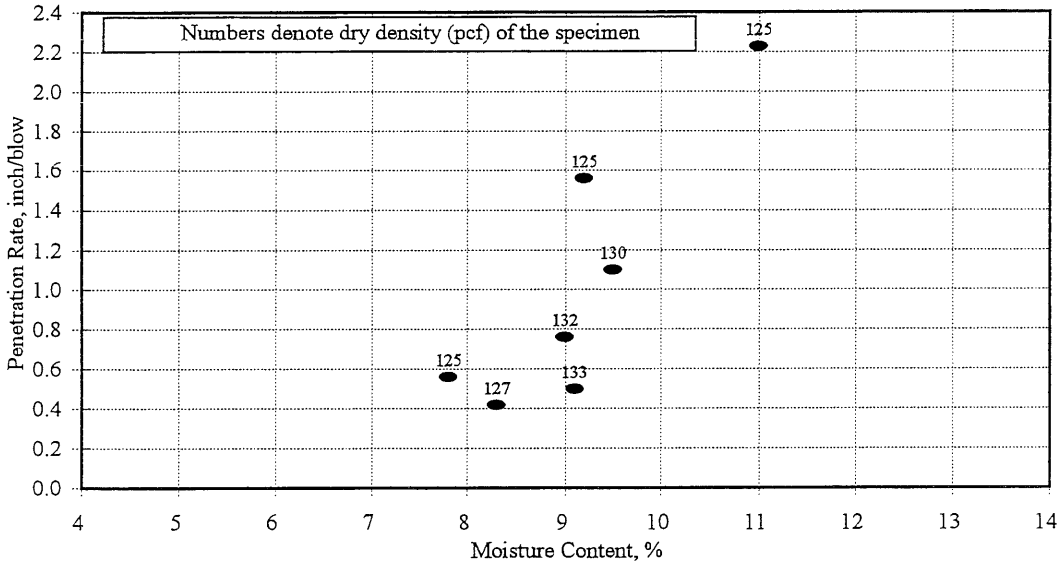

Figure 4.39. Moisture/Density Effects on DCP Test Results for CL-1Fsp

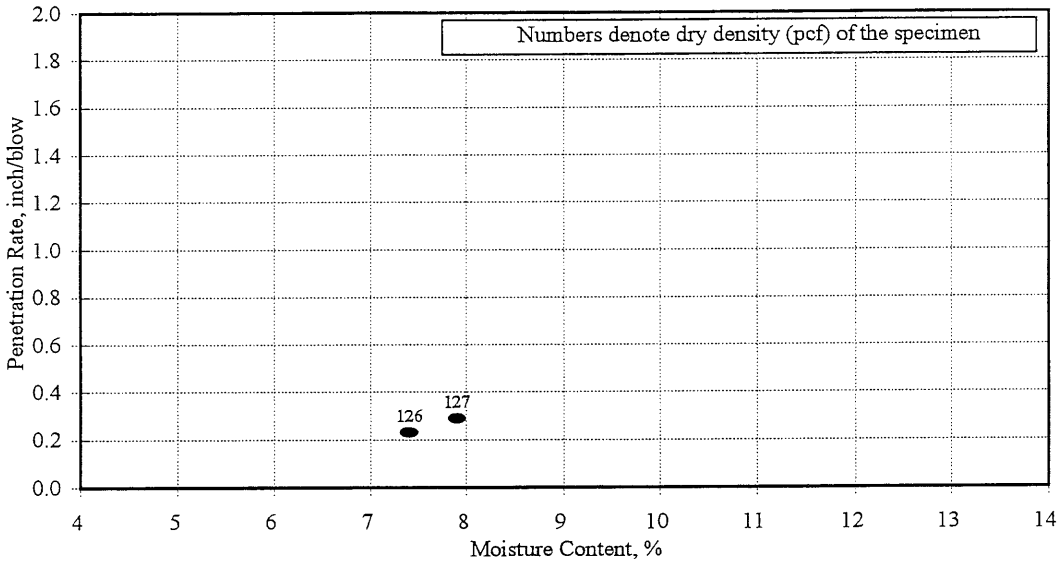

Figure 4.40. Moisture/Density Effects on DCP Test Results for CL-3sp

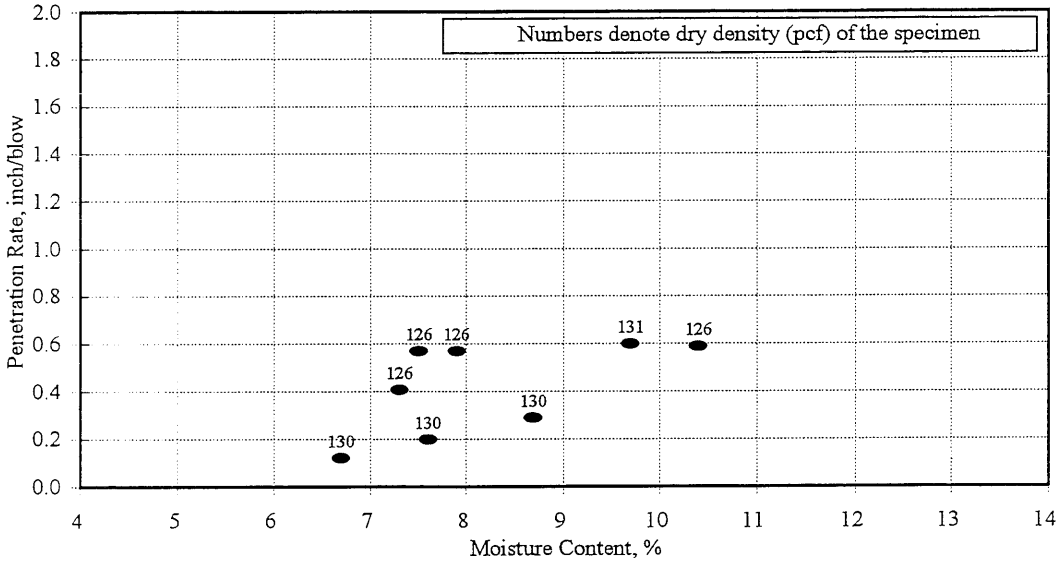

Figure 4.41. Moisture/Density Effects on DCP Test Results for CL-4sp

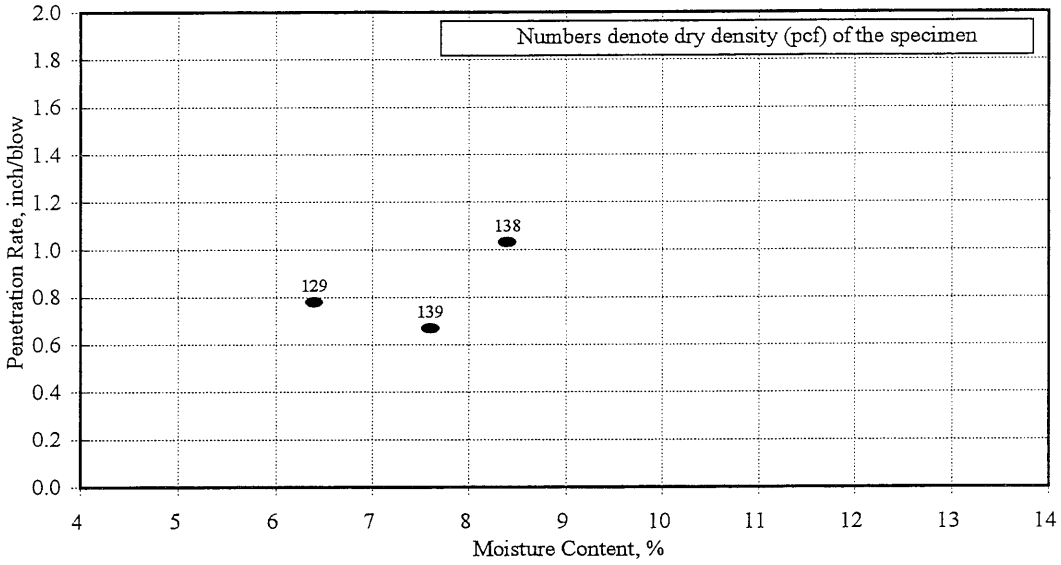

Figure 4.42. Moisture/Density Effects on DCP Test Results for CL-5sp

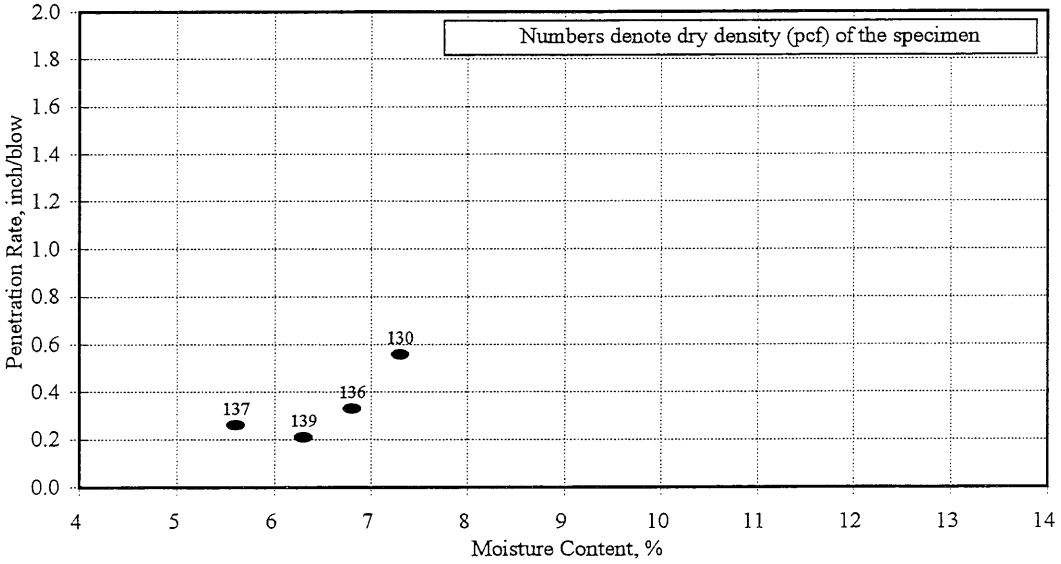

Figure 4.43. Moisture/Density Effects on DCP Test Results for CL-6sp

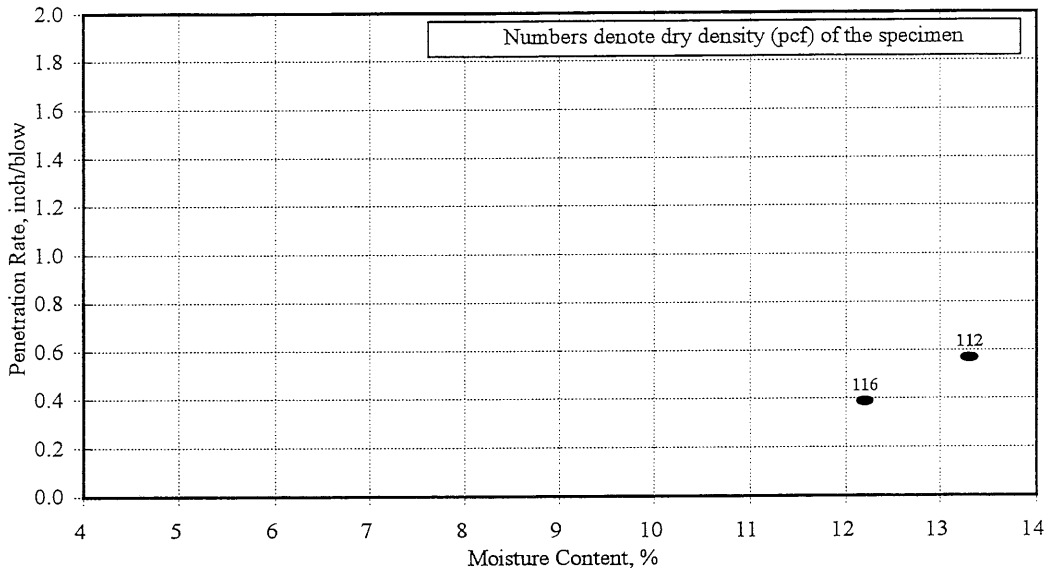

Figure 4.44. Moisture/Density Effects on DCP Test Results for Subgrade Sand

Material CL-1Csp and CL-1Fsp were found to be most susceptible to moisture changes. In case of CL-1Csp, at higher moisture content, the increase in density did not have any significant effects on the PR values. In the case of CL-1Fsp, increasing density at higher moisture contents reduced the PR values. In the case of CL-4sp, at moisture contents lower than OMC, increased density resulted in lower PR value. At moisture contents higher than OMC, the effects due to change in density were not significant. For the other materials (CL-3sp, CL-6sp, subgrade sand), PR values increased with increase in moisture content.

DCP test results are indicative of the shear strength of material. An attempt was made to correlate the peak shear strength obtained from rapid shear tests to the PR values obtained from DCP tests for the same moisture/density levels. Shear strengths obtained at a confining pressure of 15-psi gave best correlation with the PR values. Following relationship was established:

$$\sigma_D = 107.86 - 41.05*PR \quad \text{.....[4.12]}$$

$$R^2 = 0.63$$

Std. Err. of Y Est. = 7.13

where

σ_D = peak deviator stress (in psi) obtained from the rapid shear tests conducted at a confining pressure of 15-psi; and

PR = penetration rate, inch/blow.

The relationship between the PR and peak shear strength is shown in Figure 4.45.

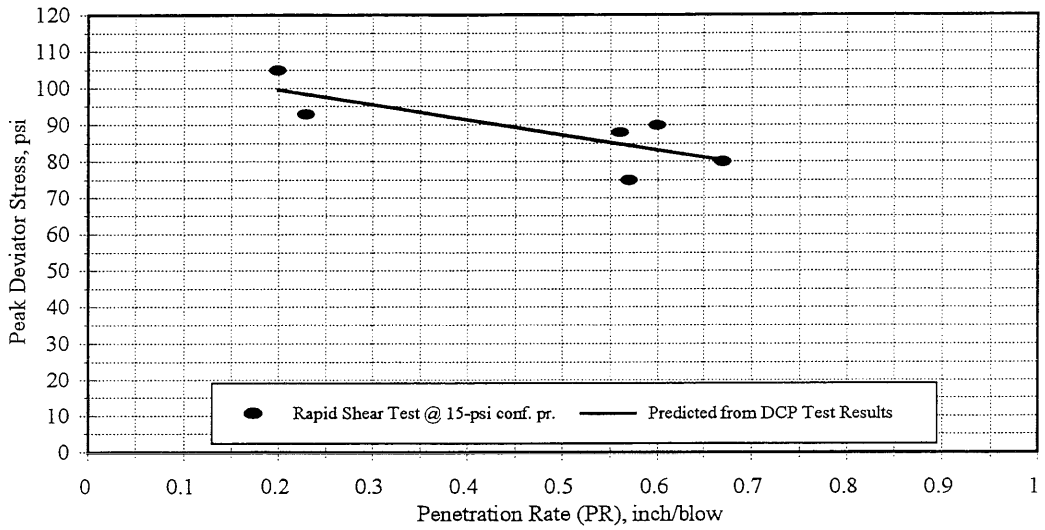

Figure 4.45. Peak Deviator Stress/Penetration Rate Relationship

Attempt was also made to correlate deviator stress at 2-percent axial strain (stated earlier: materials that achieve atleast 90-psi deviator stress at 2-percent axial strain, survive conditioning at 45/15) from rapid shear test at a confining pressure of 15-psi to the penetration rate. Following relationship was established (Figure 4.46):

$$\sigma_{D@2\% \text{ strain}} = 108.04 - 68.03*PR \quad \text{.....[4.13]}$$

$R^2 = 0.71$

Std. Err. of Y Est. = 9.92

where

$\sigma_{D@2\% \text{ strain}}$ = Deviator stress (in psi) at 2-percent axial strain obtained from the

rapid shear tests conducted at a confining pressure of 15-psi; and

PR = penetration rate, inch/blow.

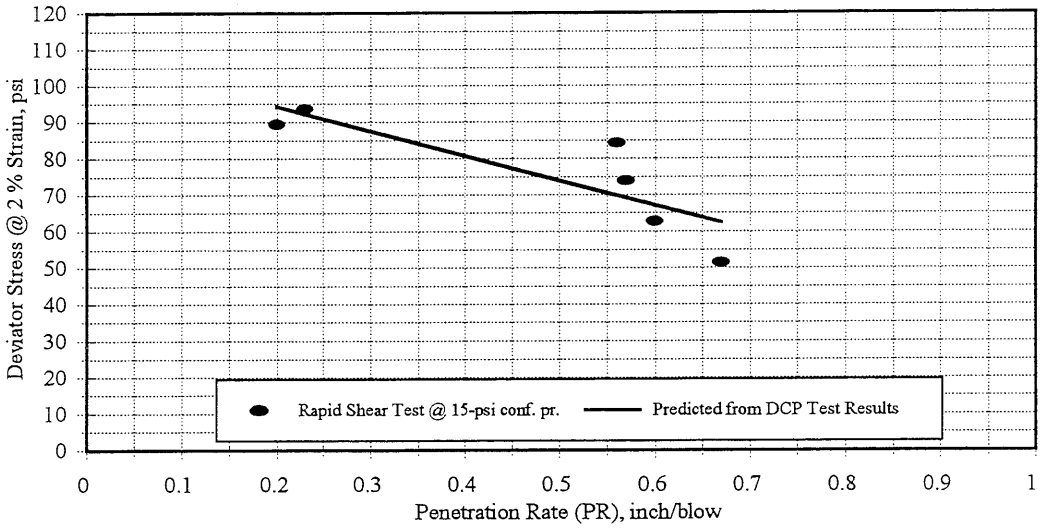

Figure 4.46. Peak Deviator Stress @ 2-percent Axial Strain/Penetration Rate Relationship

DCP test results (PR) may be used to get a fairly good estimate of the granular material shear strength.

4.8 Summary

A comprehensive laboratory program was undertaken to characterize the Mn/ROAD granular materials and subgrade sand. Dynamic cone penetrometer and rapid shear tests were conducted to determine shear strength of materials at different moisture/density levels. Repeated load tests were conducted to evaluate the rutting potential and the resilient behavior of the materials. The results have been presented in the form of various tables and figures. The results from rapid shear tests and permanent deformation tests show that the rutting potential of a granular material can be characterized from rapid shear test at a confining pressure of 15-psi. The stress-strain curve from the rapid shear test was used to predict the permanent deformation accumulation under the repeated load. Granular material that achieve at least 90-psi deviator stress at a confining pressure of 15-psi, display a low rutting potential. The laboratory test results show that rapid shear and repeated

load triaxial testing can be utilized to predict and rank the permanent deformation behavior of granular materials. Results from repeated load testing were used to develop the parameters for K-θ, UT-Austin and Uzan models for characterizing the resilient modulus. The estimated axial strain and resilient modulus values from the three models are in good agreement with the measured values. Less agreement between the measured and estimated axial strain and resilient modulus values was noted for CL-1Csp (poor quality, very low shear strength material). Laboratory tests were conducted on the subgrade sand to evaluate material properties.

Chapter-V discusses the laboratory testing performed at MnDOT on the cohesive subgrade.

CHAPTER V

LABORATORY TEST RESULTS ON COHESIVE SUBGRADE SOIL FROM MnDOT

5.1 Introduction

There are two types of subgrades at the Mn/ROAD low-volume road test track. In Cells 24 and 25, the subgrade is sand, and in the remaining cells, the subgrade is a cohesive soil. The native soils at the site are primarily silty clay and the existing topography had no more than 10 to 13-feet of relief prior to construction. The embankments for both the mainline and low-volume test track range in height from 0.3 to 10-feet and are constructed on cuts ranging from 0.7 to 2-feet. The results from laboratory tests performed at University of Illinois on sand have been presented in Chapter 4. Laboratory testing on the cohesive subgrade was performed by MnDOT. The following sections discuss the sampling procedures, testing procedures, and laboratory test results for the cohesive subgrade. These results were obtained from MnDOT.

5.2 Sampling Procedures

Subgrade soil samples were collected by MnDOT at various stages of construction for laboratory testing. Samples were obtained using Thinwall Shelby Tube (undisturbed) and bulk bag samples (disturbed). Thinwall Shelby tube was 3-inch in diameter and 30-inch in length (sample length = 24-inch). The samples were collected after subgrade completion, before placement of subbase/base materials. The samples were from depths ranging from 1-feet to over 6-feet under the right outer wheel path at various stations. All the bag samples were taken from beneath the centerline of the roadway, near the center of each cell.

5.3 Laboratory Tests

Resilient modulus of subgrade soil is an important parameter used in the design of flexible pavements. Since the test section performance is influenced by the resilient modulus of subgrade soils, it is necessary to have information to characterize the resilient modulus variation along the pavement embankment. Resilient modulus tests (SHRP Protocol P 46), and unconfined compression tests (AASHTO T 208) were performed by MnDOT personnel on the undisturbed and disturbed samples. Several other tests included Atterberg Limits (AASHTO T 90), sieve and hydrometer analysis (AASHTO T 88), Proctor Density Tests (AASHTO T 99 and T 180), and

Stabilometer (R-value) tests.

5.4 Laboratory Test Results

Gradation Tests

Sieve and hydrometer analyses on the cohesive subgrade soil were performed as per AASHTO T 88. For bag samples (Table 5.1), the percent clay (< 0.002-mm) ranged from 15.4 to 28.0 with an average value of 22.6. The percent silt (0.075-mm to 0.002-mm) ranged from 36.9 to 43.0 with a mean value of 39.4. For Shelby tube samples (Table 5.2), the percent clay (< 0.002-mm) ranged from 14.6 to 28.3 with an average value of 21. The percent silt ranged from 35.8 to 44.5 with a mean value of 40.

Stabilometer Tests

Hveem's stabilometer tests were conducted to determine R-value for the bag samples. The sample depths varied from 30 to 38-inch below the subgrade surface. Moisture content and density of the specimens is given in Table 5.1. Test results are summarized in Table 5.1. The R-value ranged from 12.0 to 14.6 with a mean value of 13.24 and a standard deviation of 0.77. The coefficient of variation (COV) was 5.84-percent.

Atterberg Limits

The laboratory testing was performed in accordance with AASHTO T 90. The liquid limit (LL) ranged from 30-percent to 48-percent (Table 5.2) with mean of 38-percent, standard deviation of 5.63-percent, and coefficient of variation of 14.93-percent. The plasticity index (PI) ranged from 12-percent to 29-percent (Table 5.2) with mean of 18-percent, standard deviation of 5.48-percent, and coefficient of variation of 29.73-percent. The subgrade soil was classified as AASHTO A-6 soil (silty-clay, more than 35 % passing No. 200 sieve, LL - 40 maximum, PI - 11 minimum).

Compressive Strength Test Results

The results from unconfined compressive strength (q_u) testing are summarized in Table 5.2 (undisturbed samples) and Table 5.3 (disturbed samples). For the undisturbed samples, unconfined compressive strength ranged from 12.6-psi to 47.18-psi (mean = 23-psi, std. = 8.95-psi, COV = 39.19-percent). Comparatively lower unconfined compressive strength values were obtained for

TABLE 5.1

Results of Soil Analyses from Bag Soil Samples

Date	Sample ID	Test Section	Station	Depth inch	Liquid Limit, %	Plasticity Index, %	Percent Clay	Percent Silt	Specific Gravity	OMC %	Max. Dry Density, pcf	R-Value @ 240 psi
6-25-92	10418A	26	17210	30.00	30	12	15.4	40.4	-	16.5	112	13.30
6-25-92	10419A	27	17775	38.03	37	19	20.4	43.0	-	18.1	108	12.80
6-25-92	10420A	28	18345	33.98	38	19	23.1	40.1	-	16.8	109	13.60
10-22-91	10421A	29	18915	32.99	43	25	25.4	38.5	2.675	17.9	107	13.30
10-22-91	10422A	30	19485	35.04	45	28	28.0	37.7	-	19.1	105	12.00
10-22-91	10423A	31	20055	36.97	37	20	21.9	38.9	-	19.6	105	12.10
10-22-91	10424A	32	20620	30.00	41	23	23.7	36.9	2.665	18.5	105	13.10
6-29-92	10425A	33	6620	35.98	34	16	-	-	-	17.9	109	14.60
6-26-92	10426A	34	7190	30.00	33	14	-	-	-	17.2	110	13.40
6-26-92	10427A	35	7740	30.00	30	11	-	-	-	15.0	111	14.20
				Mean	37	19	22.6	39.4		17.7	108	13.24
				STD	4.97	5.26	3.70	1.88		1.27	2.46	0.77
				COV, %	13.50	28.20	16.38	4.77		7.21	2.28	5.84

OMC: Optimum Moisture Content

TABLE 5.2
Results of Resilient Modulus Tests Near Optimum Moisture from Thinwall Shelby Tube Samples

Date	Sample ID	TS	Station	Depth inch	LL %	PI	K1 psi/psi	K2 psi/psi	qu psi	ERi ksi	Bulk Density pcf	Dry Density pcf	MC %	S %	% Clay	% Silt
6/25/92	10051A	26	17215	30.00	30	12	1078	333	21.8	9.5	129	111	15.9	85.1	16.4	39.9
6/25/92	10051B	26	17213	54.02	36	17	1573	484	21.0	13.7	132	113	16.7	95.0	20.9	41.5
6/25/92	10053A	27	17780	38.03	42	23	1660	472	19.0	11.0	133	112	18.1	100.0	21.7	41.5
6/25/92	10053B	27	17780	56.02	48	29	1119	306	18.0	6.6	130	109	19.8	99.8	26.5	40.8
6/26/92	10055A	28	18350	51.97	48	28	1418	384	20.5	8.1	129	107	20.0	96.7	28.3	44.5
6/26/92	10059A	30	19490	53.03	43	24	1171	310	18.9	6.3	132	112	18.1	98.8	26.7	40.7
10/24/91	10061A	31	20060	54.96	37	17	1332	412	12.6	11.8	131	112	17.4	94.5	23.7	37.4
10/24/91	10061B	31	20060	90.94	33	12	1184	420	15.7	20.6	132	115	15.3	90.7	23.0	35.8
6/26/92	10063B	32	20625	60.00	40	22	1673	475	17.7	11.0	133	114	17.2	99.1	22.8	39.7
7/1/92	10065A	33	6625	30.00	37	19	1246	433	36.6	19.1	136	119	14.1	94.2	15.5	38.9
7/1/92	10065B	33	6625	54.02	35	16	1592	447	24.0	10.1	133	113	17.3	98.2	18.7	42.1
7/1/92	10067A	34	7195	35.98	37	18	1468	370	12.9	6.9	131	111	18.2	96.4	21.6	39.5
7/1/92	10067B	34	7195	47.99	30	12	1199	365	31.2	10.0	133	115	15.7	94.0	14.6	41.7
7/1/92	10069A	35	7745	24.02	31	12	911	346	47.2	27.1	137	121	13.1	93.9	15.2	42.2
7/1/92	10069B	35	7745	60.00	38	19	1251	423	25.3	16.6	133	114	16.9	97.0	22.3	40.7
				Mean	38	18	1325	399	22.8	12.5	132	113	16.9		21.2	40.5
				STD	5.63	5.48	222.30	57.15	8.95	5.73	2.18	3.42	1.83		4.19	2.02
				COV, %	14.93	29.73	16.78	14.34	39.19	45.66	1.65	3.02	10.83		19.79	5.00

TS : Test Section
MC : Moisture Content
qu : Unconfined compressive strength
ERi : Subgrade "breakpoint" modulus
LL : Liquid limit
PI : Plasticity Index
S: Degree of Saturation

disturbed (bag) samples. For the disturbed samples, q_u ranged from 9.1-psi to 15.3-psi (mean = 12.4-psi, std. = 2.33-psi, COV = 18.85-percent). In the case of undisturbed samples (Table 5.2), a decrease in strength values was observed with increase in depth (moisture content of the soil samples increased with depth). The soil moisture content ranged from 13.1-percent to 20.0-percent.

Resilient Modulus Test Results

Resilient modulus testing was performed on the disturbed and undisturbed samples as per procedures outlined in SHRP Protocol P46. Fine-grained subgrade soils show stress softening characteristics. Resilient behavior of the subgrade soil was characterized by the following model :

$$M_R = K_1 \sigma_d^{K_2} \qquad \text{.....[5.1]}$$

where M_R is the resilient modulus of soil, σ_d is the deviator stress, and K_1 & K_2 are regression constants. The values of K_1 and K_2 were obtained from Mn/ROAD database.

Figure 5.1 shows the arithmetic model used for characterizing the stress dependent behavior of fine grained soils.

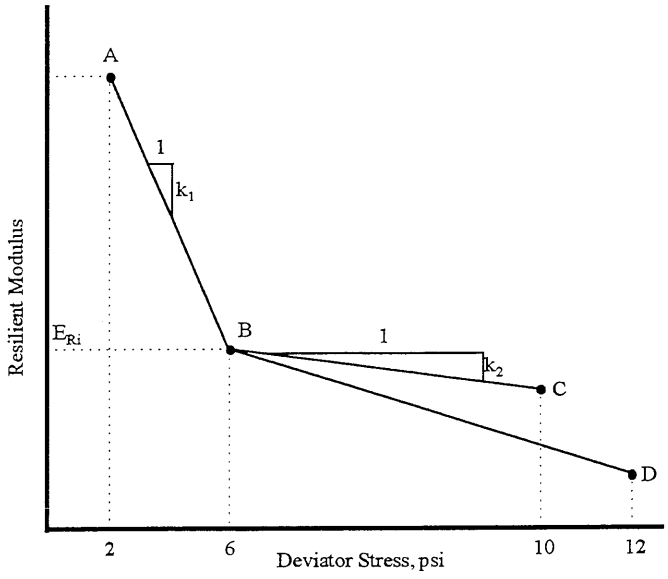

Figure 5.1. Arithmetic Model of Stress Dependency for Fine Grained Soils

This model is used in the IDOT mechanistic-empirical design procedure to characterize the stress softening behavior of fine grained soils. Points A, B, C, and D in Figure 5.1 represent several key points of the model. The deviator stresses are selected so that the parameters needed to characterize the line ABC or ABD are defined. The deviator stress at 2-psi ($\sigma_d = 2$) is used to calculate point A and $\sigma_d = 6$, 10, and 12 define points B, C, and D respectively. The slope of AB is designated as k_1. The slope k_2 may be designated between points B and C or points B and D. The lowest of the two slopes is used for k_2. Point B in Figure 5.1 is referred to as the "Break Point" resilient modulus (E_{Ri}). The term "break point" comes from the fact that point B falls at the break between the two slopes. E_{Ri}, k_1, and k_2 are inputs in the IDOT mechanistic-empirical design procedure.

Using the K_1 and K_2 values from Mn/ROAD database, and equation 5.1, resilient modulus was evaluated at σ_d = 2-psi, 6-psi, 10-psi, and 12-psi. Slopes k_1 and k_2 were evaluated for the undisturbed and disturbed samples, and are given in Tables 5.2 and 5.3 respectively. For the undisturbed samples (Table 5.2), k_1 ranged from 911-psi/psi to 1673-psi/psi, and k_2 ranged from 306-psi/psi to 484-psi/psi. For the disturbed (bag) samples (Table 5.3), k_1 ranged from 618-psi/psi to 927-psi/psi, and k_2 ranged from 207-psi/psi to 313-psi/psi. Lower k_1 and k_2 values were obtained for disturbed (bag) samples compared to the undisturbed samples. The E_{Ri} values ranged from 6.3-ksi to 27.1-ksi in the case of undisturbed samples (Table 5.2), and 5.7-ksi to 12.2-ksi in the case of disturbed (bag) samples (Table 5.3).

5.5 Analyses of Laboratory Test Results

In the arithmetic model, the value of the resilient modulus at the breakpoint in the bilinear curve, E_{Ri}, is a good indicator of a soils resilient behavior. The slope values, k_1 and k_2, display less variability and influence pavement structural response to a smaller degree than E_{Ri}. Previous studies have shown that E_{Ri} can be estimated from the unconfined compressive strength of the fine-grained soils. An attempt was made to correlate E_{Ri} to the unconfined compressive strength q_u. Test results from both, the bag and the undisturbed, samples were considered and the following regression equation was obtained:

$$E_{Ri} = 1.1714 + 0.4694 * q_u \quad \text{.....[5.2]}$$

$R^2 = 0.67$

Std. Err. of Y Est. = 3.1088

TABLE 5.3
Results of Resilient Modulus Tests Near Optimum Moisture from Bag Samples

Date	Sample ID	TS	Station	Depth inch	K1 psi/psi	K2 psi/psi	qu psi	ERi ksi	Bulk Density pcf	Dry Density pcf	MC %
6/25/92	10419A	27	17775	38.03	618	207	14.7	7.7	129	111	16.2
6/25/92	10420A	28	18345	33.98	927	313	15.3	12.0	127	109	16.3
10/22/91	10422A	30	19485	35.04	774	228	11.8	5.7	124	104	19.7
6/29/92	10425A	33	6620	35.98	680	212	10.9	6.2	128	109	17.8
6/26/92	10427A	35	7740	30.00	678	230	9.1	9.0	121	106	14.6
				Mean	735	238	12.4	8.1	126	108	16.9
				STD	107.97	38.52	2.33	2.28	2.86	2.54	1.72
				COV, %	14.68	16.21	18.85	27.98	2.27	2.36	10.16

TS : Test Section

MC : Moisture Content

qu : Unconfined compressive strength

ERi : Subgrade "breakpoint" modulus

where E_{Ri} is the "breakpoint" modulus in ksi, and q_u is unconfined compressive strength in psi. When the Y intercept is set to zero (i.e., $E_{Ri} = 0$ when $q_u = 0$), the following regression equation was obtained :

$$E_{Ri} = 0.5177 * q_u \quad \text{.....[5.3]}$$

$R^2 = 0.67$

Std. Err. of Y Est. = 3.0655

Figure 5.2 shows the relationship between the "breakpoint" modulus and the unconfined compressive strength. Comparison is made between the measured and estimated values. The regression equations can be used to predict the resilient properties of fine-grained subgrade soil.

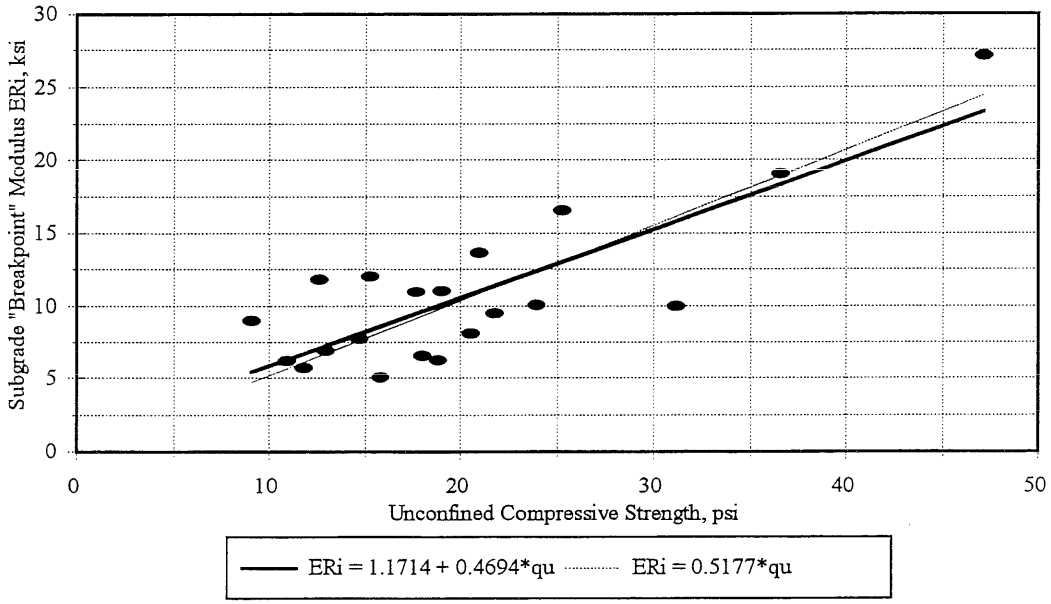

Figure 5.2. Subgrade "Breakpoint" Modulus vs Unconfined Compressive Strength

Figure 5.3 shows the variation in slopes k_1 and k_2 with unconfined compressive strength. Slope k_2 is fairly constant. Slope k_1 does not show any significant variation and values lie in a fairly narrow band.

Figures 5.4 and 5.5 show the variation in unconfined compressive strength q_u, and subgrade

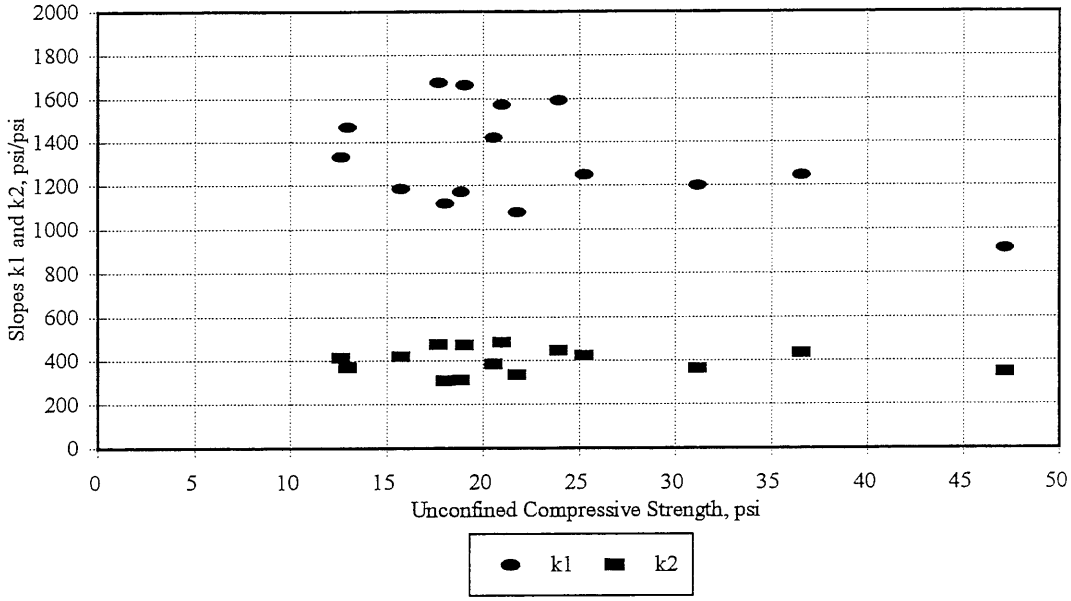

Figure 5.3. Slopes k1 and k2 vs Unconfined Compressive Strength

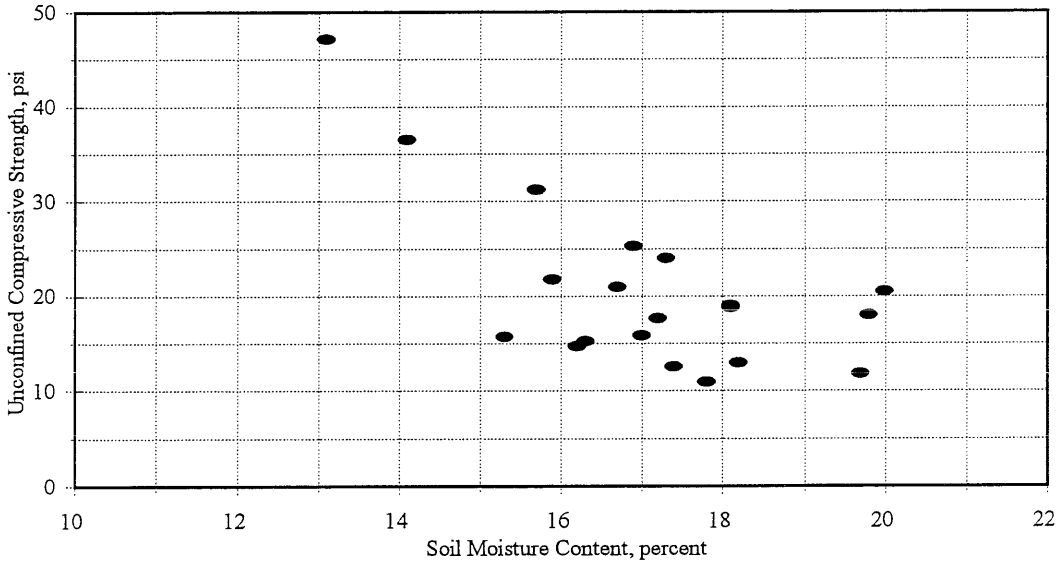

Figure 5.4. Variation in Unconfined Compressive Strength with Change in Moisture Content

"breakpoint" modulus E_{Ri}, with moisture content respectively. The figures indicate that q_u and E_{Ri} reduce with increase in moisture content. At moisture contents wet of optimum (18-percent), the decrease in q_u and E_{Ri} is not significant. A reduction of 2.19-ksi in the E_{Ri} value for every 1-percent increase in moisture content was noted. Following relationship was developed between the moisture content and E_{Ri} value:

$$E_{Ri} = 48.533 - 2.19 * \text{Moisture Content} \quad \text{.....[5.4]}$$

$$R^2 = 0.53$$

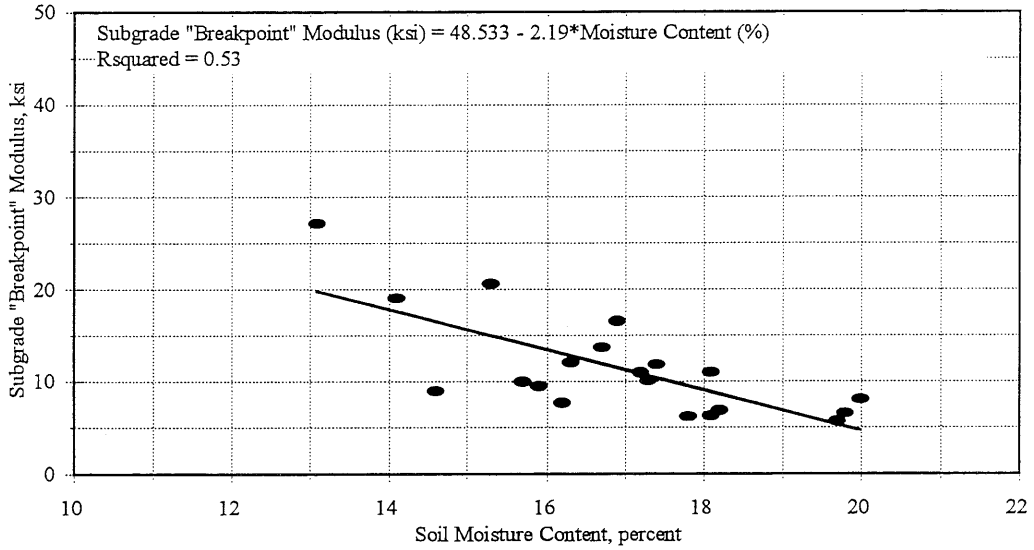

Figure 5.5. Variation in Subgrade "Breakpoint" Modulus with Change in Moisture Content

The specific gravity of soil solids (mean value = 2.67) were obtained from MnDOT and are listed in Table 5.1. It was used for estimating the degree of saturation of soil specimens. Figure 5.6 shows the effect of degree of saturation on subgrade "breakpoint" modulus E_{Ri}. An increase in degree of saturation causes reduction in E_{Ri}.

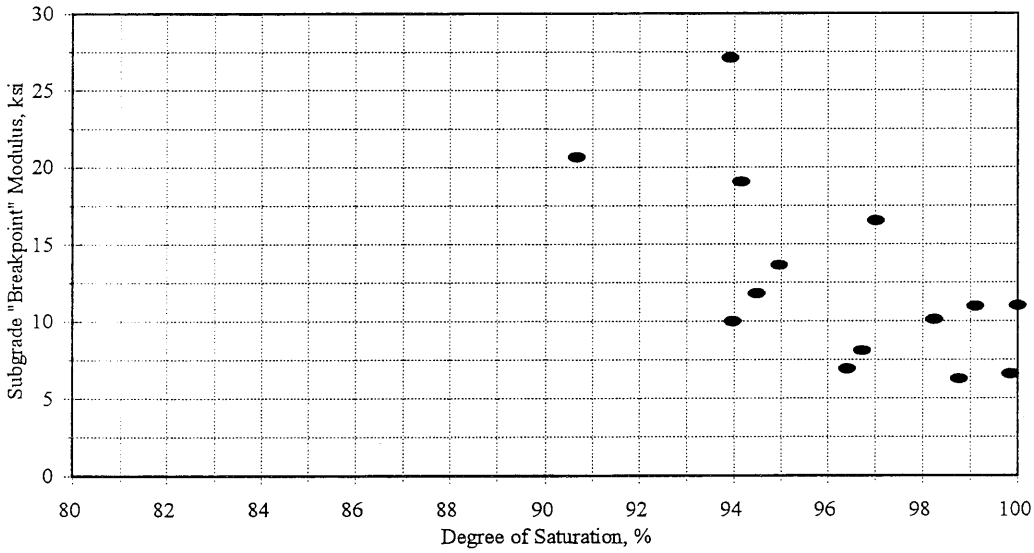

Figure 5.6. Variation in Subgrade "Breakpoint" Modulus with Degree of Saturation

Figures 5.7 and 5.8 show the effect of percent clay on E_{Ri} and q_u respectively. E_{Ri} and q_u were observed to decrease with the increase in percent clay. No particular trends could be observed while studying the effect of percent silt on E_{Ri} and q_u (Figures 5.9 & 5.10).

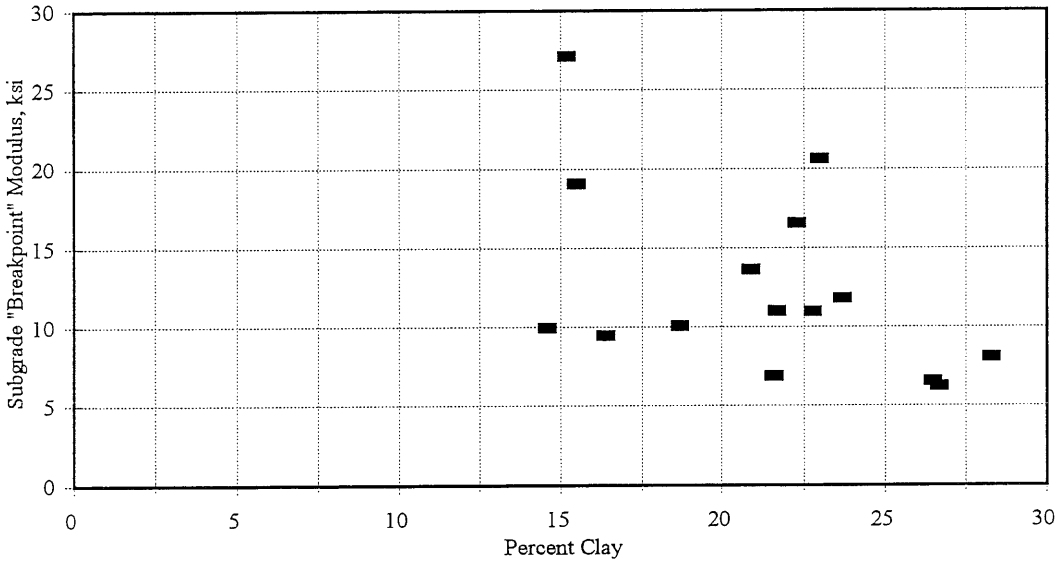

Figure 5.7. Effect of Percent Clay on Subgrade "Breakpoint" Modulus

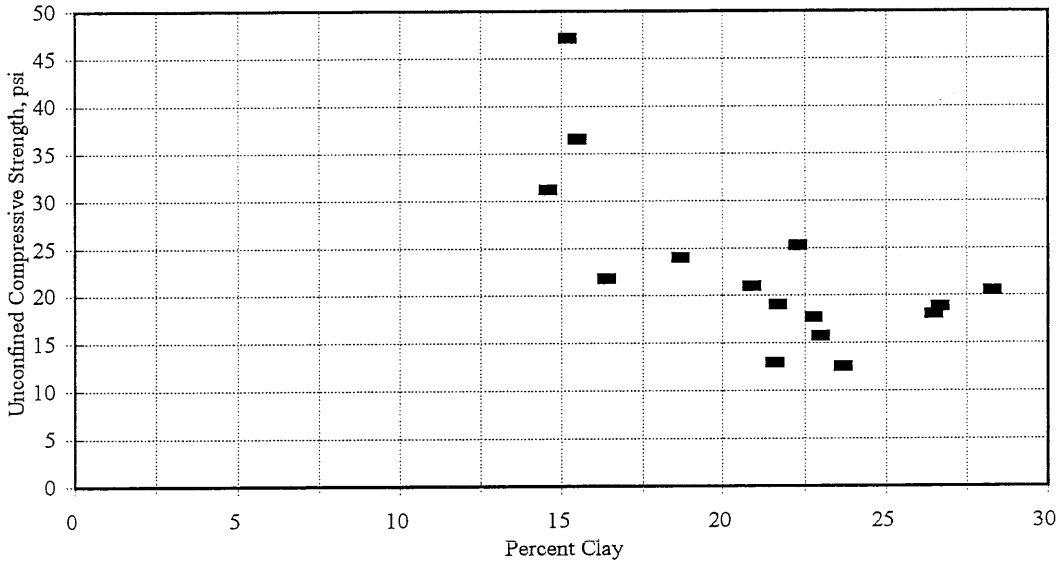

Figure 5.8. Effect of Percent Clay on Unconfined Compressive Strength

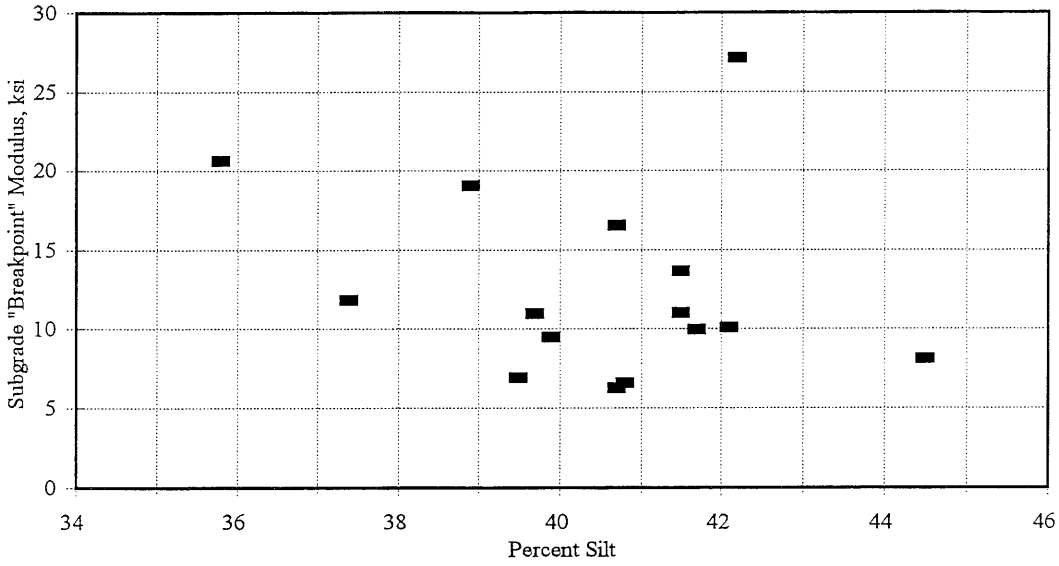

Figure 5.9. Effect of Percent Silt on Subgrade "Breakpoint" Modulus

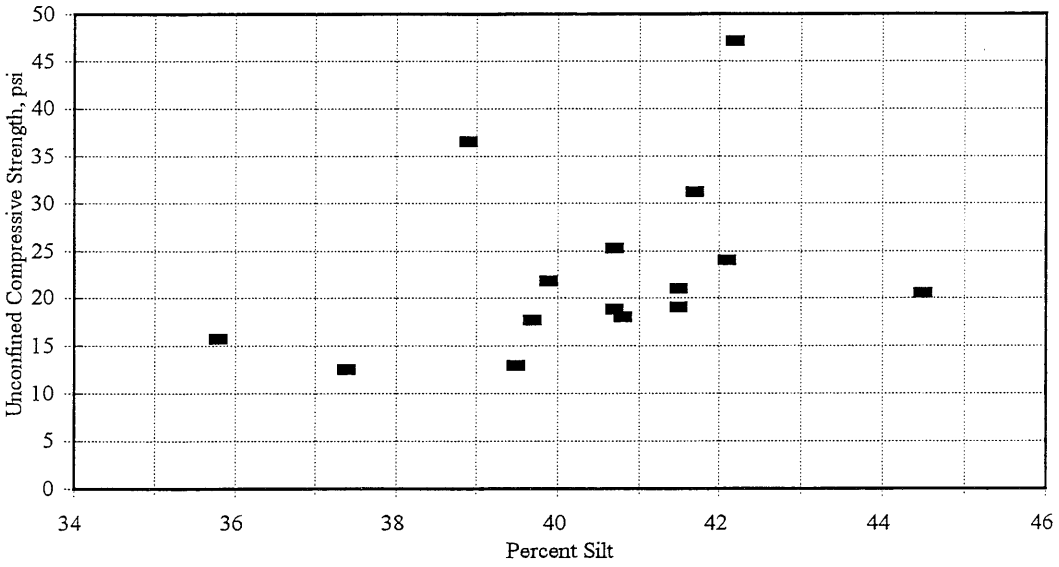

Figure 5.10. Effect of Percent Silt on Unconfined Compressive Strength

5.6 Summary

The results from laboratory testing on cohesive subgrade soil have been presented. The laboratory testing was performed at MnDOT. Field samples were collected using Thinwall Shelby Tube and

bulk bag samples. Atterberg Limits, sieve and hydrometer analysis, Proctor Density Tests, Stabilometer tests, resilient modulus tests, and unconfined compression tests were performed on undisturbed and disturbed samples. Based on the gradation test results and Atterberg limits, the soil was classified as AASHTO A-6 soil. An arithmetic model was used to characterize the stress softening behavior of fine-grained subgrade soils. A correlation between subgrade "breakpoint" modulus and unconfined compressive strength was established. Slopes k_1 and k_2 did not show any significant variation with change in unconfined compressive strength.

Chapter-VI discusses the effect of granular base material quality on pavement response and performance.

CHAPTER - VI
EFFECT OF GRANULAR MATERIAL QUALITY ON PAVEMENT RESPONSE AND PERFORMANCE

6.1 Introduction

Pavement surface deflection basins provide valuable information for the structural evaluation of flexible pavements. Among the different load responses (stress, strain, deflection), only the surface deflections are easily measurable. Pavement deflection is the basic response of the whole system to the applied load. It is frequently used as an indicator of the load carrying capacity of the pavement. Surface deflection measurements are rapid, relatively cheap, and non-destructive. A Falling Weight Deflectometer (FWD) is commonly used for non-destructive pavement testing. The FWD is an impulse-type testing device which imparts a transient load on the pavement surface. The duration and magnitude of the force applied are representative of the load pulse induced by a truck moving at moderate speeds. The load duration and magnitude can be varied by varying the height of drop and the buffer configuration. The Dynatest Model 8000 FWD equipment was used at Mn/ROAD for non-destructive testing. The testing pattern for each section consisted of ten test points spaced at 50-feet intervals with four longitudinal offsets (-9.5-feet - outer wheel track westbound lane, -6.25-feet - between wheel tracks westbound lane, +6.25-feet - between wheel tracks eastbound lane, +9.5-feet - outer wheel track eastbound lane) tested.

The performance of the test sections were monitored by measuring the rut depths, and observing for cracks (fatigue and thermal). An aluminum straight edge (6-feet long, 4-inch wide, 1/8-inch thick) was used to measure wheel path rutting in the flexible pavement test sections. The straight edge was placed across the lane and rut depth was measured in the right wheel path and left wheel path. Drill bits were slid below the straight edge (between the straight edge and the whee path). The diameter of the largest drill bit that could be slid between the straight edge and the wheel path was the rut depth. The following sections discuss the results from FWD testing on the test sections and evaluate the effect of granular material quality on the pavement response and performance.

6.2 Asphalt Concrete Thickness Measurements Using Ground Penetrating Radar

The thickness of asphalt concrete is needed as an input to use backcalculation algorithms for

estimating pavement layer properties. Ground Penetrating Radar (GPR) was used at the Mn/ROAD project to obtain accurate as-built layer thickness data. The GPR is a non-destructive, non-contact method for pavement thickness measurement. Radar data for the pavement layer thickness were collected on July 7, 1994 by Infrasense, Inc., in the two outside wheelpaths [78]. Two types of radar equipment were used: (1) air-coupled equipment normally operated at driving speeds, and (2) ground-coupled equipment normally operated at 5-10 mph. The data were analyzed using PAVLAYER© to determine layer thickness. The software is self calibrating and the analysis was executed without core data. A comparison between radar asphalt thickness data and cores showed an R-squared value of 0.98. The average deviation between radar and core data was 0.24-inches for asphalt concrete.

Figures 6.1 through 6.6 show the asphalt concrete thicknesses for test sections with cohesive subgrade (Cell-26, Cell-27, Cell-28, Cell-29, Cell-30, & Cell-31). Figures 6.6 and 6.7 show the asphalt concrete thicknesses for Cell-24 and Cell-25 (sandy subgrade) respectively. The standard deviations on the measured asphalt concrete thicknesses ranged from 0.21-inch to 0.59-inch. For test sections with 3-inch thick asphalt concrete surface (Cells 24, 27, 28, and 31), the coefficient of variation (COV) ranged from 7-percent to 16.5-percent. COV ranged from 5-percent to 10-percent for test sections with 5-inch and 6-inch thick asphalt concrete surfaces.

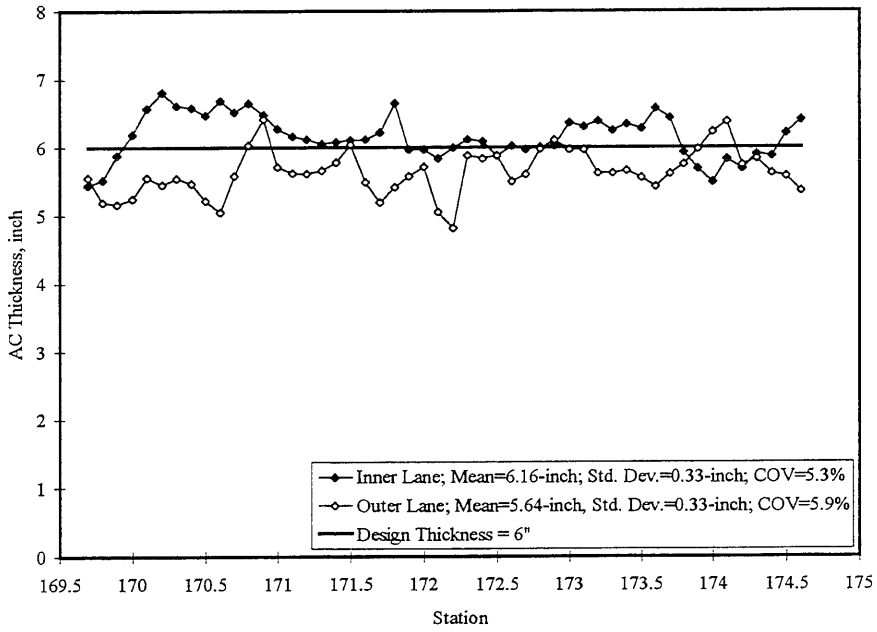

Figure 6.1. AC Thickness for Cell-26 from Ground Penetrating Radar

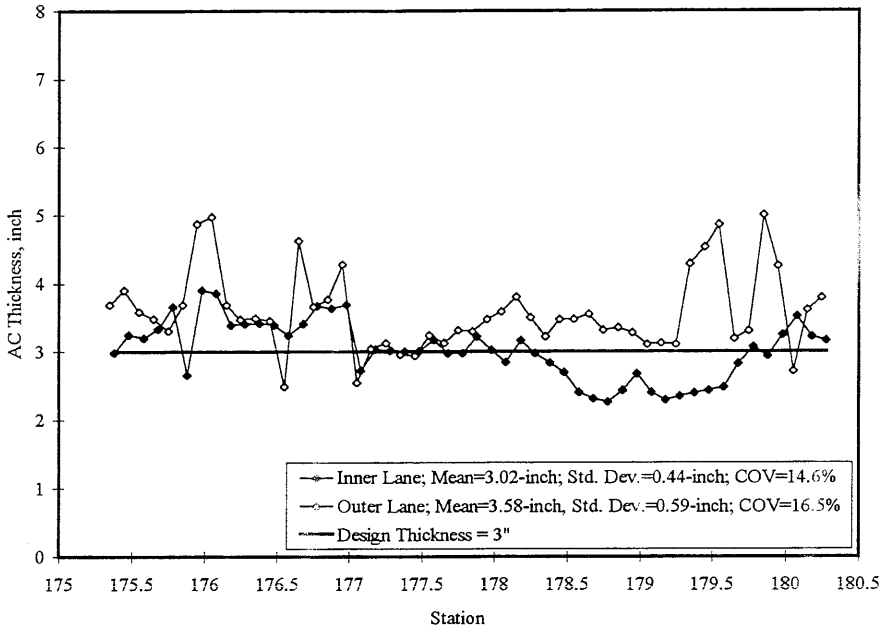

Figure 6.2. AC Thickness for Cell-27 from Ground Penetrating Radar

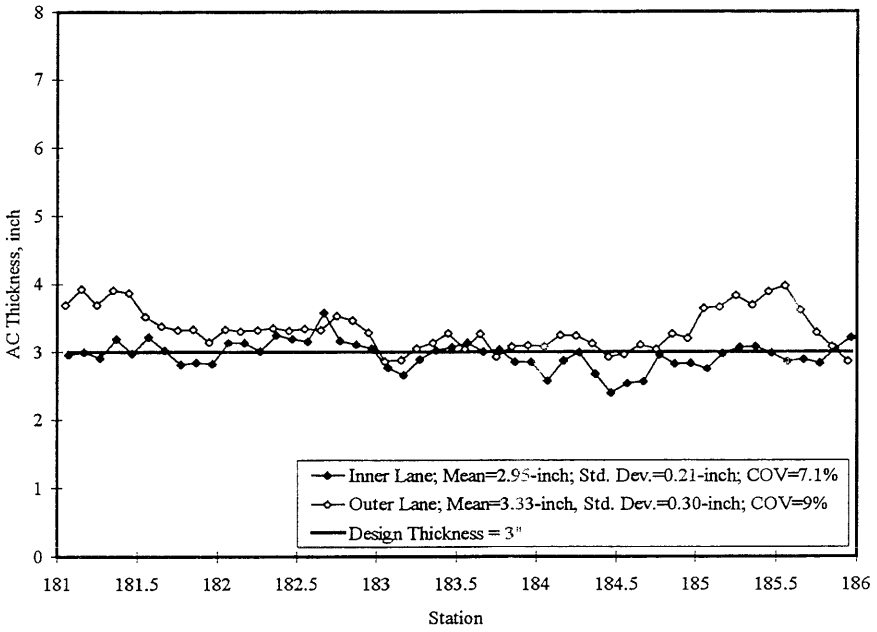

Figure 6.3. AC Thickness for Cell-28 from Ground Penetrating Radar

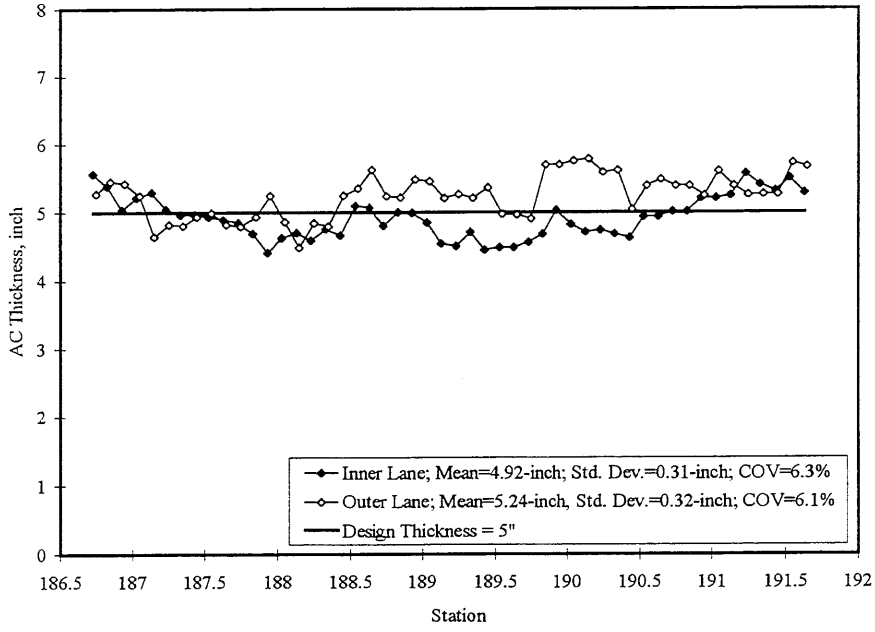

Figure 6.4. AC Thickness for Cell-29 from Ground Penetrating Radar

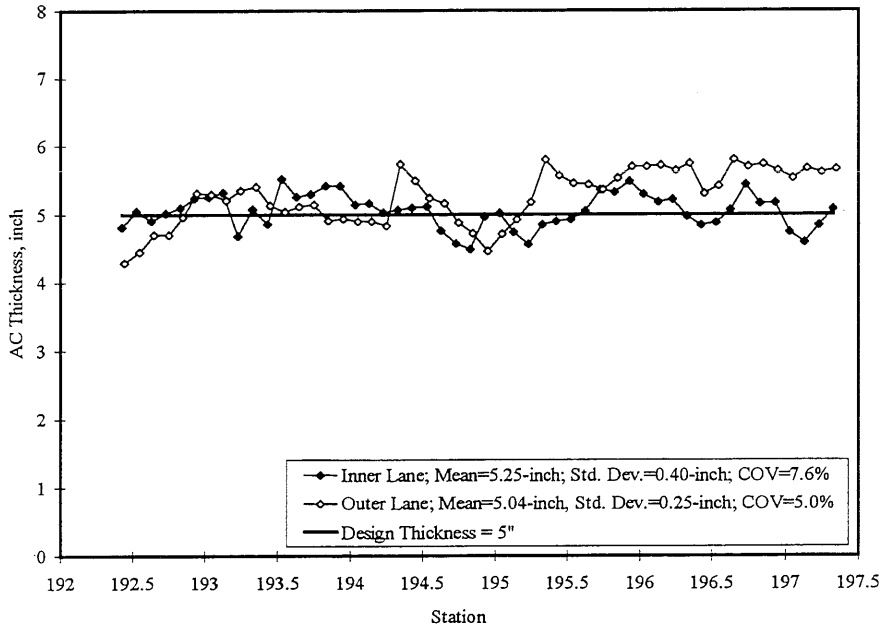

Figure 6.5. AC Thickness for Cell-30 from Ground Penetrating Radar

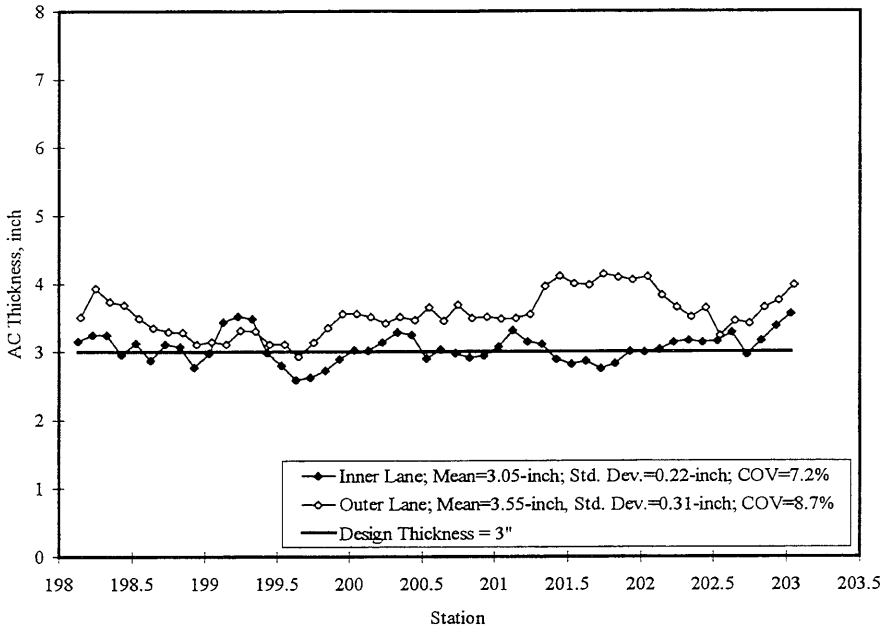

Figure 6.6. AC Thickness for Cell-31 from Ground Penetrating Radar

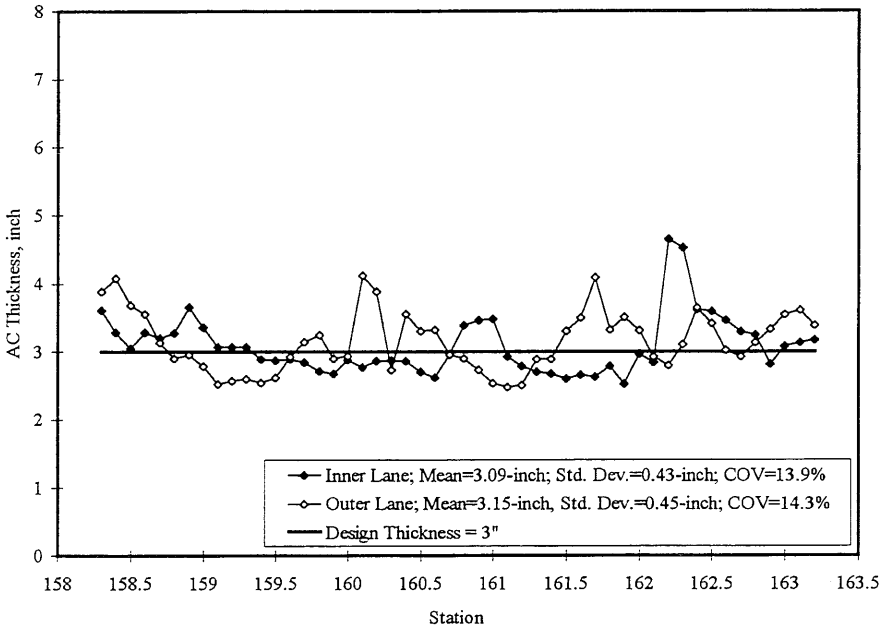

Figure 6.7. AC Thickness for Cell-24 from Ground Penetrating Radar

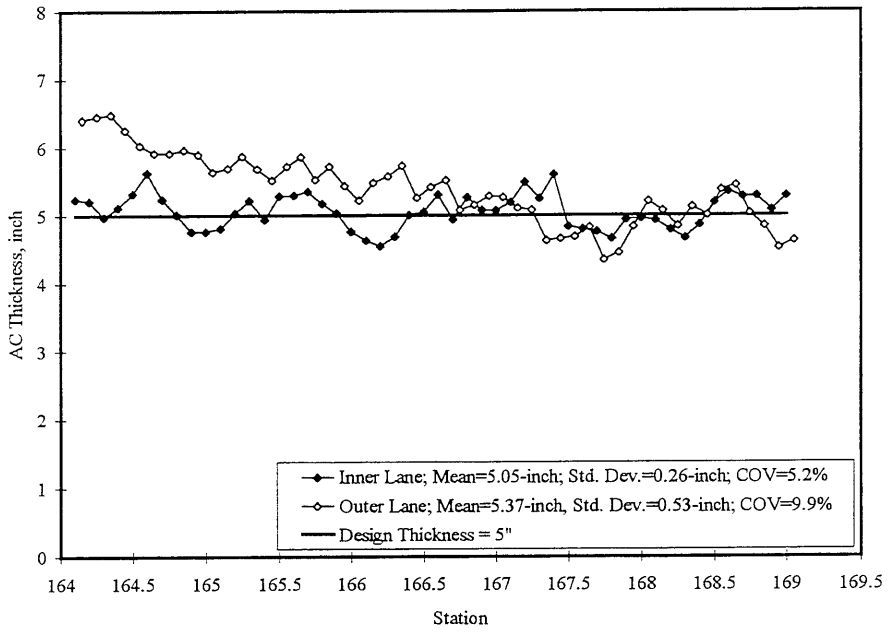

Figure 6.8. AC Thickness for Cell-25 from Ground Penetrating Radar

6.3 FWD Testing on the Mn/ROAD LVR Flexible Test Sections

FWD testing is periodically performed on the test sections to study the effect of loading and temperature on pavement deflections. Pavement surface deflections under the center of loading plate (D0), 12-inch from the load center (D1), 24-inch from the load center (D2), and 36-inch from the load center (D3), were used to backcalculate the pavement layer properties. The Illinois backcalculation algorithms were developed for 12-inch diameter loading plate, and 9000-lb load, thus Mn/ROAD data corresponding to the 12-inch diameter plate and 9000-lb were analyzed.

The algorithms developed from extensive ILLI-PAVE database [79] were used to backcalculate the stiffness of asphalt concrete (E_{AC}) and subgrade "breakpoint" modulus (E_{Ri}). The algorithms are as follows:

Conventional Flexible Pavements:

$$\text{Log } E_{AC} = 1.48 + 1.76 * \text{Log}(\text{AREA/D0}) + 0.26 * (\text{AREA}/T_{AC}) \quad \text{.....[6.1]}$$

$$R^2 = 0.95 \qquad \text{SEE} = 0.110$$

$$\text{Log } E_{Ri} = 1.51 - 0.19 * D3 + 0.27 * \text{Log}(D3) \quad \text{.....[6.2]}$$

$$R^2 = 0.99 \qquad \text{SEE} = 0.05$$

Full Depth Asphalt Concrete Pavements:

$$\text{Log } E_{AC} = 1.731 - 1.046 * \text{Log}(D0-D1) + 0.284 * (AREA/T_{AC}) + 0.393 * (D2/D3) + 0.012 * T_{AC} \quad \text{.....[6.3]}$$

$R^2 = 0.998$ SEE = 0.021

$$\text{Log } E_{Ri} = 24.7 - 5.41 * D3 + 0.31 * D3^2 \quad \text{.....[6.4]}$$

$R^2 = 0.98$ SEE = 0.64

Aggregate Surface / Surface Treated Pavements:

$$E_{Ri} = 24.2 - 5.71 * D3 + 0.35 * D3^2 \quad \text{.....[6.5]}$$

$R^2 = 0.98$ SEE = 0.57

where

E_{AC}	:	Asphalt concrete modulus, ksi;
E_{Ri}	:	Subgrade soil "breakpoint" resilient modulus, ksi;
T_{AC}	:	Asphalt concrete thickness, inch;
D0	:	Deflection at the center of loading plate, mils;
D1	:	Deflection at 12-inches from the center of loading plate, mils;
D2	:	Deflection at 24-inches from the center of loading plate, mils;
D3	:	Deflection at 36-inches from the center of loading plate, mils;
AREA	:	Deflection basin parameter, inches, and is calculated as $AREA = 6 * [D0 + 2 * D1 + 2 * D2 + D3] / D0$
R^2	:	Coefficient of Determination;
SEE	:	Standard Error of Estimate;

BELLS (an acronym for the authors Baltzer, Ertman-Larsen, Lukanen, and Stubstad) temperature [80] was used to study the variation of asphalt concrete modulus with temperature. BELLS temperature is the temperature at one-third depth of the asphalt concrete mat and is estimated based on the following parameters: asphalt concrete mat thickness, 5-day air temperature, infra-red temperature reading (at the asphalt concrete surface) at the time of FWD testing, and the time at which testing was performed. Stiffness of asphalt concrete obtained based on the temperature at

one-third depth corresponds to an asphalt concrete layer's equivalent stiffness [17]. The BELLS temperature equation is as follows [80]:

$$T_{1/3} = 8.77 + 0.649 * IR + \{\log(d) - 1.5\} * \{-0.503 * IR + 0.786 * (5\text{-day}) + 4.79 * \sin(hr-18)\} + \{\sin(hr-14)\} * \{2.20 + 0.044 * IR\} \quad \text{.....[6.6]}$$

where

$T_{1/3}$	:	Pavement temperature at third-point in asphalt concrete mat, °C;
IR	:	Infra-red temperature reading at the time of FWD test, °C;
log	:	Base 10 logarithm;
d	:	Depth at which mat temperature is to be determined, i.e. total asphalt concrete mat thickness divided by 3, mm;
5-day	:	Previous mean 5-day air temperature, sum of 5 highs and 5 lows divided by 10, °C;
sin	:	sin function in 24 hour clock system, with 2π radians equal to one 24-hour cycle.
hr	:	Time of the day, in 24 hour system. To use the time-hr function correctly, divide the number of hours in cycle by 24, multiply by 2π, and apply the sin function in radians.

Tables 6.1 through 6.10 summarize the backcalculated subgrade "breakpoint" modulus (E_{Ri}) values for Cell-26 through Cell-35. Each E_{Ri} value is an average of ten backcalculated values (ten FWD tests were conducted in one lane of a test section on a given day). The E_{Ri} values range from 5-ksi (during spring-thaw period) to 22-ksi (during winter when the subgrade is frozen). Coefficient of variation (COV) for the E_{Ri} values, for the conventional flexible test sections, ranged from 0.36-percent to 24-percent. Typically, higher COV values were observed for the lower E_{Ri} values. Figures 6.9 through 6.18 show the variation of E_{Ri} values throughout the year for the two different lanes in the test sections. The two lanes (inner and outer) generally showed similar E_{Ri} values except for Cell-29 and Cell-30. For Cell-29 (Figure 6.12), the outer lane showed higher E_{Ri} values (2.5-3 ksi) during the summer time. For Cell-30 (Figure 6.13), the E_{Ri} values for the outer lane were about 2-ksi higher than those for the inner lane during the summer time. For the surface

TABLE 6.1

Variation in Subgrade "Breakpoint" Modulus for Cell-26

	Inner Lane			Outer Lane		
Date	Subgrade "Breakpoint" Modulus, ksi	Standard Deviation, ksi	COV %	Subgrade "Breakpoint" Modulus, ksi	Standard Deviation, ksi	COV %
2/18/94	22	0.20	0.92	22	0.13	0.61
3/10/94	20	2.01	9.94	20	1.56	7.94
3/16/94	17	1.32	7.91	17	1.37	8.33
3/23/94	13	1.00	7.46	12	1.63	13.19
3/30/94	11	0.71	6.29	11	0.95	8.56
4/6/94	9	0.90	10.39	8	1.18	14.60
4/13/94	7	1.55	21.19	7	1.56	22.26
4/27/94	8	1.35	16.35	7	1.52	19.63
5/12/94	9	1.76	20.10	8	1.99	25.23
5/25/94	9	2.09	24.62	8	2.40	31.30
6/22/94	9	1.90	20.28	9	2.20	24.18
8/10/94	9	1.35	14.25	10	1.99	19.72
8/18/94	9	1.38	14.83	10	1.80	18.20
9/21/94	11	0.95	8.89	10	1.46	15.09
10/25/94	10	0.97	10.13	10	1.00	9.76

TABLE 6.2

Variation in Subgrade "Breakpoint" Modulus for Cell-27

	Inner Lane			Outer Lane		
Date	Subgrade "Breakpoint" Modulus, ksi	Standard Deviation, ksi	COV %	Subgrade "Breakpoint" Modulus, ksi	Standard Deviation, ksi	COV %
2/18/94	22	0.05	0.21	22	0.04	0.21
3/10/94	21	0.16	0.73	21	0.24	1.14
3/16/94	20	0.93	4.58	19	0.73	3.86
3/23/94	13	1.74	12.91	13	0.99	7.58
3/30/94	11	1.11	10.40	10	0.87	8.86
4/6/94	5	0.50	9.61	6	0.82	12.81
4/13/94	6	0.53	8.30	7	1.00	14.34
4/20/94	7	0.66	9.50	8	0.98	12.48
4/27/94	7	0.74	10.23	8	0.96	12.24
5/12/94	9	0.90	9.83	9	1.20	12.83
5/25/94	9	1.22	13.29	9	1.93	20.38
6/22/94	10	1.49	14.65	11	2.27	20.83
8/10/94	11	1.49	13.56	12	2.20	18.27
9/21/94	12	1.29	10.90	11	1.67	14.88
10/25/94	11	1.30	11.94	11	1.31	11.40

TABLE 6.3

Variation in Subgrade "Breakpoint" Modulus for Cell-28

	Inner Lane			Outer Lane		
Date	Subgrade "Breakpoint" Modulus, ksi	Standard Deviation, ksi	COV %	Subgrade "Breakpoint" Modulus, ksi	Standard Deviation, ksi	COV %
2/18/94	22	0.07	0.30	22	0.05	0.23
3/10/94	22	0.08	0.35	21	0.42	2.03
3/16/94	20	0.57	2.86	18	1.67	9.55
3/23/94	13	1.76	13.94	12	1.93	15.85
3/30/94	9	1.89	20.55	9	1.86	20.02
4/6/94	7	0.95	14.34	7	0.96	13.93
4/13/94	7	0.99	14.02	7	1.33	17.92
4/20/94	7	0.90	12.50	8	1.22	15.76
4/27/94	7	0.90	12.64	8	1.14	14.93
5/12/94	8	0.99	12.02	9	1.15	13.13
5/25/94	8	0.94	11.30	9	1.26	13.77
6/22/94	9	1.08	11.64	10	1.49	14.60
8/10/94	10	0.98	9.84	11	1.56	13.84
9/21/94	11	1.07	9.94	11	1.43	13.37
10/25/94	10	0.99	9.50	11	1.38	12.34

TABLE 6.4

Variation in Subgrade "Breakpoint" Modulus for Cell-29

	Inner Lane			Outer Lane		
Date	Subgrade "Breakpoint" Modulus, ksi	Standard Deviation, ksi	COV %	Subgrade "Breakpoint" Modulus, ksi	Standard Deviation, ksi	COV %
2/18/94	21	0.08	0.36	21	0.09	0.43
3/10/94	21	0.30	1.43	21	0.28	1.37
3/16/94	16	0.97	6.20	17	0.62	3.75
3/23/94	10	0.77	7.66	12	0.54	4.54
3/30/94	8	0.81	10.72	9	0.89	9.57
4/6/94	6	1.41	21.91	8	1.02	12.22
4/13/94	7	1.47	20.59	9	1.23	13.76
4/20/94	7	1.40	19.54	9	1.21	13.29
4/27/94	7	1.39	19.12	9	1.24	13.77
5/12/94	9	1.67	18.66	10	1.38	13.72
5/25/94	9	1.59	17.24	11	1.34	12.66
6/22/94	10	1.91	18.65	13	1.47	11.64
8/10/94	10	1.66	17.07	14	1.58	11.68
9/21/94	12	1.97	16.59	12	1.54	12.94
10/25/94	10	1.53	15.98	12	1.34	11.28

TABLE 6.5

Variation in Subgrade "Breakpoint" Modulus for Cell-30

	Inner Lane			Outer Lane		
Date	Subgrade "Breakpoint" Modulus, ksi	Standard Deviation, ksi	COV %	Subgrade "Breakpoint" Modulus, ksi	Standard Deviation, ksi	COV %
2/18/94	22	0.10	0.49	21	0.08	0.38
3/10/94	21	0.52	2.49	21	0.25	1.18
3/16/94	15	1.70	11.12	17	0.56	3.19
3/23/94	10	1.76	17.30	13	0.74	5.70
3/30/94	8	1.37	16.53	11	0.84	7.89
4/6/94	6	1.30	21.61	8	1.08	13.14
4/13/94	6	1.57	24.50	9	1.43	16.38
4/20/94	7	1.56	23.34	9	1.47	16.08
4/27/94	7	1.53	21.98	9	1.37	15.04
5/12/94	8	1.82	22.04	10	1.58	15.43
5/25/94	9	1.81	20.63	11	1.72	16.07
6/22/94	10	2.03	21.05	12	1.74	14.14
8/10/94	10	1.96	20.06	13	1.81	13.72
9/21/94	11	2.21	19.33	12	1.80	15.25
10/25/94	9	1.81	19.64	12	1.64	14.19

TABLE 6.6

Variation in Subgrade "Breakpoint" Modulus for Cell-31

	Inner Lane			Outer Lane		
Date	Subgrade "Breakpoint" Modulus, ksi	Standard Deviation, ksi	COV %	Subgrade "Breakpoint" Modulus, ksi	Standard Deviation, ksi	COV %
2/18/94	21	0.07	0.33	21	0.12	0.55
3/10/94	22	0.02	0.07	21	0.37	1.75
3/16/94	20	0.64	3.25	19	1.10	5.80
3/23/94	14	1.14	8.29	15	2.22	15.32
3/30/94	11	1.57	13.88	11	1.93	16.84
4/6/94	8	0.61	8.01	8	1.39	16.55
4/13/94	8	0.29	3.45	9	1.15	12.51
4/20/94	9	0.27	3.11	10	1.09	11.21
4/27/94	9	0.44	4.98	10	1.10	11.19
5/12/94	10	0.32	3.56	11	0.99	8.99
5/25/94	11	0.45	4.24	11	0.93	8.11
6/22/94	12	0.46	4.03	13	0.93	7.32
8/10/94	12	0.52	4.29	14	1.07	7.85
9/21/94	13	0.66	5.07	13	1.05	8.14
10/25/94	12	0.72	6.16	13	1.13	9.05

TABLE 6.7

Variation in Subgrade "Breakpoint" Modulus for Cell-32

	Inner Lane			Outer Lane		
Date	Subgrade "Breakpoint" Modulus, ksi	Standard Deviation, ksi	COV %	Subgrade "Breakpoint" Modulus, ksi	Standard Deviation, ksi	COV %
8/17/94	8	1.32	16.26	9	1.66	18.34
9/21/94	9	1.39	14.84	9	2.05	22.58
10/26/94	9	0.81	8.56	10	1.43	14.20

TABLE 6.8

Variation in Subgrade "Breakpoint" Modulus for Cell-33

	Inner Lane			Outer Lane		
Date	Subgrade "Breakpoint" Modulus, ksi	Standard Deviation, ksi	COV %	Subgrade "Breakpoint" Modulus, ksi	Standard Deviation, ksi	COV %
8/17/94	7	2.73	38.26	7	3.59	52.80
9/21/94	-	-	-	8	3.32	43.73
10/26/94	-	-	-	9	2.63	29.21

TABLE 6.9

Variation in Subgrade "Breakpoint" Modulus for Cell-34

	Inner Lane			Outer Lane		
Date	Subgrade "Breakpoint" Modulus, ksi	Standard Deviation, ksi	COV %	Subgrade "Breakpoint" Modulus, ksi	Standard Deviation, ksi	COV %
8/17/94	8	1.39	17.15	8	1.50	18.87
9/21/94	8	1.66	20.95	9	1.74	19.01
10/26/94	9	1.43	15.75	9	1.49	17.20

TABLE 6.10

Variation in Subgrade "Breakpoint" Modulus for Cell-35

	Inner Lane			Outer Lane		
Date	Subgrade "Breakpoint" Modulus, ksi	Standard Deviation, ksi	COV %	Subgrade "Breakpoint" Modulus, ksi	Standard Deviation, ksi	COV %
8/17/94	9	1.72	18.21	-	-	-
9/21/94	10	1.73	17.71	-	-	-
10/26/94	10	1.43	14.21	11	1.05	9.83

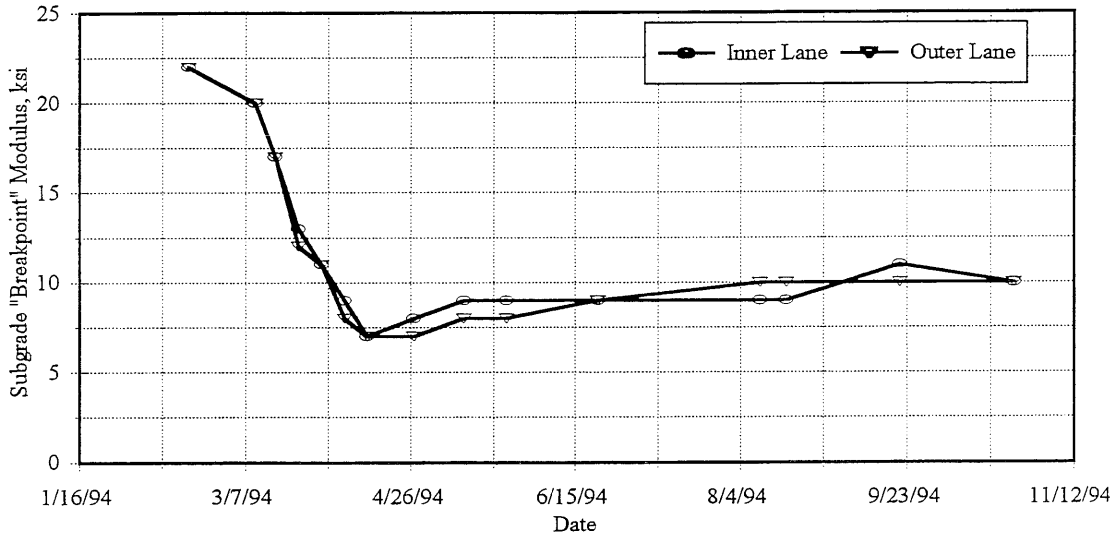

Figure 6.9. Variation in Subgrade "Breakpoint" Modulus for Cell-26

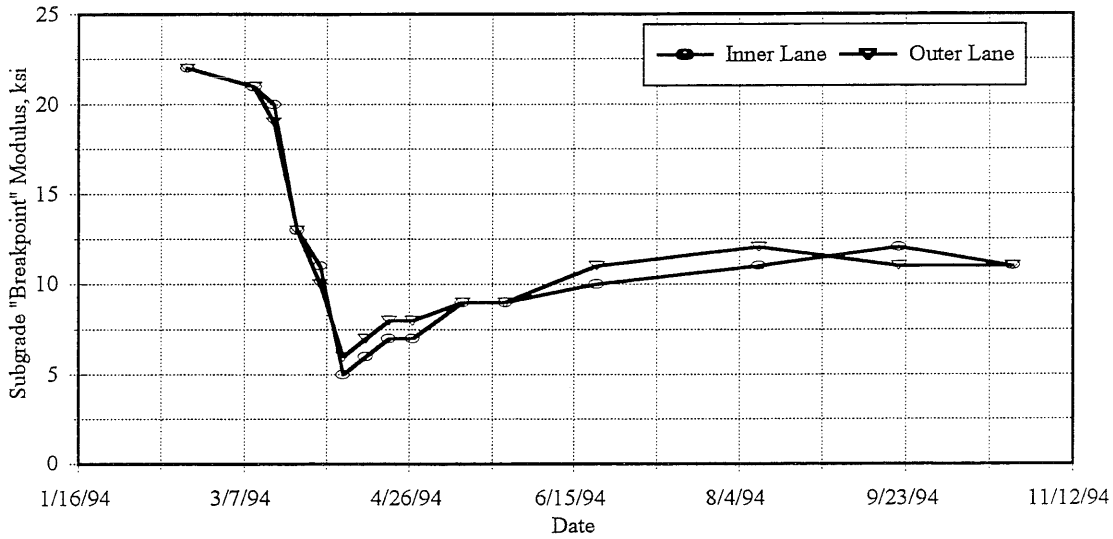

Figure 6.10. Variation in Subgrade "Breakpoint" Modulus for Cell-27

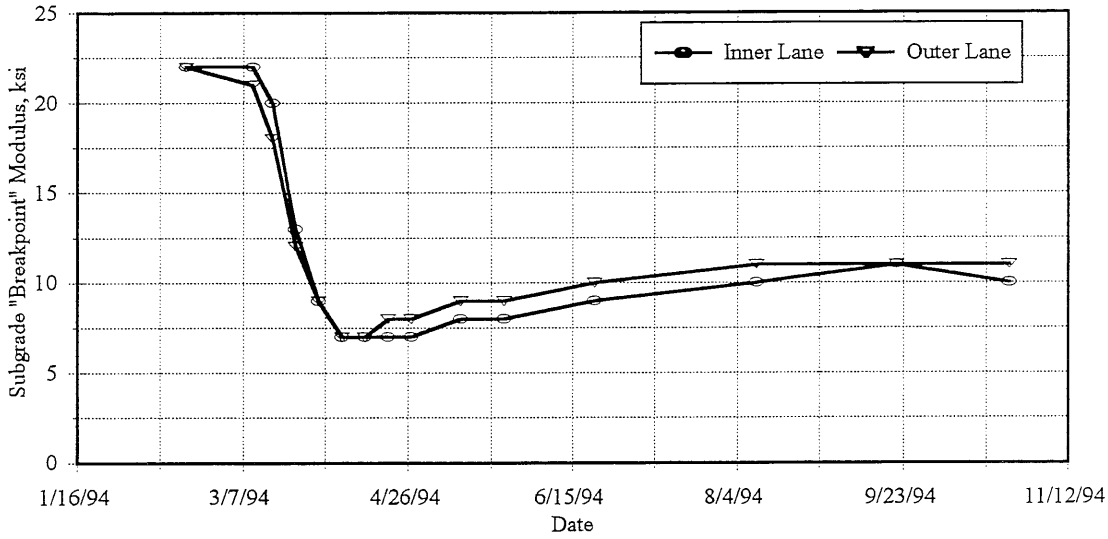

Figure 6.11. Variation in Subgrade "Breakpoint" Modulus for Cell-28

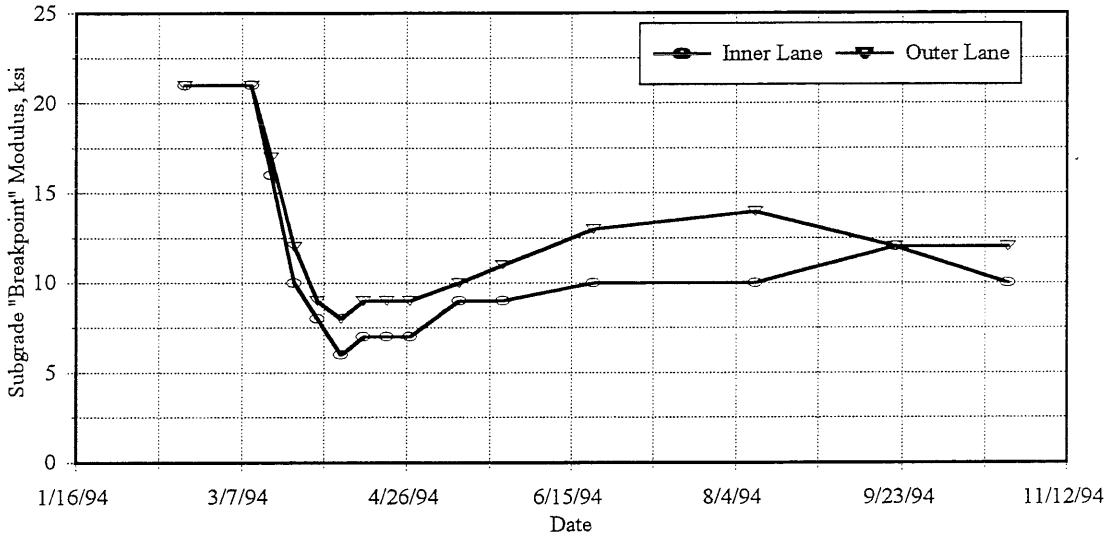

Figure 6.12. Variation in Subgrade "Breakpoint" Modulus for Cell-29

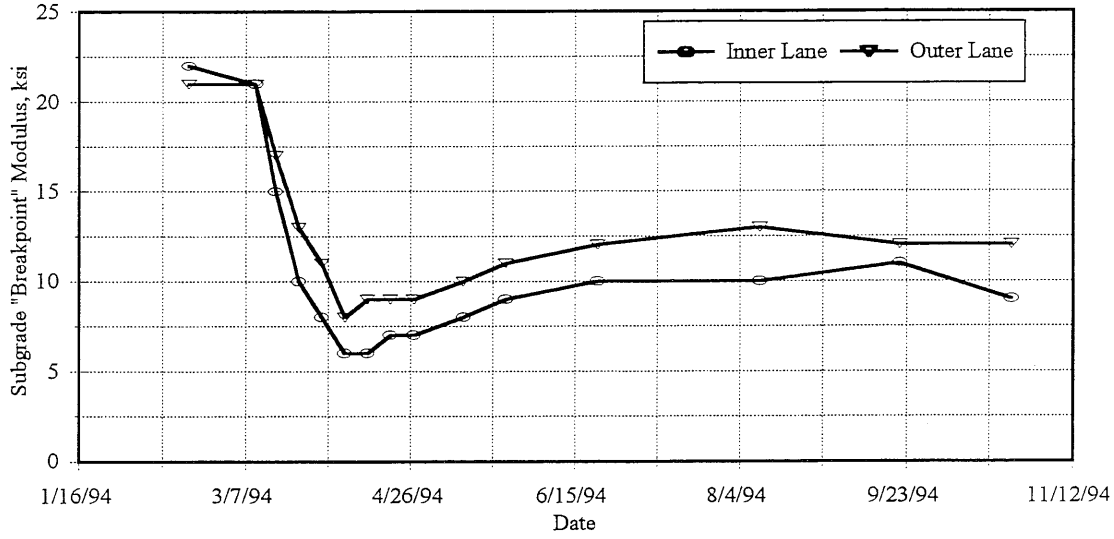

Figure 6.13. Variation in Subgrade "Breakpoint" Modulus for Cell-30

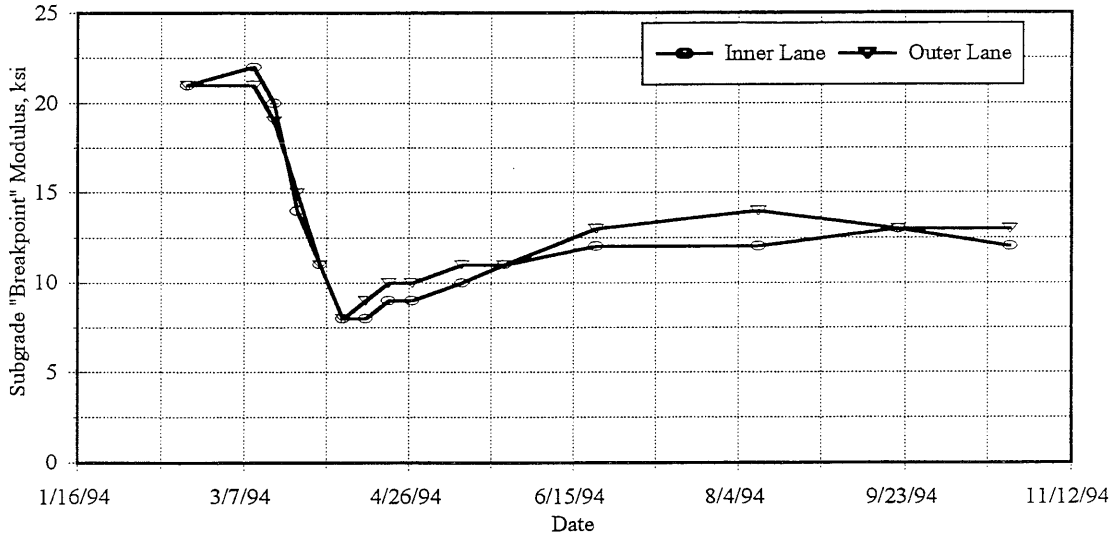

Figure 6.14. Variation in Subgrade "Breakpoint" Modulus for Cell-31

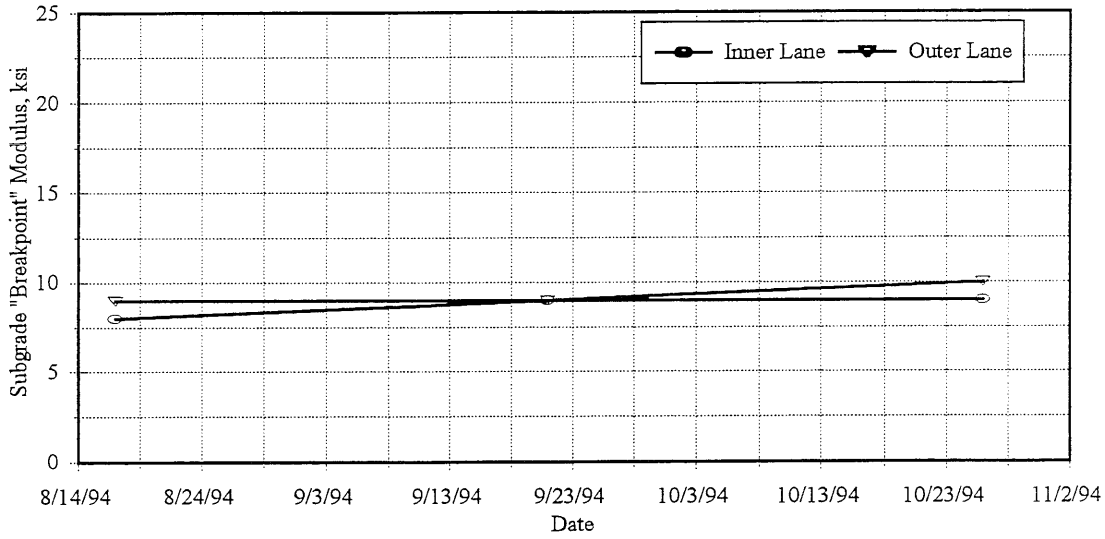

Figure 6.15. Variation in Subgrade "Breakpoint" Modulus for Cell-32

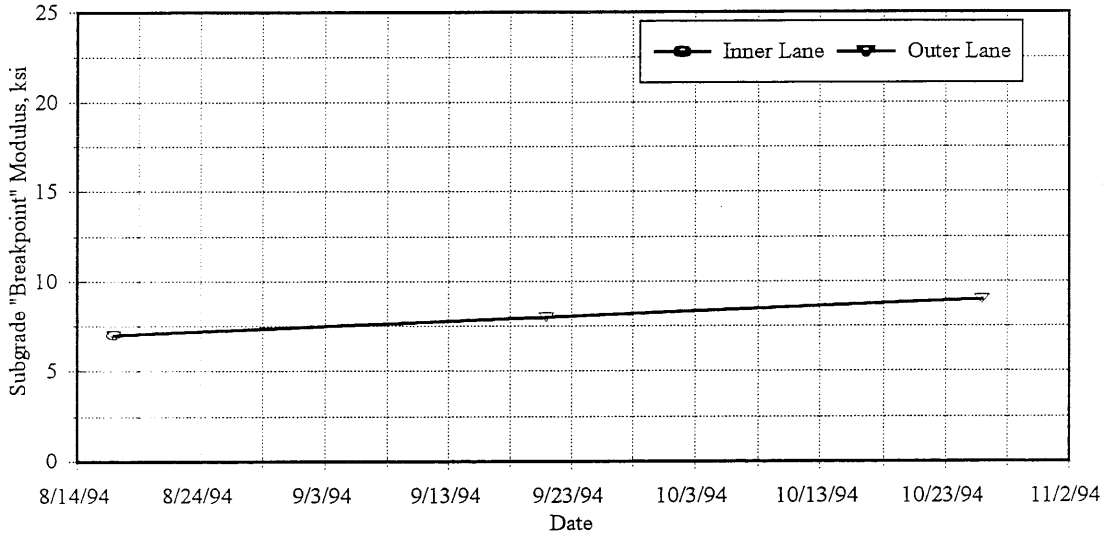

Figure 6.16. Variation in Subgrade "Breakpoint" Modulus for Cell-33

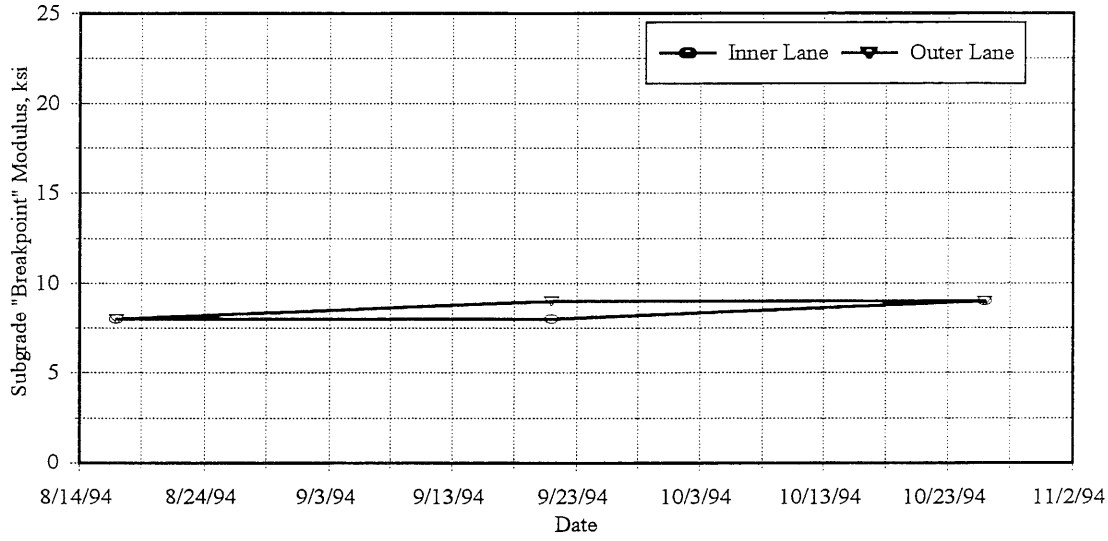

Figure 6.17. Variation in Subgrade "Breakpoint" Modulus for Cell-34

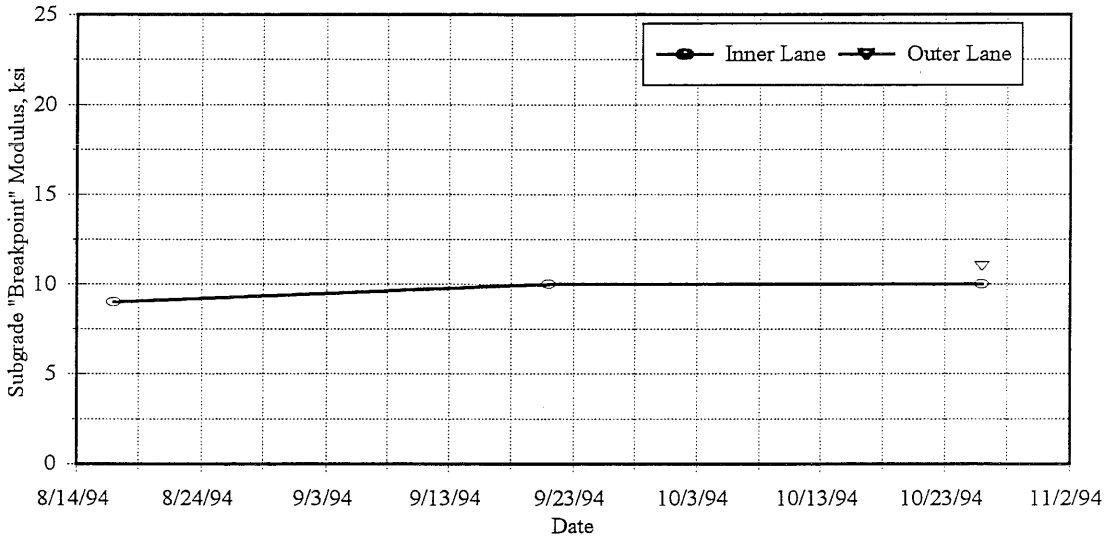

Figure 6.18. Variation in Subgrade "Breakpoint" Modulus for Cell-35

treated/aggregate surface test sections (Figures 6.15 through 6.18), similar values were observed in both the lanes. The E_{Ri} values ranged from 7 to 10-ksi. Figures 6.19 and 6.20 give a comparison of E_{Ri} values for the inner lane and outer lane respectively. All the test sections (except Cell-31) show similar E_{Ri} values. Cell-31 showed slightly higher E_{Ri} during the summer time. Figure 6.21 gives a comparison of E_{Ri} values for the surface treated/aggregate test sections.

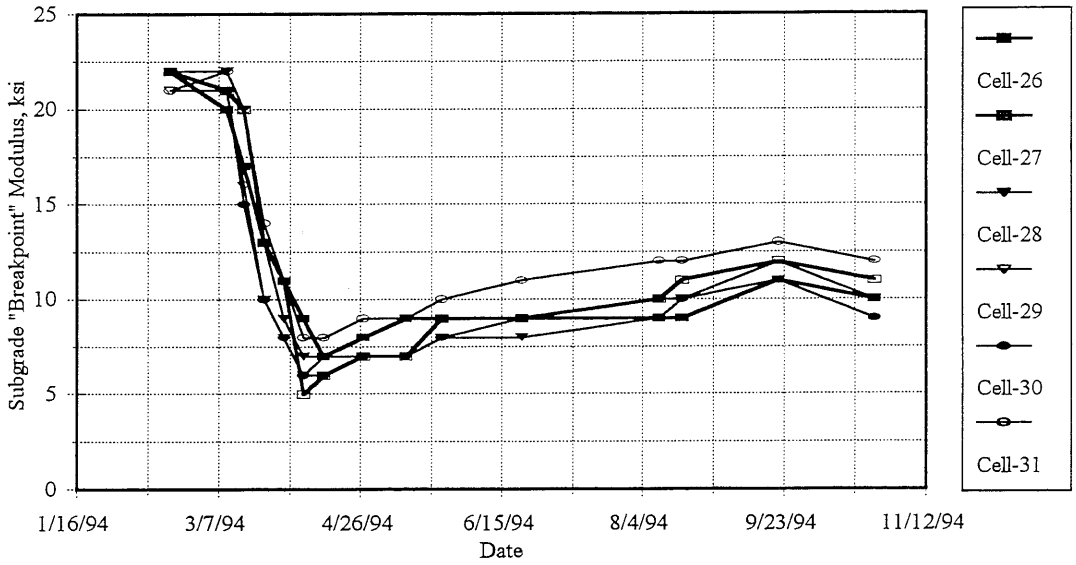

Figure 6.19. Subgrade "Breakpoint" Modulus for Inner Lane (80,000 lb Lane)

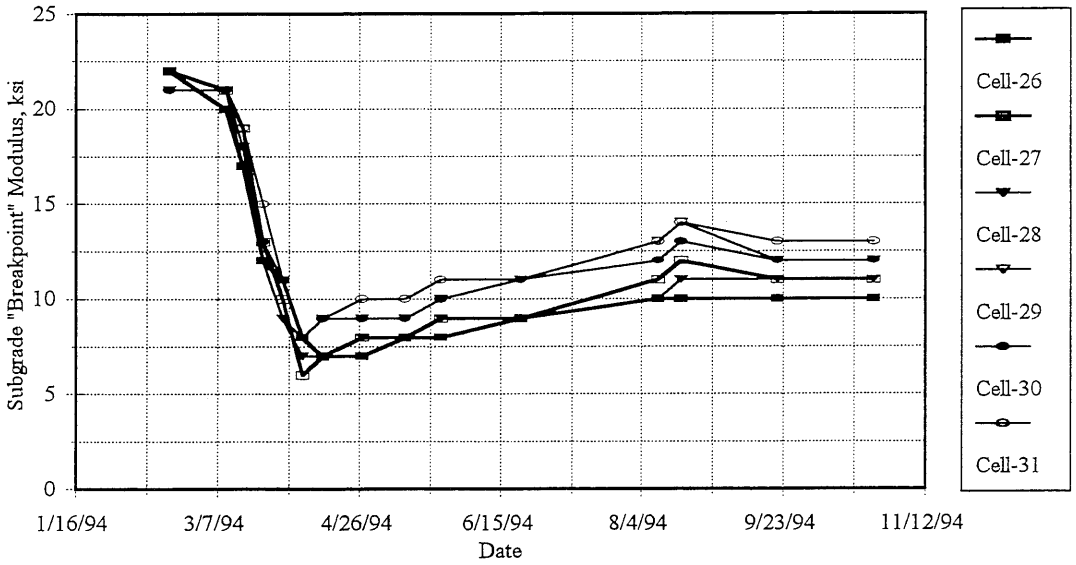

Figure 6.20. Subgrade "Breakpoint" Modulus for Outer Lane (102,500 lb Lane)

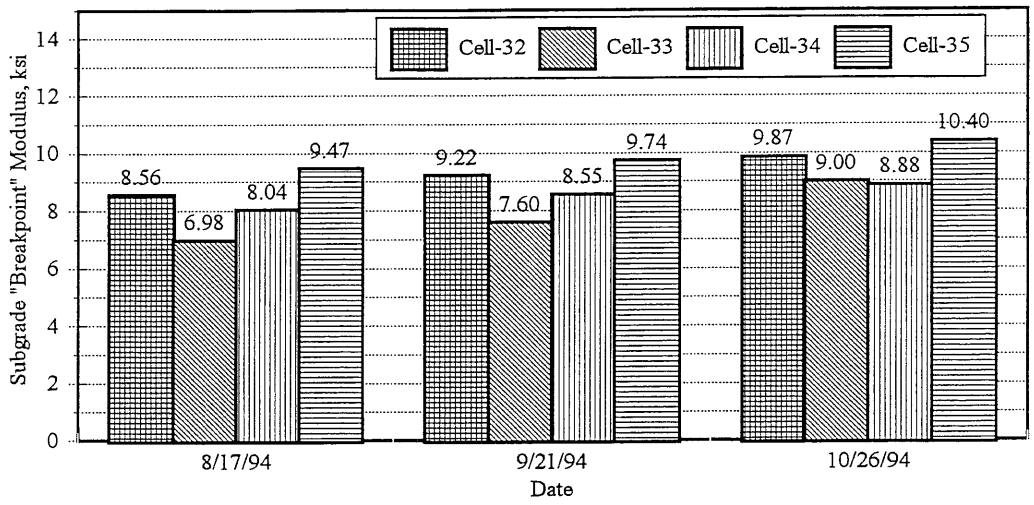

Figure 6.21. Subgrade "Breakpoint" Modulus for Surface Treated/Aggregate Test Sections

Figures 6.22 through 6.27 show the variation in asphalt concrete modulus throughout the year.

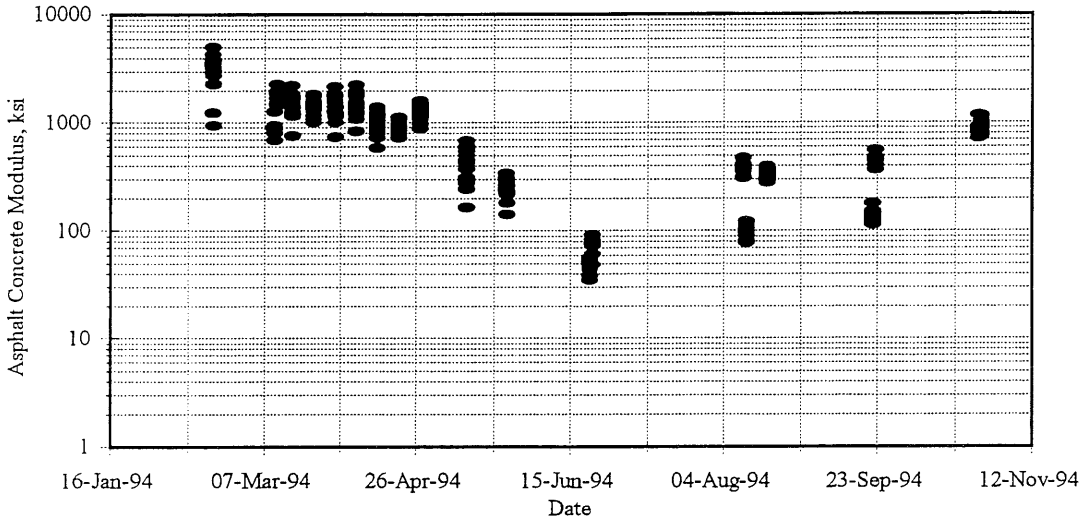

Figure 6.22. Variation in Asphalt Concrete Stiffness for Cell-26

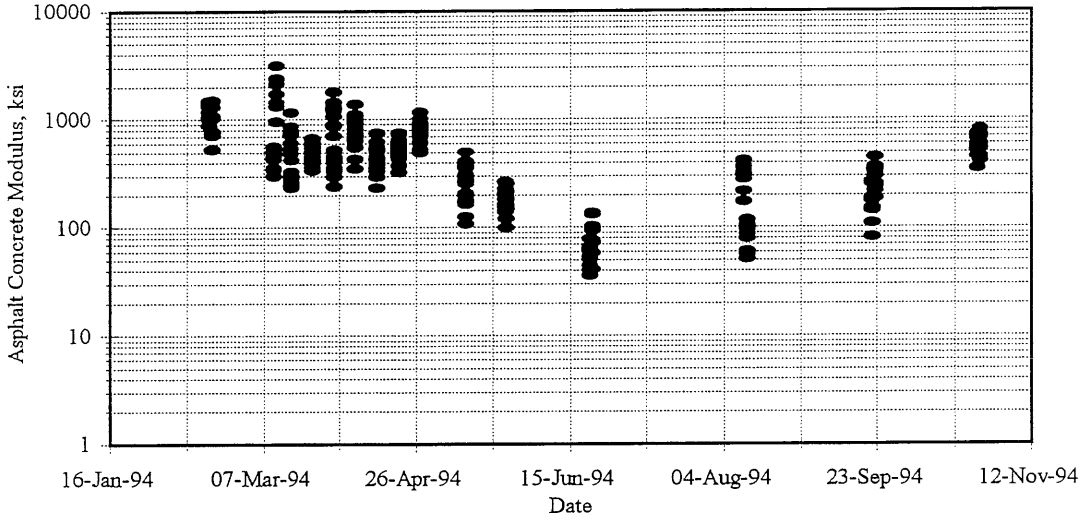

Figure 6.23. Variation in Asphalt Concrete Stiffness for Cell-27

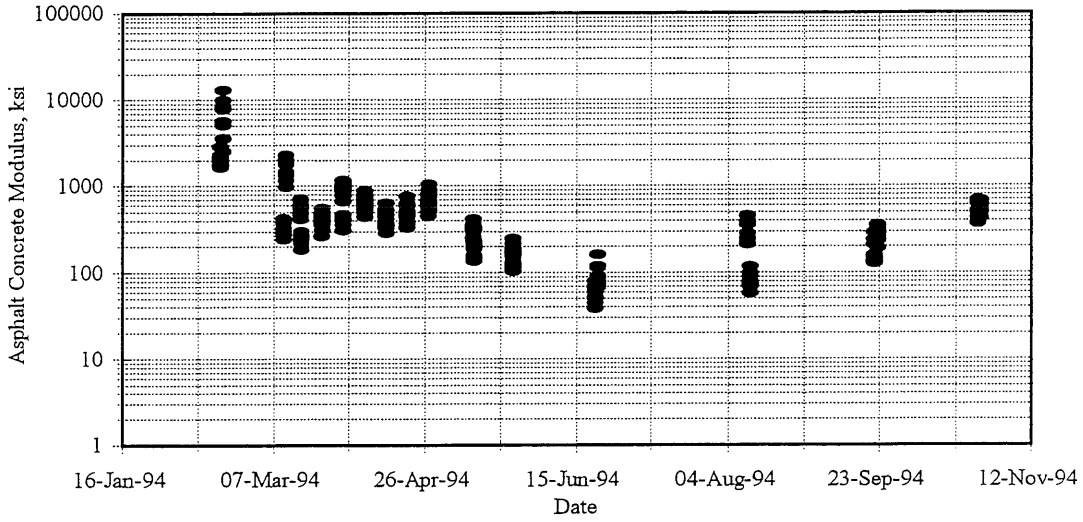

Figure 6.24. Variation in Asphalt Concrete Stiffness for Cell-28

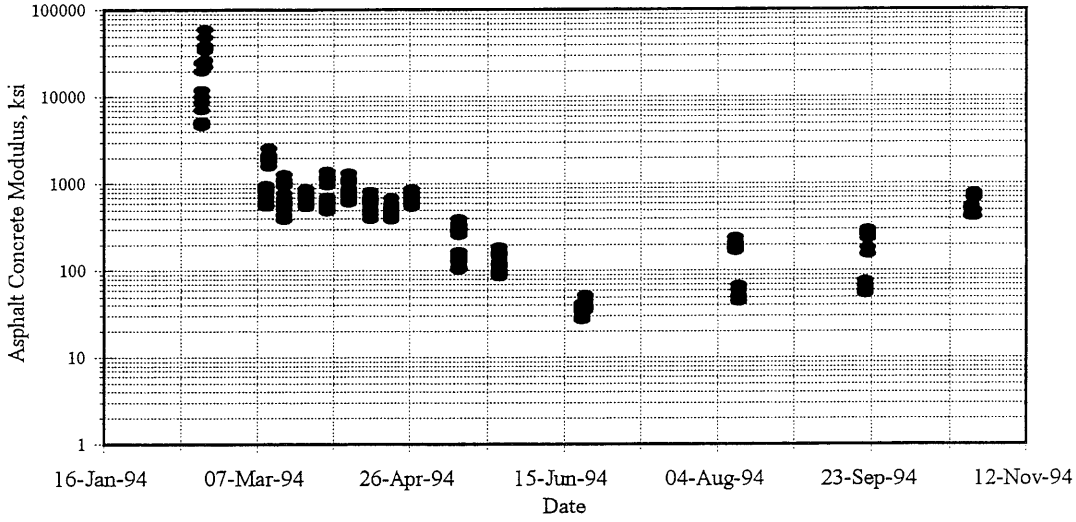

Figure 6.25. Variation in Asphalt Concrete Stiffness for Cell-29

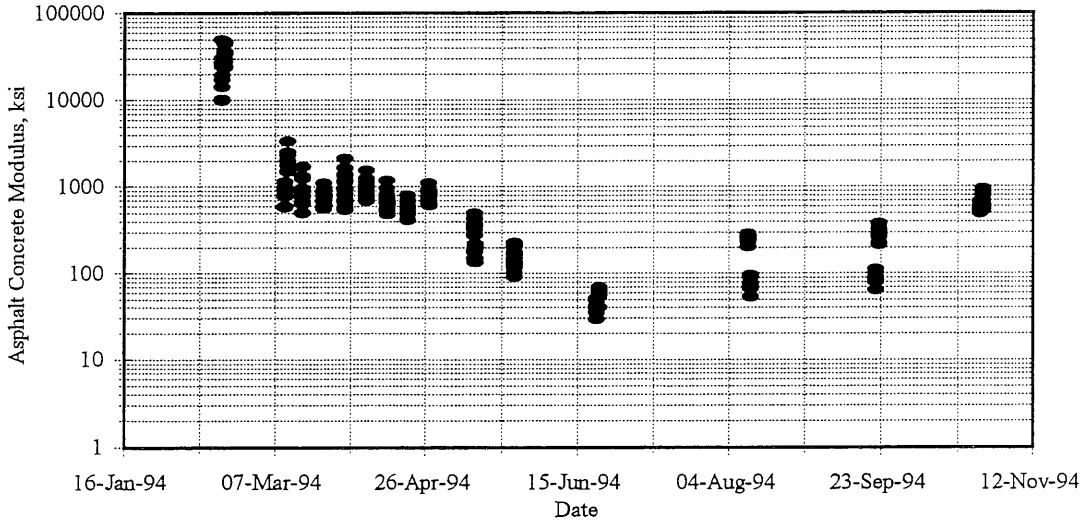

Figure 6.26. Variation in Asphalt Concrete Stiffness for Cell-30

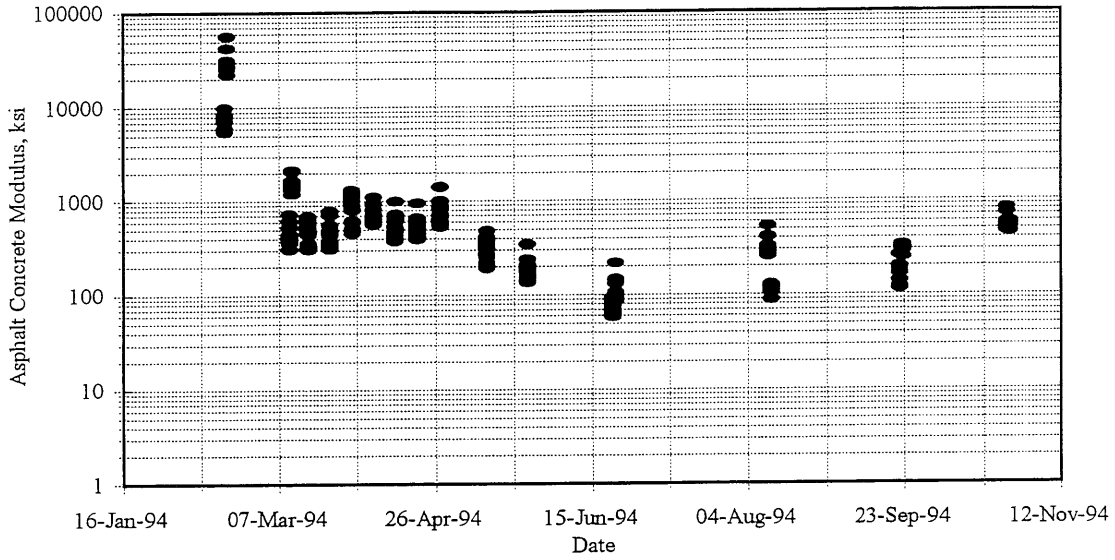

Figure 6.27. Variation in Asphalt Concrete Stiffness for Cell-31

Using the backcalculated asphalt concrete modulus results from thicker sections (Cell-26, Cell-29, Cell-30), the following relationship was established between asphalt concrete modulus and temperature:

$$\text{Log } E_{AC} = 3.3804 - 0.04771 * T \quad \text{.....[6.7]}$$

No. of observations = 755

$R^2 = 0.89$ SEE = 0.146

where

E_{AC} : Asphalt concrete modulus, ksi;

T : Temperature, degree Centigrade;

The relationship between the backcalculated asphalt concrete modulus and temperature is shown in Figure 6.28.

Only one asphalt cement (120/150 penetration grade) was used in the LVR test sections. The physical properties of asphalt cement are given in Table 6.11 [81]. Three Marshall mix designs

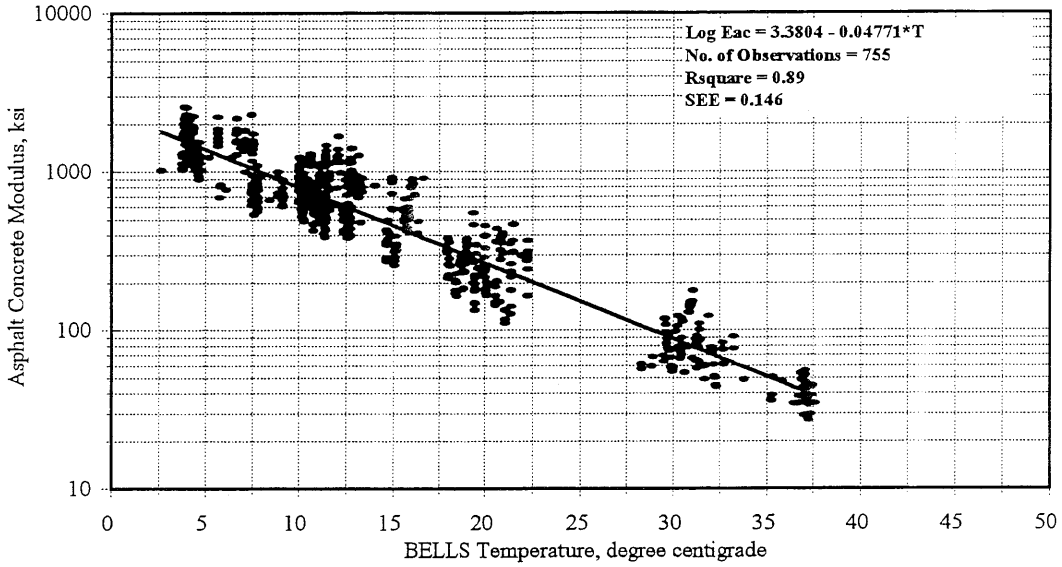

Figure 6.28. Variation in Asphalt Concrete Stiffness with Temperature

TABLE 6.11

Physical Properties of Asphalt Cement Used in LVR Test Sections

Property	Koch 120/150 Penetration Grade
Viscosity, 60 deg. C (140 F), Poise	846
Viscosity, 135 deg. C (275 F), cSt	271
Penetration, 25 deg. C (77 F), 0.1 mm	130
Ductility, 25 deg. C (77 F), 5 cm/mm	120+
Flash Point, deg. C (deg. F) min.	318 (605)
Tests on Residue from Thin Film Oven Test	
Viscosity, 60 deg. C (140 F), Poise	1880
Viscosity, 135 deg. C (275 F), cSt	439
Penetration, 25 deg. C (77 F), 0.1 mm	71
Ductility, 25 deg. C (77 F), 5 cm/mm	120+
SUPERPAVE (SHRP) Binder Specifications	
PG Grading	PG 58-28

were used in the test sections. For Cells 24 and 27, the 35-blow mix design was used. Fifty blow mix design was used in Cells 25, 26, 28, and 29. In Cells 30 and 31, 75-blow mix design was used. Marshall mix design results as reported by Mn/DOT are given in Table 6.12.

TABLE 6.12
Marshall Mix Design Results (Reported by Mn/DOT)

Asphalt Content *	Air Voids %	VMA %	VFA %	Marshall Stability, lb	Marshall Flow (0.01 in.)	Density lb./cu.ft.
			35 Blow Mix Design			
5.0	8.0	18.0	55.4	966	10	142.0
5.5	6.6	17.7	62.8	941	10	143.2
6.0	5.0	17.4	71.3	1085	11	144.5
6.5	3.7	17.4	78.7	1092	10	145.3
			50 Blow Mix Design			
5.0	7.1	17.2	28.6	1278	11	143.4
5.5	6.2	17.2	64.0	1166	10	144.0
6.0	4.3	16.8	74.4	1236	9	145.5
6.5	3.0	16.8	82.2	1216	9	146.3
			75 Blow Mix Design			
5.0	6.5	16.6	60.9	1462	10	144.3
5.5	5.4	16.5	67.2	1573	9	145.4
6.0	4.0	16.6	75.9	1480	10	146.0
6.5	2.3	16.2	85.8	1523	10	147.4

* Percent by weight of mixture

The optimum asphalt content was selected as the percentage that would produce 4-percent air voids. The optimum binder contents were selected as 6.4, 6.1, and 5.9 percent by weight of the total mix for the 35, 50, and 75 blow mix designs, respectively. Asphalt concrete mixes and cores were tested in laboratory to determine the physical properties of the mixes. The results from the laboratory testing are given in the report titled "Investigation of Hot Mix Asphalt Mixtures at Mn/ROAD - Final Report" prepared by Gardiner et. al. [81] at the University of Minnesota. Resilient modulus tests (ASTM D4123) and dynamic modulus tests were performed to study the

temperature susceptibility of the asphalt concrete mixes. The test results showed that the three mixes showed similar behavior. The results from the laboratory testing are shown in Appendix-A. For the Dynatest Model 8000 FWD equipment, the pulse duration is 25-33 milliseconds (frequency of 15-20 Hz). Figure 6.29 shows the modulus - temperature relationship obtained from Asphalt Institute equation (Table 2.1) (frequencies of 1 Hz and 15 Hz) and from backcalculation algorithms.

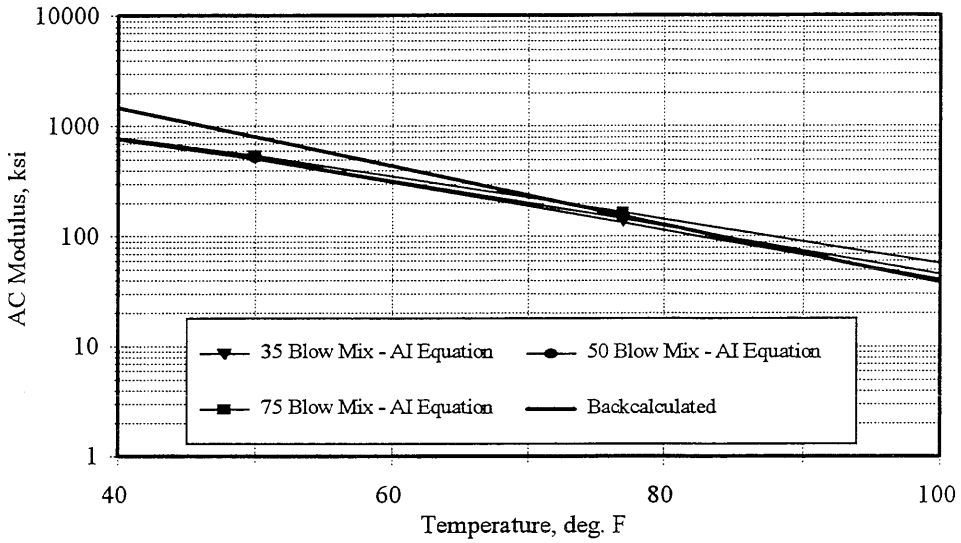

Figure 6.29. AC Stiffness from Backcalculation Algorithm and Asphalt Institute Equation

6.4 Measured Pavement Responses from FWD Testing

The Dynatest Model 8000 FWD equipment was used at Mn/ROAD for non-destructive testing. The testing pattern for each section consisted of ten test points spaced at 50-feet intervals with four longitudinal offsets from the centerline (-9.5-feet - outer wheel track westbound lane, -6.25-feet - between wheel tracks westbound lane, +6.25-feet - between wheel tracks eastbound lane, +9.5-feet - outer wheel track eastbound lane) tested. Pavement surface deflections under the center of loading plate (D0), 12 inches from the load center (D1), 24 inches from the load center (D2), and 36 inches from the load center (D3) were recorded. FWD test dates were selected to cover the entire range of pavement climatic conditions.

Based on extensive ILLI-PAVE database (unpublished report by Hill and Thompson), Area Under Pavement Profile (AUPP) was correlated to the asphalt concrete strain values for full-depth asphalt concrete pavements. AUPP is defined as follows (Figure 6.30):

$$AUPP = (5*D0 - 2*D1 - 2*D2 - D3) / 2 \quad \text{.....[6.8]}$$

where

D0 : Deflection at the center of loading plate, mils;

D1 : Deflection at 12-inches from the center of loading plate, mils;

D2 : Deflection at 24-inches from the center of loading plate, mils;

D3 : Deflection at 36-inches from the center of loading plate, mils;

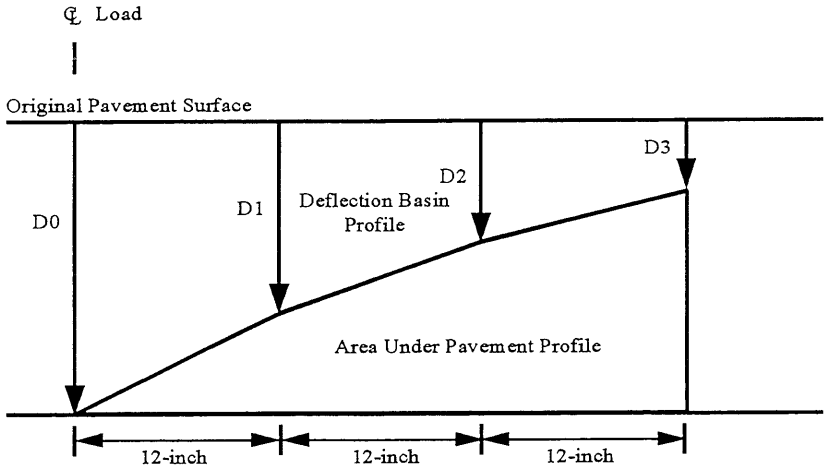

AUPP = (Area Under Pavement Profile) / 12
= (5*D0 - 2*D1 - 2*D2 - D3) / 2

Figure 6.30. Area Under Pavement Profile (AUPP)

The relationship established by Hill and Thompson is as follows:

$$\text{Log}(\varepsilon_{ac}) = 1.001 + 1.024 * \text{Log}(AUPP) \quad \text{.....[6.9]}$$

$R^2 = 0.997$ SEE = 0.025

where ε_{ac} is strain (microstrain) at the bottom of asphalt concrete layer. The relationship was developed from a database in which asphalt concrete thicknesses ranged from 9.5 to 14 inches, asphalt concrete modulus ranged from 100-ksi to 1100-ksi and E_{Ri} ranged from 1-ksi to 12.3-ksi.

For the conventional flexible pavements, the IDOT algorithm relating AUPP to asphalt concrete strain is as follows:

$$\text{Log}(\varepsilon_{ac}) = 1.2105 + 0.821 * \text{Log}(\text{AUPP}) \quad \text{.....[6.10]}$$

$$R^2 = 0.973 \qquad SEE = 0.0579$$

where ε_{ac} is strain (microstrain) at the bottom of asphalt concrete layer. The relationship was developed from an ILLI-PAVE database in which asphalt concrete thicknesses ranged from 3 to 8 inches, asphalt concrete modulus ranged from 100-ksi to 1400-ksi and E_{Ri} ranged from 1-ksi to 12.3-ksi.

The study by Hill and Thompson (unpublished report) and this study (described in detail in Chapter 7) showed that AUPP is a powerful geometrical property of pavement deflection basin that can be used to predict asphalt concrete strains fairly accurately. Further analyses on Mn/ROAD FWD data showed that AUPP is primarily controlled by the peak center deflection D0. The results are summarized in Table 6.13 and Figure 6.31.

Table 6.13.
AUPP-D0 Algorithms for Mn/ROAD LVR Test Sections

Test Section	AC Thickness inch	Granular Base Type	Granular Base Thickness, inch	AUPP Algorithm	R^2
24	3	CL-6sp	4	AUPP = 1.665 * D0	0.90
27	3	CL-6sp	11	AUPP = 1.621 * D0	0.92
28	3	CL-5sp	13	AUPP = 1.631 * D0	0.93
31	3	CL-5sp/CL-3sp	16	AUPP = 1.627 * D0	0.93
All 3-inch				**AUPP = 1.6312 * D0**	**0.93**
29	5	CL-4sp	10	AUPP = 1.5078 * D0	0.91
30	5	CL-3sp	12	AUPP = 1.4563 * D0	0.90
All 5-inch				**AUPP = 1.4843 * D0**	**0.90**

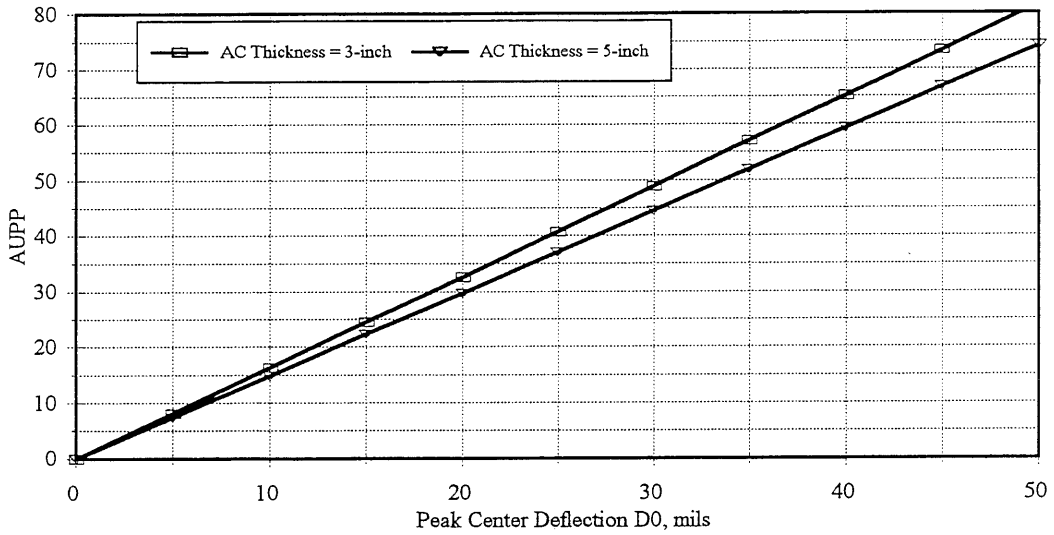

Figure 6.31. AUPP-D0 Relationship for Mn/ROAD LVR Test Sections

6.5 Effect of Granular Material Quality on Pavement Response

Mn/ROAD LVR test sections include six conventional flexible pavements, two full-depth asphalt concrete pavements, and four surface-treated/aggregate-surface pavements. The conventional flexible pavements have 5-inch and 3-inch thick asphalt concrete surfaces with varying granular base quality and thickness. Analyses were performed on the Mn/ROAD project FWD data for the conventional flexible pavements (with cohesive subgrade) and the surface-treated/aggregate-surface pavements to study the effect of granular material quality on the pavement deflection response. The cross-sections for the conventional flexible pavements and for the surface-treated/aggregate-surface pavements are given in Figure 1.3.

The pavement deflection response, in the case of a conventional flexible pavement, is affected by the stiffness and thickness of asphalt concrete, thickness and quality of granular base, and the stiffness of the subgrade soil. When comparing two conventional flexible pavements with the same asphalt concrete thickness, if the deflections for two pavements are normalized for the same asphalt concrete stiffness and the same subgrade stiffness, the difference in the deflection response is a function of granular base thickness and quality.

In the case of surface treated/aggregate surface pavements, the pavement deflection response is affected by the thickness and quality of the granular base, and the stiffness of the subgrade. The surface treatment is generally not considered as a structural component. When comparing two surface treated/aggregate surface pavements with the same granular base thickness, if the deflections for two pavements are normalized for the same subgrade stiffness, the difference in the deflection response is a function of granular base quality. Mn/ROAD FWD data were analyzed to study the effect of granular material quality on the pavement deflection response.

Conventional Flexible Pavements:

For 3-inch asphalt concrete surface, Cells 27, 28 and 31 were compared. For 5-inch asphalt concrete surface, Cells 29 and 30 were compared. The FWD data were used to backcalculate the asphalt concrete moduli and subgrade "breakpoint" moduli values using the algorithms developed at the University of Illinois (equations 6.1 and 6.2 respectively). The asphalt concrete modulus and temperature relation (equation 6.7) was utilized.

Mean values for measured surface deflections (D0), pavement temperature at one-third depth, and subgrade "breakpoint" modulus (E_{Ri}), were evaluated for each of the test sections for different test dates. Asphalt concrete stiffness were evaluated using equation 6.7. To normalize the surface deflections to benchmark asphalt concrete stiffness and subgrade stiffness, a correction factor (or adjustment factor) needs to be established. When this adjustment factor is applied to the field measured surface deflection values, the adjusted surface deflection values will correspond to the benchmark asphalt concrete and subgrade stiffness. The adjusted surface deflections can then be compared to evaluate the effect of granular base thickness and quality on the pavement response. Based on extensive ILLI-PAVE database, Thompson & Elliot [73] developed an algorithm to predict pavement surface deflection (D0) as a function of asphalt concrete thickness and stiffness, granular base thickness, and subgrade "breakpoint" modulus. The algorithm is:

$$\text{Log } D0 = 1.9692 + 0.0465 * T_{AC} - 0.5637 * (\text{Log } T_{bse})/T_{AC} - 0.0464 * (\text{Log } E_{AC}) * T_{AC} - 0.2079 * (\text{Log } E_{Ri}) \quad \text{.....[6.11]}$$

$R^2 = 0.974$ SEE = 0.04586

where

E_{AC} : Asphalt concrete modulus, ksi;

T_{AC} : asphalt concrete thickness, inch;

T_{bse} : Granular base thickness, inch;

E_{Ri} : Subgrade "breakpoint" modulus, ksi; and

D0 : FWD deflection at the center of loading plate, mils;

Equation 6.11 was used to establish the adjustment factor to be applied to the measured surface deflections. The peak center deflections (D0), for various test sections were evaluated using equation 6.11 from the backcalculated asphalt concrete modulus and subgrade E_{Ri}. This estimated surface deflection is D0′. Use equation 6.11 again to estimate the surface deflection for the mean (benchmark) asphalt concrete and subgrade stiffness. This estimated surface deflection is D″. The adjustment factor is the ratio of D0′ and D″:

$$\text{Adjustment Factor} = D0' / D'' \quad \text{.....[6.12]}$$

where

D0′ : Estimated D0 from backcalculated asphalt concrete and subgrade stiffness; and

D″ : Estimated D0 from mean (benchmark) asphalt concrete and subgrade stiffness.

The field measured deflections (D0's) were adjusted to the bench mark asphalt concrete stiffness and subgrade stiffness using the adjustment factors. The adjusted D0's were obtained as:

$$\text{Adjusted D0} = \text{Field Measured D0} / \text{Adjustment Factor} \quad \text{.....[6.13]}$$

Table 6.14 gives the adjusted D0 values along with the adjustment factors for Cells 27, 28, and 31 (test sections with asphalt concrete thickness = 3-inch).

TABLE 6.14

Adjusted Surface Deflections for Test Sections with AC Thickness = 3-inch

Date	Cell No.	Granular Base Thickness, inch	Measured D0, mils	Std. Dev. for Measured D0, mils	Adjustment Factor	Adjusted D0, mils
03-23-94	27	11	25.93	3.55	0.978	26.52
(981, 12.0)	28	13	28.40	3.23	1.019	27.88
	31	16	23.26	1.84	0.955	24.34
04-06-94	27	11	31.06	3.84	1.087	28.58
(771, 6.4)	28	13	29.47	2.39	1.022	28.83
	31	16	24.82	1.31	0.949	26.14
04-20-94	27	11	29.81	3.41	1.011	29.48
(610, 7.4)	28	13	29.28	1.93	1.011	28.95
	31	16	24.86	1.16	0.955	26.04
05-25-94	27	11	34.02	2.52	1.009	33.71
(249, 9.2)	28	13	35.13	2.05	1.027	34.19
	31	16	28.36	1.34	0.947	29.93
06-22-94	27	11	38.76	3.44	1.052	36.86
(80, 10.2)	28	13	38.40	2.33	1.042	36.87
	31	16	30.30	1.24	0.946	32.04
08-10-94	27	11	27.16	2.61	0.999	27.19
(255, 10.5)	28	13	28.70	2.13	1.027	27.93
	31	16	24.51	0.98	0.961	25.51
09-21-94	27	11	30.09	2.42	1.009	29.81
(74, 11.8)	28	13	31.28	2.35	1.021	30.65
	31	16	27.95	1.08	0.993	28.15
10-25-94	27	11	23.48	2.13	1.004	23.38
(398, 10.4)	28	13	24.95	2.05	1.009	24.73
	31	16	22.50	1.03	0.970	23.20

Note: Values in paranthesis in the date column represent mean asphalt concrete stiffness (ksi) and mean subgrade "breakpoint" modulus (ksi), to which the deflections were adjusted.

Figure 6.32 shows the comparison between the adjusted D0's for Cells 27, 28, and 31.

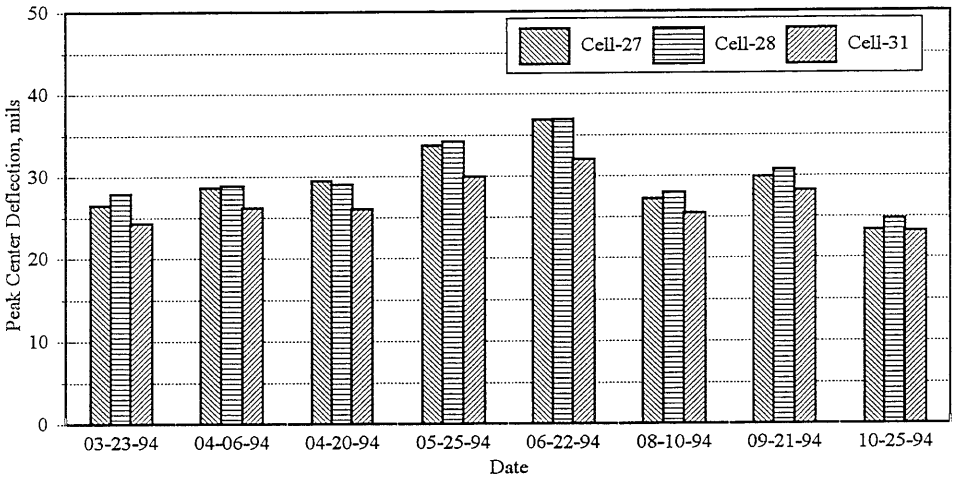

Figure 6.32. Adjusted Pavement Deflection Response (D0) for Test Sections with 3-inch Thick Asphalt Concrete Surface

Table 6.15 gives the adjusted D0 values along with the adjustment factors for Cells 29, and 30 (test sections with asphalt concrete thickness = 5-inch). Figure 6.33 shows the comparison between the adjusted D0's for Cells 29, and 30.

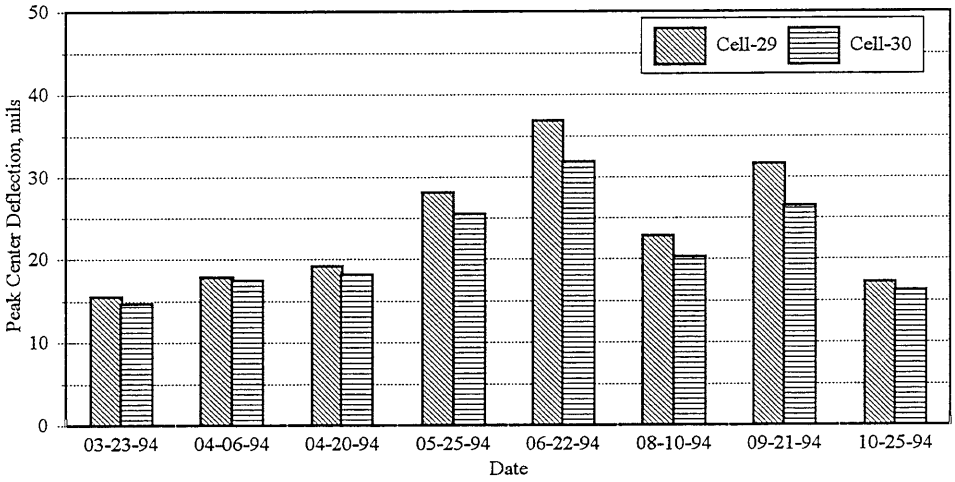

Figure 6.33. Adjusted Pavement Deflection Response (D0) for Test Sections with 5-inch Thick Asphalt Concrete Surface

TABLE 6.15

Adjusted Surface Deflections for Test Sections with AC Thickness = 5-inch

Date	Cell No.	Granular Base Thickness, inch	Measured D0, mils	Std. Dev. for Measured D0, mils	Adjustment Factor	Adjusted D0, mils
03-23-94	29	10	16.03	1.68	1.033	15.52
(981, 12.0)	30	12	15.00	1.75	1.018	14.73
04-06-94	29	10	17.34	1.96	0.973	17.83
(771, 6.4)	30	12	16.55	1.68	0.947	17.47
04-20-94	29	10	19.43	2.07	1.011	19.23
(610, 7.4)	30	12	18.54	2.02	1.020	18.18
05-25-94	29	10	28.42	2.69	1.012	28.09
(249, 9.2)	30	12	25.95	3.24	1.017	25.52
06-22-94	29	10	36.09	3.02	0.980	36.84
(80, 10.2)	30	12	30.54	3.70	0.960	31.80
08-10-94	29	10	23.02	2.35	1.008	22.83
(255, 10.5)	30	12	20.33	2.00	1.000	20.32
09-21-94	29	10	30.54	2.87	0.967	31.58
(74, 11.8)	30	12	26.38	3.32	0.996	26.48
10-25-94	29	10	17.34	1.93	1.005	17.26
(398, 10.4)	30	12	16.27	1.58	1.004	16.21

Note: Values in paranthesis in the date column represent mean asphalt concrete stiffness (ksi) and mean subgrade "breakpoint" modulus (ksi), to which the deflections were adjusted.

The measured surface deflections were also normalized for a 12-inch granular base thickness. Tables 6.16 and 6.17 show the adjusted surface deflections for test sections with asphalt concrete thickness of 3-inch and 5-inch respectively, for a 12-inch granular base thickness. Figures 6.34 and 6.35 show the effect of granular material quality on the pavement deflection response for test sections with asphalt concrete thickness of 3-inch and 5-inch respectively.

Statistical analyses were carried out to determine if there is a significant difference between the means of adjusted surface deflections. The least significant difference (LSD) test was performed. The LSD method performs a t-test for each pair of means using the within mean square (MSW) as

TABLE 6.16

Adjusted Surface Deflections (for granular base thickness = 12-inch) for Test Sections with AC Thickness = 3-inch

Date	Cell No.	Granular Base Thickness, inch	Measured D0, mils	Std. Dev. for Measured D0, mils	Adjustment Factor	Adjusted D0, mils
03-23-94	27	11	25.93	3.55	0.994	26.09
(981, 12.0)	28	13	28.40	3.23	1.003	28.30
	31	16	23.26	1.84	0.905	25.70
04-06-94	27	11	31.06	3.84	1.105	28.11
(771, 6.4)	28	13	29.47	2.39	1.007	29.27
	31	16	24.82	1.31	0.899	27.59
04-20-94	27	11	29.81	3.41	1.028	29.00
(610, 7.4)	28	13	29.28	1.93	0.996	29.39
	31	16	24.86	1.16	0.905	27.48
05-25-94	27	11	34.02	2.52	1.026	33.16
(249, 9.2)	28	13	35.13	2.05	1.012	34.71
	31	16	28.36	1.34	0.898	31.60
06-22-94	27	11	38.76	3.44	1.069	36.26
(80, 10.2)	28	13	38.40	2.33	1.026	37.42
	31	16	30.30	1.24	0.896	33.82
08-10-94	27	11	27.16	2.61	1.015	26.75
(255, 10.5)	28	13	28.70	2.13	1.012	28.36
	31	16	24.51	0.98	0.910	26.93
09-21-94	27	11	30.09	2.42	1.026	29.33
(74, 11.8)	28	13	31.28	2.35	1.005	31.12
	31	16	27.95	1.08	0.941	29.72
10-25-94	27	11	23.48	2.13	1.021	23.00
(398, 10.4)	28	13	24.95	2.05	0.994	25.11
	31	16	22.50	1.03	0.919	24.49

Note: Values in paranthesis in the date column represent mean asphalt concrete stiffness (ksi) and mean subgrade "breakpoint" modulus (ksi), to which the deflections were adjusted.

TABLE 6.17

Adjusted Surface Deflections (for granular base thickness = 12-inch) for Test Sections with AC Thickness = 5-inch

Date	Cell No.	Granular Base Thickness, inch	Measured D0, mils	Std. Dev. for Measured D0, mils	Adjustment Factor	Adjusted D0, mils
03-23-94	29	10	16.03	1.68	1.055	15.20
(981, 12.0)	30	12	15.00	1.75	1.018	14.73
04-06-94	29	10	17.34	1.96	0.993	17.47
(771, 6.4)	30	12	16.55	1.68	0.947	17.47
04-20-94	29	10	19.43	2.07	1.032	18.84
(610, 7.4)	30	12	18.54	2.02	1.020	18.18
05-25-94	29	10	28.42	2.69	1.033	27.52
(249, 9.2)	30	12	25.95	3.24	1.017	25.52
06-22-94	29	10	36.09	3.02	1.000	36.09
(80, 10.2)	30	12	30.54	3.70	0.960	31.80
08-10-94	29	10	23.02	2.35	1.029	22.36
(255, 10.5)	30	12	20.33	2.00	1.000	20.32
09-21-94	29	10	30.54	2.87	0.987	30.93
(74, 11.8)	30	12	26.38	3.32	0.996	26.48
10-25-94	29	10	17.34	1.93	1.026	16.91
(398, 10.4)	30	12	16.27	1.58	1.004	16.21

Note: Values in paranthesis in the date column represent mean asphalt concrete stiffness (ksi) and mean subgrade "breakpoint" modulus (ksi), to which the deflections were adjusted.

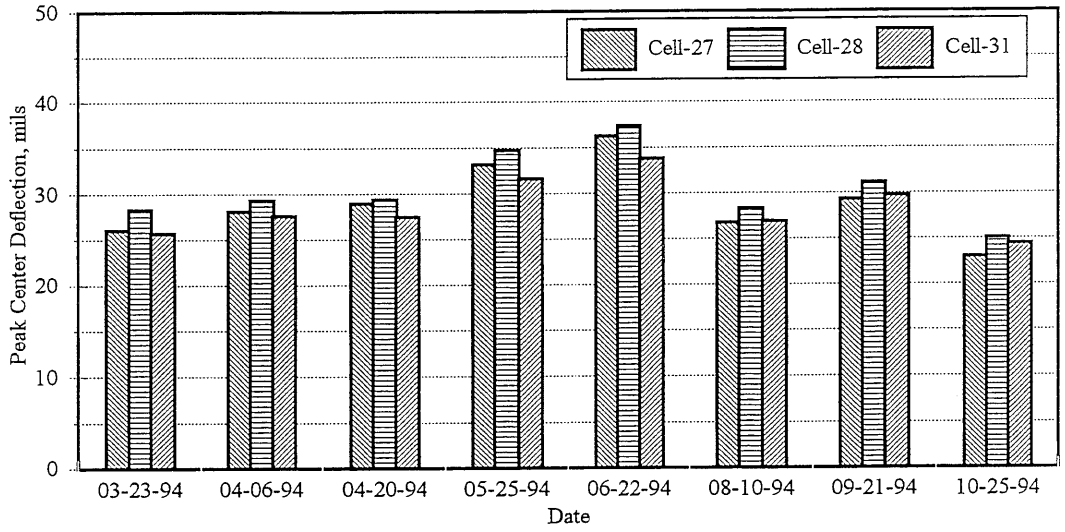

Figure 6.34. Adjusted Pavement Deflection Response (D0) for Test Sections with 3-inch Thick Asphalt Concrete Surface & Granular Base Thickness = 12-inch

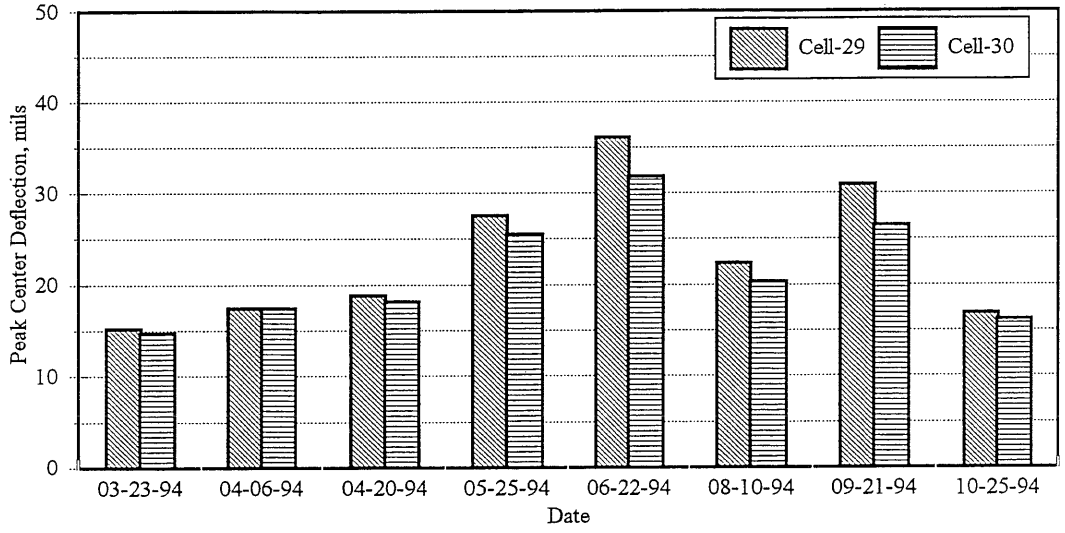

Figure 6.35. Adjusted Pavement Deflection Response (D0) for Test Sections with 5-inch Thick Asphalt Concrete Surface & Granular Base Thickness = 12-inch

the estimate of variance (σ^2). Since all of the tests have same denominator, it is easier to compute the minimum difference between means that will result in "significance" at some desired level. This difference is known as the least significance difference (LSD) and is calculated as [82]:

$$LSD = t_{\alpha/2} * \sqrt{[2 * MSW/n]} \quad \text{.....[6.14]}$$

where $t_{\alpha/2}$ is the $\alpha/2$ tail probability value from the t-distribution, and the degrees of freedom correspond to those of the estimated variance. Any difference between a pair of sample means exceeding the LSD value is considered to be statistically significant.

Tables 6.18 and 6.19 show the LSD values for test sections with asphalt concrete thickness of 3-inch and 5-inch respectively. In most of the cases, the difference between the means are less than the LSD. In some cases, the difference between the means was slightly higher than the LSD. Cell-27 has high shear strength (peak σ_d = 177-psi @ σ_3 = 15-psi, at OMC) material CL-6sp as the granular base. In Cell-28, CL-5sp is used as granular base (peak σ_d = 81-psi @ σ_3 = 15-psi, at OMC). CL-6sp has highest shear strength, and CL-5sp has lowest shear strength among the granular bases used in the conventional flexible pavements. In the case of test sections 27 and 28 (Table 6.19), the difference between the means were always less than the LSD suggesting that there is no significant difference between Cell-27 and Cell-28. Difference between means for Cell-27 or Cell-28 and Cell-31 were slightly higher than the LSD. The reason for this could be the difference in the thickness of granular base (in Cell-28, granular base thickness is 13-inch and for Cell-31, it is 16-inch). Based on the analysis, it can be concluded that the Cells 27, 28, and 31 show no significant difference in the pavement surface deflection response because of the difference in granular material quality. Similar trends were noted for test sections 29 and 30 (Table 6.19).

Tables 6.20 and 6.21 show the LSD values for test sections with asphalt concrete thickness of 3-inch and 5-inch respectively, and a granular base thickness of 12-inch. In most of the cases, the difference between the means are less than the LSD. In some cases, (Table 6.20, for dates 05-25-94, & 06-22-94, and Table 6.21, for 06-22-94, & 09-21-94), the difference between the means was slightly higher than the LSD. Based on the analysis, it can be concluded that the Cells 27, 28, and

TABLE 6.18

LSD for Comparing Mean Adjusted Surface Deflections for Test Sections with 3-inch Thick Asphalt Concrete Surface (Cells 27, 28, & 31)

	AC Modulus	Subgrade "breakpoint"	Mean Adjusted Surface Deflections, mils			
Date	ksi	Modulus, ksi	Cell-27	Cell-28	Cell-31	LSD for P = 0.05
03-23-94	981	12.0	26.52	27.88	24.34	2.87
04-06-94	771	6.4	28.58	28.83	26.14	2.63
04-20-94	610	7.4	29.48	28.95	26.04	2.28
05-25-94	249	9.2	33.71	34.19	29.93	1.96
06-22-94	80	10.2	36.86	36.87	32.04	2.42
08-10-94	255	10.5	27.19	27.93	25.51	1.96
09-21-94	74	11.8	29.81	30.65	28.15	1.98
10-25-94	398	10.4	23.38	24.73	23.2	1.75

LSD - Least Significant Difference

TABLE 6.19

LSD for Comparing Mean Adjusted Surface Deflections for Test Sections with 5-inch Thick Asphalt Concrete Surface (Cells 29, & 30)

Date	AC Modulus ksi	Subgrade "breakpoint" Modulus, ksi	Mean Adjusted Surface Deflections, mils		LSD for P = 0.05
			Cell-29	Cell-30	
03-23-94	981	12.0	15.52	14.73	1.70
04-06-94	771	6.4	17.83	17.47	1.81
04-20-94	610	7.4	19.23	18.18	2.02
05-25-94	249	9.2	28.09	25.52	2.95
06-22-94	80	10.2	36.84	31.8	3.34
08-10-94	255	10.5	22.83	20.32	2.16
09-21-94	74	11.8	31.58	26.48	3.07
10-25-94	398	10.4	17.26	16.21	1.75

LSD - Least Significant Difference

TABLE 6.20

LSD for Comparing Mean Adjusted Surface Deflections for Test Sections with 3-inch Thick Asphalt Concrete Surface (Cells 27, 28, & 31) with Granular Base Thickness = 12-inch

Date	AC Modulus ksi	Subgrade "breakpoint" Modulus, ksi	Mean Adjusted Surface Deflections, mils			LSD for P = 0.05
			Cell-27	Cell-28	Cell-31	
03-23-94	981	12.0	26.09	28.30	25.70	2.87
04-06-94	771	6.4	28.11	29.27	27.59	2.63
04-20-94	610	7.4	29.00	29.39	27.48	2.28
05-25-94	249	9.2	33.16	34.71	31.60	1.96
06-22-94	80	10.2	36.26	37.42	33.82	2.42
08-10-94	255	10.5	26.75	28.36	26.93	1.96
09-21-94	74	11.8	29.33	31.12	29.72	1.98
10-25-94	398	10.4	23.00	25.11	24.49	1.75

LSD - Least Significant Difference

TABLE 6.21

LSD for Comparing Mean Adjusted Surface Deflections for Test Sections with 5-inch Thick Asphalt Concrete Surface (Cells 29, & 30) with Granular Base Thickness = 12-inch

Date	AC Modulus ksi	Subgrade "breakpoint" Modulus, ksi	Mean Adjusted Surface Deflections, mils		LSD for P = 0.05
			Cell-29	Cell-30	
03-23-94	981	12.0	15.20	14.73	1.70
04-06-94	771	6.4	17.47	17.47	1.81
04-20-94	610	7.4	18.84	18.18	2.02
05-25-94	249	9.2	27.52	25.52	2.95
06-22-94	80	10.2	36.09	31.80	3.34
08-10-94	255	10.5	22.36	20.32	2.16
09-21-94	74	11.8	30.93	26.48	3.07
10-25-94	398	10.4	16.91	16.21	1.75

LSD - Least Significant Difference

31 show no significant difference in the pavement surface deflection response. Test sections 29 and 30 also show similar behavior.

Aggregate Surface/Surface Treated Pavements:

FWD data were used to backcalculate the subgrade "breakpoint" modulus using equation 6.5. Based on extensive ILLI-PAVE database, Thompson [76] developed an algorithm to predict pavement surface deflection (D0) as a function of granular base thickness, and subgrade "breakpoint" modulus. The algorithm is as follows:

$$\text{Log D0} = 2.434 - 0.5648 * (\text{Log } T_{bse}) - 0.0288 * E_{Ri} \quad \text{.....[6.15]}$$

$$R^2 = 0.96 \qquad \text{SEE} = 0.06$$

where

T_{bse} : Granular base thickness, inch;

E_{Ri} : Subgrade "breakpoint" modulus, ksi; and

D0 : FWD deflection at the center of loading plate, mils;

Equation 6.15 was used to evaluate the adjustment factor to be applied to the measured surface deflections. The peak center deflections (D0), for various test sections were evaluated using equation 6.15 from the backcalculated subgrade E_{Ri}. This estimated surface deflection is D0′. Use equation 6.15 again to estimate the surface deflection for the mean (benchmark) subgrade stiffness. This estimated surface deflection is D″. The adjustment factor is the ratio of D0′ and D″:

$$\text{Adjustment Factor} = D0' / D'' \quad \text{.....[6.16]}$$

where

D0′ : Estimated D0 from backcalculated subgrade stiffness; and

D″ : Estimated D0 from mean (benchmark) subgrade stiffness.

The field measured deflections (D0's) were adjusted to the bench mark subgrade stiffness using the adjustment factors. The adjusted D0's were obtained as:

$$\text{Adjusted D0} = \text{Field Measured D0} / \text{Adjustment Factor} \quad \text{.....[6.17]}$$

CL-1Csp is the granular material in Cells 32 and 33, and CL-1Fsp is the granular material in Cells 34 and 35. The peak shear strength, obtained from rapid shear test at a confining pressure of 15-psi, is 50-psi for CL-1Csp and 88-psi for CL-1Fsp. CL-1Csp also showed highest moisture susceptibility (Chapter-IV). Figure 6.36 shows the mean of adjusted surface deflections for Cells 32, 33, 34, and 35.

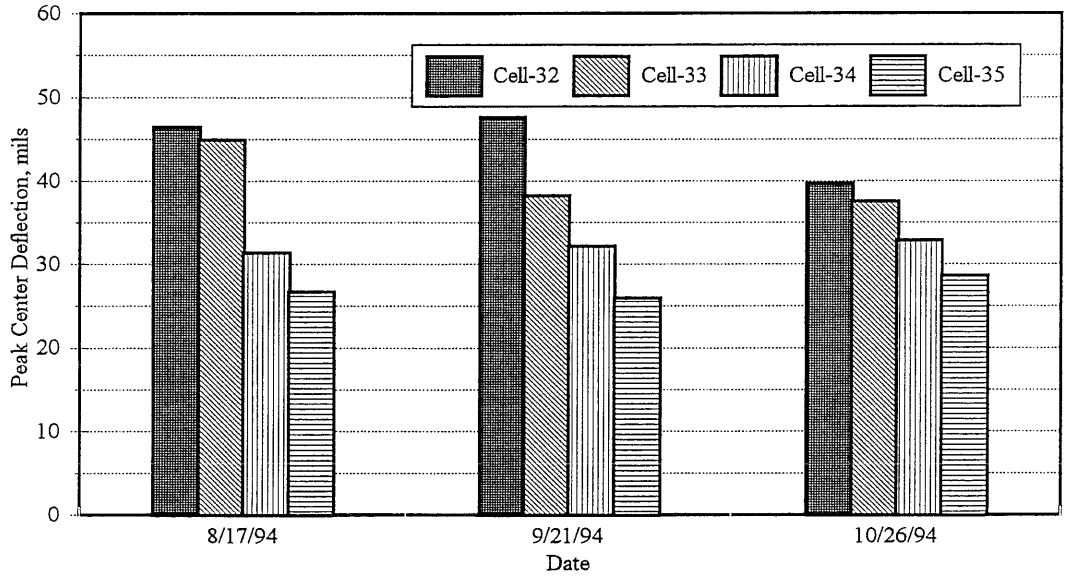

Figure 6.36. Adjusted Pavement Deflection Response (D0) for Aggregate Surface/Surface Treated Test Sections

The figure shows that the deflections for Cells 32 and 33 (granular material CL-1Csp) were always higher than that for Cells 34 and 35 (granular material CL-1Fsp). Analysis of variance was performed to study the effect of material and type of surface (double chip seal or no double chip seal) on the surface deflections. The results showed that both, the granular material and the type of surface, were significant factors. Results from statistical analysis (ANOVA) are shown in Table 6.22. Higher deflections were observed for test sections with double chip seal (Cells 32 and 34). The reason for this could be the deteriorated double chip seal. The material quality effects are significant because of the high stress states occurring in the granular base layer which in turn determines the resilient modulus of the granular base. Figure 6.37 shows the distribution of bulk stress ($\theta = \sigma_1 + 2 * \sigma_3$) within the granular layer. The magnitude of bulk stress ranges from 220-psi to 25-psi for a 12-inch thick granular layer with no asphalt concrete surface. Presence of 3-inch

TABLE 6.22
ANOVA Table for Deflection Response of Aggregate/Surface Treated Pavements

```
(formula = Deflection ~ Material + Surface + Date + Material:Surface +
           Material:Date, data = naf1)

Residuals:
    Min     1Q   Median    3Q   Max
 -16.88 -2.979 0.008521 3.155 18.45

Coefficients:
                   Value Std. Error  t value Pr(>|t|)
     (Intercept)  38.2610   0.6996    54.6878   0.0000
        Material  10.4084   0.6996    14.8771   0.0000
         Surface   2.3996   0.2616     9.1731   0.0000
            Date  -0.9788   0.3550    -2.7574   0.0060
Material:Surface  -0.0763   0.2616    -0.2916   0.7707
   Material:Date  -1.8840   0.3550    -5.3076   0.0000

Residual standard error: 5.447 on 478 degrees of freedom
Multiple R-Squared: 0.6547
F-statistic: 181.3 on 5 and 478 degrees of freedom, the p-value is 0

Correlation of Coefficients:
                (Intercept) Material Surface    Date Material:Surface
        Material  0.0396
         Surface -0.1842      0.0930
            Date -0.9184     -0.1627   0.0806
Material:Surface  0.0930     -0.1842   0.1094 -0.0892
   Material:Date -0.1627     -0.9184  -0.0892  0.3216  0.0806

Analysis of Variance Table

Response: Deflection

Terms added sequentially (first to last)
                  Df Sum of Sq  Mean Sq  F Value     Pr(F)
Material           1  23613.81 23613.81 795.9613 0.0000000
Surface            1   2404.98  2404.98  81.0659 0.0000000
Date               1     35.96    35.96   1.2121 0.2714737
Material:Surface   1      0.55     0.55   0.0186 0.8916240
Material:Date      1    835.72   835.72  28.1701 0.0000002
Residuals        478  14180.84    29.67
```

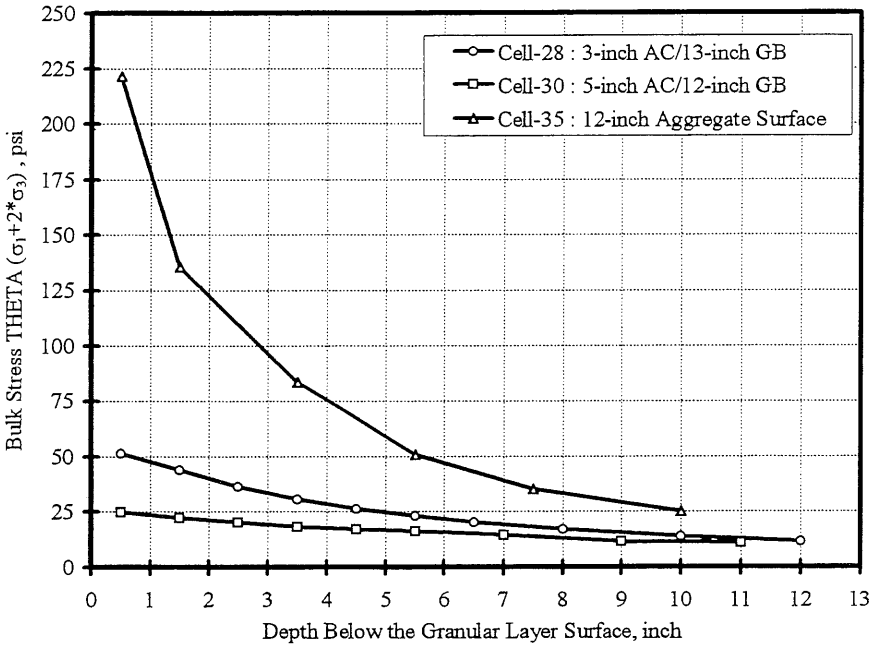

Figure 6.37. Bulk Stress Distribution within the Granular Layer

thick asphalt concrete surface reduces the bulk stress to 50-psi near the surface of granular layer. Granular materials exhibit stress hardening behavior. Generally, the modulus for granular material is estimated as a function of bulk stress (K-θ model is the most commonly used model). If the magnitude of bulk stress in granular layer is low, granular material quality effects on pavement structural response are not observed.

6.6 Effect of Granular Material Quality on Pavement Performance

Development of distresses (asphalt concrete fatigue, pavement rutting, pot-hole formation, etc.), are used to quantify pavement performance/serviceability. The low-volume road test sections at Mn/ROAD are loaded by a 5-axle tractor-trailer. In the inner lane, the tractor-trailer is loaded to 80,000-pounds (16-kip drive axle, 32-kip dual tandems on the trailer, tire pressure 100-psi). In the outer lane, the tractor-trailer travels in the opposite direction loaded to 102,500-pounds (13.2-kip drive axle, 41.5-kip front dual tandems on the trailer, 47.8-kip rear dual tandem on the trailer, tire pressure 100-psi). The axle load configuration for the LVR test vehicle is shown in Figure 1.5. The number of ESAL's corresponding to each pass of tractor-trailer are listed in Table 6.23 (per

TABLE 6.23

Load Equivalency Factors for Low-Volume Road Test Sections at Mn/ROAD Project

Test Section	AC Thickness in.	Asphalt Cement	Marshall Design	Granular Base (GB)	GB Thickness in.	Cell Number	Equivalency Factor 80-kip Lane	Equivalency Factor 102.5-kip Lane
LVR-F11	3	AC 120/150	35 Blow	CL-6sp	11	27	2.338	6.832
LVR-F12	3	AC 120/150	50 Blow	CL-5sp	13	28	2.330	6.981
LVR-F13	5	AC 120/150	50 Blow	CL-4sp	10	29	2.357	6.765
LVR-F14	5	AC 120/150	75 Blow	CL-3sp	12	30	2.345	6.871
LVR-F15	3	AC 120/150	75 Blow	CL-5sp, CL-3sp*	16	31	2.322	7.000
LVR-A1	0	-	-	CL-1Csp	12	33	-	-
LVR-A2	0	-	-	CL-1Fsp w/DCS	12	34	-	-
LVR-A3	0	-	-	CL-1Fsp	12	35	-	-
LVR-A4	0	-	-	CL-1Csp w/DCS	12	32	-	-

Note : DCS - 1" thick Double Chip Seal

* 4-inch CL-5sp Base & 12-inch CL-3sp Subbase

Mn/ROAD database). Table 6.23 lists the Mn/ROAD low-volume road test sections and the granular materials used. At this time, the rut depth measurements on the test sections are available. Some thermal cracking of asphalt concrete was observed in the winter of 1996. Forty feet of fatigue cracking was observed on March 10, 1997, in the right wheel path of the 80-kip lane of Cell-28 from station 184+35 to station 184+75. Ground penetrating radar recorded a minimal asphalt concrete thickness of 2.39-inches in the area experiencing this distress. Cell-28 was originally designed for 3-inch of asphalt concrete over 13-inches of Class-5sp base. This was the first occurrence of fatigue cracking at Mn/ROAD. As of 15th April, 1997, the fatigue cracking in the right wheel path of 80-kip lane has spread to a total length of 114-feet from station 183+88 to station 185+02.

The results from permanent deformation tests in laboratory on the granular materials showed that permanent deformation accumulation reduced with increase in the shear strength (Chapter-V). The 'A' term in the model $\varepsilon_p \% = A N^b$ is a function of shear strength (obtained from rapid shear test at 15-psi confining pressure). CL-6sp is the best material and CL-1Csp is the worst material.

Conventional Flexible Pavements:

Figures 6.38 and 6.39 show the rut depth measurements on 3-inch asphalt concrete and 5-inch asphalt concrete test sections respectively, loaded by 80,000-pound tractor-trailer. The 80,000-lb lane had experienced 16553 passes (38700 ESALs) of the tractor-trailer. The rapid shear test results reflect the rutting trends observed in the field, except for test section LVR-F11 (Cell-27) which experienced higher rutting than expected. One of the reasons for higher rutting in Cell-27 could be the 2.4-inch asphalt concrete thickness (design thickness is 3-inch) at the location where rut depths were measured. The asphalt concrete thickness for Cells 28 and 31 was 3 inches at the location of rut depth measurement. Similar trends were observed (Figures 6.40 and 6.41) on the lane trafficked by the tractor-trailer loaded to 102,5000-pounds. The 102,500-lb lane had experienced 5812 passes (40000 ESALs) of tractor-trailer.

The following model was used to characterize rutting in the test sections:

$$RD = A' N^B \qquad \text{.....[6.18]}$$

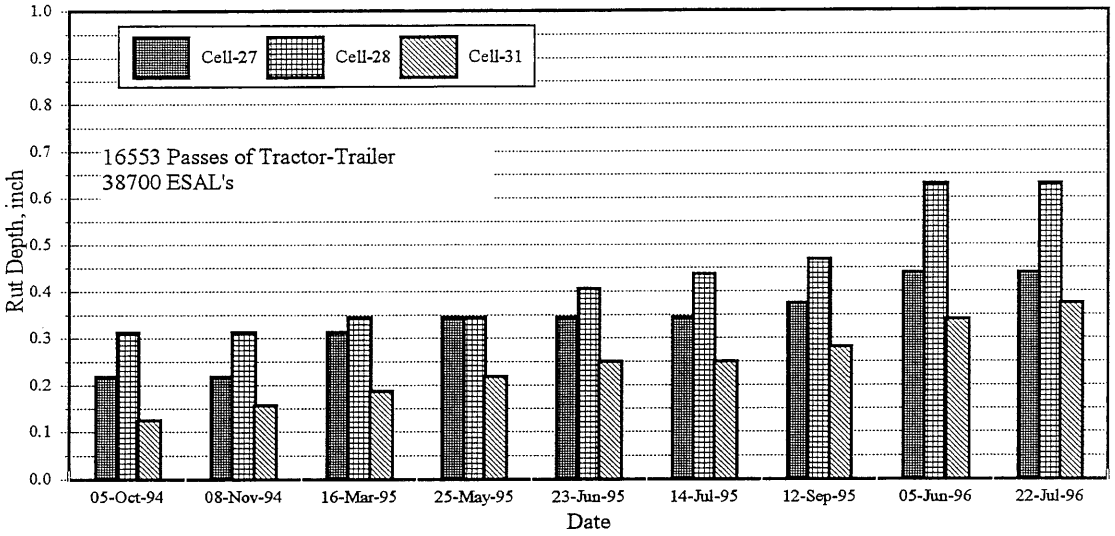

Figure 6.38. Rut Depth Measurements on 3-inch AC LVR Mn/ROAD Test Sections on the 80,000 lb Lane

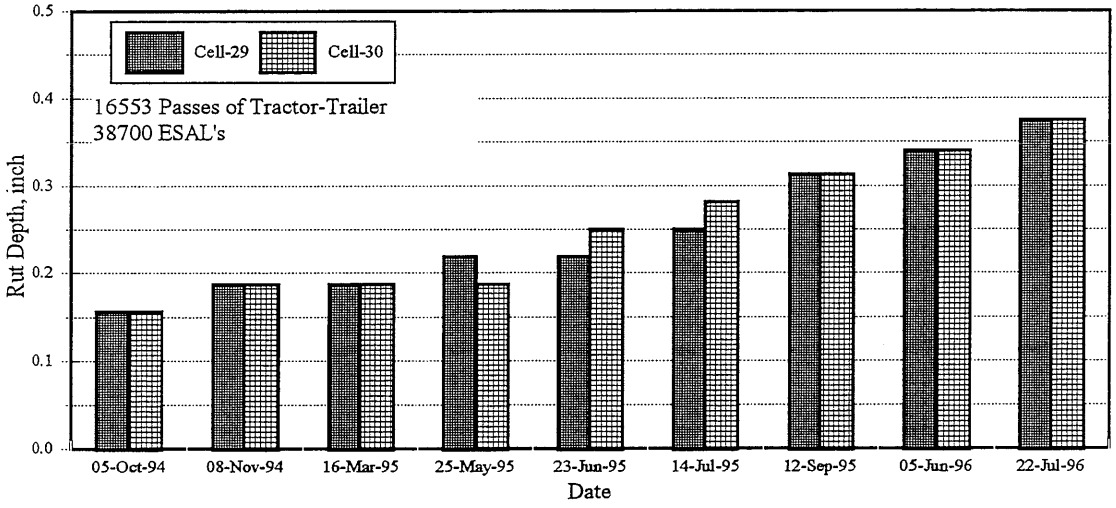

Figure 6.39. Rut Depth Measurements on 5-inch AC LVR Mn/ROAD Test Sections on 80,000 lb Lane

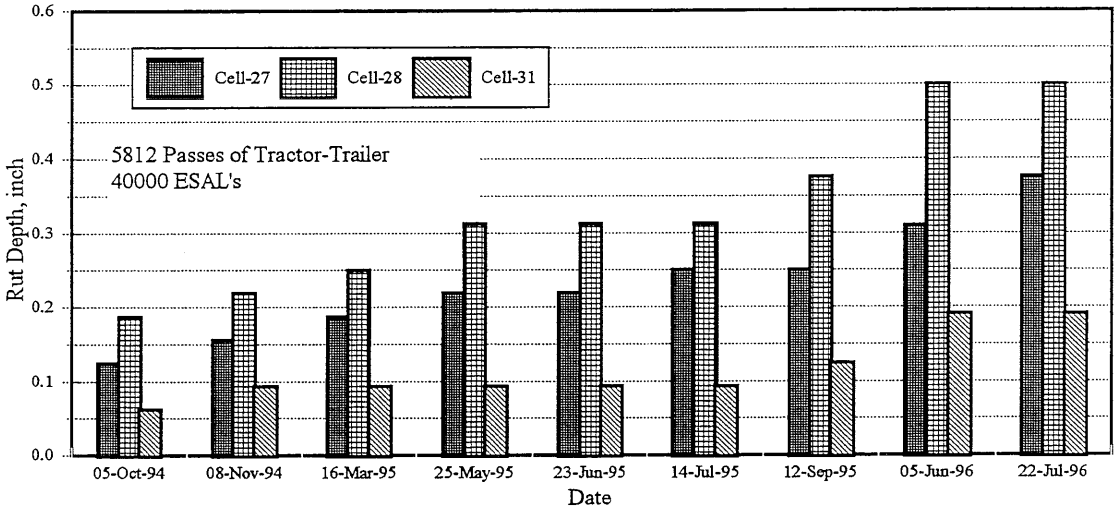

Figure 6.40. Rut Depth Measurements on 3-inch AC LVR Mn/ROAD Test Sections on the 102,500 lb Lane

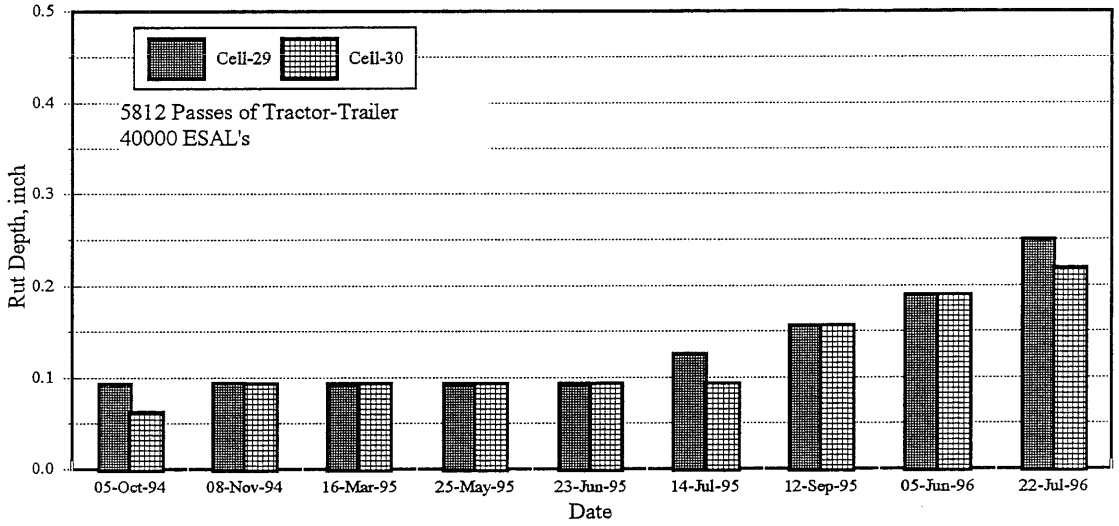

Figure 6.41. Rut Depth Measurements on 5-inch AC LVR Mn/ROAD Test Sections on the 102,500 lb Lane

where RD is rut depth in inches, and N is the number of tractor trailer passes (In Tables 6.24 & 6.25, when the parameters A′ and B are evaluated based on number of passes, N in the above equation is the number of passes of tractor trailer, and when the parameters A′ and B are evaluated based on number of ESAL's, N in the above equation is the number of ESAL's). The 'A'' and 'B' values for test sections are summarized in Table 6.24 and 6.25 for 80-kip lane and 102.5-kip lane respectively. Tables 6.24 and 6.25 give the rut depths measured on 07-22-96. This is the last set of useful rut depth data on the LVR test sections because the rut depth profiles were disturbed by the trucks hauling material for the rehabilitation of aggregate test sections. The lane with 80-kip loading experienced higher rutting compared to 102.5-kip lane. No particular trends were observed in the A′ and B values for the 80-kip lane and 102.5-kip lane.

Except for Cell 31, the A′ values were lower for the 102.5-kip lane.

For Cell 31, the A′ value was higher and B value was lower for the 102.5-kip lane.

Rutting can occur in the asphalt concrete surface, granular base, and subgrade. Khedr [83] showed that the rutting parameter A_a (in the model $\varepsilon_p/N = A_a*N^{-m}$) is a function of the resilient modulus and the applied stress. A study conducted at University of Minnesota [81] on the Mn/ROAD asphalt concrete mixes showed that all the three mixes (35-blow, 50-blow, & 75-blow) had similar modulus values. Therefore, according to Khedr's [83] analyses the asphalt concrete mixes should show similar rutting trends. Analysis of Falling Weight Deflectometer (FWD) tests showed that the backcalculated subgrade "breakpoint" modulus (E_{Ri}) values were similar for all the test sections. The trends observed for the parameter 'A' from laboratory tests on granular bases reflect the trends for parameter 'A'' from the field results. This suggests that the rutting is probably occurring in the granular base layer.

Aggregate Surface/Surface Treated Pavements:

The unsurfaced test sections Cell-33 (LVR-A1) and Cell-35 (LVR-A3) experienced severe rutting in the first few weeks of trafficking. Severe washboarding/corrugations occurred in Cell-35. The results from rapid shear tests showed CL-1Csp to be very low shear strength material (50-psi, Table 4.4), compared to 100-psi tire pressure, and had very high moisture susceptibility. Even

TABLE 6.24

Results from Rut Depth Measurements at Mn/ROAD Test Sections for 80-kip Lane

Cell No.	AC	Granular	Based on No. of Passes			Based on No. of ESALs			Rut Depth
	Thickness, inch	Base	Parameter A', inch	Parameter B	R^2	Parameter A', inch	Parameter B	R^2	inch*
27	3	CL-6 sp	0.0143	0.36	0.98	0.0106	0.36	0.98	0.44
28	3	CL-5 sp	0.0188	0.35	0.84	0.0140	0.35	0.84	0.63
29	5	CL-4 sp	0.0076	0.39	0.87	0.0054	0.39	0.87	0.38
30	5	CL-3 sp	0.0072	0.40	0.83	0.0051	0.40	0.83	0.38
31	3	CL-5 sp, CL-3sp	0.0030	0.49	0.98	0.0024	0.47	0.98	0.38

* *measured on 07/22/96*

TABLE 6.25

Results from Rut Depth Measurements at Mn/ROAD Test Sections for 102.5-kip Lane

Cell No.	AC	Granular	Based on No. of Passes			Based on No. of ESALs			Rut Depth
	Thickness, inch	Base	Parameter A', inch	Parameter B	R^2	Parameter A', inch	Parameter B	R^2	inch*
27	3	CL-6 sp	0.0099	0.41	0.95	0.0045	0.41	0.95	0.38
28	3	CL-5 sp	0.0136	0.41	0.95	0.0061	0.41	0.95	0.50
29	5	CL-4 sp	0.0073	0.37	0.63	0.0036	0.37	0.63	0.25
30	5	CL-3 sp	0.0041	0.43	0.73	0.0018	0.43	0.73	0.22
31	3	CL-5 sp, CL-3sp	0.0055	0.39	0.74	0.0026	0.39	0.74	0.19

* *measured on 07/22/96*

though CL-1Fsp achieved a peak deviator stress of 88-psi at 15-psi confining pressure (Table 4.4), the material did not perform well in the field due to high moisture susceptibility (discussed in Chapter 4). The poor performance of test sections LVR-A1 and LVR-A3 was predicted after conducting rapid shear and permanent deformation tests in the laboratory. Test sections LVR-A1 and LVR-A4 (CL-1Csp granular material) experienced higher rutting compared to test sections LVR-A3 and LVR-A2 (CL-1Fsp granular material), respectively, as predicted by the laboratory tests. Figure 6.42 shows a comparison of subgrade stress ratio in the surface treated/aggregate surface test sections.

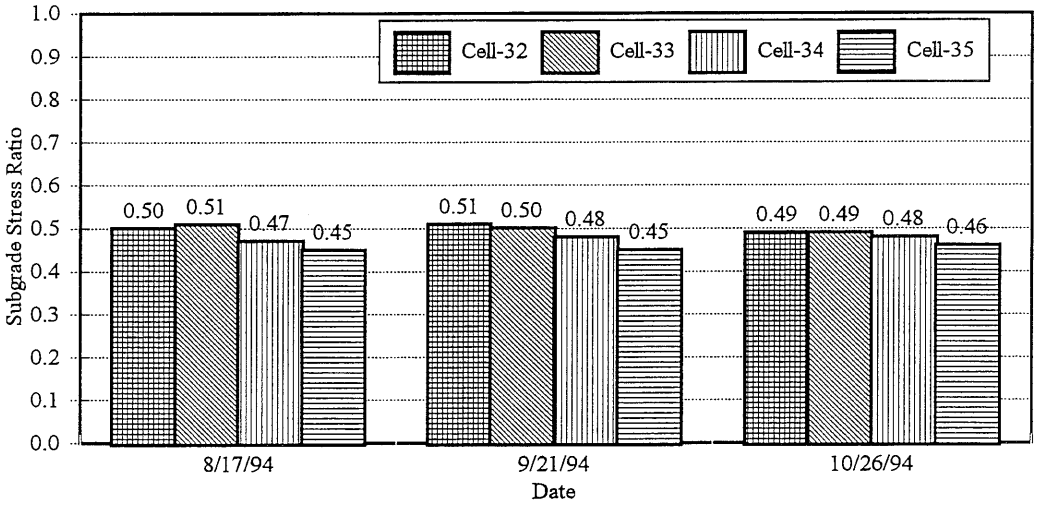

Figure 6.42. Comparison of Subgrade Stress Ratio for Surface Treated/Aggregate Surface Test Sections

The subgrade stress ratios are similar in the four test sections and the values range from 0.45 to 0.51. Thompson [76] reported that satisfactory performance can be obtained from surface treated /aggregate surface pavements if the subgrade stress ratio are lower than 0.65 for heavy traffic (< 80000 ESAL's), and lower than 0.75 for light traffic (< 20000 ESAL's). Recent (Summer' 1996) Mn/ROAD staff trenching studies in the aggregate test sections showed the rutting was primarily in the granular base and not in the subgrade.

Three types of distresses were observed on the surface/ aggregate surface treated test sections.

These were rutting, washboarding, and pothole formation. All these distresses are related to the quality and strength of the granular material used. Laboratory tests showed that the granular materials (CL-1Csp & CL-1Fsp) used in these test sections had very low shear strength and were highly moisture susceptible. The materials consisted of rounded gravel particles. All these properties contribute to rutting, washboarding, and pothole formation.

6.7 South African Mechanistic Approach for Pavement Life Prediction

In the South African mechanistic design method (SAMDM), the concept of "safety factor" for limiting the permanent deformation accumulation in granular material is used [84]. Permanent deformation accumulation in granular layer is caused due to densification and gradual shear caused by the moving traffic. The safety factor against shear failure is based on Mohr-Coulomb theory for static loading and is defined as [84]:

Safety Factor F = (Material Shear Strength) / (Applied Stress Causing Shear) .....[6.19]

$$F = (\sigma_3 * \phi_{term} + c_{term}) / (\sigma_1 - \sigma_3) \quad \text{.....[6.20]}$$

where

ϕ_{term}	=	$K * [\tan^2(45 + \phi/2) - 1]$
c_{term}	=	$2 * K * C * \tan(45 + \phi/2)$
σ_1	=	Major principal stress acting at a point in granular layer
σ_3	=	Minor principal stress acting at a point in granular layer
C	=	Cohesion
ϕ	=	Angle of internal friction
K	=	Constant = 0.65 for saturated conditions, 0.8 for moderate moisture conditions, and 0.95 for normal moisture conditions.

At values of safety factor below a certain critical value, the permanent deformation in the granular material increases rapidly under a few load applications because of shear failure [85]. At values above the critical value of safety factor, the permanent deformation increases gradually with increasing load applications. In both instances, the mode of failure will be the deformation in granular layer, and the rate of deformation is controlled by the magnitude of safety factor against

shear failure. The major and minor principal stresses, and hence the safety factor, are generally calculated at the midpoint of granular layer.

ILLI-PAVE (finite element program) was used to evaluate the major and minor principal stresses in the granular layer in the Mn/ROAD test sections. The seasonal variation in the safety factor for conventional flexible test sections with 3-inch thick asphalt concrete surface (Cells 27, 28, and 31) is shown in Figure 6.43.

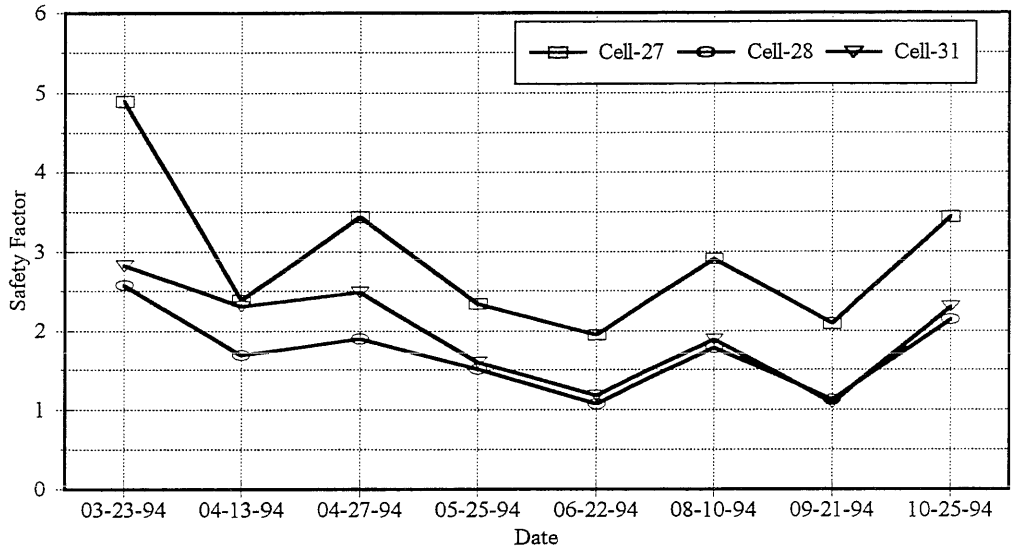

Figure 6.43. Safety Factors Against Shear Failure in Granular Material for Test Sections with 3-inch Asphalt Concrete Surface

Safety factor is lowest during summer because the asphalt concrete surface has lowest stiffness and stresses in the granular layer are high. Material CL-6sp showed higher safety factors compared to other materials (CL-3sp, and CL-5sp). Figure 6.44 shows the seasonal variation in safety factors for conventional flexible test sections with 5-inch thick asphalt concrete surface (Cells 29, and 30). For material CL-1Csp (Cells 32, and 33), the safety factor value of 0.8 was obtained. Cells 32 and 33 experienced more than one inch of rutting in less than one week of traffic. For material CL-1Fsp (Cells 34, and 35), safety factor value of 1.1 was obtained. Cells 34 and 35 also experienced severe rutting but the rate of permanent deformation accumulation was slower than Cells 32 and 33.

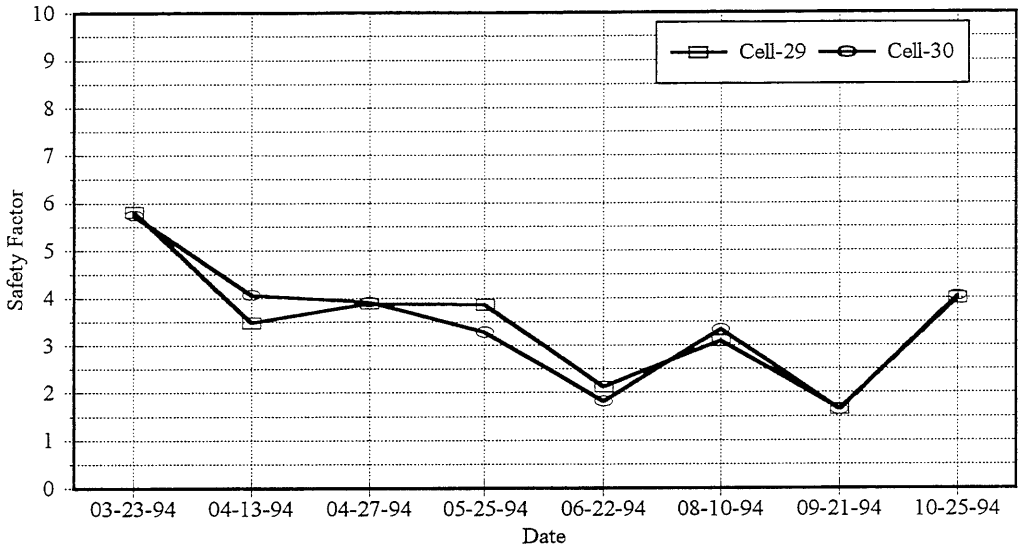

Figure 6.44. Safety Factors Against Shear Failure in Granular Material for Test Sections with 5-inch Asphalt Concrete Surface

Mean safety factors for different materials are as follows:

Material	Safety Factor
CL-1Csp	0.8
CL-1Fsp	1.1
CL-3sp	2.0 (Cell-31), 3.5 (Cell-30)
CL-4sp	3.5
CL-5sp	1.7
CL-6sp	2.9

Figures 6.45 through 6.50 show the safety factors for Cell-24, Cell-27, Cell-28, Cell-29, Cell-30, and Cell-31 (conventional flexible pavements), respectively. Safety factors are plotted as a function of pavement temperature (the temperature at one-third depth of the asphalt concrete layer) and depth below the granular base surface. Safety factor reduces with increase in pavement temperature. Pavement temperature affects the asphalt concrete stiffness which in turn affects the stresses within the granular layer. High pavement temperature correspond to reduced asphalt concrete stiffness and higher stresses in the granular base layer. Safety factor increases within the

granular layer with increase in depth. Low safety factor values are observed within the top half of the granular layer thickness.

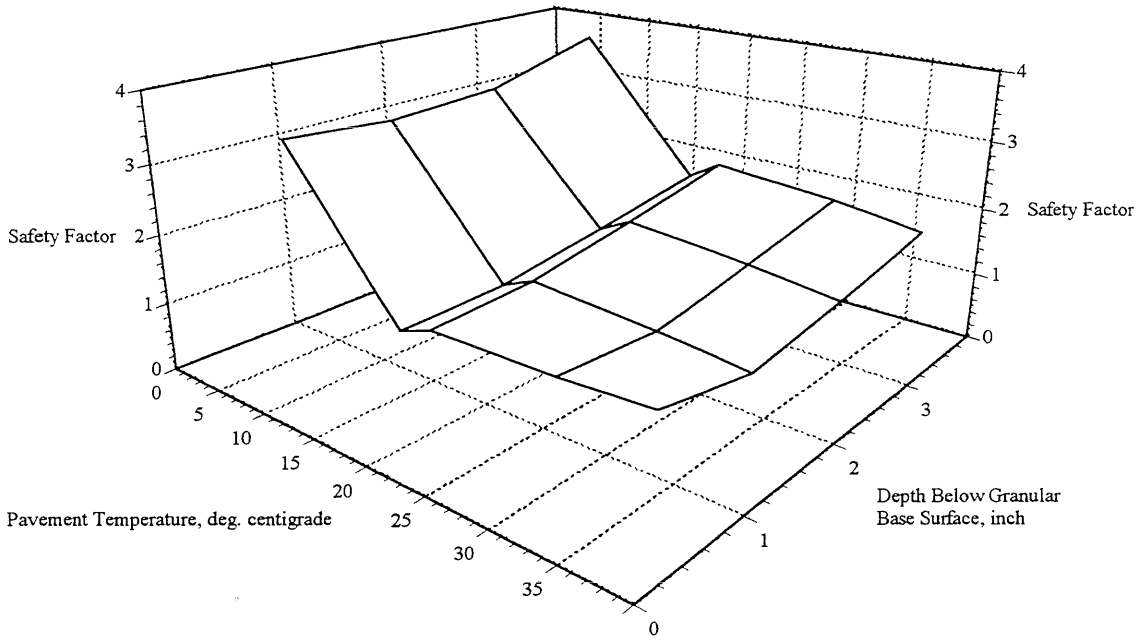

Figure 6.45. Safety Factor for Cell-24 [3-inch AC/4-inch GB]

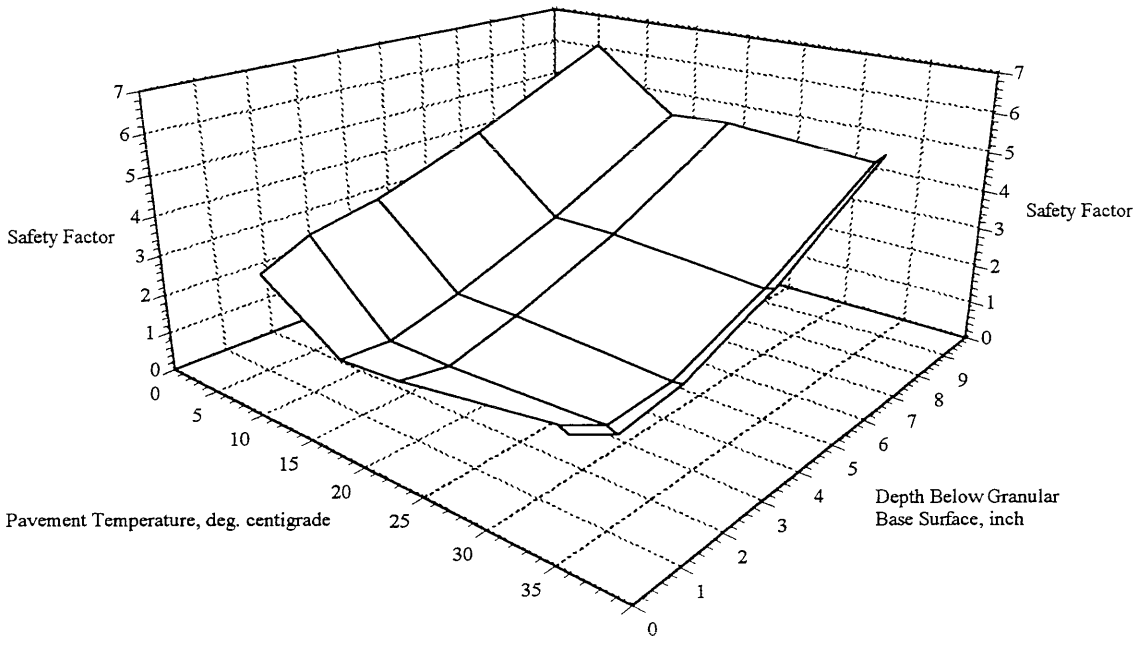

Figure 6.46. Safety Factor for Cell-27 [3-inch AC/11-inch GB]

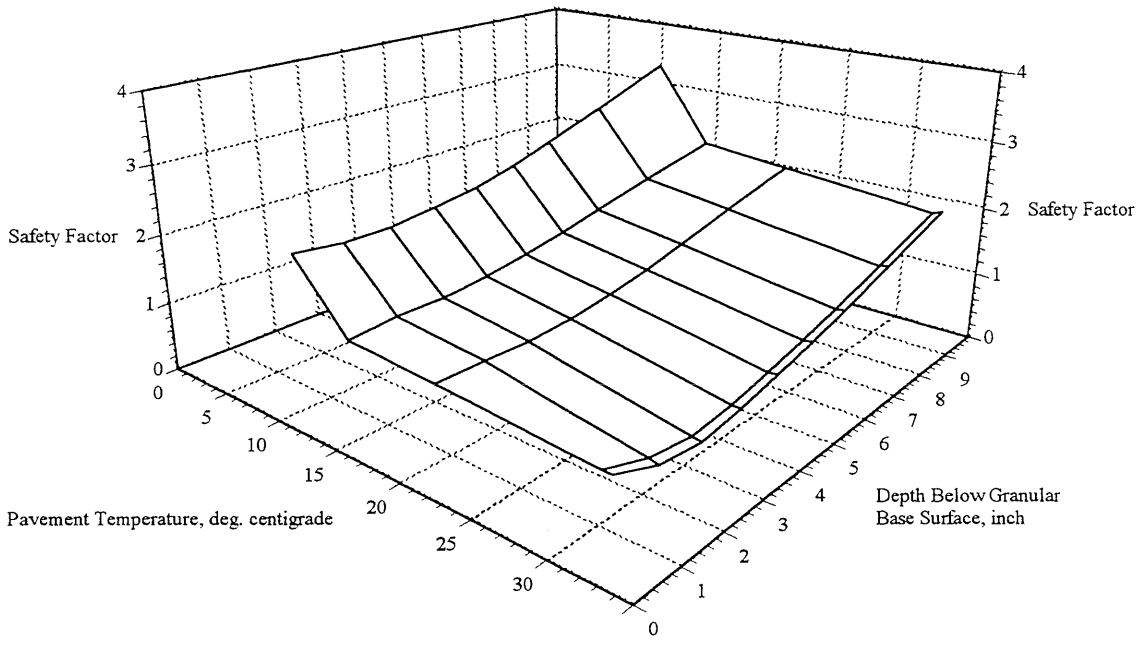

Figure 6.47. Safety Factor for Cell-28 [3-inch AC/13-inch GB]

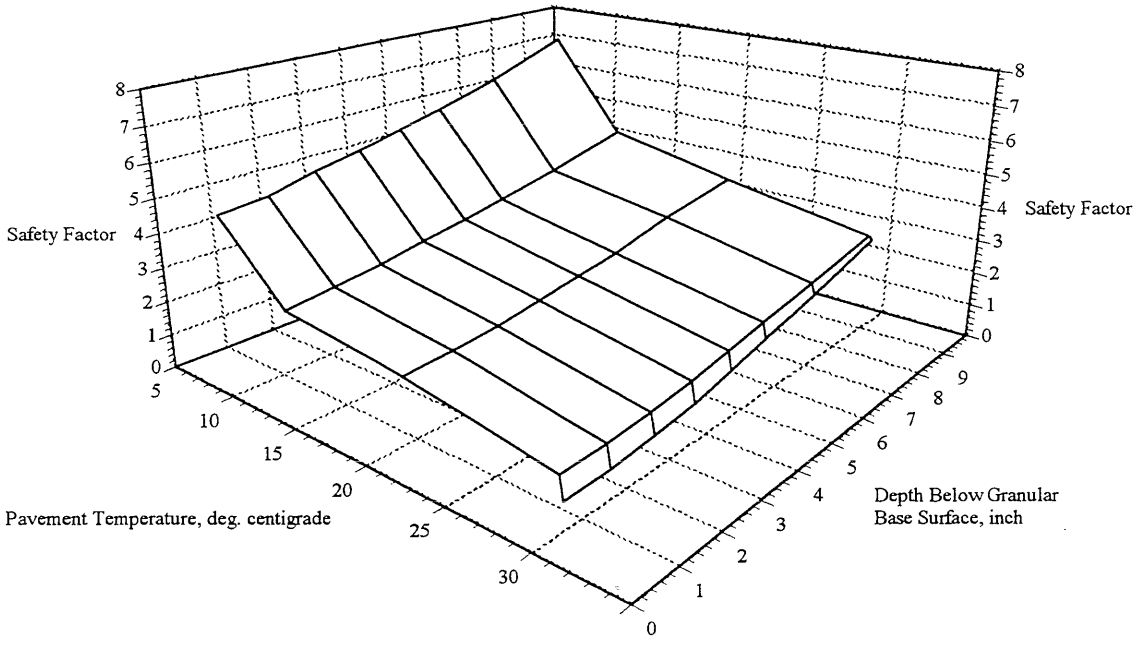

Figure 6.48. Safety Factor for Cell-29 [5-inch AC/10-inch GB]

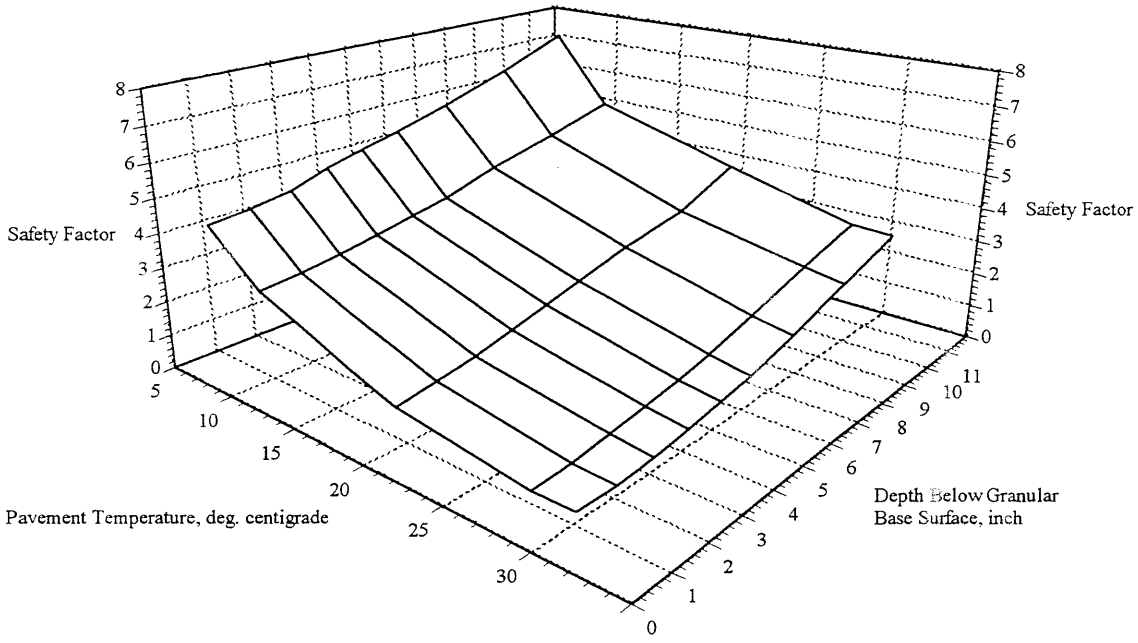

Figure 6.49. Safety Factor for Cell-30 [5-inch AC/12-inch GB]

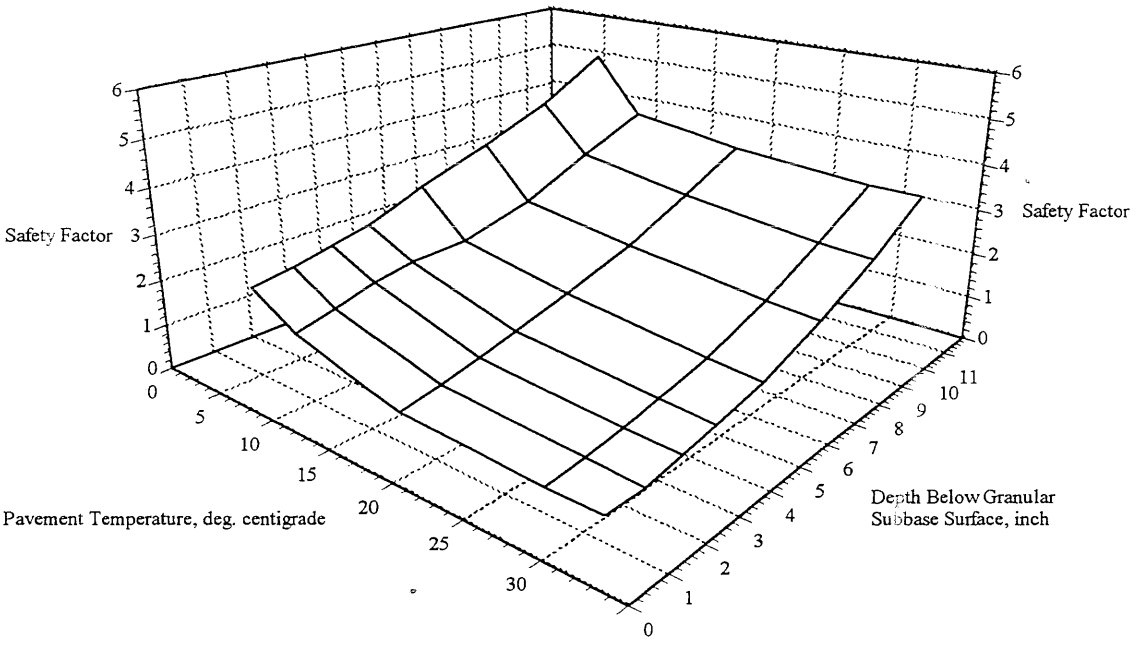

Figure 6.50. Safety Factor for Cell-31 [3-inch AC/4-inchGB/12-inch Subbase]

Figures 6.51 shows the safety factors for aggregate surface test sections Cell-33 and Cell-35.

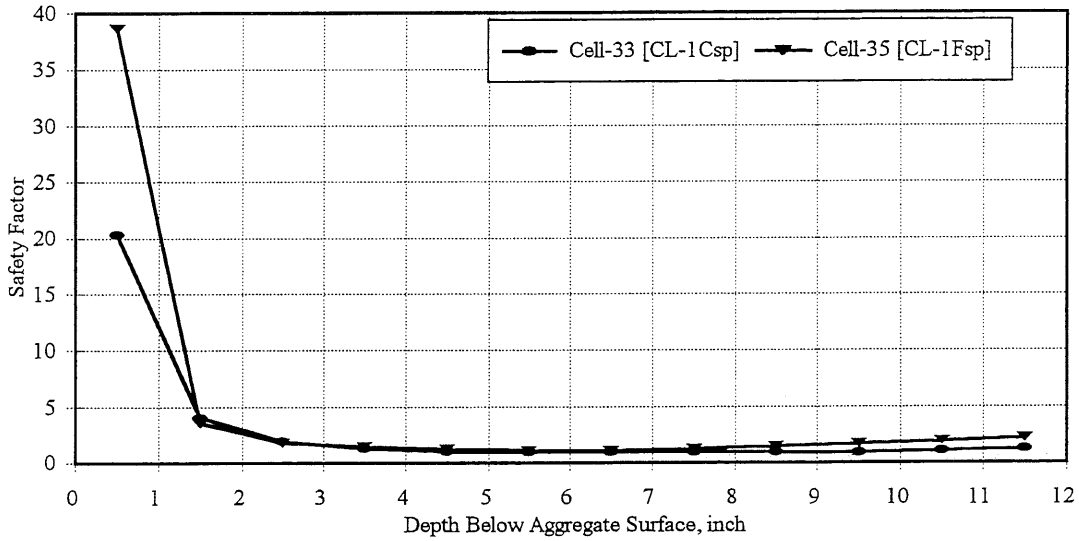

Figure 6.51. Comparison of Safety Factors for Aggregate Surface Test Sections

High safety factor values (20-38) are observed in the top 1-inch of the granular layer because of high confining stresses. Figure 6.52 shows a magnified view of the safety factor as a function of depth within the granular base layer.

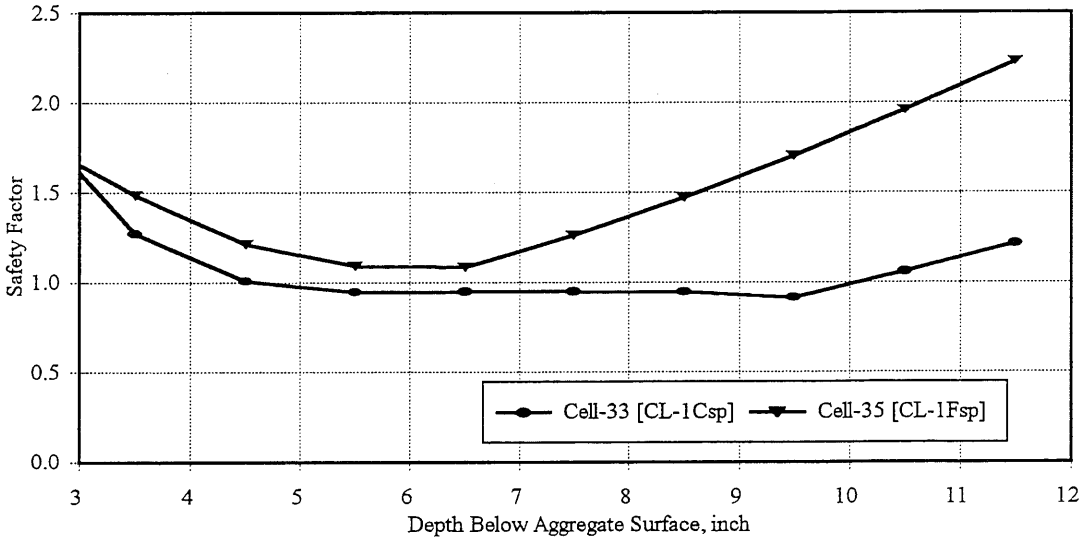

Figure 6.52. Comparison of Safety Factors for Aggregate Surface Test Sections

The safety factor values are lower than one in the middle one-third thickness of granular base in Cell-33 (granular base - CL-1Csp). Cell-35 (granular base - CL-1Fsp) showed higher safety factor values than Cell-33. Cell-32 and Cell-33 (granular base - CL-1Csp) experienced higher rutting than Cell-34 and Cell-35 (granular base - CL-1Fsp).

The granular materials used in Mn/ROAD test sections can be ranked in the order of performance based on the laboratory (rapid shear) tests, South African method (based on safety factor), and the field performance (rut depth measurements). Table 6.26 gives the comparison between the rankings based on the three methods. The rankings of the materials are same from all the three methods except for material CL-6sp, which for some reason gave slightly poor performance in the field than expected.

6.8 Summary

Results from the FWD testing on the test sections have been presented. Asphalt concrete stiffness and subgrade "breakpoint" modulus were backcalculated using the algorithms developed at the University of Illinois. Similar subgrade "breakpoint" modulus values were observed in the test sections. The FWD data were analyzed to study the effect of granular material quality on the pavement surface deflection response. The surface deflections were normalized to same asphalt concrete and subgrade stiffness. The analysis showed that there is no significant effect of granular material quality on the pavement deflection response in the case of conventional flexible pavements (asphalt concrete surface and granular base). There is an inverse relationship between the 'K' and 'n' parameters in the granular material K-θ resilient modulus model ($E_r = K\theta^n$; θ is bulk stress). As a result, for a certain range of bulk stresses, two granular materials (one with high 'K' and low 'n', and the other with low 'K' but high 'n') can exhibit similar moduli values in a pavement system (Figure 6.53). When this occurs, the resilient load responses (stresses, strains, deflections) of the pavement system are similar, regardless of the granular material. Because of higher stresses within the granular layer, the granular material quality effects on the pavement surface deflection response of surface treated/aggregate surface pavements are significant. Increased asphalt concrete thickness reduces the effect of granular base quality on the pavement deflection response.

The granular material quality significantly affects the performance of the pavement. The shear

TABLE 6.26

Granular Material Ranking Based on Laboratory Triaxial Tests, the South African Safety Factor Approach, and Field Performance

Rank	Material Ranking Based on		
	Laboratory Shear Tests	Safety Factor Approach	Field Performance
3-inch Thick Asphalt Concrete Surface			
1	CL-6sp	CL-6sp	CL-3sp
2	CL-3sp	CL-3sp	CL-6sp
3	CL-5sp	CL-5sp	CL-5sp
5-inch Thick Asphalt Concrete Surface			
1	CL-3sp, CL-4sp	CL-3sp, CL-4sp	CL-3sp, CL-4sp
Surface_Treated/Aggregate_Surface_Pavements			
1	CL-1Fsp	CL-1Fsp	CL-1Fsp
2	CL-1Csp	CL-1Csp	CL-1Csp

Note: Superior material is ranked 1.

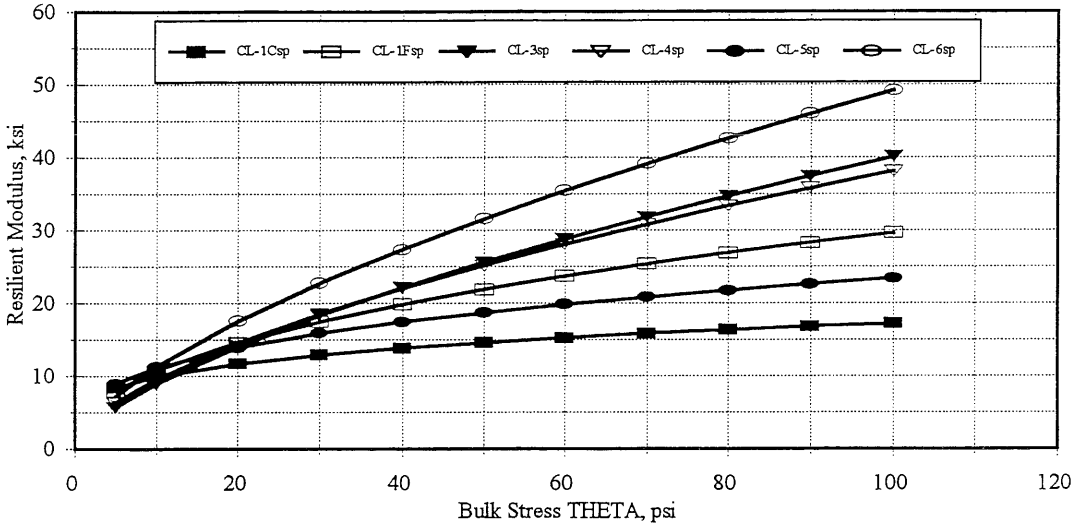

Figure 6.53. Resilient Modulus - Bulk Stress Relationship for Mn/ROAD Base Materials

strength results obtained from rapid shear tests performed at a confining pressure of 15-psi reflect the rutting trends observed in the low-volume road test sections at Mn/ROAD project. The aggregate layer in pavement must posses sufficient shear strength/rutting resistance (for a given asphalt concrete thickness) to minimize rutting within the layer. Adequate asphalt concrete and granular layer thickness must be provided to protect the subgrade. In the case of surface treated/aggregate surface test sections, the distresses observed were attributed to the poor quality of the granular materials used. Even though the subgrade stress ratio were within acceptable limits, the test sections experienced severe rutting, washboarding, and pothole formation.

Chapter-VII discusses the results obtained from finite element modeling of the test sections. The results from ILLI-PAVE runs are compared with the field measured responses.

CHAPTER - VII

COMPARISON OF FIELD MEASURED PAVEMENT RESPONSES WITH THE ILLI-PAVE PREDICTED PAVEMENT RESPONSES

7.1 Introduction

In a mechanistic-design procedure for the pavements, pavement responses (stresses, strains, deflections) are used to predict pavement distresses through the use of transfer functions. At the Mn/ROAD project, approximately 4500 sensors were embedded in different pavement layers to measure the pavement responses to different loading and climatic conditions. FWD testing was performed to measure the surface deflection response of the pavement. Among the sensors, only asphalt concrete strain data for some test sections (Cell-25 and Cell-27) corresponding to the FWD testing are available in the database. For Cells 25 and 27, the FWD loading plate was placed at the top of asphalt concrete surface above the strain gauge location. The FWD testing equipment used at Mn/ROAD project is described in Chapter VI. The Dynatest PAST-2AC strain gauges were used to monitor the longitudinal and transverse strains at the bottom of asphalt concrete layer. This type of embedment gauge consists of an electrical resistance strain gauge embedded within a strip of glass-fiber reinforced epoxy surrounded by several protective layers of various materials. There are transverse steel anchors at each end to form an H-shape. The sensor is coated with an asphalt material to help bond the gauge to the mix and to protect against mechanical and chemical damage.

In this chapter, the field measured pavement responses are compared to the ILLI-PAVE (finite element program) predicted pavement responses.

7.2 Measured Pavement Responses from FWD Testing

The Dynatest Model 8000 FWD equipment was used at Mn/ROAD for non-destructive testing. The testing pattern for each section consisted of ten test points spaced at 50-feet intervals with four longitudinal offsets from the centerline (-9.5-feet - outer wheel track westbound lane, -6.25-feet - between wheel tracks westbound lane, +6.25-feet - between wheel tracks eastbound lane, +9.5-feet - outer wheel track eastbound lane) tested. Pavement surface deflections under the center of loading plate (D0), 12 inches from the load center (D1), 24 inches from the load center (D2), and 36 inches from the load center (D3) were recorded. FWD test dates were selected to cover the entire range of

pavement climatic conditions. Tables 7.1 through 7.12 present the summary of FWD measurements for Cell-24 through Cell-35 respectively. Each deflection value listed in the tables is a mean of ten test points spaced at 50-feet intervals in the test section. BELLS temperature corresponding to each test date is also listed in the tables.

Figure 1.3 gives the cross-sections of test sections in the LVR loop. The asphalt concrete strain data corresponding to the FWD tests were available for Cell-4, Cell-22, Cell-25, and Cell-27. Cells 4 and 22 are mainline tests sections over cohesive subgrade. Cell-4 is an 8.75-inch full depth asphalt concrete pavement and Cell-22 is a conventional flexible pavement with 7.75-inch asphalt concrete and 18-inch granular base. Cell-25 is 5-inch full depth asphalt concrete pavement over sandy subgrade, and Cell-27 is a conventional flexible pavement with 3-inch asphalt concrete and 11-inch granular base over cohesive subgrade. The FWD deflection data were correlated with the measured asphalt concrete strain values for Cells 4, 22, and 25. Data from Cell-27 were not used since the 3-inch asphalt concrete thickness is not considered as a structural layer (behaves more like an enhanced surface treatment). Based on extensive ILLI-PAVE database (unpublished report by Hill and Thompson), Area Under Pavement Profile (AUPP) was correlated to the asphalt concrete strain values for full-depth asphalt concrete pavements. AUPP is defined as follows (Figure 7.1):

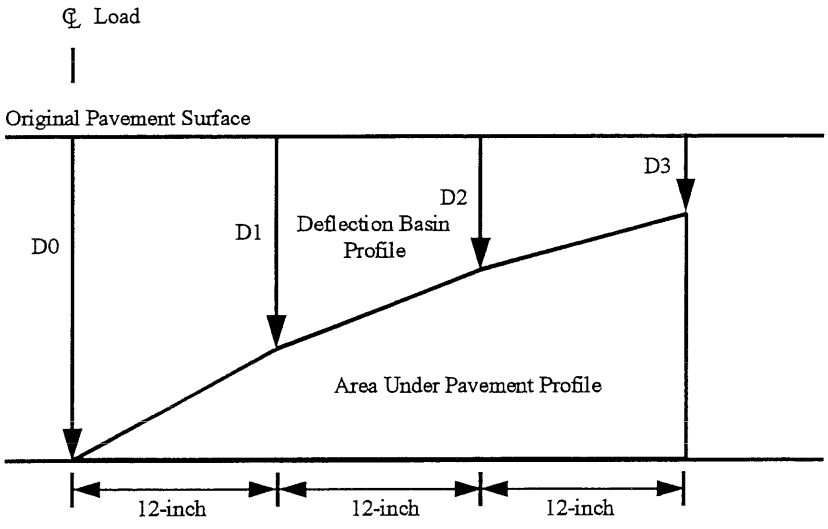

AUPP = (Area Under Pavement Profile) / 12
= (5*D0 - 2*D1 - 2*D2 - D3) / 2

Figure 7.1. Area Under Pavement Profile (AUPP)

TABLE 7.1
Summary of Measured Pavement Responses from FWD Tests on Cell-24

Date	D0, mils	D1, mils	D2, mils	D3, mils	Tac, in	Bell's Temperature, deg. C.
3/23/94						
Mean	15.68	9.58	4.73	2.72	3.20	8.78
Std.	0.83	0.36	0.13	0.12	0.57	0.19
COV, %	5.28	3.78	2.76	4.39	17.72	2.12
4/13/94						
Mean	17.35	9.15	4.06	2.55	3.20	19.00
Std.	0.77	0.31	0.17	0.13	0.57	0.41
COV, %	4.47	3.39	4.17	5.04	17.72	2.16
4/27/94						
Mean	14.98	8.97	4.29	2.59	3.20	11.69
Std.	0.77	0.32	0.16	0.13	0.57	0.02
COV, %	5.13	3.58	3.68	4.87	17.72	0.21
5/25/94						
Mean	17.95	7.77	3.55	2.52	3.20	21.63
Std.	0.53	0.23	0.20	0.15	0.57	0.21
COV, %	2.95	2.95	5.54	6.01	17.72	0.98
6/22/94						
Mean	19.69	7.45	3.76	2.66	3.20	38.25
Std.	0.28	0.25	0.22	0.16	0.57	0.87
COV, %	1.43	3.34	5.74	5.88	17.72	2.27
8/10/94						
Mean	18.15	9.41	4.47	2.75	3.20	23.52
Std.	0.55	0.24	0.19	0.15	0.57	0.33
COV, %	3.03	2.52	4.18	5.57	17.72	1.42
9/21/94						
Mean	19.58	9.30	4.43	2.90	3.20	31.50
Std.	0.52	0.27	0.20	0.17	0.57	0.19
COV, %	2.63	2.85	4.54	5.92	17.72	0.62
10/25/94						
Mean	17.64	10.62	5.38	3.22	3.20	17.73
Std.	0.75	0.30	0.20	0.17	0.57	0.20
COV, %	4.23	2.79	3.75	5.15	17.72	1.13

TABLE 7.2
Summary of Measured Pavement Responses from FWD Tests on Cell-25

Date	D0, mils	D1, mils	D2, mils	D3, mils	Tac, in	Bell's Temperature, deg. C.
3/23/94						
Mean	11.67	8.37	5.00	3.00	5.11	7.60
Std.	0.76	0.45	0.19	0.11	0.30	1.16
COV, %	6.51	5.38	3.78	3.64	5.79	15.33
4/13/94						
Mean	14.75	10.14	5.86	3.61	5.11	15.66
Std.	1.24	0.89	0.56	0.35	0.30	0.41
COV, %	8.41	8.78	9.48	9.72	5.79	2.64
4/27/94						
Mean	12.94	9.40	5.71	3.64	5.11	11.66
Std.	1.11	0.80	0.51	0.34	0.30	0.01
COV, %	8.59	8.51	8.93	9.27	5.79	0.11
5/25/94						
Mean	18.11	10.07	5.17	3.35	5.11	21.85
Std.	1.45	0.91	0.51	0.30	0.30	0.08
COV, %	8.00	9.08	9.91	9.04	5.79	0.35
6/22/94						
Mean	22.46	10.33	5.20	3.51	5.11	34.11
Std.	1.73	1.00	0.51	0.29	0.30	0.30
COV, %	7.72	9.69	9.79	8.38	5.79	0.88
8/10/94						
Mean	17.47	11.04	6.21	3.85	5.11	22.42
Std.	1.10	0.76	0.49	0.32	0.30	0.65
COV, %	6.32	6.88	7.87	8.23	5.79	2.88
9/21/94						
Mean	20.19	11.10	5.92	3.87	5.11	30.85
Std.	1.06	0.70	0.44	0.28	0.30	0.24
COV, %	5.24	6.31	7.44	7.23	5.79	0.77
10/25/94						
Mean	15.40	11.11	6.96	4.48	5.11	16.59
Std.	0.96	0.67	0.43	0.29	0.30	0.06
COV, %	6.24	6.01	6.21	6.56	5.79	0.35

TABLE 7.3
Summary of Measured Pavement Responses from FWD Tests on Cell-26

Date	D0, mils	D1, mils	D2, mils	D3, mils	Tac, in	Bell's Temperature, deg. C.
3/23/94						
Mean	9.21	6.94	4.27	2.44	6.15	7.12
Std.	0.83	0.54	0.33	0.26	0.23	0.03
COV, %	9.02	7.79	7.84	10.78	3.75	0.42
4/13/94						
Mean	14.60	11.05	7.01	4.29	6.15	16.81
Std.	1.38	1.14	0.84	0.55	0.23	2.30
COV, %	9.46	10.33	11.98	12.81	3.75	13.71
4/27/94						
Mean	11.76	9.21	6.08	3.94	6.15	10.71
Std.	1.08	0.91	0.66	0.45	0.23	0.16
COV, %	9.16	9.85	10.88	11.32	3.75	1.45
5/25/94						
Mean	23.41	14.19	7.04	3.89	6.15	21.39
Std.	3.51	2.70	1.50	0.69	0.23	0.00
COV, %	15.00	19.04	21.27	17.74	3.75	0.00
6/22/94						
Mean	38.48	18.44	6.92	3.60	6.15	32.74
Std.	7.51	4.68	1.66	0.61	0.23	0.54
COV, %	19.51	25.38	24.00	16.97	3.75	1.64
8/10/94						
Mean	18.45	12.09	6.47	3.55	6.15	21.13
Std.	2.05	1.49	0.83	0.43	0.23	0.27
COV, %	11.10	12.33	12.86	12.04	3.75	1.28
9/21/94						
Mean	27.29	14.55	6.09	3.16	6.15	30.81
Std.	3.40	1.96	0.70	0.28	0.23	0.26
COV, %	12.46	13.47	11.46	8.78	3.75	0.85
10/25/94						
Mean	12.42	9.20	5.70	3.51	6.15	16.17
Std.	1.05	0.72	0.43	0.30	0.23	0.25
COV, %	8.45	7.78	7.54	8.60	3.75	1.56

TABLE 7.4
Summary of Measured Pavement Responses from FWD Tests on Cell-27

Date	D0, mils	D1, mils	D2, mils	D3, mils	Tac, in	Bell's Temperature, deg. C.
3/23/94						
Mean	25.93	16.31	6.90	2.61	3.04	8.25
Std.	3.55	1.60	0.53	0.39	0.45	0.28
COV, %	13.70	9.82	7.68	15.01	14.73	3.40
4/13/94						
Mean	33.58	21.23	9.75	4.65	3.04	15.81
Std.	4.15	1.84	0.40	0.22	0.45	0.40
COV, %	12.35	8.67	4.08	4.80	14.73	2.54
4/27/94						
Mean	25.89	17.16	8.44	4.34	3.04	10.14
Std.	2.83	1.24	0.35	0.28	0.45	0.02
COV, %	10.94	7.24	4.17	6.36	14.73	0.17
5/25/94						
Mean	34.02	17.60	7.04	3.71	3.04	21.14
Std.	2.52	1.02	0.55	0.38	0.45	0.38
COV, %	7.40	5.78	7.79	10.19	14.73	1.79
6/22/94						
Mean	38.76	17.52	6.49	3.42	3.04	34.25
Std.	3.44	1.65	0.66	0.43	0.45	0.48
COV, %	8.87	9.43	10.16	12.45	14.73	1.41
8/10/94						
Mean	27.16	14.98	6.35	3.21	3.04	20.90
Std.	2.61	1.35	0.72	0.40	0.45	0.30
COV, %	9.59	9.00	11.27	12.35	14.73	1.42
9/21/94						
Mean	30.09	14.54	5.60	2.99	3.04	32.30
Std.	2.42	1.27	0.60	0.32	0.45	0.50
COV, %	8.04	8.76	10.68	10.76	14.73	1.55
10/25/94						
Mean	23.48	14.04	6.38	3.22	3.04	17.36
Std.	2.13	0.86	0.58	0.35	0.45	0.31
COV, %	9.08	6.15	9.14	10.74	14.73	1.81

TABLE 7.5
Summary of Measured Pavement Responses from FWD Tests on Cell-28

Date	D0, mils	D1, mils	D2, mils	D3, mils	Tac, in	Bell's Temperature, deg. C.
3/23/94						
Mean	28.40	17.56	7.35	2.80	2.93	10.03
Std.	3.23	1.92	0.84	0.40	0.22	0.58
COV, %	11.39	10.91	11.38	14.30	7.67	5.78
4/13/94						
Mean	31.02	18.94	8.64	4.41	2.93	14.31
Std.	1.66	0.83	0.50	0.38	0.22	0.01
COV, %	5.36	4.38	5.84	8.52	7.67	0.10
4/27/94						
Mean	26.80	17.27	8.32	4.38	2.93	11.29
Std.	2.16	1.18	0.51	0.33	0.22	0.28
COV, %	8.08	6.85	6.11	7.62	7.67	2.52
5/25/94						
Mean	35.13	17.23	6.95	3.98	2.93	20.97
Std.	2.04	0.82	0.38	0.31	0.22	0.10
COV, %	5.81	4.73	5.47	7.80	7.67	0.50
6/22/94						
Mean	38.40	16.87	6.65	3.66	2.93	32.41
Std.	2.33	0.93	0.44	0.33	0.22	0.51
COV, %	6.07	5.51	6.58	8.91	7.67	1.57
8/10/94						
Mean	28.70	15.32	6.63	3.46	2.93	21.47
Std.	2.13	1.02	0.44	0.28	0.22	0.20
COV, %	7.41	6.64	6.70	7.95	7.67	0.94
9/21/94						
Mean	31.28	14.97	6.09	3.25	2.93	31.80
Std.	2.35	1.10	0.45	0.28	0.22	0.52
COV, %	7.52	7.36	7.43	8.76	7.67	1.64
10/25/94						
Mean	24.95	14.48	6.55	3.35	2.93	16.98
Std.	2.05	0.98	0.46	0.27	0.22	0.05
COV, %	8.23	6.75	7.03	8.00	7.67	0.28

TABLE 7.6
Summary of Measured Pavement Responses from FWD Tests on Cell-29

Date	D0, mils	D1, mils	D2, mils	D3, mils	Tac, in	Bell's Temperature deg. C.
3/23/94						
Mean	16.03	11.79	6.81	3.45	4.92	7.96
Std.	1.68	1.07	0.47	0.21	0.36	0.42
COV, %	10.49	9.04	6.87	6.17	7.36	5.26
4/13/94						
Mean	19.16	13.87	8.05	4.41	4.92	12.81
Std.	2.14	1.40	0.81	0.54	0.36	0.16
COV, %	11.18	10.13	10.09	12.18	7.36	1.26
4/27/94						
Mean	17.50	12.97	7.70	4.35	4.92	11.09
Std.	1.89	1.28	0.74	0.50	0.36	0.16
COV, %	10.78	9.85	9.67	11.56	7.36	1.46
5/25/94						
Mean	28.42	16.59	7.46	3.71	4.92	21.07
Std.	2.69	1.47	0.75	0.47	0.36	0.01
COV, %	9.45	8.88	10.10	12.64	7.36	0.05
6/22/94						
Mean	36.09	17.98	7.04	3.42	4.92	30.20
Std.	3.02	1.42	0.76	0.51	0.36	0.41
COV, %	8.37	7.88	10.73	15.03	7.36	1.37
8/10/94						
Mean	23.02	14.60	7.28	3.55	4.92	20.12
Std.	2.35	1.38	0.75	0.47	0.36	0.19
COV, %	10.22	9.47	10.32	13.17	7.36	0.92
9/21/94						
Mean	30.54	16.11	6.51	2.99	4.92	30.42
Std.	2.87	1.51	0.75	0.47	0.36	0.60
COV, %	9.39	9.34	11.58	15.83	7.36	1.98
10/25/94						
Mean	17.34	12.13	6.75	3.59	4.92	15.91
Std.	1.93	1.22	0.68	0.43	0.36	0.23
COV, %	11.15	10.04	10.04	12.11	7.36	1.47

TABLE 7.7
Summary of Measured Pavement Responses from FWD Tests on Cell-30

Date	D0, mils	D1, mils	D2, mils	D3, mils	Tac, in	Bell's Temperature, deg. C.
3/23/94						
Mean	15.00	11.17	6.59	3.44	5.07	7.51
Std.	1.75	1.39	0.90	0.53	0.23	0.01
COV, %	11.70	12.44	13.70	15.33	4.53	0.13
4/13/94						
Mean	18.06	13.47	8.21	4.73	5.07	11.31
Std.	1.96	1.57	1.06	0.66	0.23	0.48
COV, %	10.85	11.69	12.93	13.93	4.53	4.28
4/27/94						
Mean	16.38	12.40	7.62	4.50	5.07	10.51
Std.	1.73	1.39	0.94	0.59	0.23	0.01
COV, %	10.55	11.25	12.28	13.14	4.53	0.06
5/25/94						
Mean	25.95	15.53	7.35	3.86	5.07	20.87
Std.	3.24	2.25	1.15	0.56	0.23	0.08
COV, %	12.48	14.51	15.59	14.63	4.53	0.36
6/22/94						
Mean	30.54	15.64	6.76	3.60	5.07	28.92
Std.	3.70	2.34	1.11	0.59	0.23	0.38
COV, %	12.12	14.93	16.38	16.29	4.53	1.30
8/10/94						
Mean	20.33	13.14	6.85	3.56	5.07	19.82
Std.	2.00	1.55	0.93	0.57	0.23	0.22
COV, %	9.82	11.77	13.64	15.90	4.53	1.09
9/21/94						
Mean	26.38	14.50	6.18	3.11	5.07	31.30
Std.	3.32	2.23	1.07	0.57	0.23	0.19
COV, %	12.58	15.39	17.37	18.20	4.53	0.60
10/25/94						
Mean	16.27	11.62	6.70	3.72	5.07	15.56
Std.	1.58	1.28	0.86	0.55	0.23	0.20
COV, %	9.68	11.04	12.77	14.80	4.53	1.27

TABLE 7.8
Summary of Measured Pavement Responses from FWD Tests on Cell-31

Date	D0, mils	D1, mils	D2, mils	D3, mils	Tac, in	Bell's Temperature, deg. C.
3/23/94						
Mean	23.26	14.44	6.32	2.54	3.06	7.01
Std.	1.84	0.97	0.44	0.26	0.24	0.03
COV, %	7.91	6.70	7.00	10.14	7.79	0.41
4/13/94						
Mean	25.12	15.85	7.67	3.95	3.06	10.71
Std.	1.29	0.66	0.24	0.09	0.24	0.30
COV, %	5.15	4.18	3.11	2.35	7.79	2.78
4/27/94						
Mean	22.73	14.68	7.22	3.82	3.06	9.65
Std.	1.27	0.72	0.29	0.14	0.24	0.10
COV, %	5.57	4.88	4.03	3.58	7.79	1.06
5/25/94						
Mean	28.36	13.93	5.73	3.27	3.06	19.08
Std.	1.34	0.62	0.18	0.12	0.24	0.49
COV, %	4.73	4.47	3.21	3.61	7.79	2.58
6/22/94						
Mean	30.30	13.16	5.38	3.06	3.06	28.97
Std.	1.24	0.46	0.17	0.11	0.24	0.35
COV, %	4.09	3.47	3.13	3.71	7.79	1.19
8/10/94						
Mean	24.51	13.16	5.67	2.90	3.06	19.75
Std.	0.98	0.38	0.19	0.13	0.24	0.31
COV, %	3.98	2.87	3.38	4.36	7.79	1.58
9/21/94						
Mean	27.95	12.93	5.03	2.70	3.06	32.54
Std.	1.08	0.38	0.20	0.15	0.24	0.44
COV, %	3.86	2.92	3.98	5.65	7.79	1.35
10/25/94						
Mean	22.50	13.46	6.13	3.01	3.06	15.97
Std.	1.03	0.41	0.24	0.19	0.24	0.35
COV, %	4.58	3.05	3.84	6.20	7.79	2.19

TABLE 7.9
Summary of Measured Pavement Responses from FWD Tests on Cell-32

Date	D0, mils	D1, mils	D2, mils	D3, mils
8/17/94				
Mean	49.11	21.13	7.67	3.65
Std.	6.57	3.11	0.94	0.43
COV, %	13.39	14.73	12.29	11.73
9/21/94				
Mean	46.12	19.28	6.73	3.27
Std.	5.82	2.87	0.91	0.41
COV, %	12.61	14.89	13.56	12.60
10/26/94				
Mean	40.45	15.93	5.90	3.06
Std.	2.84	0.84	0.53	0.41
COV, %	7.03	5.24	8.91	13.29

TABLE 7.10
Summary of Measured Pavement Responses from FWD Tests on Cell-33

Date	D0, mils	D1, mils	D2, mils	D3, mils
8/17/94				
Mean	42.72	21.30	8.20	4.24
Std.	3.01	2.64	1.98	1.22
COV, %	7.05	12.40	24.17	28.89
9/21/94				
Mean	41.83	20.17	7.65	3.94
Std.	4.47	3.48	1.83	1.14
COV, %	10.69	17.27	23.91	28.88
10/26/94				
Mean	40.07	18.10	6.15	3.42
Std.	4.75	3.36	1.45	0.82
COV, %	11.86	18.55	23.66	24.00

TABLE 7.11
Summary of Measured Pavement Responses from FWD Tests on Cell-34

Date	D0, mils	D1, mils	D2, mils	D3, mils
8/17/94				
Mean	29.88	12.26	5.89	3.64
Std.	3.07	1.33	0.86	0.44
COV, %	10.27	10.84	14.68	12.17
9/21/94				
Mean	34.48	14.86	6.37	3.72
Std.	5.12	2.36	1.11	0.56
COV, %	14.86	15.85	17.45	15.12
10/26/94				
Mean	34.18	12.89	5.47	3.35
Std.	4.36	1.73	0.86	0.44
COV, %	12.75	13.42	15.78	13.24

TABLE 7.12
Summary of Measured Pavement Responses from FWD Tests on Cell-35

Date	D0, mils	D1, mils	D2, mils	D3, mils
8/17/94				
Mean	24.12	10.88	5.32	3.24
Std.	1.44	1.36	0.68	0.51
COV, %	5.97	12.50	12.73	15.68
9/21/94				
Mean	24.77	11.51	5.57	3.16
Std.	2.61	1.61	0.88	0.52
COV, %	10.53	13.95	15.76	16.40
10/26/94				
Mean	29.44	12.15	5.36	3.06
Std.	2.60	1.20	0.78	0.42
COV, %	8.83	9.85	14.63	13.62

$$AUPP = (5*D0 - 2*D1 - 2*D2 - D3) / 2 \quad \text{.....[7.1]}$$

where

D0 : Deflection at the center of loading plate, mils;

D1 : Deflection at 12-inches from the center of loading plate, mils;

D2 : Deflection at 24-inches from the center of loading plate, mils;

D3 : Deflection at 36-inches from the center of loading plate, mils;

The relationship established by Hill and Thompson is as follows:

$$\text{Log}(\varepsilon_{ac}) = 1.001 + 1.024 * \text{Log}(AUPP) \quad \text{.....[7.2]}$$

$R^2 = 0.997$ SEE = 0.025

where ε_{ac} is strain (microstrain) at the bottom of asphalt concrete layer. The relationship was developed from a database in which asphalt concrete thicknesses ranged from 9.5 to 14 inches, asphalt concrete modulus ranged from 100-ksi to 1100-ksi and E_{Ri} ranged from 1-ksi to 12.3-ksi.

For the conventional flexible pavements, the IDOT algorithm relating AUPP to asphalt concrete strain is as follows:

$$\text{Log}(\varepsilon_{ac}) = 1.2105 + 0.821 * \text{Log}(AUPP) \quad \text{.....[7.3]}$$

$R^2 = 0.973$ SEE = 0.0579

where ε_{ac} is strain (microstrain) at the bottom of asphalt concrete layer. The relationship was developed from an ILLI-PAVE database in which asphalt concrete thicknesses ranged from 3 to 8 inches, asphalt concrete modulus ranged from 100-ksi to 1400-ksi and E_{Ri} ranged from 1-ksi to 12.3-ksi.

Following relationship was obtained between the AUPP and asphalt concrete strain values when the FWD data for Cells 4, 22, and 25 were used:

$$\text{Log}(\varepsilon_{ac}) = 1.15 + 0.89 * \text{Log}(AUPP) \quad \text{.....[7.4]}$$

$R^2 = 0.92$ SEE = 0.030

where ε_{ac} is strain (microstrain) at the bottom of asphalt concrete layer.

The following relationship is for Cells 4 and 22 (thicker asphalt concrete surface):

$$\text{Log}(\varepsilon_{ac}) = 1.15 + 0.92 * \text{Log}(\text{AUPP}) \quad \text{.....[7.5]}$$

$R^2 = 0.99$ SEE = 0.019

There is not a significant difference in equations 7.4 and 7.5, but the R^2 and SEE values for equation 7.5 are much better, reinforcing the fact that the pavement responses can be predicted with much higher accuracy for thicker asphalt concrete pavements. Figures 7.2 and 7.3 show the comparison between the predicted and measured asphalt concrete strain values for Cell-25 and Cell-27 respectively.

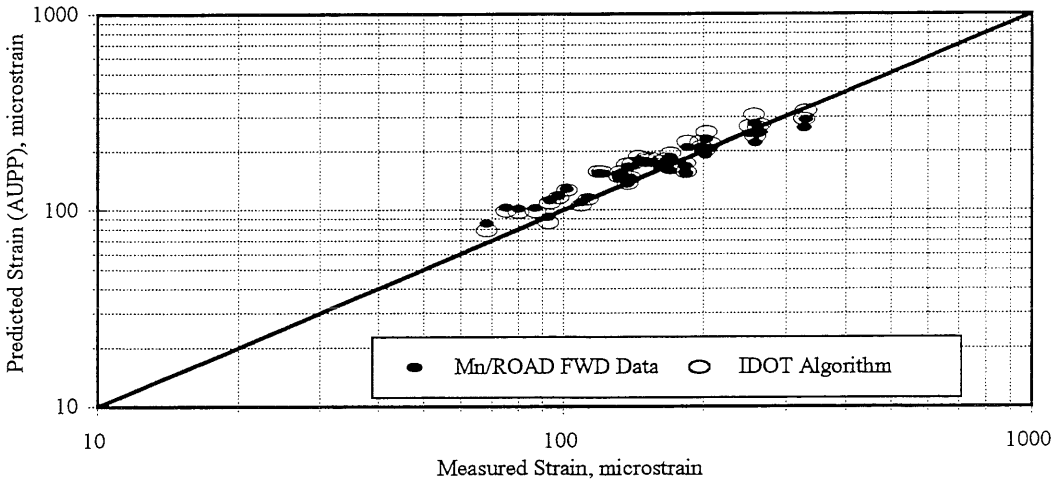

Figure 7.2. Measured and Predicted Asphalt Concrete Strain Values for Cell-25

The predicted asphalt concrete strain values are fairly accurate in the case of Cell-25. The asphalt concrete strain values predicted from FWD data (Eq. 7.5) and IDOT algorithm (Eq. 7.2) are consistent with the field measured values. In the case of Cell-27 (3-inch asphalt concrete thickness), the predicted strain values from FWD data (Eq. 7.5) and IDOT algorithm (Eq. 7.3) are approximately 75-percent higher than the measured values. The IDOT algorithm (Eq. 7.3) and

FWD data (Eq. 7.5) gave similar results. A 3-inch thick asphalt concrete surface exhibits a membrane type behavior which makes predicting pavement responses accurately more difficult.

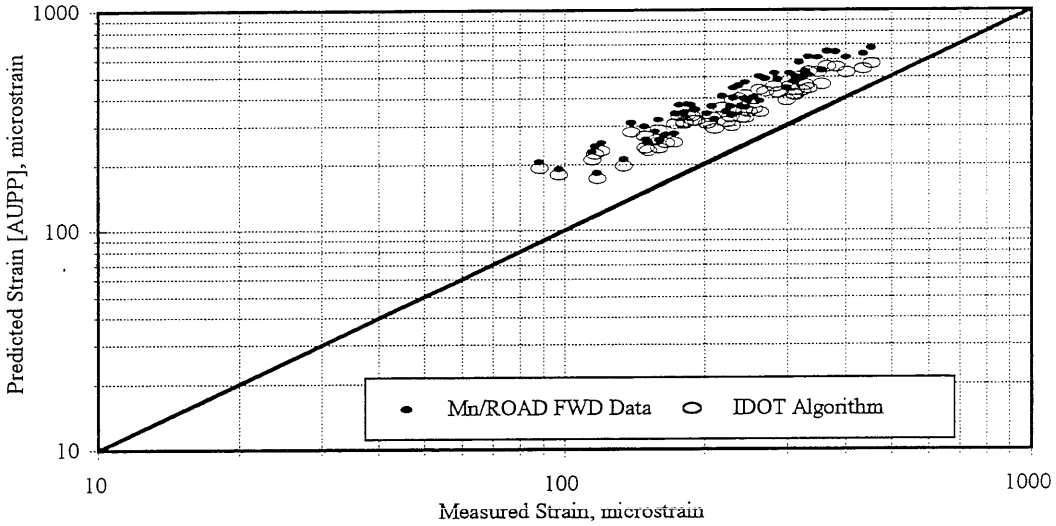

Figure 7.3. Measured and Predicted Asphalt Concrete Strain Values for Cell-27

AUPP is a geometric property of the pavement deflection basin. This is one of the reasons why the relationship between AUPP and asphalt concrete strain is not affected by the type of subgrade (Cells 4 and 22 have cohesive subgrade, and Cell-25 has sandy subgrade), and type of pavement (Cells 4 and 25 are full depth asphalt concrete pavement and Cell-22 is a conventional flexible pavement).

7.3 Estimated Pavement Responses from ILLI-PAVE

ILLI-PAVE [73] is a finite element computer program for plane strain analysis of elastic solids with stress dependent properties. The pavement is modeled as a three-dimensional pavement section by using a two-dimensional half space of a finite solid of revolution as shown in Figure 7.4. By symmetry, the solution of the three-dimensional solid may be specified in terms of a plane radial section of rectangular configuration as shown in Figure 7.5. This rectangular half space is then divided into a set of rectangular elements connected at their node points. Spatial location of the elements and nodes are in terms of the elevation boundaries (rows of node points) and radial boundaries (columns of node points). The elevations are specified as distances up from the

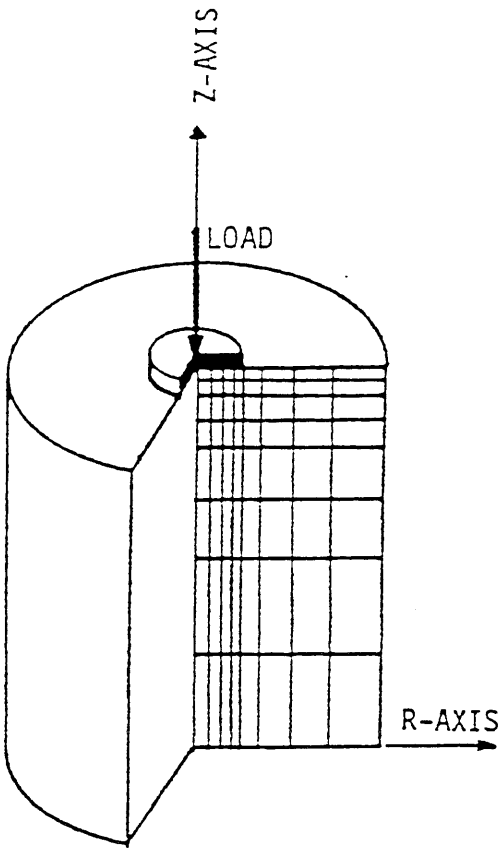

Figure 7.4. Cylindrical Pavement Configuration

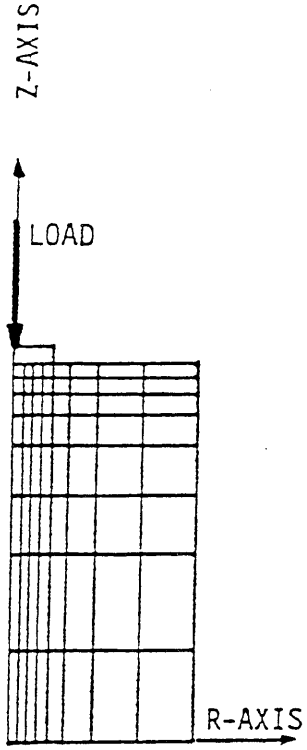

Figure 7.5. Rectangular Half Space of an Axisymmetric Solid

horizontal fixed lower boundary and the radial distances are specified in offset distances from the axial centerline of applied load. The nodes at the inner and outer vertical boundaries are constrained to move only in the vertical direction. The lower boundary is constrained of vertical and horizontal movement. All other elements and nodes are free to move vertically and horizontally. Loading is specified in terms of the surface contact pressure and radius of loaded area. Only one load can be accommodated. It includes stress-strain characterization models that realistically represent the nonlinear stress dependent resilient behavior of granular materials and fine-grained soils. The failure of unbound granular materials is incorporated into the analysis by Mohr-Coulomb failure criteria. The Mohr-Coulomb failure criteria allows for the stress redistribution in the elements so that the granular materials do not achieve unrealistic stress values (i.e. tensile stress at the bottom of the unbound granular layer). The stresses in the granular layer are modified so that the stresses lie within the Mohr-Coulomb failure envelope. The stress adjustment is made assuming that the vertical stress is predicted more accurately. The vertical stress, therefore is used as the basis for adjusting the other stresses. Since directly beneath the point of loading the vertical stress is the major principal stress (σ_1), only the minor principal stress (σ_3) is adjusted in this area. Away from the point of loading, both σ_1 and σ_3 may be adjusted. The major advantage of the stress adjustment is in the selection of realistic modulus values. ILLI-PAVE utilizes an iterative approach to predicting responses. Moduli values are assumed for use in the first iteration. The predicted stresses are then examined and adjusted as necessary. The adjusted stresses are used to calculate the resilient modulus values used in the next iteration. ILLI-PAVE has been found to predict realistic flexible pavement structural responses [72, 73, 74, 75, 76].

ILLI-PAVE runs were conducted for test sections to compare the predicted pavement responses with the FWD measured pavement responses. Pavement deflection responses measured from FWD testing for Cells 24 through 35 are summarized in Tables 7.1 through 7.12. On any given FWD test date, 10 FWD tests were conducted in one lane of the test section. Each deflection value, listed in Tables 7.1 through 7.12, is an average of values measured from 10 FWD tests conducted on the same test date. Variability observed in the measured deflection values within a test section are also summarized in Tables 7.1 through 7.12. The material properties used for the ILLI-PAVE runs correspond to the field conditions at the time of FWD testing. The asphalt concrete layer is modeled as constant modulus material in ILLI-PAVE. Backcalculation algorithms were used to

estimate asphalt concrete modulus (explained in detail in Chapter-VI, section 6.3). A relationship was established between the backcalculated asphalt concrete modulus and the pavement temperature (BELL's temperature). The asphalt concrete modulus was estimated from the following relationship (Chapter-VI):

$$\text{Log } E_{AC} = 3.3804 - 0.04771 * T \quad \text{.....[7.6]}$$

No. of observations = 755

$R^2 = 0.89$ SEE = 0.146

where

E_{AC} : Asphalt concrete modulus, ksi;

T : Temperature, degree Centigrade;

The relationship between the backcalculated asphalt concrete modulus and temperature is shown in Figure 6.28. The temperatures at the time of each FWD test are listed in Tables 7.1 through 7.8. Knowing the test temperature, asphalt concrete stiffness values for ILLI-PAVE were evaluated corresponding to the FWD test conditions. The granular base material is modeled as a stress hardening material. The K-θ model was used to estimate modulus values. The 'K' and 'n' values, used in ILLI-PAVE analysis, for the K-θ model (for different granular materials used) are listed in Table 4.3 (Chapter IV). For the subgrade soils, the "breakpoint" modulus (E_{Ri}) was estimated from the FWD data using the following backcalculation algorithms:

Conventional Flexible Pavements [79]:

$$\text{Log } E_{Ri} = 1.51 - 0.19 * D3 + 0.27 * \text{Log}(D3) \quad \text{.....[7.7]}$$

$R^2 = 0.99$ SEE = 0.05

Full Depth Asphalt Concrete Pavements [79]:

$$\text{Log } E_{Ri} = 24.7 - 5.41 * D3 + 0.31 * D3^2 \quad \text{.....[7.8]}$$

$R^2 = 0.98$ SEE = 0.64

Aggregate Surface / Surface Treated Pavements [79]:

$$E_{Ri} = 24.2 - 5.71 * D3 + 0.35 * D3^2 \quad \text{.....[7.9]}$$

$R^2 = 0.98$ SEE = 0.57

Table 7.13 gives a brief summary of properties used in the ILLI-PAVE runs. Asphalt concrete modulus values listed were obtained from Equation 7.6. The coefficient of lateral pressure at rest and Poisson's ratio values for asphalt concrete, granular material, and subgrade soil were obtained from Reference 73. The granular base material was modeled as a stress hardening material. The K-θ model was used to estimate modulus values. Since two types of subgrades (cohesive and sand) were used in the LVR loop, the subgrades were modeled differently.

Two test sections (Cell-24 & Cell-25) in the LVR loop have a sand subgrade. Cell-24 is a conventional flexible pavement with 3-inch asphalt concrete and 4-inch granular base. Cell-25 is a 5-inch full-depth asphalt concrete section. Sand is a granular material and exhibits stress-hardening behavior (increased modulus with increased stresses). At 3-feet depth in the sand subgrade, the confining stresses exceed deviator stresses (Figure 7.6.a).

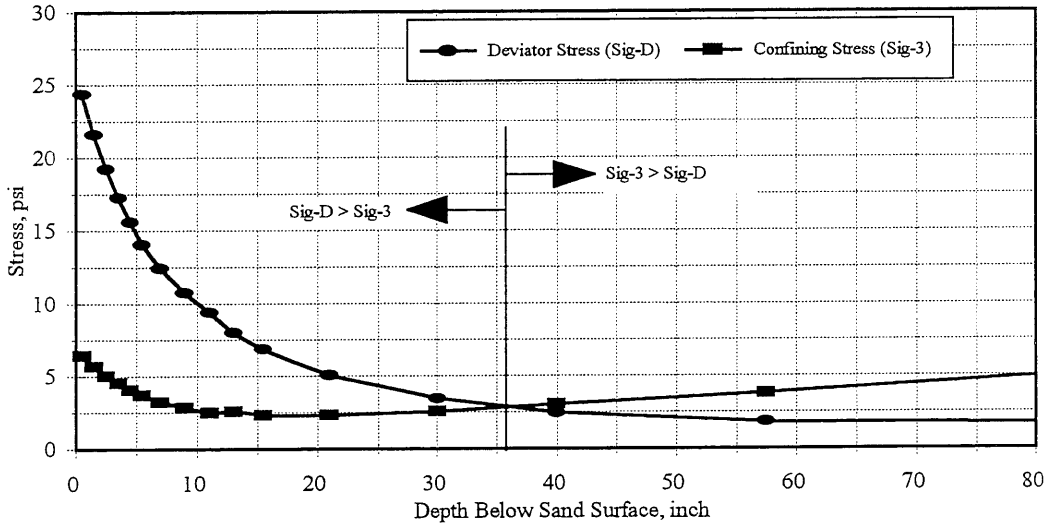

Figure 7.6.a. Stresses in the Sand Subgrade with Depth
[Cell-25: 5-inch full-depth asphalt concrete pavement]

When the confining stress is higher than the deviator stress, granular material exhibits descending behavior (Figure 7.6.b) of resilient modulus with axial strain [50]. The K-θ model (Chapter-IV)

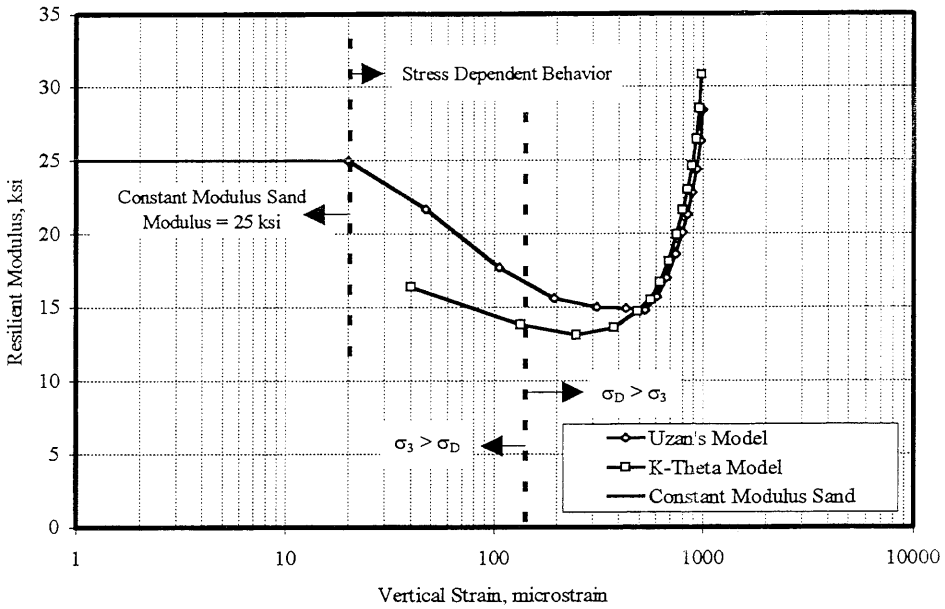

Figure 7.6.b. Behavior of Subgrade Sand Predicted by K-Θ Model and Uzan's Model
[Cell-25: 5-inch full-depth asphalt concrete pavement]

does not describe the descending behavior of resilient modulus with axial strain because it neglects the effect of shear stress on resilient modulus. Uzan's model (Chapter-IV) considers the effect of shear stress on resilient modulus. Figure 7.6.b shows the comparison in the behavior of subgrade sand predicted by K-θ model and Uzan's model. Uzan's model was incorporated in the ILLI-PAVE program recently (April 1997). For Cells 24 and 25, the resilient behavior of top 6-feet of subgrade sand was modeled using Uzan's model. At a depth of 6-feet (72-inches) in the sand subgrade, the magnitude of shear strain is 80-microstrain and it reduces as the depth increases (Figure 7.6.c). Figure 7.6.d [86] shows that as the magnitude of shear strain reduces (lower than 100-microstrain) G/Gmax (G is shear modulus and Gmax is shear modulus at very low or zero shear strain) approaches 1. Since the magnitude of shear strain is very low (lower than 80-microstrain) as the depth in sand increases, the resilient modulus of sand predicted by Uzan's model at six-feet depth (resilient modulus @ 6-feet depth = 25-ksi) was assigned to the sand at depths greater than 6-feet. In other words, the subgrade sand below 6-feet depth was modeled as a constant modulus material with a resilient modulus of 25-ksi.

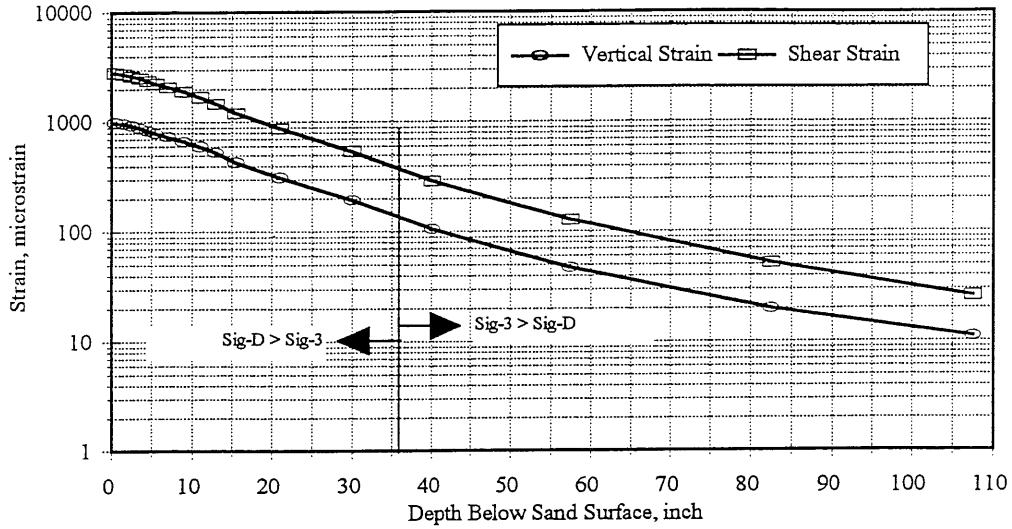

Figure 7.6.c. Vertical and Shear Strains in the Sand Subgrade with Depth
[Cell-25: 5-inch full-depth asphalt concrete pavement]

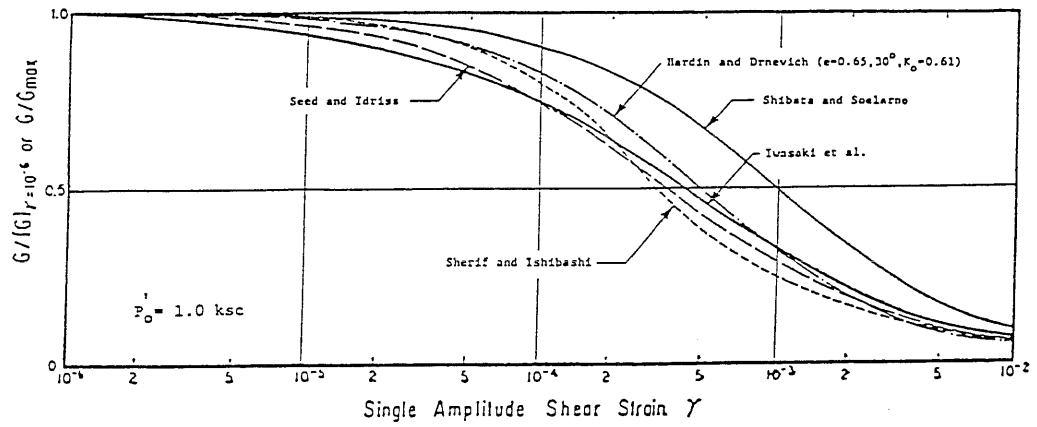

Figure 7.6.d. Comparison of Normalized Modulus Reduction Relationships for Sands [86]

TABLE 7.13
Summary of Material Properties for ILLI-PAVE Runs

Property	Asphalt Concrete			Subgrade			
	40 deg. F	70 deg. F	100 deg. F	Stiff	Medium	Soft	Very Soft
Unit Weight, pcf	145	145	145	125	120	115	110
Lateral Pressure							
Coefficient at res	0.37	0.67	0.85	0.82	0.82	0.82	0.82
Poisson's Rati	0.27	0.40	0.46	0.45	0.45	0.45	0.45
Unconfined Compressive Strength, psi				32.80	22.85	12.90	6.21
Deviator Stress, psi							
Upper Limi				32.80	22.85	12.90	6.21
Lower Limi				2.00	2.00	2.00	2.00
K1, ksi/psi				-1.11	-1.11	-1.11	-1.11
K2, ksi/psi				-0.178	-0.178	-0.178	-0.178
Deviator Stress @ Breakpoint, psi				6.20	6.20	6.20	6.20
Eri, ksi				12.34	7.68	3.02	1.00
E failure, ksi				7.605	4.716	1.827	1.00
E Constant Modulus, ksi	1475	240	38				
Friction Angle, degrees				0.00	0.00	0.00	0.00
Cohesion, psi				16.40	11.43	6.45	3.11

The remaining test sections have cohesive subgrades. The arithmetic model (defined in Chapter-V, Figure 5.1) was used to characterize the stress softening behavior of cohesive soils. In the arithmetic model, the value of the resilient modulus at the breakpoint in the bilinear curve, E_{Ri}, is a good indicator of a soil's resilient behavior. The slope values, K_1 and K_2, display less variability and influence pavement structural response to a smaller degree than E_{Ri}.

7.4 Comparison Between Estimated (from ILLI-PAVE) & Measured (from FWD Testing) Pavement Responses

Cell-24 :

3-inch Asphalt Concrete Surface / 4-inch Granular Base (CL-6sp) / Sandy Subgrade

Figures 7.7 through 7.10 show the comparison between the measured and ILLI-PAVE predicted deflections under a 9000-lb load applied on a 12-inch diameter plate.

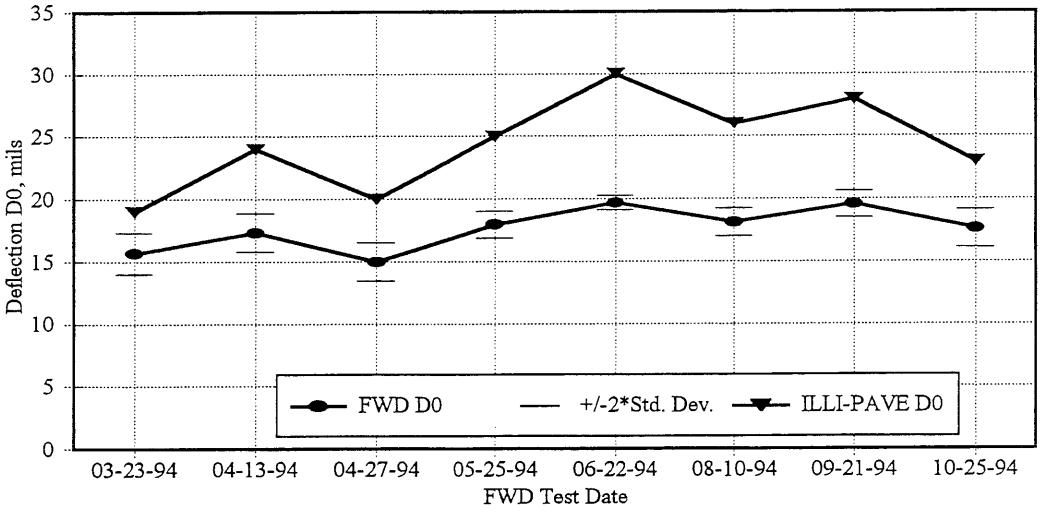

Figure 7.7. Comparison Between FWD Peak Center Deflection and ILLI-PAVE Predicted Peak Center Deflection for Cell-24

The peak center deflections (Figure 7.7) were over-predicted by about 30-percent. The predicted deflections D1 (deflection at 12-inch distance from the center of plate) were fairly constant and ranged from 11-12 mils (Figure 7.8). The difference between the measured and predicted deflections ranged from 2-4 mils (15-65 percent). The predicted deflections D2 (deflection at 24-inch distance from the center of plate) were almost same as the field measured deflections. The

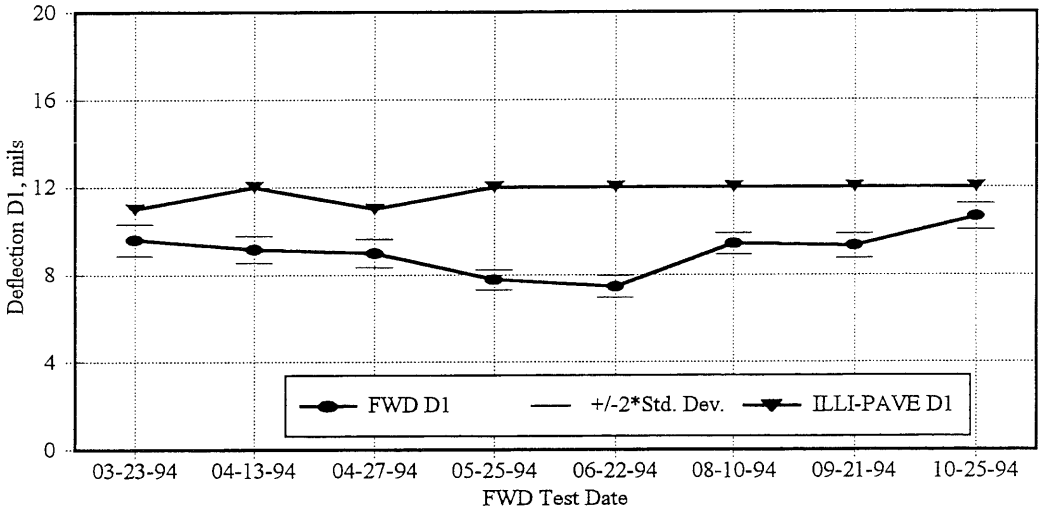

Figure 7.8. Comparison Between FWD D1 and ILLI-PAVE D1 for Cell-24

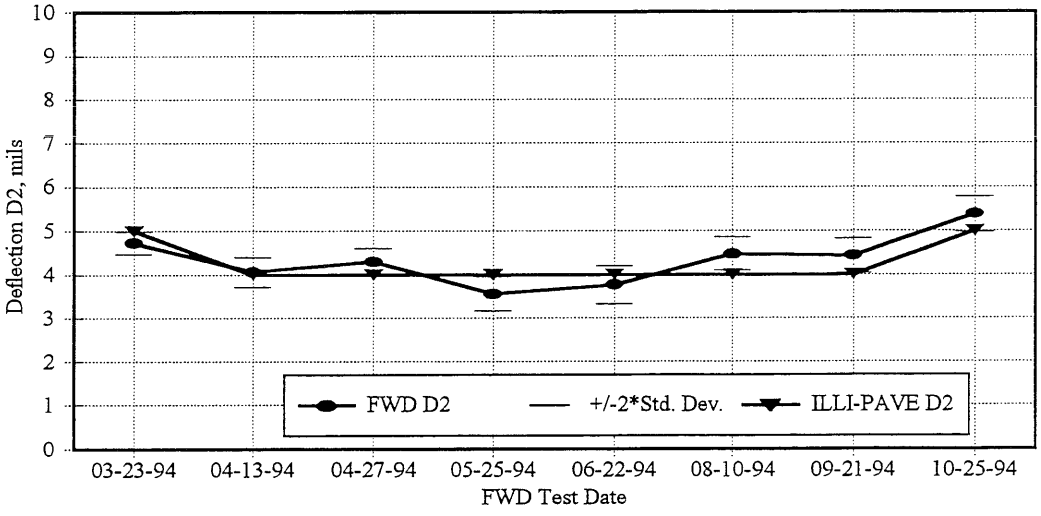

Figure 7.9. Comparison Between FWD D2 and ILLI-PAVE D2 for Cell-24

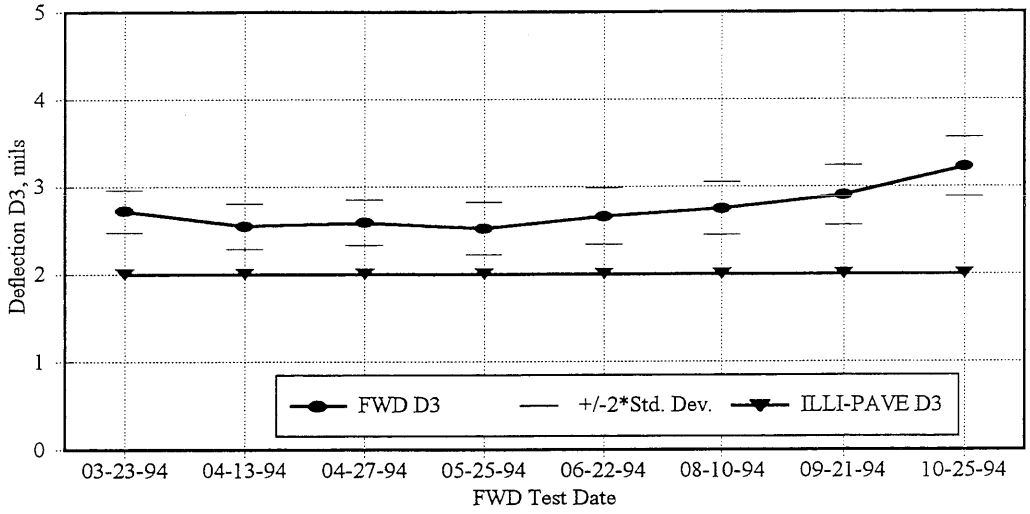

Figure 7.10. Comparison Between FWD D3 and ILLI-PAVE D3 for Cell-24

difference between the measured and predicted D3 (deflection at 36-inch distance from the center of plate) ranged from 0.5-1.0 mils (20-35 percent). ILLI-PAVE under-predicted the D3 deflections (Figure 7.10). Figure 7.11 shows the comparison between the measured and the predicted AREA. The "AREA" of the deflection basin is a parameter combining all measured deflections in the basin. Combining the different sensor deflections into one number minimizes the effect of a possible sensor malfunction. AREA is defined as [75]:

$$AREA = 6 * [1 + 2*D1/D0 + 2*D2/D0 + D3/D0] \quad \text{.....[7.10]}$$

where D0, D1, D2, and D3 are sensor deflections from FWD testing at distance of 0-inch, 12-inch, 24-inch, and 36-inch respectively. AREA is a function of sensor location and has units of length (inches in this case). Stiffer the pavement, larger the AREA. The stiffness of the pavement section predicted by ILLI-PAVE (ILLI-PAVE AREA) is lower than the observed stiffness (FWD AREA) in the field. AREA and AUPP are used to characterize the shape of deflection basin. Figure 7.12 shows the comparison between measured and predicted AUPP. The predicted AUPP values are about 33-60 percent higher than the measured values and the difference increases with the increase in the measured AUPP values.

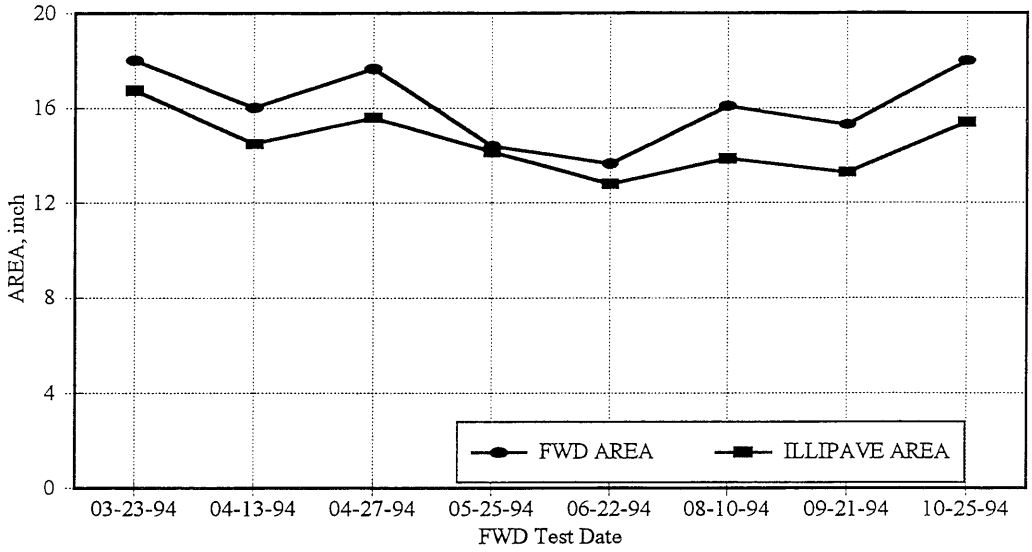

Figure 7.11. Comparison Between FWD AREA and ILLI-PAVE Predicted AREA for Cell-24

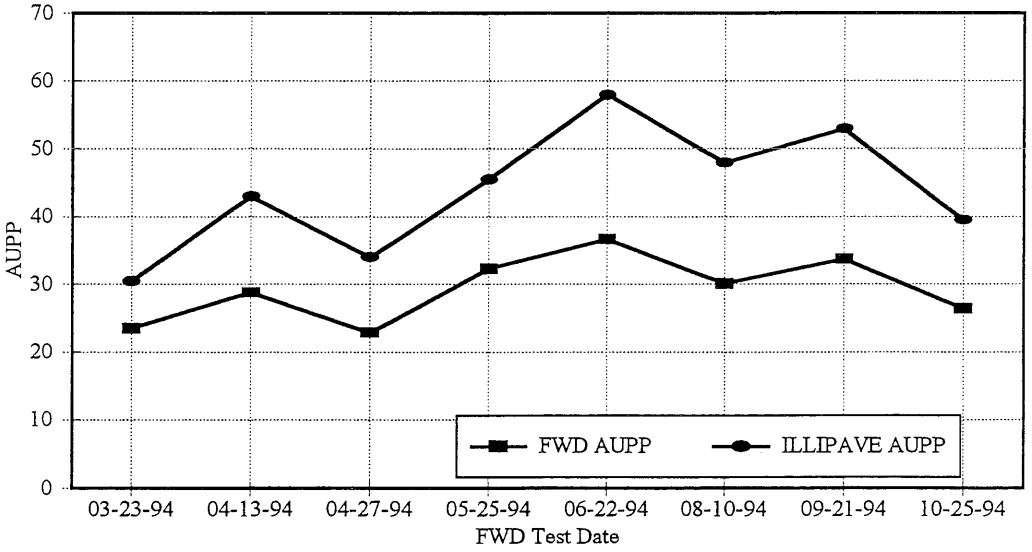

Figure 7.12. Comparison Between FWD AUPP and ILLI-PAVE Predicted AUPP for Cell-24

Cell-25 :

5-inch Full-Depth Asphalt Concrete Pavement / Sandy Subgrade

The peak center deflections (Figure 7.13) were over-predicted by about 1-7 mils (2-33 percent).

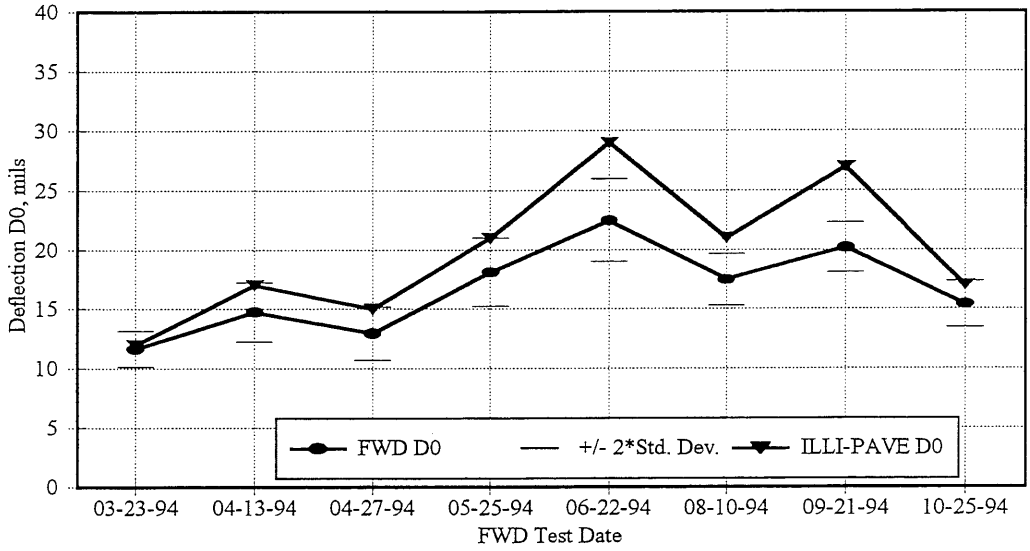

Figure 7.13. Comparison Between FWD Peak Center Deflection and ILLI-PAVE Predicted Peak Center Deflection for Cell-25

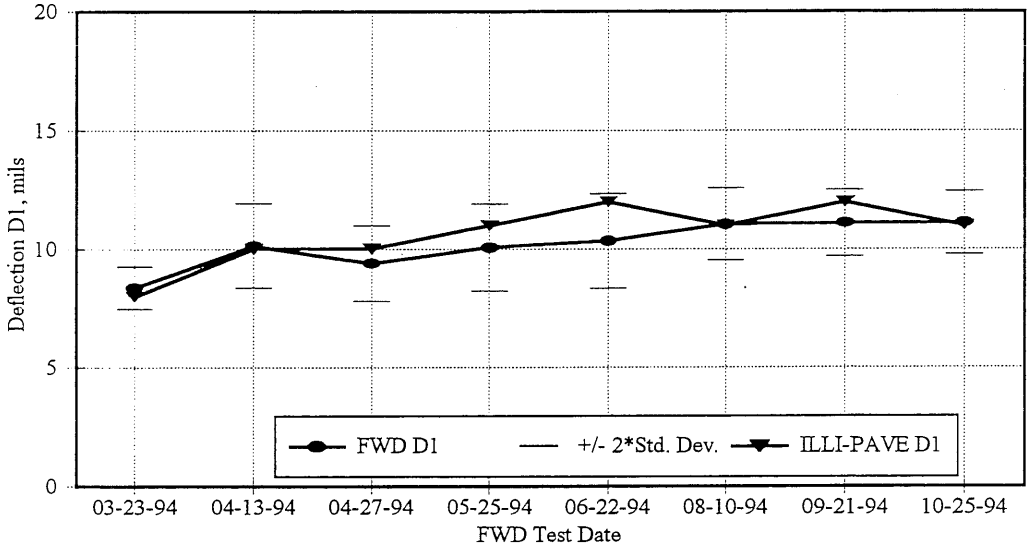

Figure 7.14. Comparison Between FWD D1 and ILLI-PAVE D1 for Cell-25

The deflections D1 are shown in Figure 7.14. The difference between the measured and predicted deflections ranged from 1-2 mils (1-16 percent). The difference between the predicted and measured deflections D2 (Figure 7.15) ranged from 1-2 mils (4-28 percent).

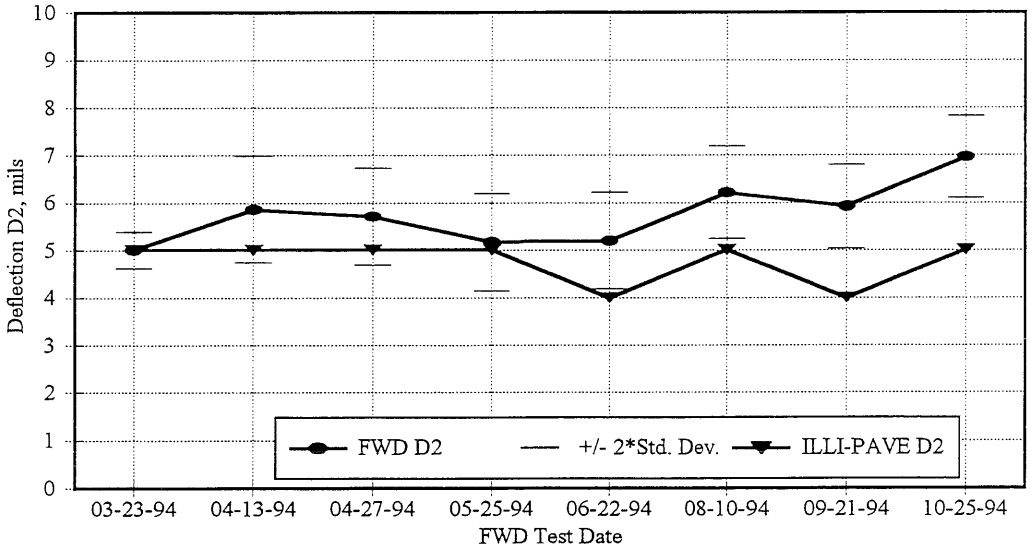

Figure 7.15. Comparison Between FWD D2 and ILLI-PAVE D2 for Cell-25

The difference between the measured and predicted D3 ranged from 1-2 mils (13-48 percent). ILLI-PAVE under-predicted the D3 deflections (Figure 7.16).

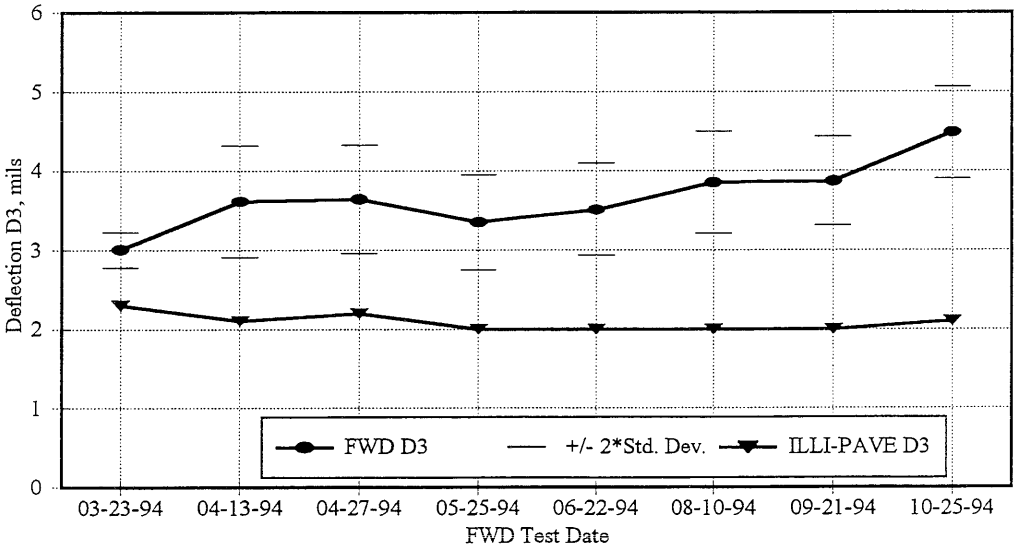

Figure 7.16. Comparison Between FWD D3 and ILLI-PAVE D3 for Cell-25

Figure 7.17 shows the comparison between the measured AUPP and the predicted AUPP. The predicted AUPP values are about 16-55 percent higher than the measured values and the difference increases with the increase in the measured AUPP values.

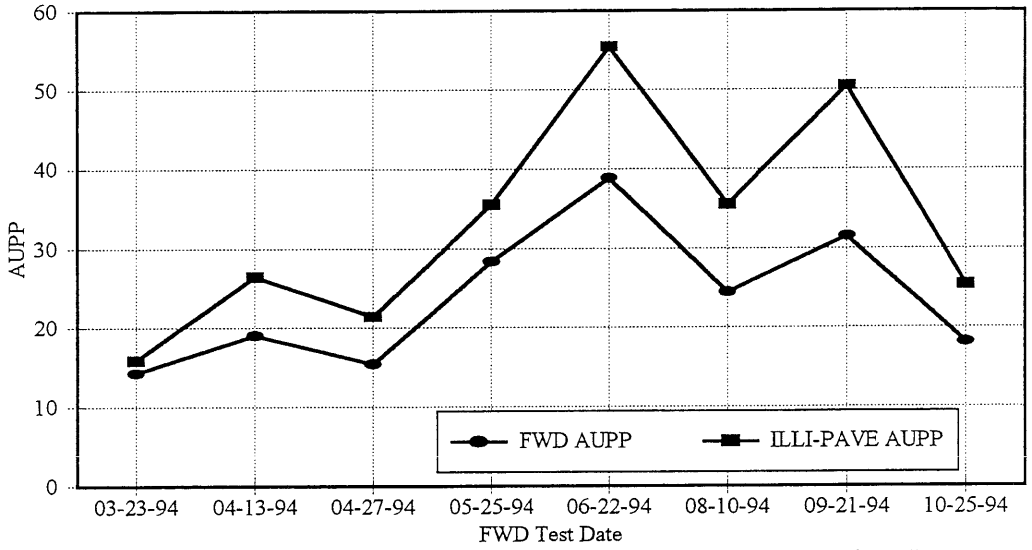

Figure 7.17. Comparison Between FWD AUPP and ILLI-PAVE Predicted AUPP for Cell-25

Figure 7.18 shows the measured and predicted asphalt concrete strain values. ILLI-PAVE over predicted the asphalt concrete strain values by about 40-percent.

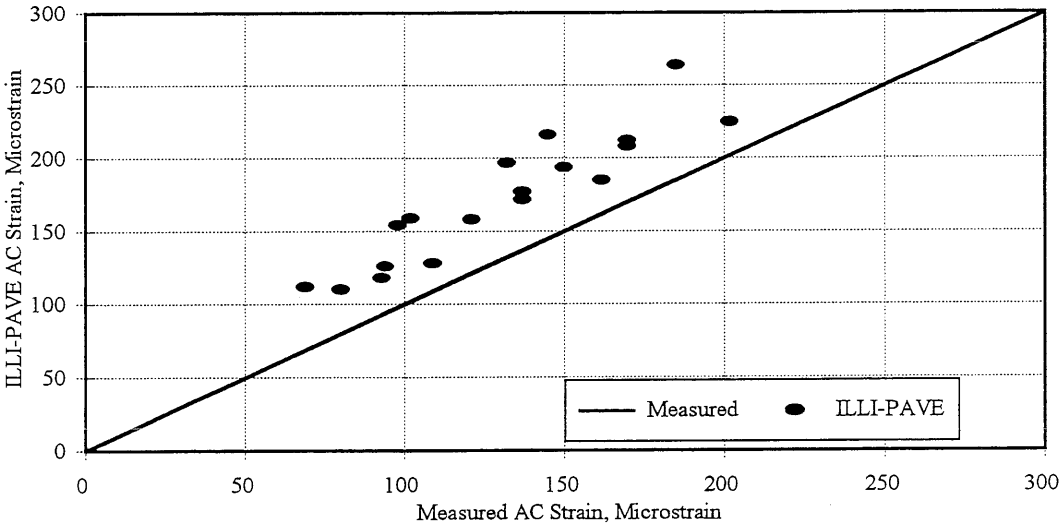

Figure 7.18. Comparison Between Measured Asphalt Concrete Strain and ILLI-PAVE Predicted Asphalt Concrete Strain for Cell-25

Figure 7.19 shows comparison between measured and ILLI-PAVE predicted AREA. ILLI-PAVE predicted lower stiffness (lower AREA) compared to the stiffness measured in the field.

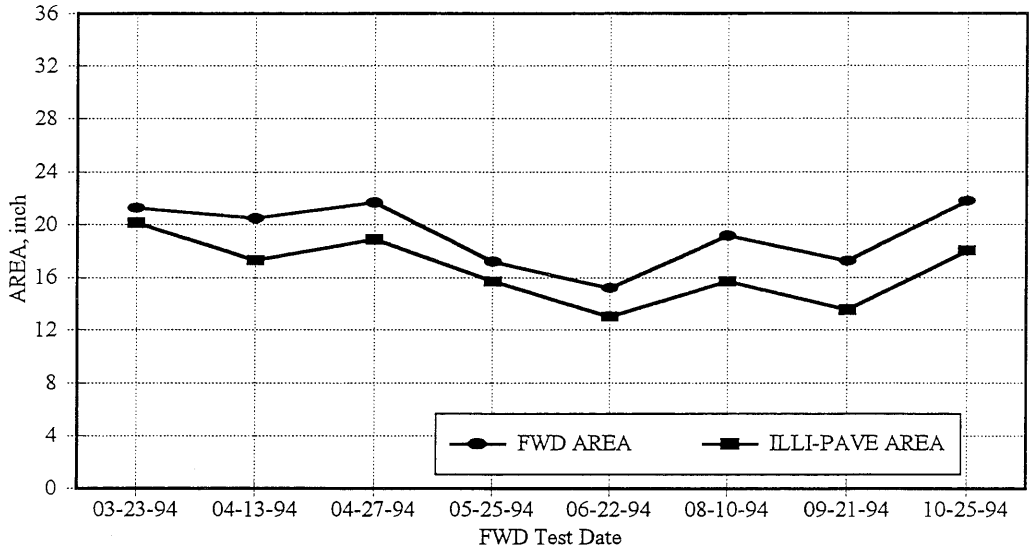

Figure 7.19. Comparison Between FWD AREA and ILLI-PAVE Predicted AREA for Cell-25

Cell-26 :

6-inch Full-Depth Asphalt Concrete Pavement / Cohesive Subgrade

Figures 7.20 through 7.23 show the comparison between the measured FWD deflections and ILLI-PAVE predicted deflections.

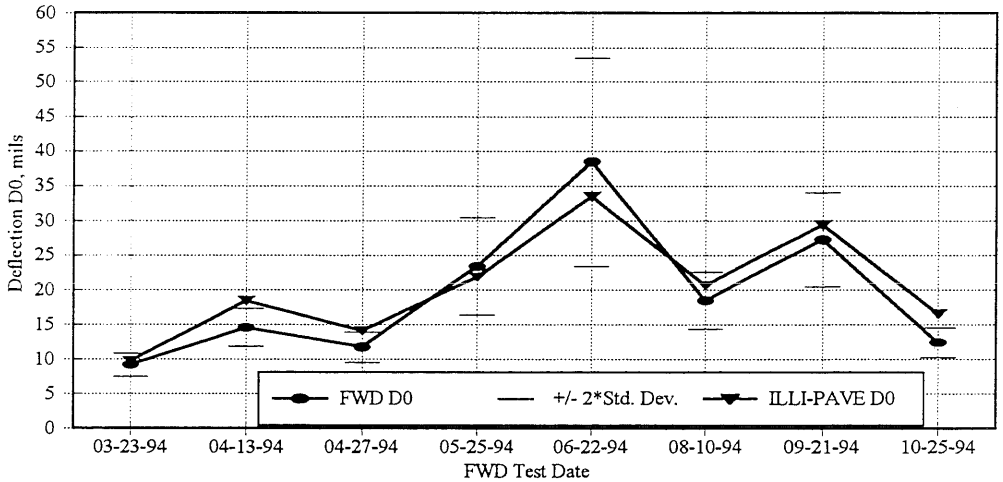

Figure 7.20. Comparison Between FWD Peak Center Deflection and ILLI-PAVE Predicted Peak Center Deflection for Cell-26

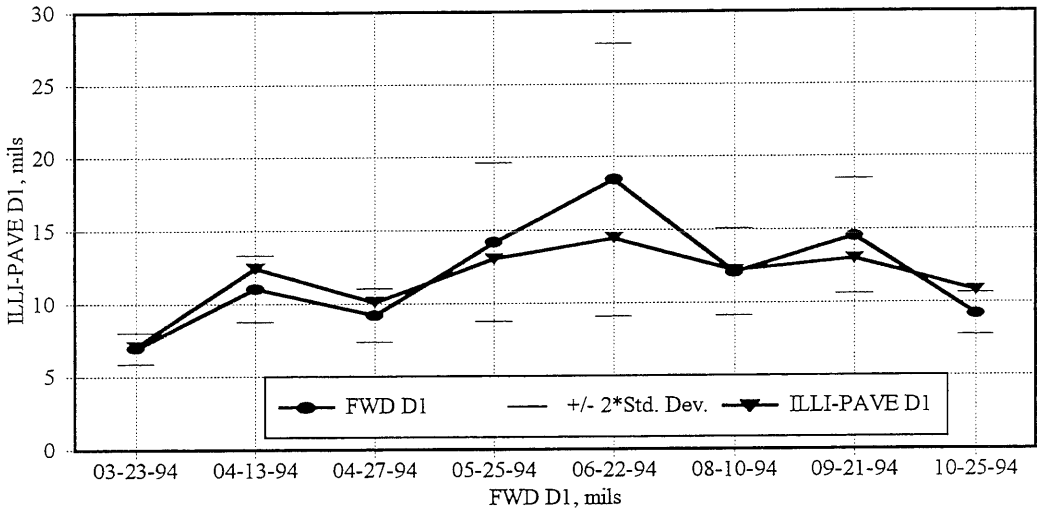

Figure 7.21. Comparison Between FWD D1 and ILLI-PAVE Predicted D1 for Cell-26

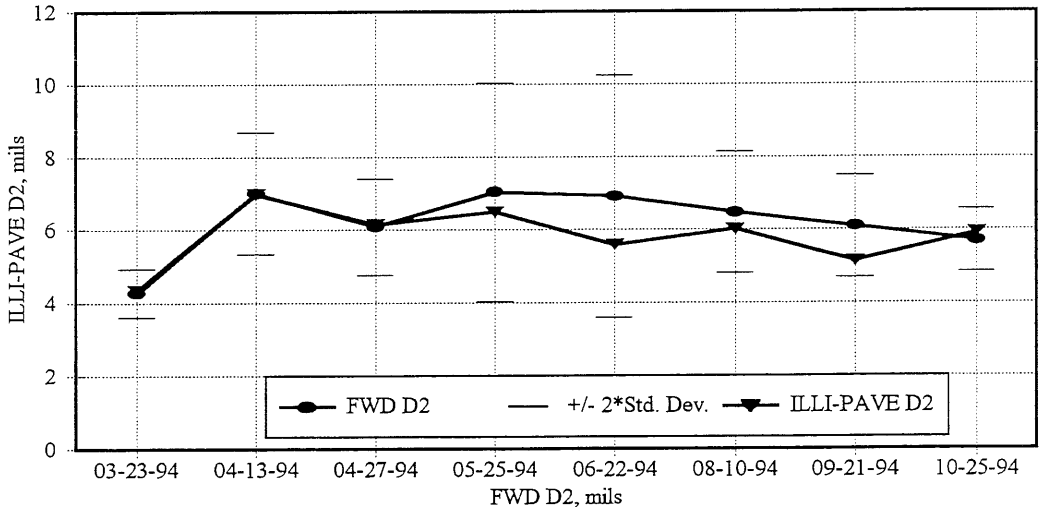

Figure 7.22. Comparison Between FWD D2 and ILLI-PAVE Predicted D2 for Cell-26

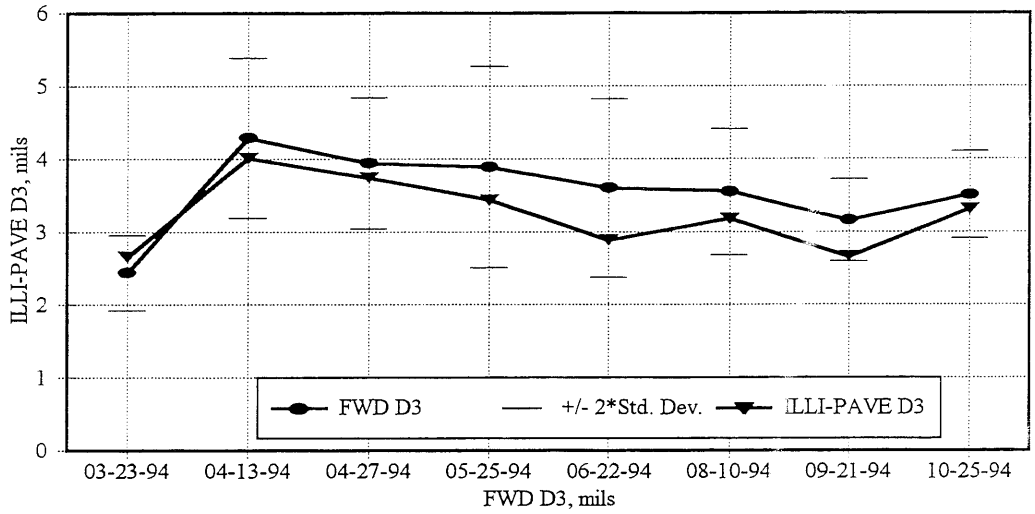

Figure 7.23. Comparison Between FWD D3 and ILLI-PAVE Predicted D3 for Cell-26

The ILLI-PAVE predicted deflections are within two standard deviation of the field measured values. There is variability in the field measured values because of the inherent variability in the materials and the variation in the layer thickness. Figure 7.24 shows the comparison between the measured and predicted AUPP values.

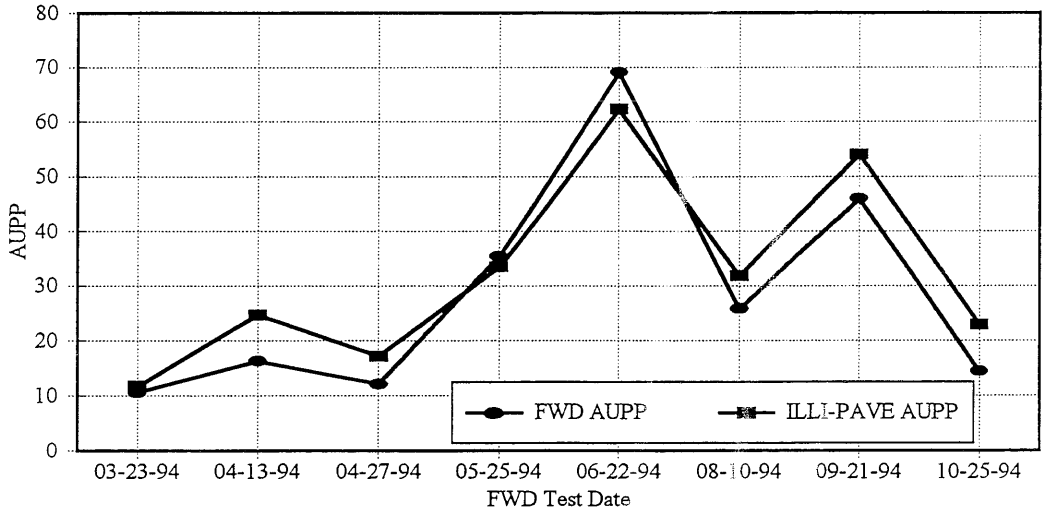

Figure 7.24. Comparison Between FWD AUPP and ILLI-PAVE Predicted AUPP for Cell-26

The predicted values are fairly accurate considering the material and thickness variability in the

field. Comparison between measured and predicted AREA is shown in Figure 7.25. The AREA predicted from ILLI-PAVE is comparable to FWD AREA.

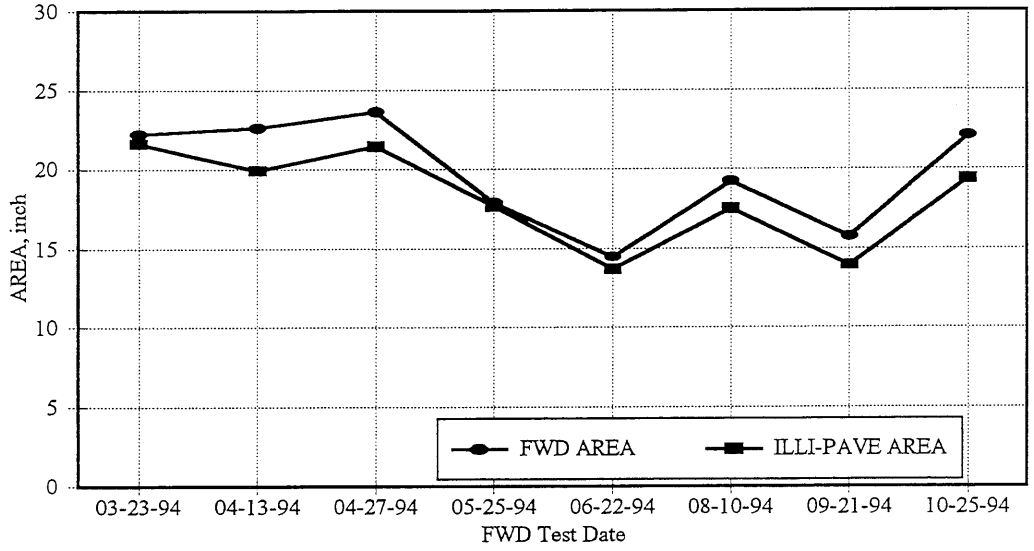

Figure 7.25. Comparison Between FWD AREA and ILLI-PAVE Predicted AREA for Cell-26

Cell-27 :

3-inch Asphalt Concrete Surface / 11-inch Granular Base (CL-6sp) / Cohesive Subgrade

Deflection D0 values (Figure 7.26) are under-predicted by 6-33 percent, higher differences being at higher D0 values (high pavement temperatures).

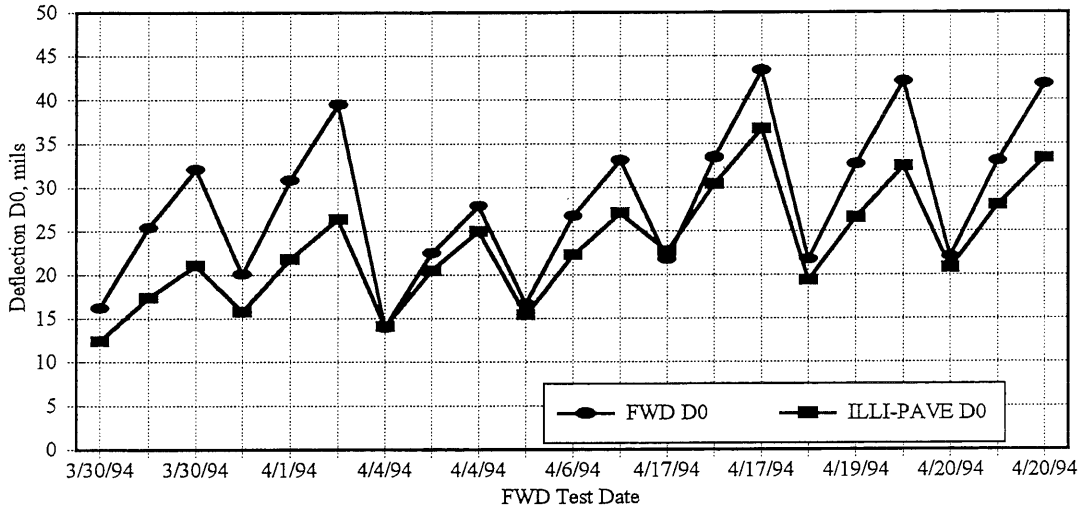

Figure 7.26. Comparison Between FWD Peak Center Deflection and ILLI-PAVE Predicted Peak Center Deflection for Cell-27

Similar pattern was observed for deflections D1 and D2 (Figures 7.27 & 7.28 respectively).

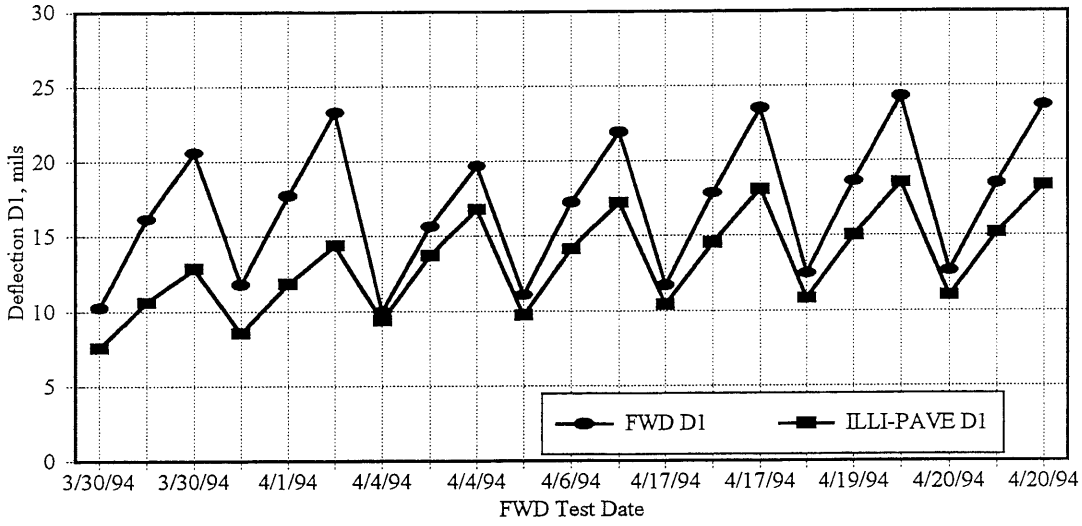

Figure 7.27. Comparison Between FWD D1 and ILLI-PAVE D1 for Cell-27

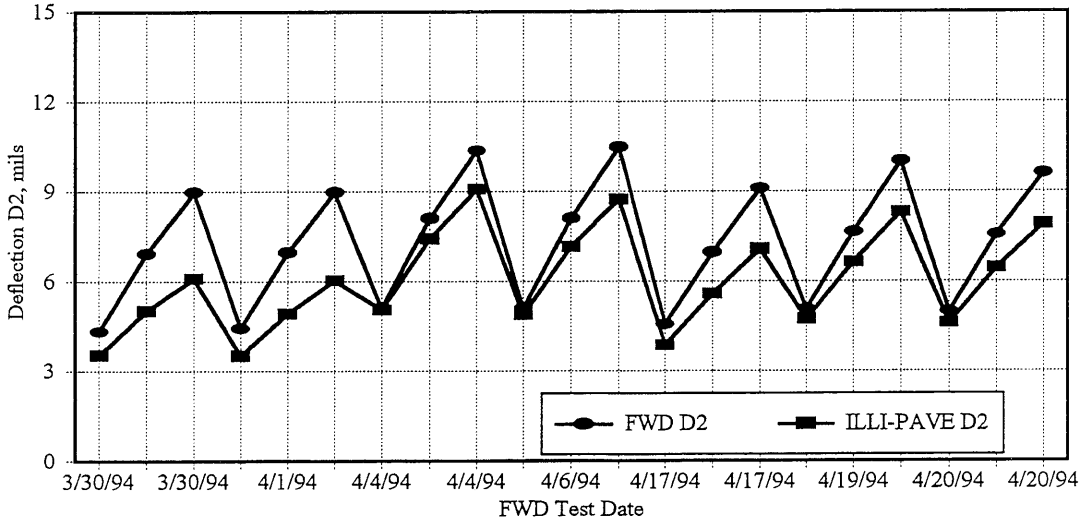

Figure 7.28. Comparison Between FWD D2 and ILLI-PAVE D2 for Cell-27

The difference in predicted and measured deflection D3 values were less than 1-mil (Figure 7.29).

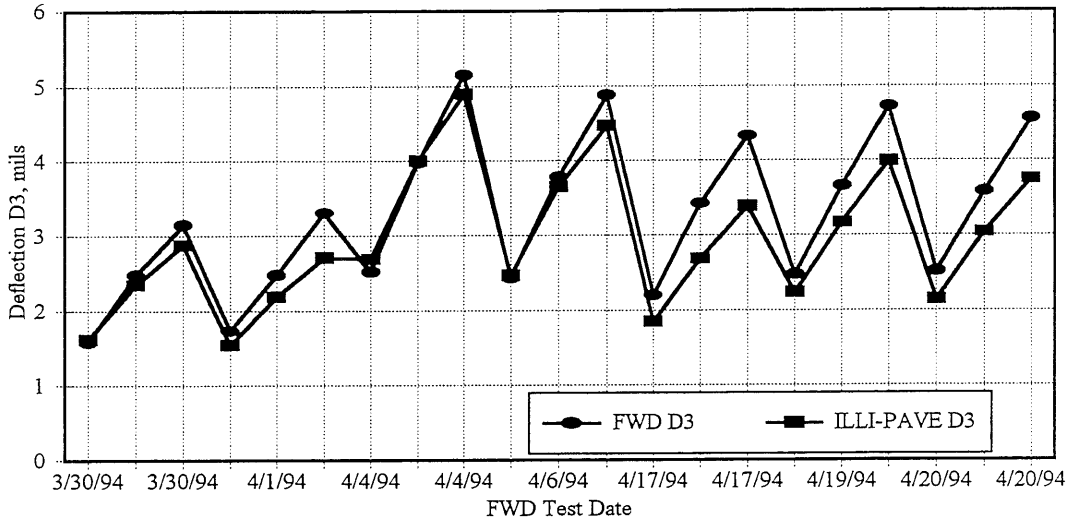

Figure 7.29. Comparison Between FWD D3 and ILLI-PAVE D3 for Cell-27

Figure 7.30 shows the comparison between the measured and predicted AUPP values. The predicted AUPP values were lower by 3-30 percent compared to the measured AUPP values.

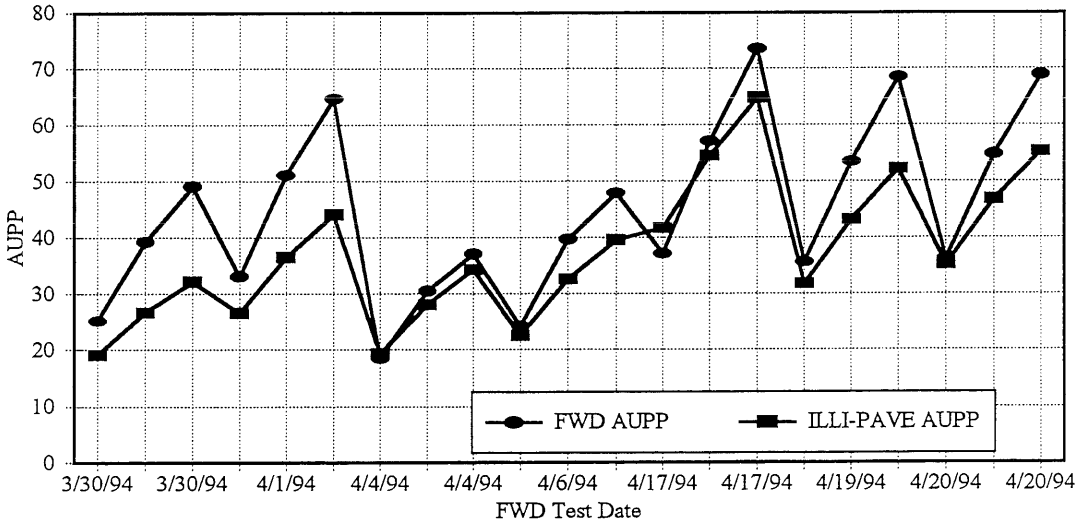

Figure 7.30. Comparison Between FWD AUPP and ILLI-PAVE AUPP for Cell-27

ILLI-PAVE predicted AREA were similar to the field measured AREA (Figure 7.31).

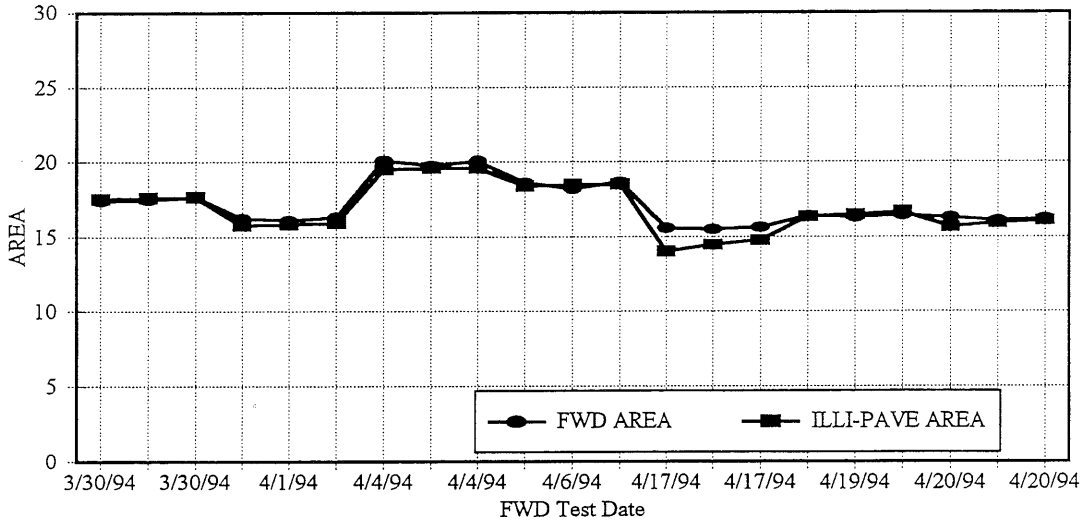

Figure 7.31. Comparison Between FWD AREA and ILLI-PAVE AREA for Cell-27

The predicted asphalt concrete strain values were 20-90 percent higher than the measured values (Figure 7.32).

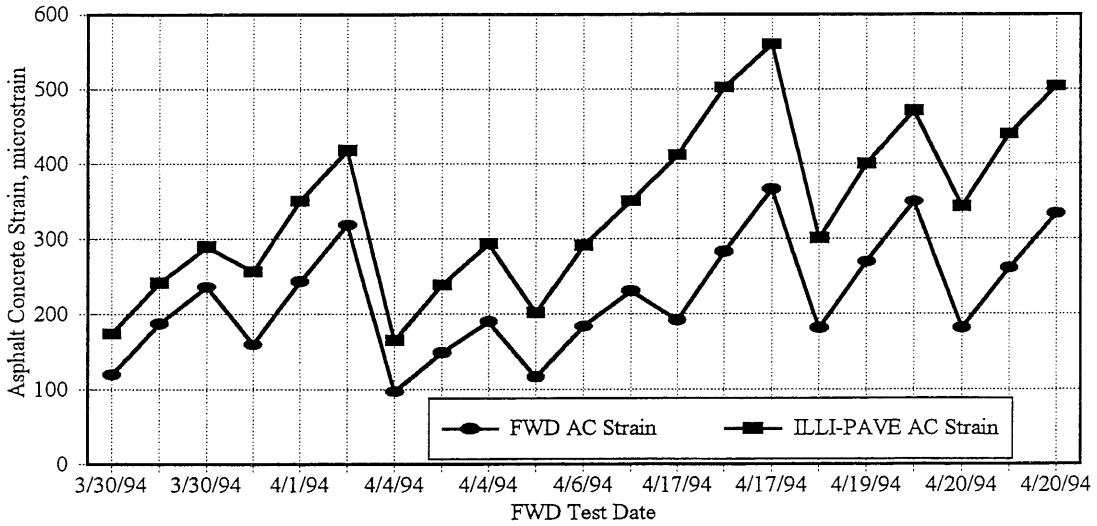

Figure 7.32. Comparison Between Measured and ILLI-PAVE Predicted Asphalt Concrete Strain for Cell-27

Cell-28 :

3-inch Asphalt Concrete Surface / 13-inch Granular Base (CL-5sp) / Cohesive Subgrade

Predicted deflection D0 values (Figure 7.33) were fairly accurate. The difference in the predicted and measured values ranged from 1-25 percent. Most of the predicted values were within two standard deviations of the measured values.

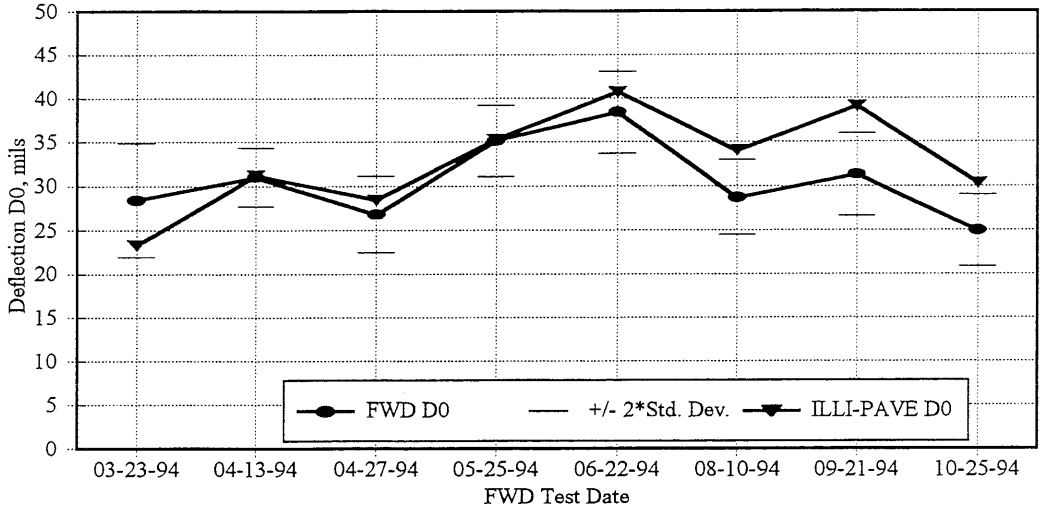

Figure 7.33. Comparison Between FWD Peak Center Deflection and ILLI-PAVE Predicted Peak Center Deflection for Cell-28

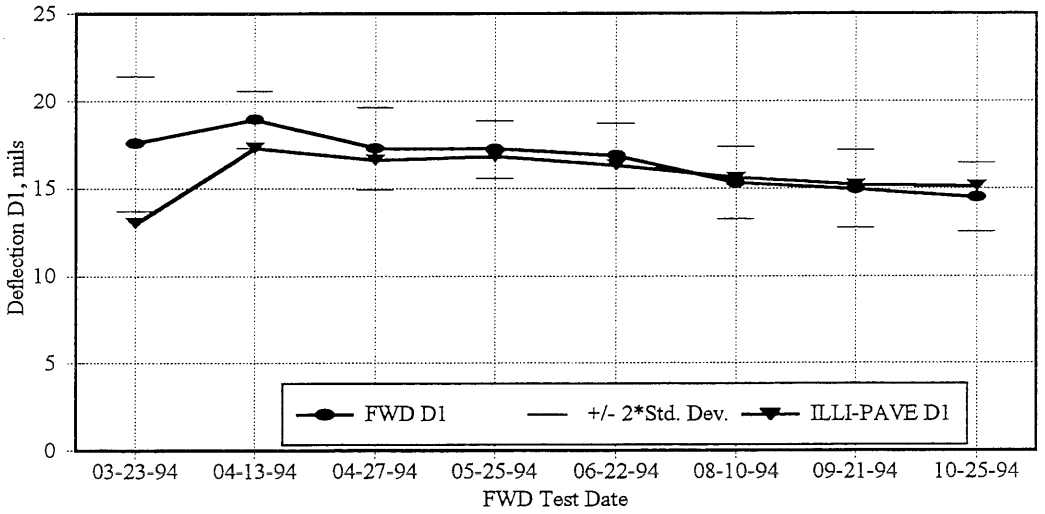

Figure 7.34. Comparison Between FWD D1 and ILLI-PAVE Predicted D1 for Cell-28

Predicted deflection D1 values were within 2-8 percent of the measured values (Figure 7.34). Deflection D2 values were under predicted by 5-16 percent (Figure 7.35).

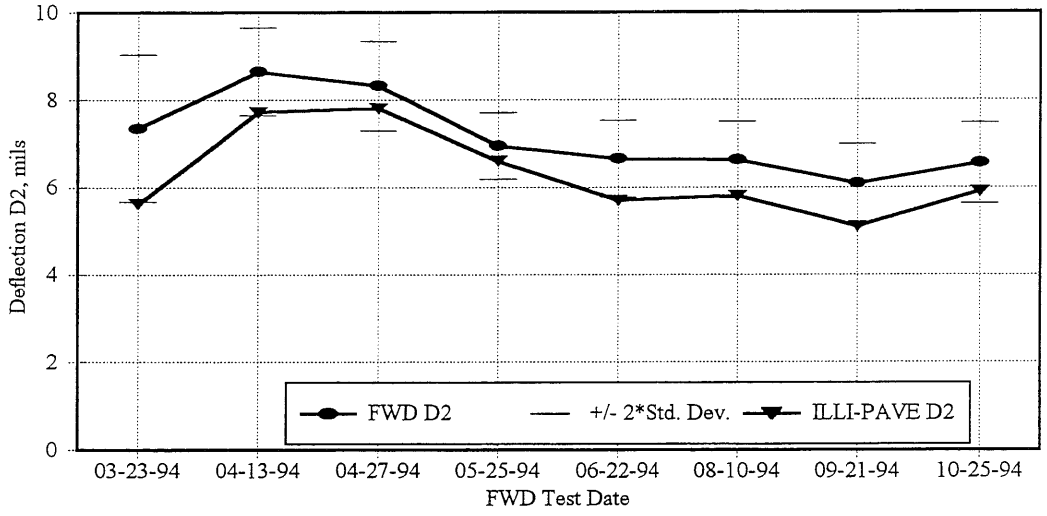

Figure 7.35. Comparison Between FWD D2 and ILLI-PAVE Predicted D2 for Cell-28

Figure 7.36 shows that the D3 values were under predicted by 11-23 percent. The difference between the measured and predicted values was about 1-mil.

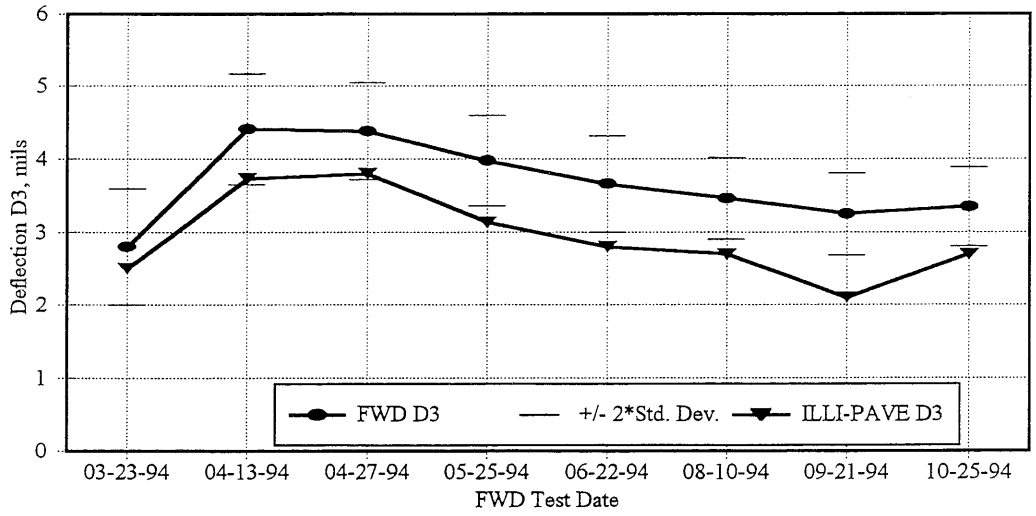

Figure 7.36. Comparison Between FWD D3 and ILLI-PAVE Predicted D3 for Cell-28

Figure 7.37 shows the comparison between the measured and predicted AUPP values. The predicted AUPP values were higher by 3-37 percent compared to the measured AUPP values. ILLI-PAVE predicted slightly lower stiffness (lower AREA) compared to the stiffness measured in the field (Figure 7.38).

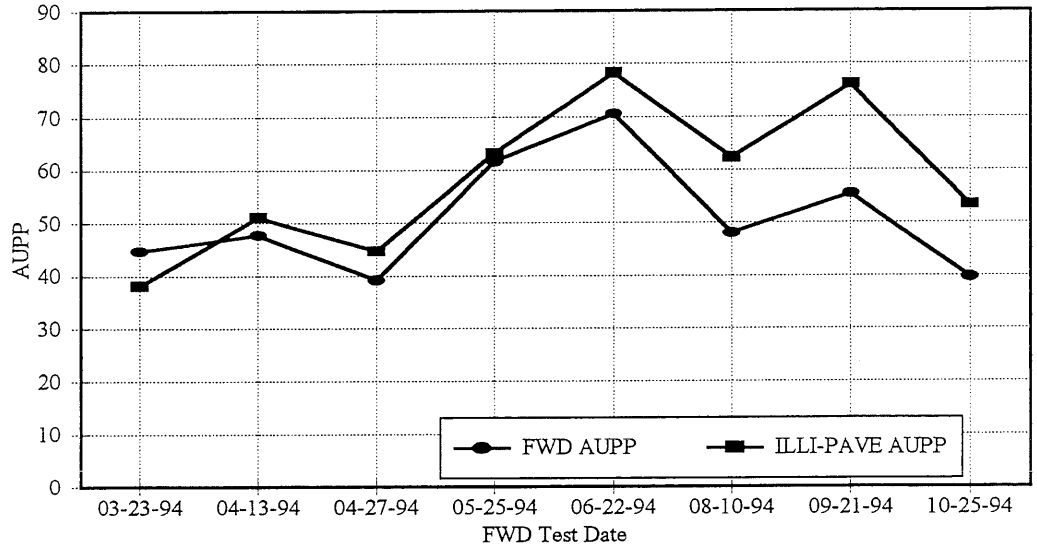

Figure 7.37. Comparison Between FWD AUPP and ILLI-PAVE Predicted AUPP for Cell-28

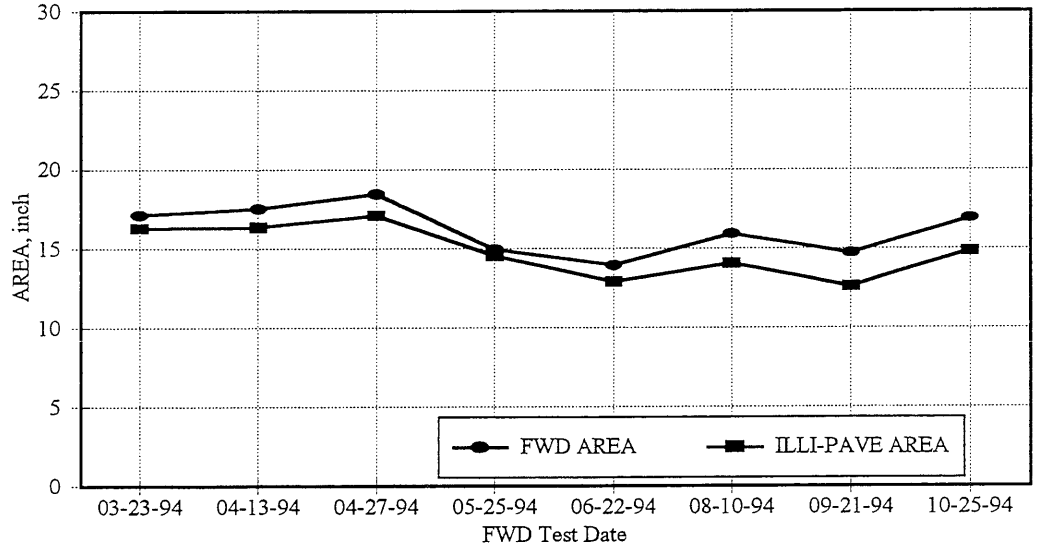

Figure 7.38. Comparison Between FWD AREA and ILLI-PAVE Predicted AREA for Cell-28

Cell-29 :

5-inch Asphalt Concrete Surface / 10-inch Granular Base (CL-4sp) / Cohesive Subgrade

Figures 7.39 through 7.42 show the comparison between the measured FWD deflections and ILLI-PAVE predicted deflections.

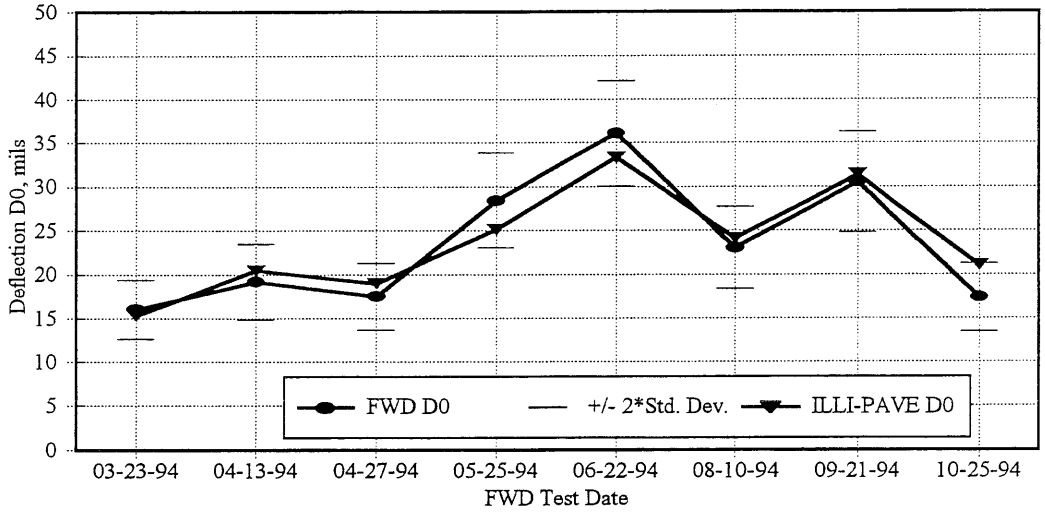

Figure 7.39. Comparison Between FWD Peak Center Deflection and ILLI-PAVE Predicted Peak Center Deflection for Cell-29

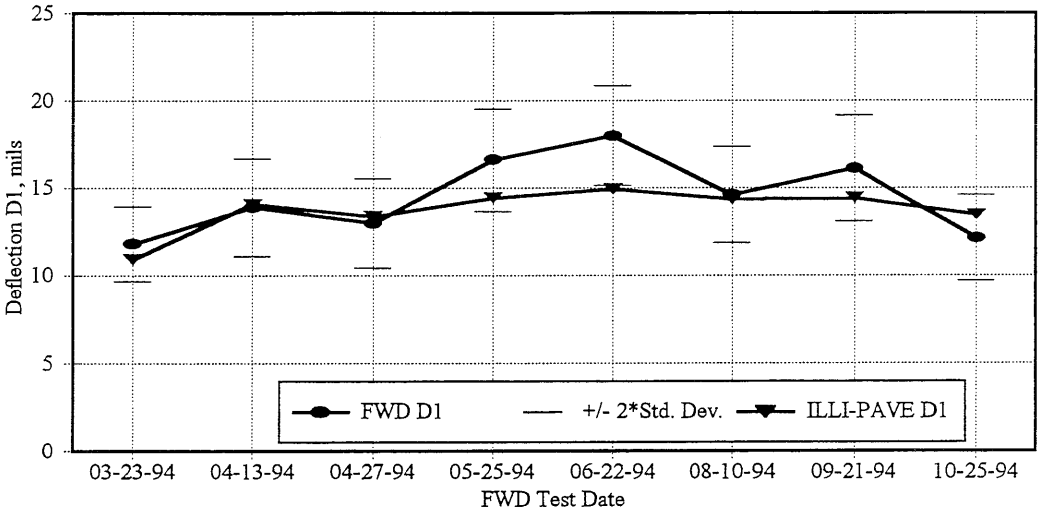

Figure 7.40. Comparison Between FWD D1 and ILLI-PAVE Predicted D1 for Cell-29

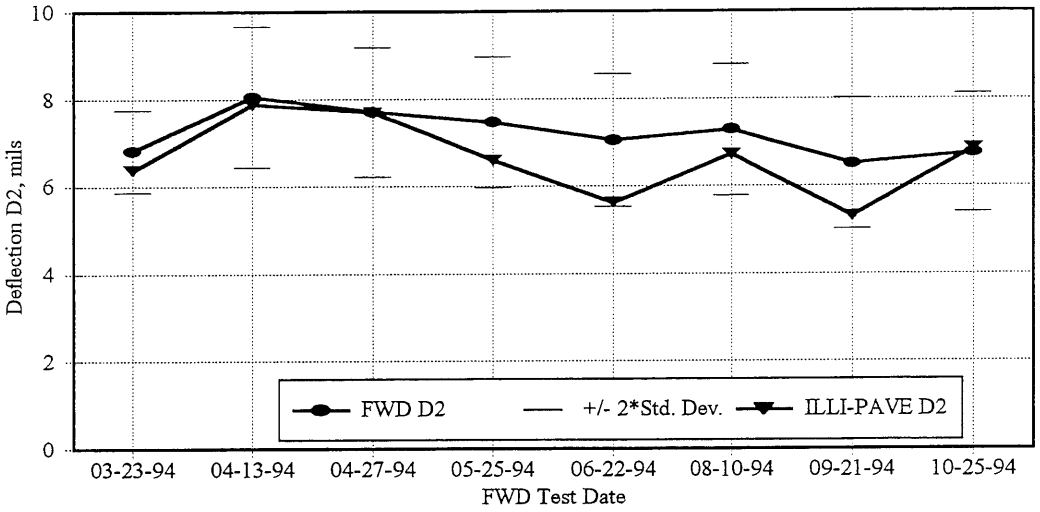

Figure 7.41. Comparison Between FWD D2 and ILLI-PAVE Predicted D2 for Cell-29

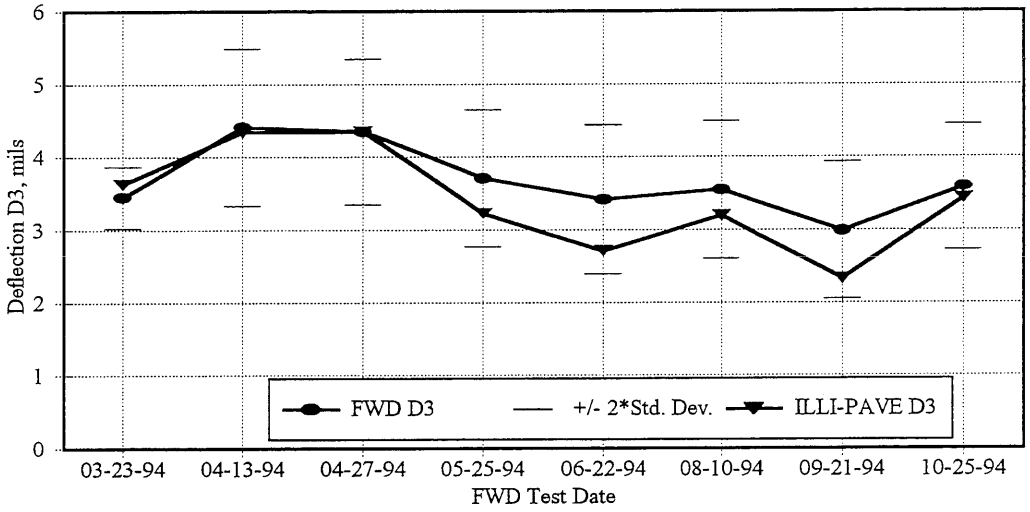

Figure 7.42. Comparison Between FWD D3 and ILLI-PAVE Predicted D3 for Cell-29

The ILLI-PAVE predicted deflections are within two standard deviation of the field measured values. The difference between the predicted and measured D0 values is 2-10 percent. In the case of deflection D1, the difference is about 2-14 percent. Deflections D2 were under predicted by 2-10

percent. The differences for deflection D3 were less than 1-mil (2-20 percent). Figure 7.43 shows the comparison between the measured and predicted AUPP values.

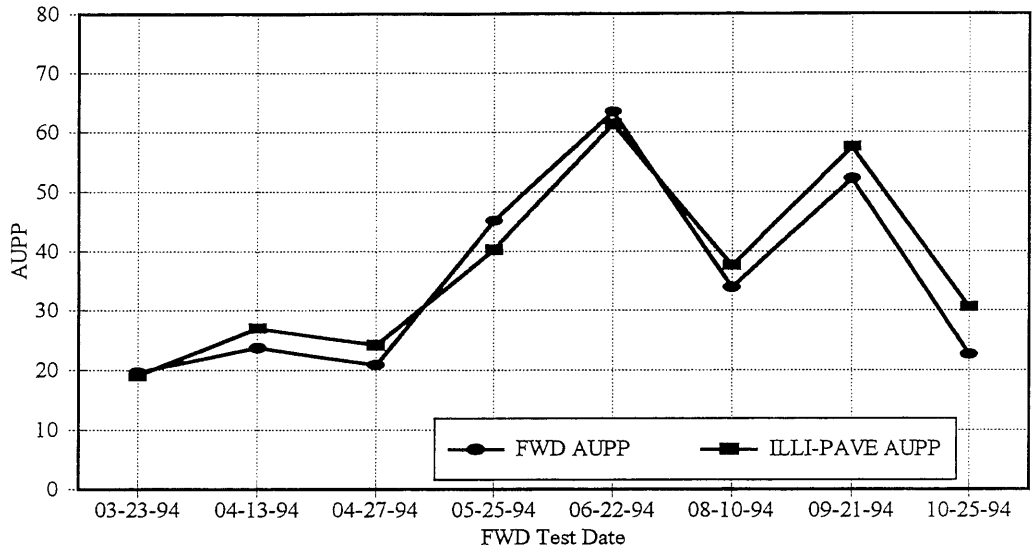

Figure 7.43. Comparison Between FWD AUPP and ILLI-PAVE Predicted AUPP for Cell-29

The predicted values are similar in magnitude to the field measured values. The deviation observed could be due to the inherent variability in the material and layer thickness. ILLI-PAVE predicted similar stiffness as the stiffness measured in the field (similar AREA, Figure 7.44).

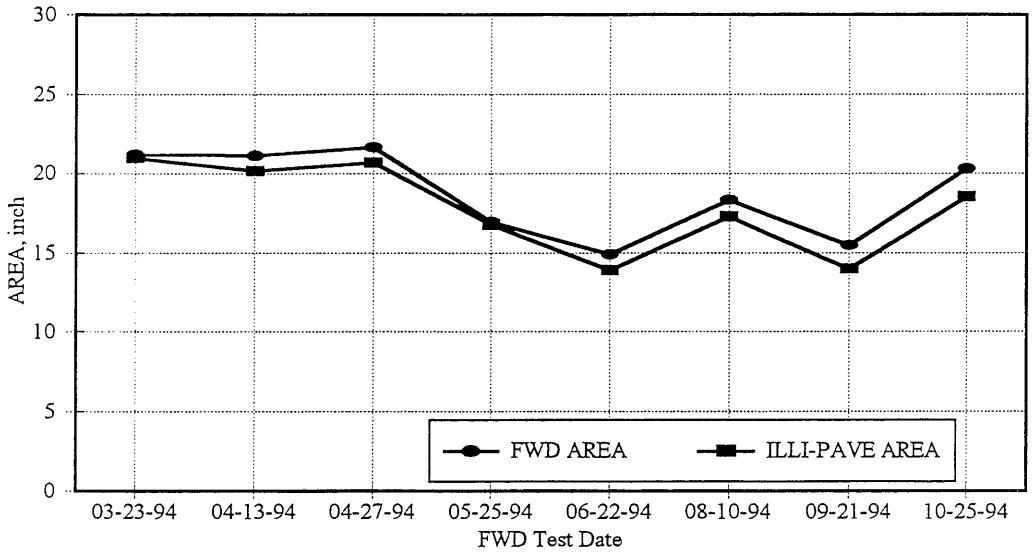

Figure 7.44. Comparison Between FWD AREA and ILLI-PAVE Predicted AREA for Cell-29

Cell-30 :

5-inch Asphalt Concrete Surface / 12-inch Granular Base (CL-3sp) / Cohesive Subgrade

Figures 7.45 through 7.48 show the comparison between the measured FWD deflections and ILLI-PAVE predicted deflections.

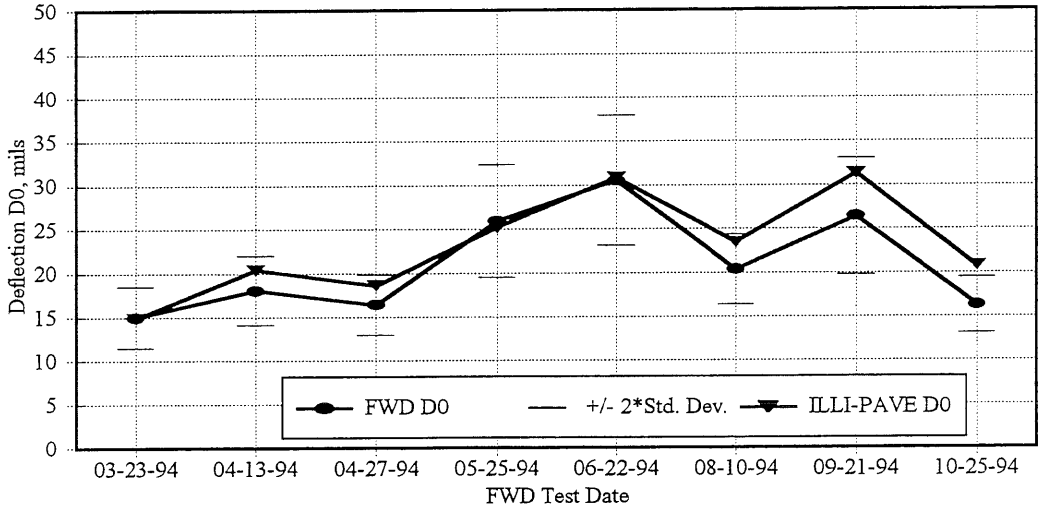

Figure 7.45. Comparison Between FWD Peak Center Deflection and ILLI-PAVE Predicted Peak Center Deflection for Cell-30

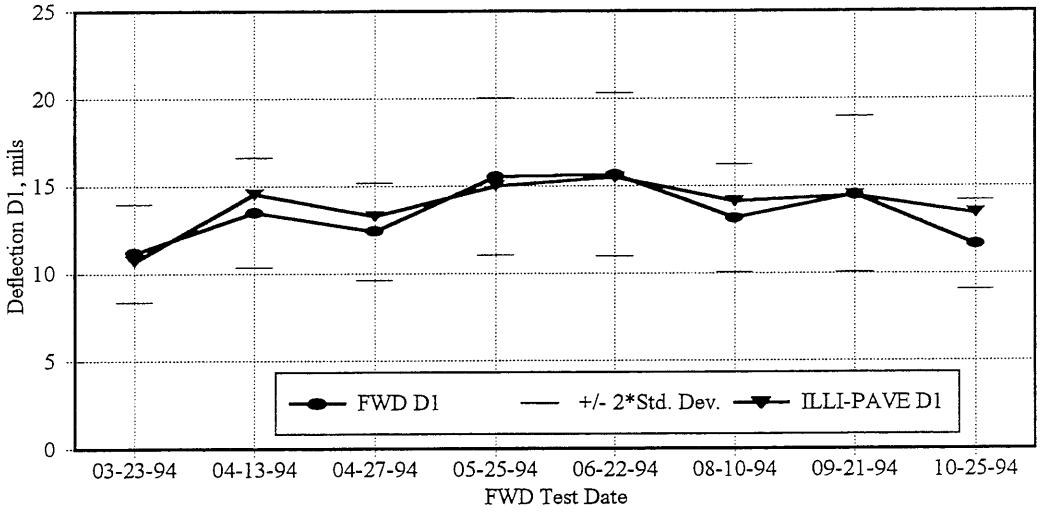

Figure 7.46. Comparison Between FWD D1 and ILLI-PAVE Predicted D1 for Cell-30

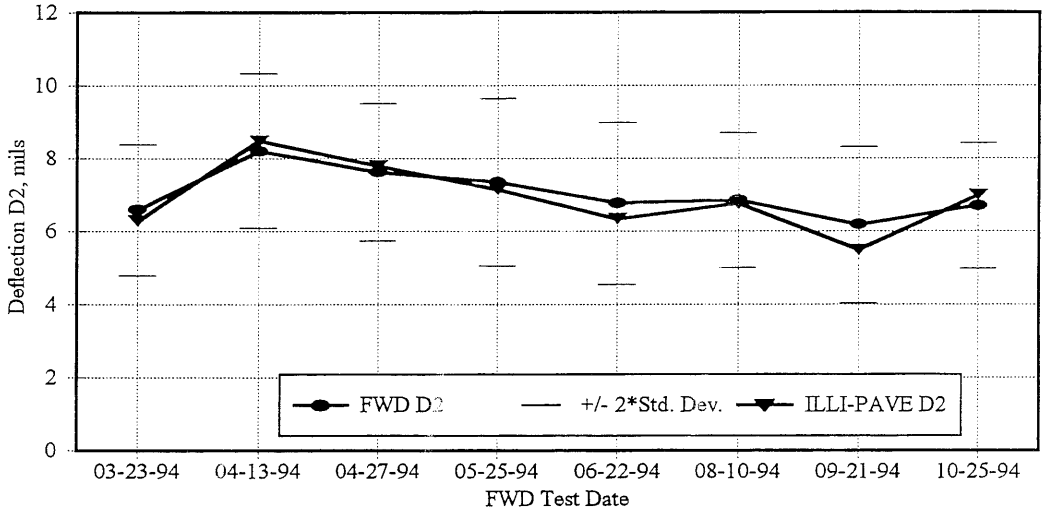

Figure 7.47. Comparison Between FWD D2 and ILLI-PAVE Predicted D2 for Cell-30

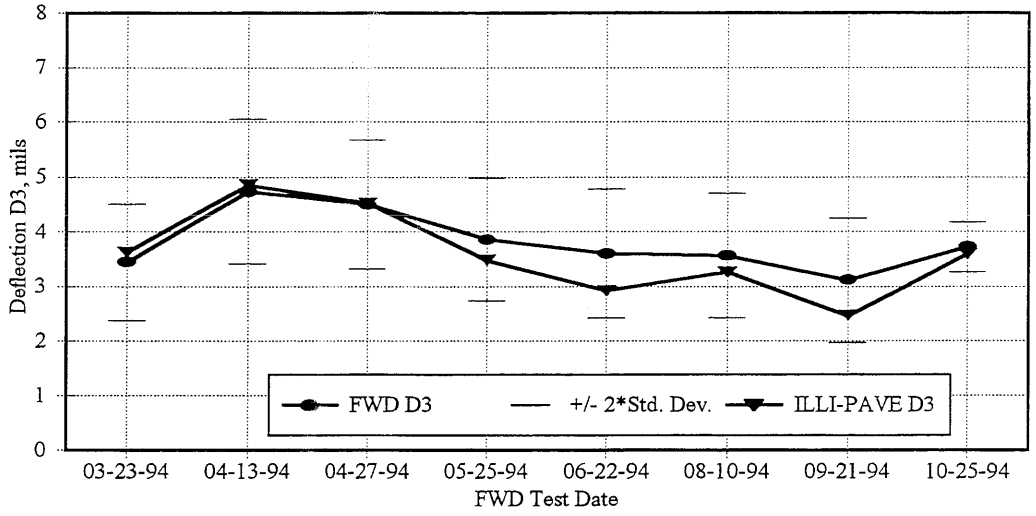

Figure 7.48. Comparison Between FWD D3 and ILLI-PAVE Predicted D3 for Cell-30

The ILLI-PAVE predicted deflections are within two standard deviation of the field measured values. The difference between the predicted and measured D0 values is 1-18 percent. In the case of deflection D1, the difference is about 2-7 percent. Deflections D2 were different by 2-10 percent. The differences for deflection D3 were less than 1-mil (2-20 percent). Figure 7.49 shows

the comparison between the measured and predicted AUPP values. The difference between the predicted and measured values is in the range of 1-30 percent. AREA predicted from ILLI-PAVE were similar to AREA estimated from the FWD data (Figure 7.50).

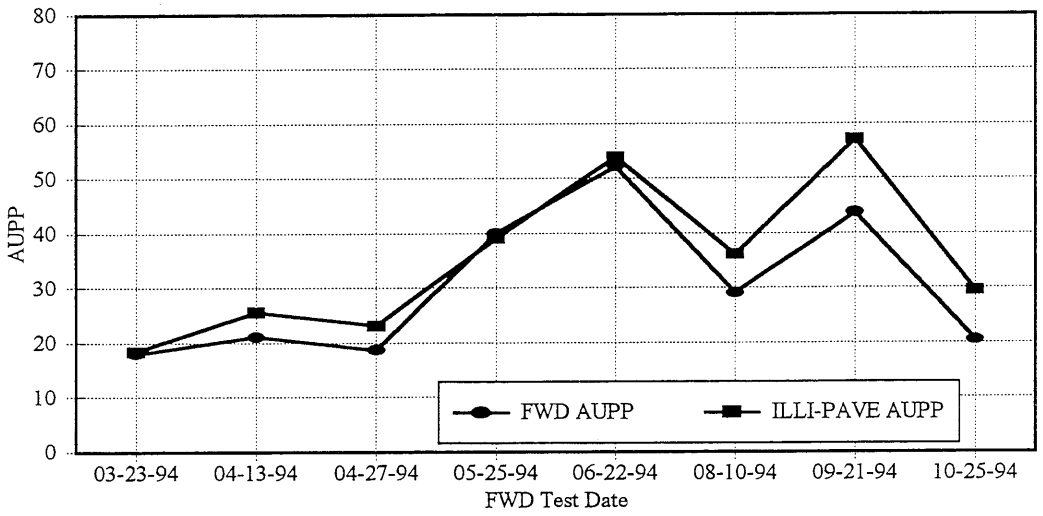

Figure 7.49. Comparison Between FWD AUPP and ILLI-PAVE Predicted AUPP for Cell-30

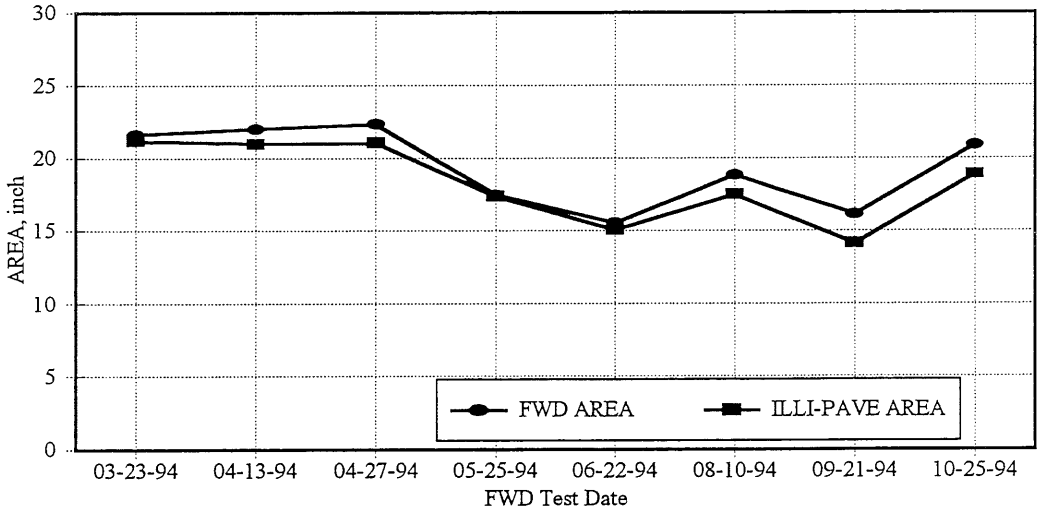

Figure 7.50. Comparison Between FWD AREA and ILLI-PAVE Predicted AREA for Cell-30

Cell-31 :

3-inch Asphalt Concrete Surface / 4-inch Base (CL-5sp) / 12-inch Granular Subbase (CL-3sp) / Cohesive Subgrade

Deflection D0 values (Figure 7.51) are 12-29 percent higher than the measured values.

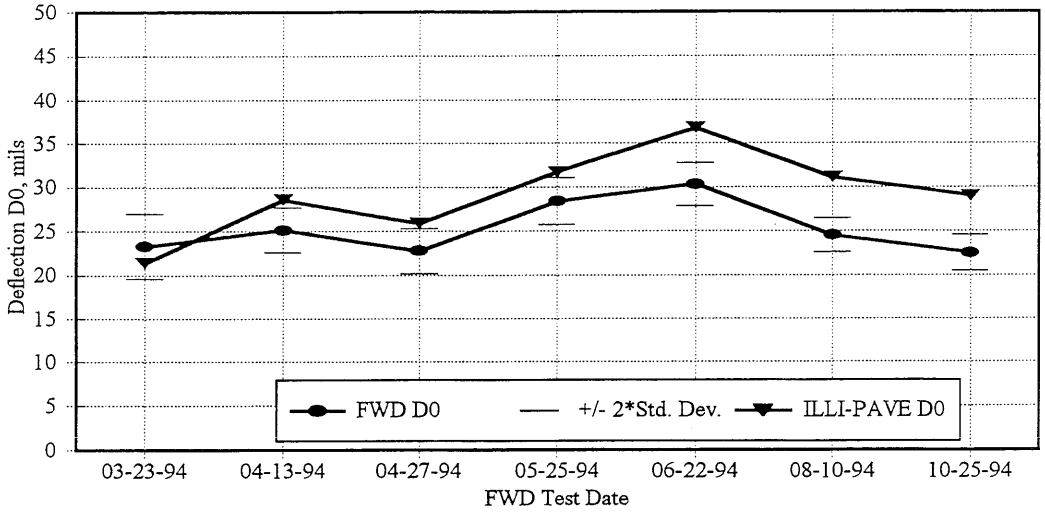

Figure 7.51. Comparison Between FWD Peak Center Deflection and ILLI-PAVE Predicted Peak Center Deflection for Cell-31

Similar pattern was observed for deflection D1 (Figures 7.52).

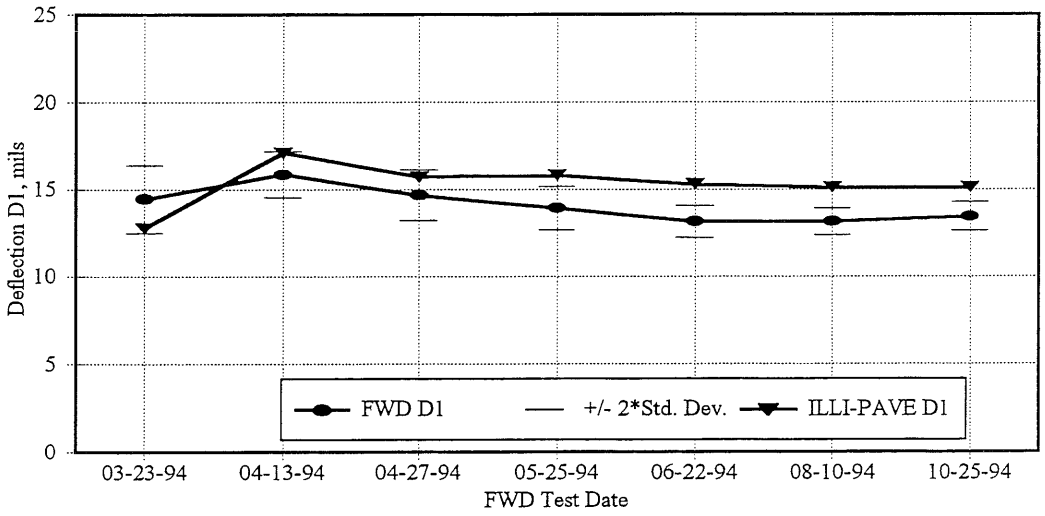

Figure 7.52. Comparison Between FWD D1 and ILLI-PAVE Predicted D1 for Cell-31

The predicted values were 7-17 percent higher than the measured values. In the case of deflection D2 (Figure 7.53), the difference between the predicted and measured values ranged from 1-7 percent. The predicted values were within two standard deviations of the field measured values.

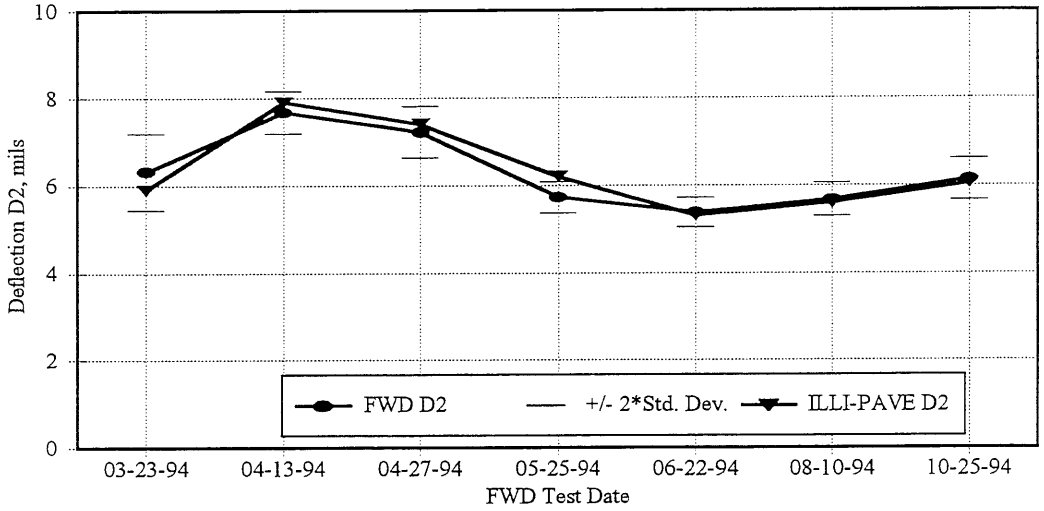

Figure 7.53. Comparison Between FWD D2 and ILLI-PAVE Predicted D2 for Cell-31

The difference in predicted and measured deflection D3 values were less than 1-mil (Figure 7.54).

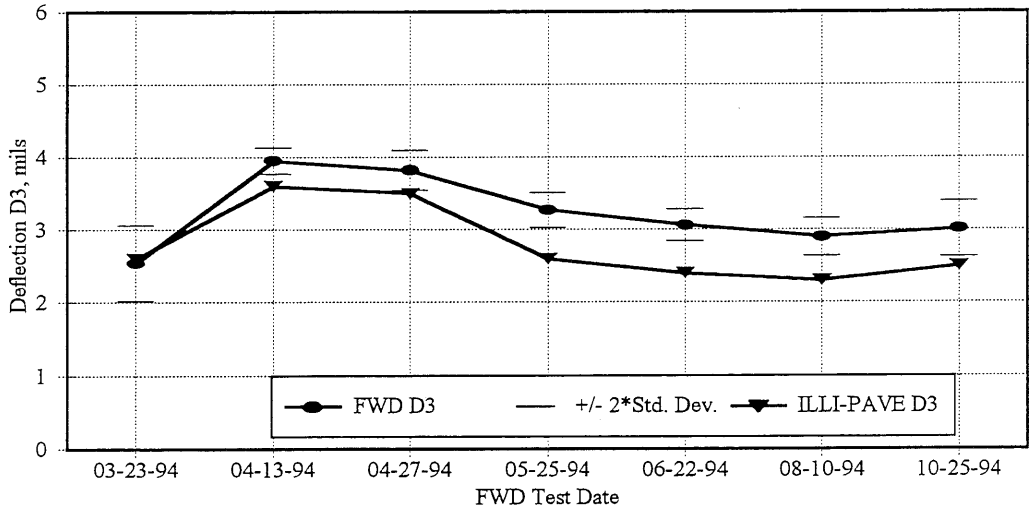

Figure 7.54. Comparison Between FWD D3 and ILLI-PAVE Predicted D3 for Cell-31

Figure 7.55 shows the comparison between the measured and predicted AUPP values. The predicted AUPP values were higher by 12-40 percent compared to the measured AUPP values. The AREA predicted from ILLI-PAVE were comparable to the FWD AREA (Figure 7.56).

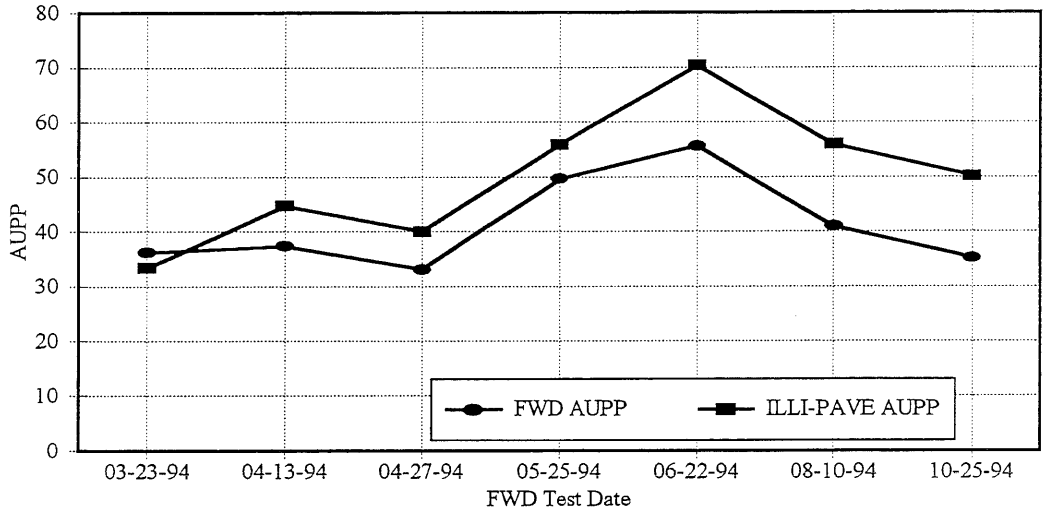

Figure 7.55. Comparison Between FWD AUPP and ILLI-PAVE Predicted AUPP for Cell-31

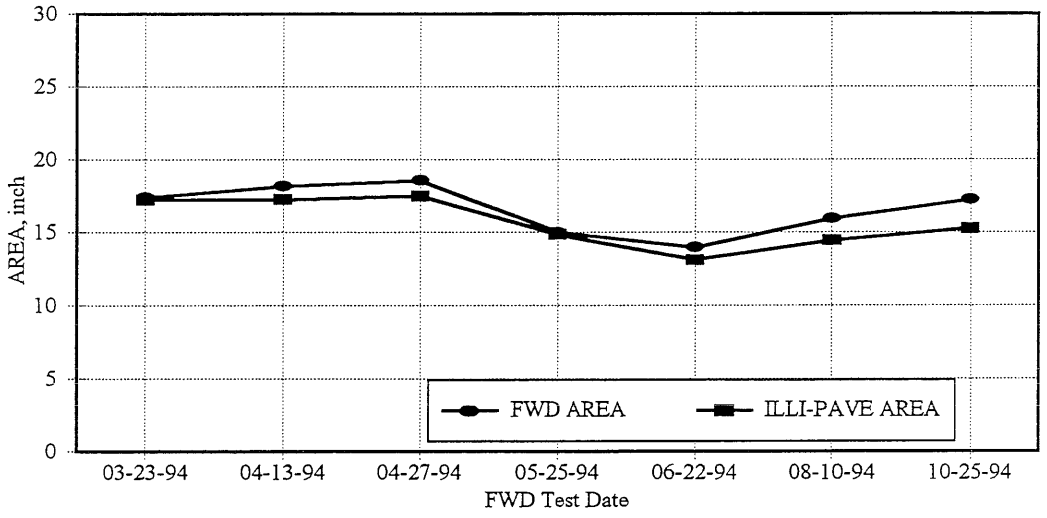

Figure 7.56. Comparison Between FWD AREA and ILLI-PAVE Predicted AREA for Cell-31

Cell-32 & Cell-33 :

12-inch Granular Base (CL-1Csp) / Cohesive Subgrade

Cell-32 has 1-inch thick double chip seal as a surface treatment. Double chip seal was not considered as a structural layer but was considered as a part of the aggregate surface. Therefore the analyses for Cell-32 and Cell-33 was same. Figure 7.57 shows the comparison between the field measured and ILLI-PAVE predicted deflection basins. The predicted D0 was 35-percent higher than the measured value. Deflections D1, D2, and D3 were fairly accurate with the difference between measured and predicted values being less than 1-mil for D2 and D3.

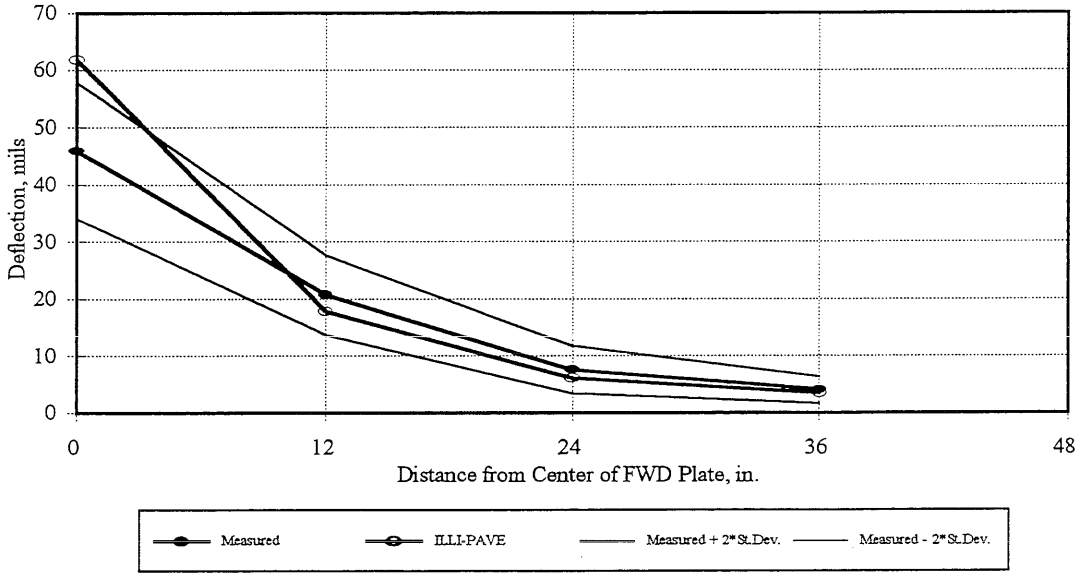

Figure 7.57. Comparison of FWD Deflection Basin with the ILLI-PAVE Predicted Deflection Basin for Cell-33

Cell-34 & Cell-35 :

12-inch Granular Base (CL-1Fsp) / Cohesive Subgrade

Cell-34 has 1-inch thick double chip seal as a surface treatment. Double chip seal was not considered as a structural layer but was considered as a part of the aggregate surface. Therefore the analyses for Cell-34 and Cell-35 was same. Figure 7.58 shows the comparison between the field measured and ILLI-PAVE predicted deflection basins. The predicted D0 was 91-percent higher than the measured value. In the case of deflection D1, the predicted value was 43-percent higher than the measured value. Deflections D2 and D3 were fairly accurate with the difference

between measured and predicted values being less than 1-mil.

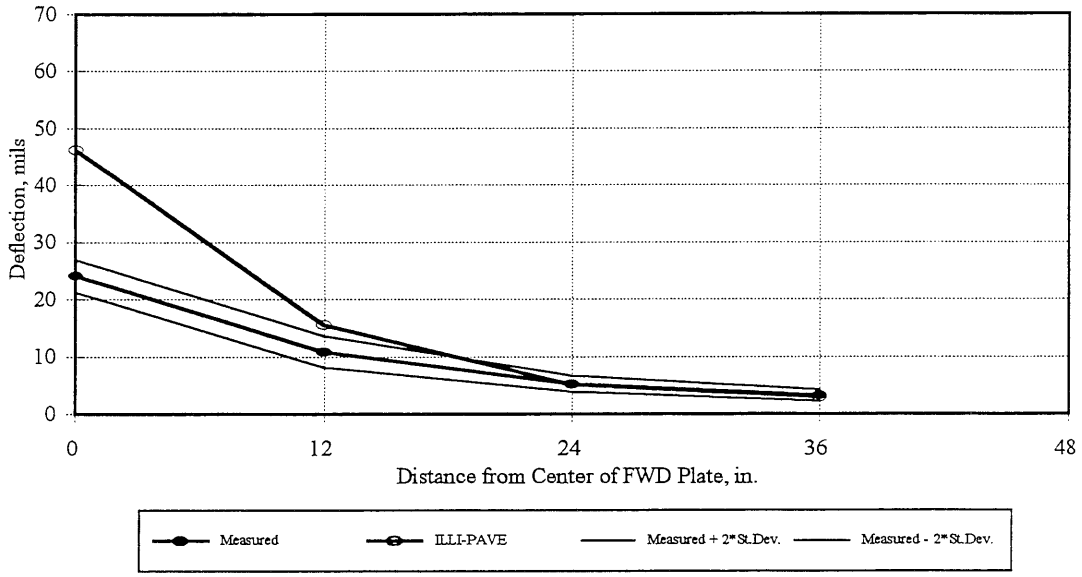

Figure 7.58. Comparison of FWD Deflection Basin with the ILLI-PAVE Predicted Deflection Basin for Cell-35

7.5 Summary

ILLI-PAVE was used to predict the pavement deflections and the results were compared with the field measured responses. The analyses showed that more accurate pavement response predictions are achieved if the asphalt concrete surface is thick (5-inch or higher). The behavior of thin asphalt concrete surfaces (3-inch in the case of Mn/ROAD test sections) is midway between a surface treatment and a structural layer. Thin asphalt concrete surface exhibits a 'membrane' type behavior. This makes the modeling of stress states occurring in the pavement cross-section slightly difficult. Predicting exact deflection basins is not important. If the geometry (e.g. AUPP, AREA, curvature, etc.) of the deflection basin can be predicted with a reasonable amount of accuracy, critical pavement response like strain at the bottom of the asphalt concrete surface can be predicted. In the previous section, it was found that the asphalt concrete strains for Cell-27 (3-inch asphalt concrete surface) were over predicted by 75-percent when the geometry of deflection basin (AUPP) was used to estimate them. AUPP was evaluated from the FWD deflection basins. Similar results were obtained from ILLI-PAVE analysis also. The ILLI-PAVE predicted strains were about 20-90 percent higher than the measured strain values.

In the case of surface treated/aggregate surface pavements, except for the peak center deflection, the rest of the deflection basin was predicted fairly accurately. The test sections Cell-32 and Cell-33 performed poorly and failed before Cell-34 and Cell-35. All the four test sections had similar subgrade-stress ratios (described in the previous chapter). The results from ILLI-PAVE analysis are shown in Figure 7.57 (Cell-33) and Figure 7.58 (Cell-35). Cell-33 had CL-1Csp as the granular base and Cell-35 had CL-1Fsp as the granular base. As discussed in Chapter-4, the shear strength of CL-1Fsp was considerably higher than CL-1Csp. Figures 7.59 and 7.60 show the development of failure zones in Cell-33 and Cell-35 respectively.

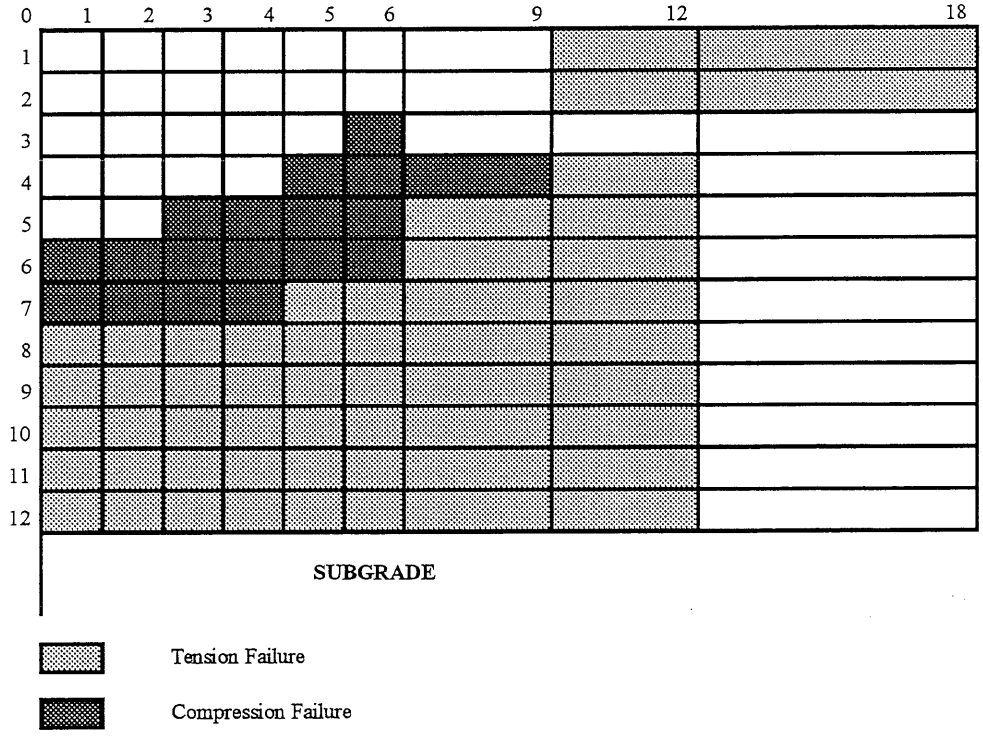

Figure 7.59. Failure Zones in the Granular Base in Cell-33 Under 9000-lb Load Applied on a 12-inch Diameter Plate (80-psi Pressure)

The shear strength has a significant effect in the development of plastic zones (failure zones) in the pavement cross-section. Failure occurs when the state of stress in the material exceeds its shear strength. If a failure zone exists, the rate of permanent deformation accumulation will increase under repetitive loads. In general, improved shear strength will contribute to the development of

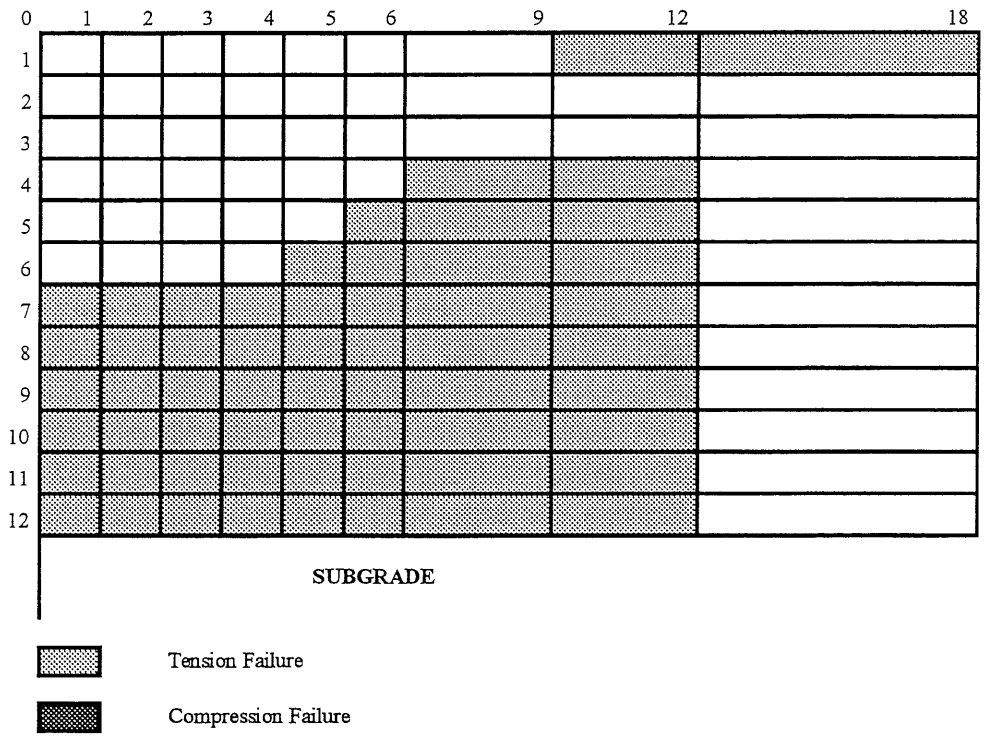

Figure 7.60. Failure Zones in the Granular Base in Cell-35 Under 9000-lb Load Applied on a 12-inch Diameter Plate (80-psi Pressure)

smaller plastic zones. A careful study of Figure 7.59 and Figure 7.60 shows that Cell-33 developed more plastic zones than Cell-35. In Chapter-VI, safety factor values against shear failure were estimated based on Mohr-Coulomb theory for static loading. Lower safety factor values were observed (Figures 6.49 and 6.50) for Cell-33 (granular base - CL-1Csp) compared to Cell-35 (granular base - CL-1Fsp). This contributed to a higher rate of permanent deformation accumulation in the granular base in Cell-33. For this reason Cells 32 and 33 experienced severe rutting.

An important step in a mechanistic-empirical pavement design procedure is the accurate estimate of critical pavement responses. Strain at the bottom of asphalt concrete layer, vertical stress/strain at the top of the subgrade, and subgrade stress ratio (SSR) are typically considered. The strain at the bottom of asphalt concrete layer is related to the fatigue life of the pavement; higher strains are associated with reduced fatigue life. The stress/strain at the top of subgrade and SSR are related to

the permanent deformation accumulation in the subgrade. Higher stress/strain and SSR are associated with higher permanent deformation accumulation. Pavement thickness should be designed in such a way so as to limit the strain at the bottom of asphalt concrete surface, and the stress at the top of the subgrade. The stresses in the granular base should also be kept lower than the shear strength of the base. This chapter showed that the finite element program ILLI-PAVE can be used to estimate the pavement responses. Estimate of pavement responses is fairly accurate in the case of pavement cross-sections where the asphalt concrete surface behaves like a structural layer (asphalt concrete thickness higher than 5-inch). In the case of thinner asphalt concrete surfaces, the exact match may not be obtained on the deflections, but the predicted geometry of deflection basin was comparable to the measured one. The analysis of field FWD data showed how powerful a single term containing the differences of deflections (AUPP) can be in predicting the strains at the bottom of asphalt concrete layer.

Chapter-VIII discusses the effect of climatic conditions on the temperature gradients within the asphalt concrete layer and the fatigue life of the pavement.

CHAPTER - VIII

"DESIGN TIME" CONCEPT FOR ASPHALT CONCRETE FATIGUE

8.1 Introduction

The previous two chapters discussed the effect of material quality on pavement performance and response. Climatic effects impact both pavement response and performance. Climatic factors like maximum and minimum air temperature, sunshine, wind velocity, precipitation, etc., vary with geographical location and should be considered in an a priori pavement design procedure. There are large daily and seasonal temperature variations in a pavement system. The asphalt concrete layer is characterized as a constant modulus material and the modulus is temperature dependent. Asphalt concrete mean monthly pavement temperatures (MMPT) are estimated based on mean monthly air temperatures (MMAT). MMPT's are then used to estimate asphalt concrete modulus from an appropriate asphalt concrete modulus - temperature relation. A "Design Time" concept [26] is used to consider the effect of climate on pavement structure. The fatigue life of an asphalt concrete layer estimated based on design time asphalt concrete modulus is equal to the fatigue life calculated based on the 12-monthly asphalt concrete modulus inputs. The Climatic-Materials-Structural (CMS) model [5] was used to estimate mean monthly pavement temperatures as a function of mean monthly air temperatures.

This chapter describes the effect of climatic conditions on the asphalt concrete fatigue life. It discusses the effect of asphalt concrete thickness, granular base thickness, and subgrade type on the design time.

8.2 CMS Modeling of Mn/ROAD Test Sections

The Climatic-Materials-Structural (CMS) program is a climatic model used to analyze multilayered flexible pavement systems. It simulates field conditions by considering the climatic characteristics (minimum and maximum air temperature, sunshine, wind velocity, precipitation, etc.) that vary with geographical location. CMS includes a one-dimensional forward-finite-difference heat transfer model that calculates temperatures and moisture profiles as a function of time based on pertinent climatic inputs. The required climatic data inputs are:

i. Weekly high/low/average air temperatures.

ii. Average weekly wind speed.

iii. Average weekly percentage of sunlight.

iv. Daily solar radiation.

These inputs were obtained from National Oceanic and Atmospheric Administration (NOAA) in Asheville, NC for Minneapolis-St. Paul in Minnesota. The Mn/ROAD facility is located approximately 40-miles northwest of the Minneapolis-St. Paul metropolitan area. The input temperatures are weekly averages of the high and low temperatures. The daily air temperature-time relation is established by indicating the time when the low and high temperature occur. In this analysis, the low is assumed to occur at 4-a.m. and the high at 1-p.m. The daily air temperature-time relation is repeated for seven days to represent a week.

The following pavement system inputs are required for CMS:

i. Number and types of layers.

ii. Thickness of each layer.

iii. Thermal and physical properties of each layer.

iv. Radiation absorptivity and emmissivity of surface layer.

The thermal properties of different layer materials used in the analysis are given in Table 8.1. CMS analyses were conducted for the following test sections in the low-volume road loop:

Cell No.	AC Thickness, inches	Granular Base Thickness, inches	Subgrade
24	3	4	Sand
25	5	-	Sand
26	6	-	Cohesive
27	3	11	Cohesive
28	3	13	Cohesive
29	5	10	Cohesive
30	5	12	Cohesive
31	3	4 + 12 = 16	Cohesive

TABLE 8.1

Thermal Properties of Pavement Layer Materials for CMS Model

Material	Density	Moisture	Thermal Conductivity, (BTU/Hr-Ft-F)			Heat Capacity, (BTU/lb-Ft)		
	pcf	Content, %	Unfrozen	Freezing	Frozen	Unfrozen	Freezing	Frozen
Asphalt Concrete*	148	2	0.7	0.7	0.7	0.22	1.44	0.22
Sand	117	10	1.361	1.6	1.78	0.231	5.8	0.19
Cohesive Subgrade	129	17	0.92	1.02	1.13	0.29	10.49	0.22
Aggregate Base	147	5	2.18	2.28	2.38	0.21	3.6	0.19

* Surface short-wave absorptivity for asphalt concrete is 0.85

Pavement temperatures were calculated for nodes spaced at 1-inch depth intervals in the asphalt concrete layer. The yearly condition was represented by calculating pavement temperatures six times a day (2,6,10 a.m. and 2,6,10 p.m.), seven days a week, for fifty two weeks.

8.3 Results from CMS Modeling of Mn/ROAD Test Sections

The CMS generated asphalt concrete pavement temperature (for various depths from the pavement surface)-time data were analyzed to establish pavement temperature-air temperature algorithms. Air temperature-pavement temperature relations of the following form [4] were derived for each node depth using a linear regression procedure:

$$\text{Pavement Temperature} = a + b * \text{Air Temperature} \quad \text{.....[8.1]}$$

where 'a' and 'b' are regression coefficients. The intercept 'a' and slope 'b' were then related to depth 'z' in the pavement by linear regression. A relation of following form was obtained:

$$MMPT = [A + B*z] + [C - D*z] * MMAT \quad \text{.....[8.2]}$$

where

MMPT	:	Mean Monthly Pavement Temperature (°F) at depth 'z';
MMAT	:	Mean Monthly Air Temperature (°F);
z	:	Pavement Depth from Surface, inch;
A, B, C, D	:	Regression Coefficients.

Table 8.2 summarizes the values of A, B, C, and D for the different test sections.

The asphalt concrete temperature at a depth of one-third layer thickness was utilized to estimate the asphalt concrete modulus. Equation 8.2 was used to calculate the pavement temperature at one-third depth. The asphalt concrete modulus was estimated from the following relationship (developed in Chapter VI):

$$\text{Log } E_{\text{asphalt concrete}} = 3.3804 - 0.04771 * T \quad \text{.....[8.3]}$$

$R^2 = 0.89$ SEE = 0.146

where

$E_{asphalt\ concrete}$: Asphalt concrete modulus, ksi;

T : Temperature, degree Centigrade;

TABLE 8.2

Algorithms for Predicting Pavement Temperatures

Cell No.	A	B	C	D	R^2
24	1.957	0.545	1.09	0.012	0.99
25	1.873	0.509	1.09	0.011	0.99
26	3.830	1.265	1.05	0.027	0.99
27	4.001	1.365	1.05	0.029	0.99
28	4.022	1.370	1.05	0.029	0.99
29	3.866	1.303	1.05	0.027	0.99
30	3.880	1.308	1.05	0.027	0.99
31	4.016	1.369	1.05	0.029	0.99

Algorithm: MMPT = [A + B*z] + [C - D*z]*MMAT

MMPT : Mean Monthly Pavement Temperature, degree F

MMAT : Mean Monthly Air Temperature, degree F

For Cells 24 and 25 (sandy subgrade), the tensile strains at the bottom of the asphalt concrete layer were obtained from ILLI-PAVE. For Cells 26 through 31, the asphalt concrete strain calculations were based on previously developed ILLI-PAVE algorithms for the full-depth asphalt concrete (eq. 2.23) and conventional flexible pavements (eq. 2.19). The algorithms used were as follows:

Conventional Flexible Pavements

$$Log(\varepsilon_{ac}) = 2.9496 + 0.1289*T_{ac} - 0.5195*Log(T_g)/T_{ac} - 0.0807*(LogE_{ac})*T_{ac} - 0.0408*Log(E_{Ri}) \quad \text{.....[8.4]}$$

Full-Depth Asphalt Concrete Pavements

$$Log(\varepsilon_{ac}) = 5.746 - 1.589*Log(T_{ac}) - 0.774*(LogE_{ac}) - 0.097*Log(E_{Ri}) \quad \text{.....[8.5]}$$

where

ε_{ac} = Tensile strain at the bottom of the AC layer, in micro-in/in

T_{ac} = Thickness of AC layer, in inches

T_g = Thickness of granular base course, in inches

E_{ac} = Resilient modulus of AC layer, in ksi

E_{Ri} = "breakpoint" resilient modulus of the subgrade, in ksi

The IDOT (Illinois Department of Transportation) fatigue algorithm was used to calculate asphalt concrete fatigue life. The algorithm is:

$$N = 5 * 10^{-6} * (1/\varepsilon)^{3.0} \quad \text{.....[8.6]}$$

where

N = Number of load repetitions to asphalt concrete fatigue failure

ε = Radial tensile strain at the bottom of asphalt concrete layer

The cumulative damage from traffic loading were calculated based on the Miner cumulative damage model. The relation is as follows:

$$Nf = 12 / [\sum_{a=1}^{12} (1/Na)] \quad \text{.....[8.7]}$$

where

Nf = Fatigue life based on cumulative damage for 12-month data inputs

Na = Fatigue life for a given month

For calculating the "Design Time", the asphalt concrete fatigue life Nf is calculated (based on eq. 8.7). This Nf value is then associated with a particular asphalt concrete strain value (for a given asphalt concrete thickness and subgrade E_{Ri}) and asphalt concrete modulus. The relationship between asphalt concrete modulus and asphalt concrete temperature (eq. 8.3) is used to establish the "Design Time Pavement Temperature". The air temperature and calendar week corresponding

to the "Design Time Pavement Temperature" can be calculated. Thus for each test section, the following "Design Time" data are established:

- Design Time (week number; week number 1 is the first week of January)
- Design Time Asphalt Concrete Pavement Temperature
- Design Time Air Temperature

Table 8.3 through Table 8.10 show the design time computations for Cell-24 through Cell-31. Design time relations for Cell-24 through Cell-31 are shown in Figure 8.1 through Figure 8.8. Table 8.11 gives the summary of Design Time data. Design time ranged from early April (Cells 24, 27, 28, 31) to middle of May (Cell-26). The design pavement temperatures ranged from 55-°F (for Cell-24) to 68-°F (for Cell-26). The design air temperatures ranged from 48-°F (for Cell-24) to 62-°F (for Cell-26).

8.4 Effect of Asphalt Concrete Thickness on "Design Time" Data

In the Mn/ROAD LVR test sections, the asphalt concrete thickness ranged from 3-inch to 6-inch. Figure 8.9 shows the effect of asphalt concrete thickness on "Design Time". For 3-inch thick asphalt concrete test sections on cohesive subgrade (Cells 27, 28, 31), the "Design Time" was second week of April (16 weeks after January 1). For Cell-24 (3-inch thick asphalt concrete/4-inch granular base on sandy subgrade), the "Design Time" was first week of April (15 weeks from January 1). For 5-inch thick asphalt concrete test sections (Cells 25, 29, 30), the "Design Time" was 4th week of April (18 weeks from January 1). For Cell-26 (6-inch full-depth asphalt concrete pavement), the "Design Time" was second week of May (20 weeks from January 1). The general trend was that with increase in asphalt concrete thickness, the "Design Time" also increased.

Figure 8.10 shows the effect of asphalt concrete thickness on design time pavement temperature and design time air temperature. The design time pavement temperature and design time air temperature increased with the increase in asphalt concrete thickness. For test sections with 3-inch thick asphalt concrete surface (except for Cell-24 : 4-inch granular base and sandy subgrade), the design time pavement temperature was 60-°F and design time air temperature was 53-°F. For test sections with 5-inch thick asphalt concrete surface (Cells 25, 29, 30), the design time pavement

TABLE 8.3.

Design Time Computations for Cell-24

Month	MMAT deg. F	MMPT deg. F	MMPT deg. C	AC Modulus ksi	AC Strain microstrain	IDOT Na
January	13.10	16.65	-8.53	6127	79.44	9973608
February	17.15	21.02	-6.10	4692	97.70	5361500
March	30.05	34.96	1.64	2005	178.37	881058
April	46.10	52.29	11.27	696	313.96	161561
May	58.25	65.41	18.56	312	390.67	83859
June	67.95	75.89	24.38	165	420.19	67397
July	73.25	81.61	27.56	116	429.91	62927
August	70.65	78.80	26.00	138	425.56	64875
September	61.45	68.87	20.48	253	402.55	76649
October	49.60	56.07	13.37	553	342.64	124296
November	32.80	37.93	3.29	1672	199.87	626220
December	19.15	23.18	-4.90	4112	107.92	3977995
					Nf	**135411**

Design Time : 15 weeks from January 1 [1st week of April]

DT Pavement Temperature: 55 deg. F

DT Air Temperature: 48 deg. F

Table 8.4.

Design Time Computations for Cell-25

Month	MMAT deg. F	MMPT deg. F	MMPT deg. C	AC Modulus ksi	AC Strain microstrain	IDOT Na
January	13.10	16.76	-8.47	6086	45.85	51874268
February	17.15	21.10	-6.06	4670	58.13	25454762
March	30.05	34.92	1.62	2009	117.55	3078237
April	46.10	52.12	11.18	703	239.48	364062
May	58.25	65.14	18.41	318	357.79	109166
June	67.95	75.54	24.19	168	452.24	54057
July	73.25	81.22	27.34	119	503.85	39089
August	70.65	78.43	25.80	141	478.54	45628
September	61.45	68.57	20.32	258	388.95	84975
October	49.60	55.87	13.26	559	273.56	244240
November	32.80	37.87	3.26	1678	125.95	2502508
December	19.15	23.24	-4.86	4097	65.19	18047916
					Nf	**126842**

Design Time: 18 weeks from January 1 [4th week of April]

DT Pavement Temperature: 63 deg. F

DT Air Temperature: 57 deg. F

TABLE 8.5.

Design Time Computations for Cell-26

Month	MMAT deg. F	MMPT deg. F	MMPT deg. C	AC Modulus ksi	Subgrade "Breakpoint" Modulus, ksi	AC Strain microstrain	IDOT Na
January	13.10	19.41	-7.00	5178	22	31.95	153254909
February	17.15	23.44	-4.75	4048	22	38.66	86526780
March	30.05	36.29	2.38	1848	15	73.62	12530885
April	46.10	52.28	11.26	697	7	168.68	1041843
May	58.25	64.38	17.99	333	8	294.91	194933
June	67.95	74.04	23.35	185	9	460.19	51306
July	73.25	79.32	26.29	134	9	590.52	24282
August	70.65	76.73	24.85	157	10	517.21	36139
September	61.45	67.56	19.76	274	10	335.49	132412
October	49.60	55.76	13.20	563	10	192.11	705228
November	32.80	39.03	3.90	1563	15	83.79	8499777
December	19.15	25.43	-3.65	3585	20	42.87	63460843
						Nf =	**115789**

Design Time: 20 weeks from January 1 [2nd week of May]

DT Pavement Temperature: 68 deg. F

DT Air Temperature: 62 deg. F

TABLE 8.6.

Design Time Computations for Cell-27

Month	MMAT deg. F	MMPT deg. F	MMPT deg. C	AC Modulus ksi	Subgrade "Breakpoint" Modulus, ksi	AC Strain microstrain	IDOT Na
January	13.10	18.74	-7.37	5393	22	157.67	1275655
February	17.15	22.88	-5.07	4190	22	167.60	1062012
March	30.05	36.05	2.25	1876	16	206.27	569703
April	46.10	52.43	11.35	690	7	271.80	249022
May	58.25	64.84	18.24	324	9	323.14	148178
June	67.95	74.74	23.75	177	10	372.46	96768
July	73.25	80.15	26.75	127	11	401.90	77024
August	70.65	77.50	25.28	149	12	385.07	87569
September	61.45	68.11	20.06	265	11	336.36	131388
October	49.60	56.01	13.34	555	11	281.30	224631
November	32.80	38.85	3.81	1580	15	215.58	499075
December	19.15	24.92	-3.93	3699	20	173.41	958854
						Nf =	**187233**

Design Time: 16 weeks from January 1 [2nd week of April]

DT Pavement Temperature: 60 deg. F

DT Air Temperature: 53 deg. F

TABLE 8.7.

Design Time Computations for Cell-28

Month	MMAT deg. F	MMPT deg. F	MMPT deg. C	AC Modulus ksi	Subgrade "Breakpoint" Modulus, ksi	AC Strain microstrain	IDOT Na
January	13.10	18.77	-7.35	5385	22	153.22	1390119
February	17.15	22.90	-5.06	4184	22	162.87	1157306
March	30.05	36.07	2.26	1873	15	200.98	615937
April	46.10	52.46	11.37	689	7	264.12	271366
May	58.25	64.86	18.26	323	9	314.02	161474
June	67.95	74.77	23.76	177	10	361.94	105450
July	73.25	80.18	26.77	127	11	390.55	83935
August	70.65	77.52	25.29	149	11	375.53	94416
September	61.45	68.13	20.07	265	11	326.86	143177
October	49.60	56.03	13.35	554	11	273.35	244787
November	32.80	38.88	3.82	1578	15	209.49	543857
December	19.15	24.94	-3.92	3694	20	168.51	1044891
						Nf =	**203601**

Design Time: 16 weeks from January 1 [2nd week of April]

DT Pavement Temperature: 60 deg. F

DT Air Temperature: 53 deg. F

TABLE 8.8.

Design Time Computations for Cell-29

Month	MMAT deg. F	MMPT deg. F	MMPT deg. C	AC Modulus ksi	Subgrade "Breakpoint" Modulus, ksi	AC Strain microstrain	IDOT Na
January	13.10	19.21	-7.11	5242	22	86.02	7855574
February	17.15	23.28	-4.85	4089	21	95.27	5782613
March	30.05	36.24	2.35	1854	15	132.91	2129677
April	46.10	52.37	11.31	693	9	201.88	607676
May	58.25	64.58	18.10	329	11	270.47	252695
June	67.95	74.32	23.51	181	13	341.52	125524
July	73.25	79.65	26.47	131	13	389.38	84692
August	70.65	77.04	25.02	154	14	364.01	103661
September	61.45	67.79	19.88	270	12	291.73	201394
October	49.60	55.88	13.27	559	12	217.58	485419
November	32.80	39.00	3.89	1566	15	142.27	1736392
December	19.15	25.28	-3.73	3617	20	100.30	4955029
						Nf =	**275249**

Design Time: 18 weeks from January 1 [4th week of April]

DT Pavement Temperature: 63 deg. F

DT Air Temperature: 57 deg. F

TABLE 8.9.

Design Time Computations for Cell-30

Month	MMAT deg. F	MMPT deg. F	MMPT deg. C	AC Modulus ksi	Subgrade "Breakpoint" Modulus, ksi	AC Strain microstrain	IDOT Na
January	13.10	19.23	-7.09	5234	22	84.47	8297003
February	17.15	23.30	-4.83	4083	21	93.55	6107556
March	30.05	36.26	2.37	1851	15	130.51	2249350
April	46.10	52.39	11.33	692	9	198.24	641824
May	58.25	64.60	18.11	328	11	265.59	266895
June	67.95	74.35	23.53	181	12	336.45	131285
July	73.25	79.68	26.49	131	12	383.60	88579
August	70.65	77.06	25.04	153	13	358.52	108497
September	61.45	67.82	19.90	270	12	286.46	212711
October	49.60	55.91	13.28	558	12	213.65	512697
November	32.80	39.03	3.90	1564	15	139.70	1833965
December	19.15	25.31	-3.72	3611	20	98.49	5233467
						Nf =	**288844**

Design Time: 18 weeks from January 1 [4th week of April]

DT Pavement Temperature: 63 deg. F

DT Air Temperature: 57 deg. F

TABLE 8.10.

Design Time Computations for Cell-31

Month	MMAT deg. F	MMPT deg. F	MMPT deg. C	AC Modulus ksi	Subgrade "Breakpoint" Modulus, ksi	AC Strain microstrain	IDOT Na
January	13.10	18.76	-7.35	5385	22	147.81	1548357
February	17.15	22.90	-5.06	4184	21	157.42	1281724
March	30.05	36.07	2.26	1873	16	193.37	691491
April	46.10	52.46	11.37	689	9	252.20	311698
May	58.25	64.86	18.26	323	11	300.46	184328
June	67.95	74.77	23.76	177	13	345.45	121287
July	73.25	80.18	26.77	127	13	374.20	95420
August	70.65	77.52	25.29	149	14	358.73	108314
September	61.45	68.13	20.07	265	13	313.18	162770
October	49.60	56.03	13.35	554	13	261.92	278284
November	32.80	38.88	3.82	1578	15	202.09	605764
December	19.15	24.94	-3.92	3694	20	162.56	1163832
						Nf =	**232064**

Design Time: 16 weeks from January 1 [2nd week of April]

DT Pavement Temperature: 60 deg. F

DT Air Temperature: 53 deg. F

TABLE 8.11

Summary of Design Time Data

Cell	Design Time Week *		Design Time Pavement Temperature, deg. F	Design Time Air Temperature, deg. F
24	15	1st week of April	55	48
25	18	4th week of April	63	57
26	20	2nd week of May	68	62
27	16	2nd week of April	60	53
28	16	2nd week of April	60	53
29	18	4th week of April	63	57
30	18	4th week of April	63	57
31	16	2nd week of April	60	53

* Week 1 is first week of January

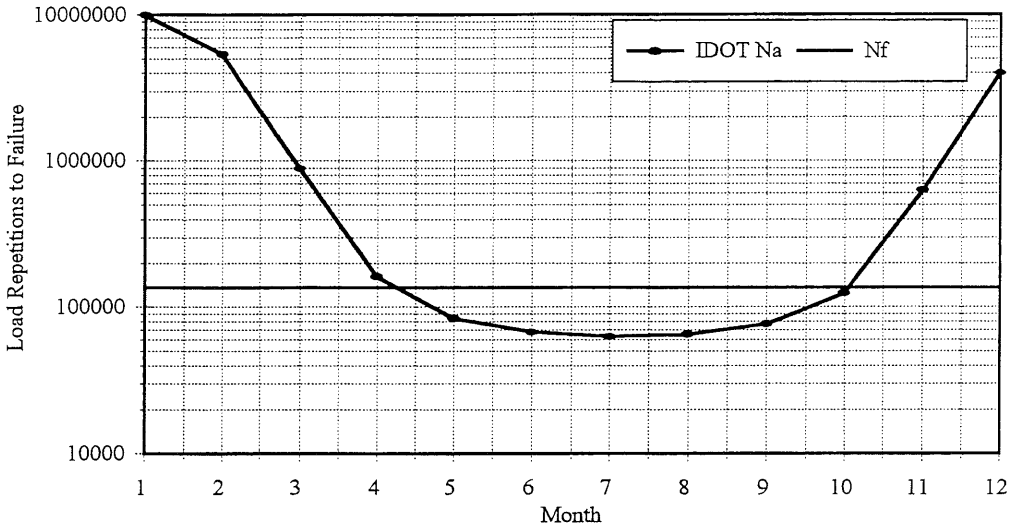

Figure 8.1. Design Time Relation for Cell-24
[3-inch AC/4-inch GB/Sandy Subgrade]

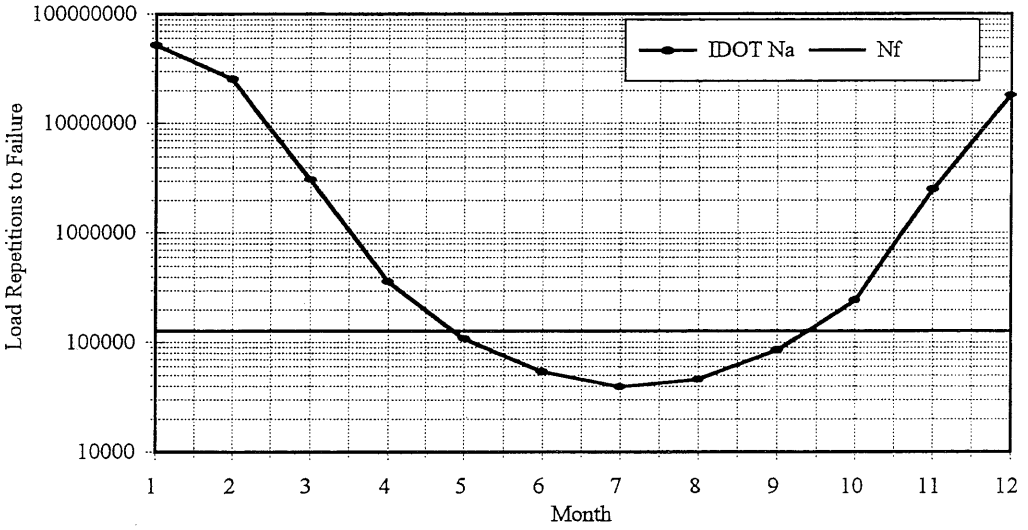

Figure 8.2. Design Time Relation for Cell-25
[5-inch Full-Depth AC/Sandy Subgrade]

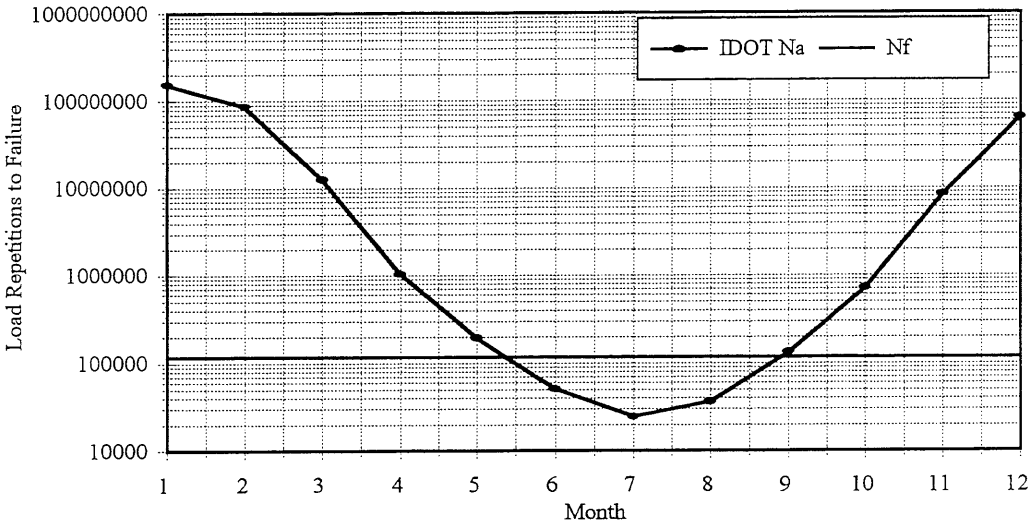

Figure 8.3. Design Time Relation for Cell-26
[6-inch Full Depth AC Pavement]

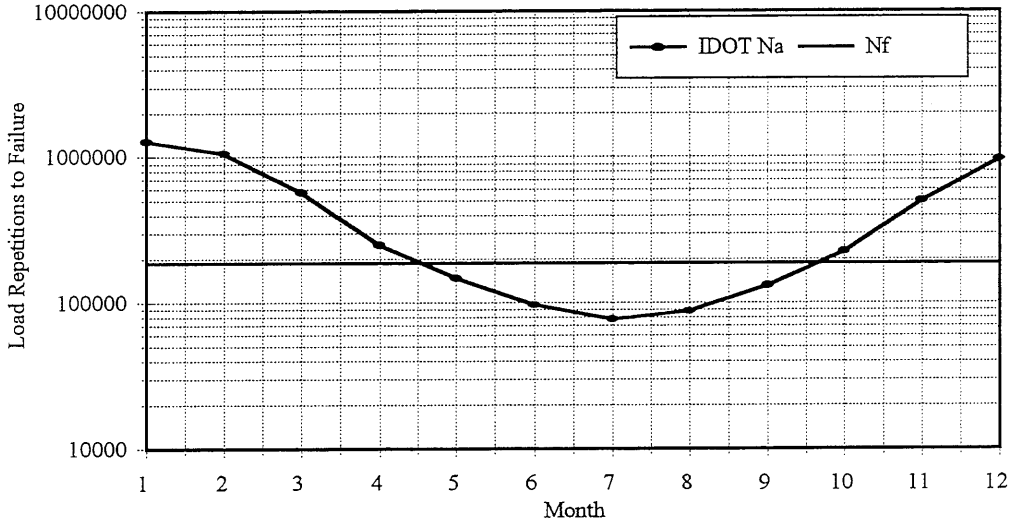

Figure 8.4. Design Time Relation for Cell-27
[3-inch AC/11-inch GB/Cohesive Subgrade]

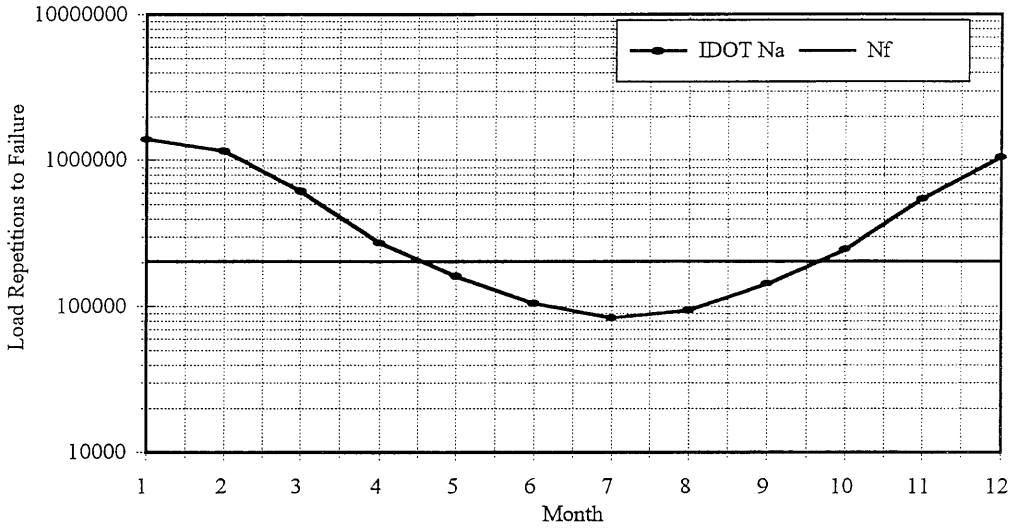

Figure 8.5. Design Time Relation for Cell-28
[3-inch AC/13-inch GB/Cohesive Subgrade]

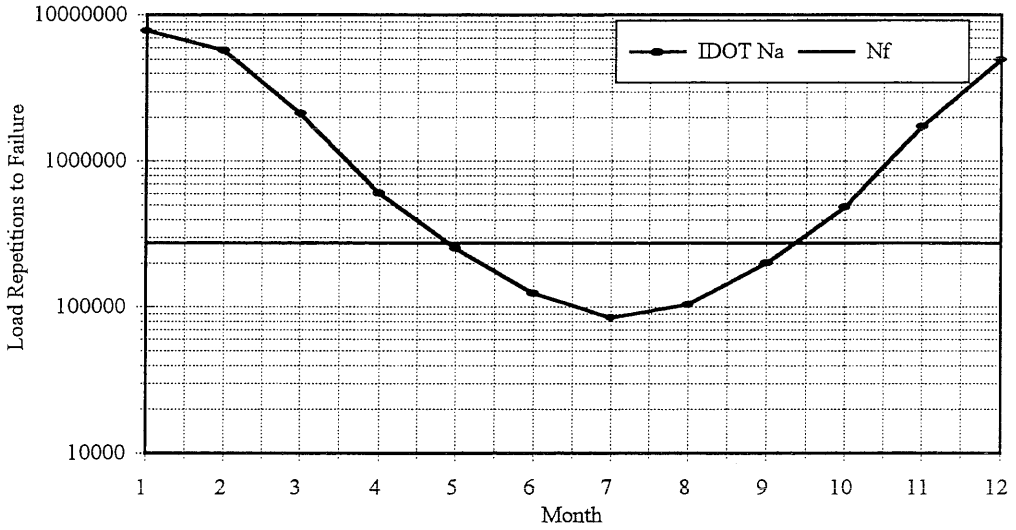

Figure 8.6. Design Time Relation for Cell-29
[5-inch AC/10-inch GB/Cohesive Subgrade]

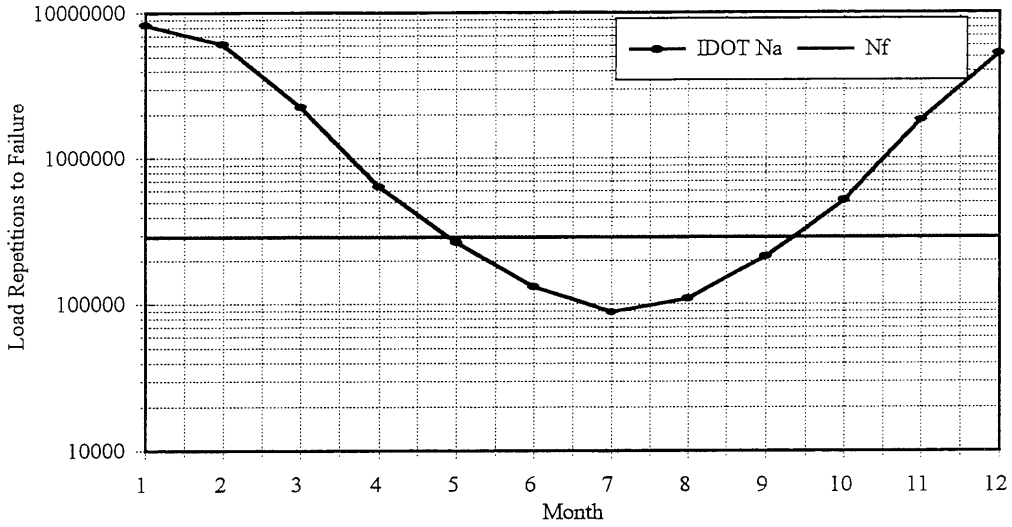

Figure 8.7. Design Time Relation for Cell-30
[5-inch AC/12-inch GB/Cohesive Subgrade]

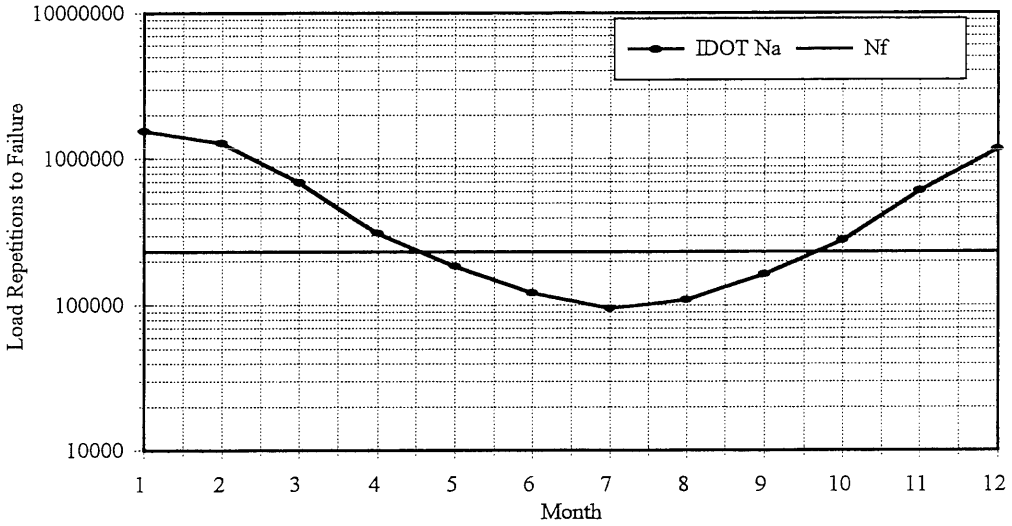

Figure 8.8. Design Time Relation for Cell-31
[3-inch AC/16-inch GB/Cohesive Subgrade]

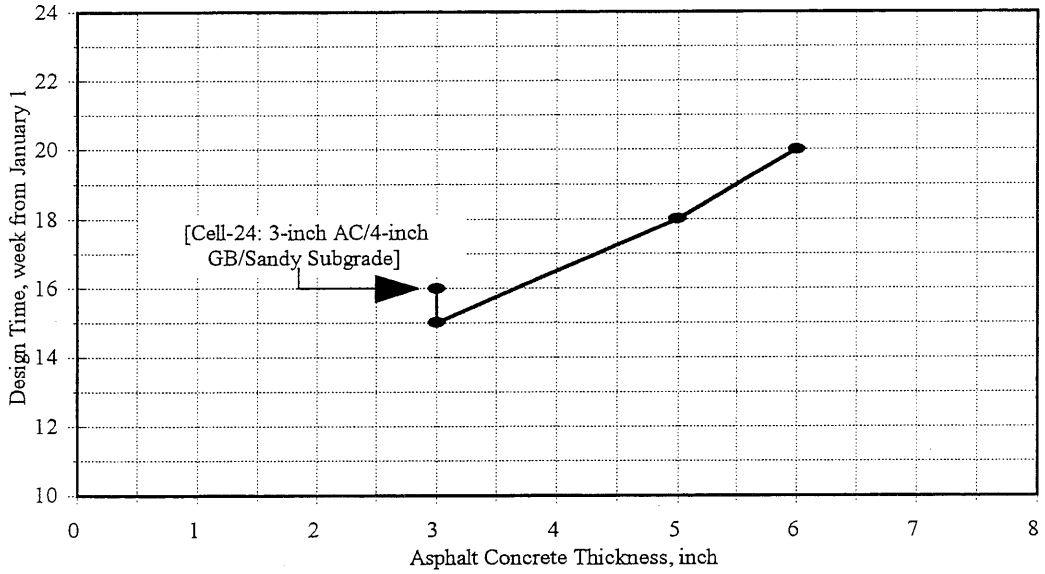

Figure 8.9. Effect of Asphalt Concrete Thickness on "Design Time"

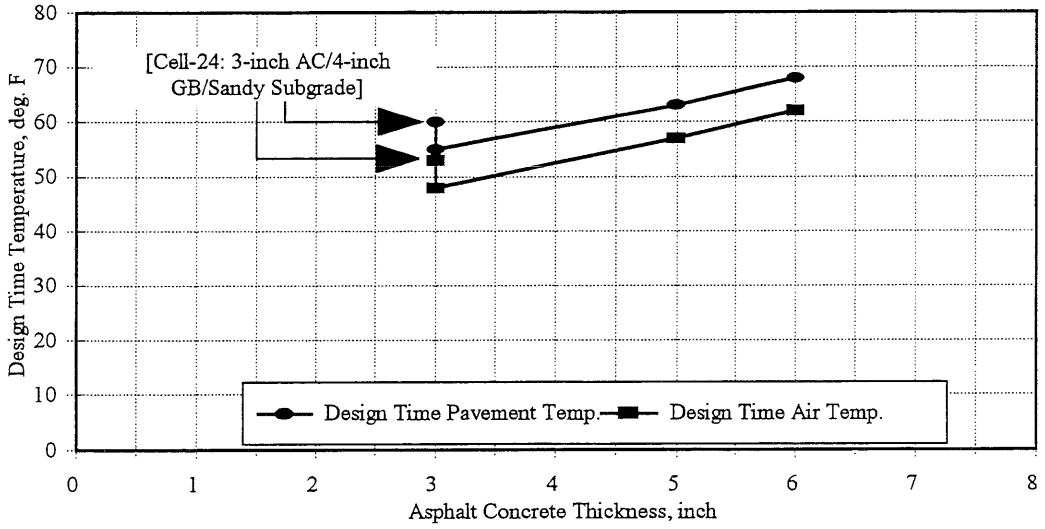

Figure 8.10. Effect of Asphalt Concrete Thickness on "Design Time" Temperatures

temperature was 63-°F and design time air temperature was 57-°F. In the case of Cell-26 (6-inch full depth asphalt concrete pavement), the design time pavement temperature was 68-°F and design time air temperature was 62-°F.

8.5 Effect of Granular Base Layer Thickness on "Design Time" Data

Four different type of granular materials were used as bases in the Mn/ROAD LVR test sections. No differentiation was made between the granular materials when CMS modeling was done for the test sections. The same thermal properties (Table 8.1) were used for all the four granular materials. Therefore, from the CMS results, the effect of granular layer thickness on "Design Time" was studied. The granular base thickness ranged from 4-inch (Cell-24) to 16-inch (Cell-31). Figure 8.11 shows the effect of granular layer thickness on the "Design Time". For test sections with 5-inch asphalt concrete surface (Cells 29 and 30), granular layer thickness did not have any effect on the "Design Time". In the case of test sections with 3-inch asphalt concrete surface (Cells 24, 27, 28 and 31), granular layer thickness did have some effect on the "Design Time". The granular layer thickness in Cells 24, 27, 28, and 31 were 4-inch, 11-inch, 13-inch, and 16-inch respectively. The "Design Time" for Cell-24 was one week earlier than the "Design Time" for Cells 27, 28 and 31.

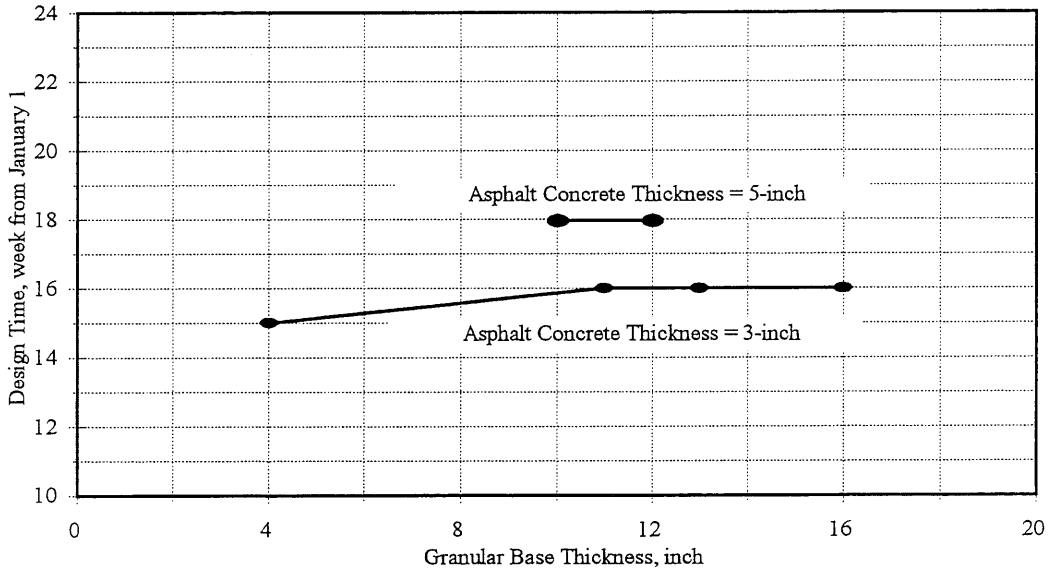

Figure 8.11. Effect of Granular Base Thickness on "Design Time"

Figures 8.12 and 8.13 show the effect of granular base thickness on the design time pavement temperature and design time air temperature for 3-inch thick and 5-inch thick asphalt concrete surfaces, respectively. The granular base thickness does not have any effect on the design time

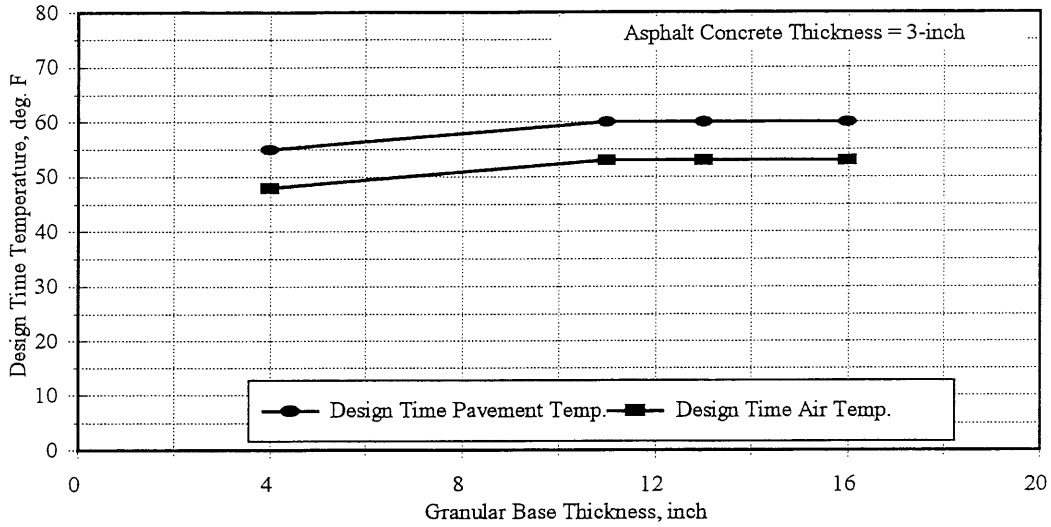

Figure 8.12. Effect of Granular Base Thickness on "Design Time" Temperatures

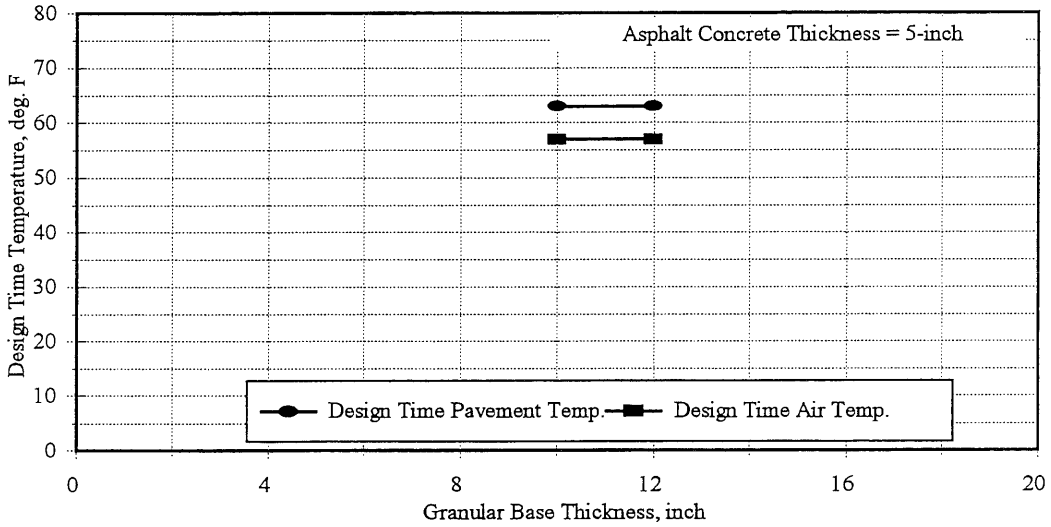

Figure 8.13. Effect of Granular Base Thickness on "Design Time" Temperatures

pavement temperature and design time air temperature except for Cell-24 (Figure 8.12). The design time pavement temperature and design time air temperature are lower for Cell-24 when compared to the other test sections (Cells 27, 28, and 31) with 3-inch thick asphalt concrete surface. Thin granular layer thickness in Cell-24 results in higher stresses in the sandy subgrade which shows

stress hardening behavior, thereby reducing the tensile strains at the bottom of the asphalt concrete layer.

8.6 Effect of Subgrade Type on "Design Time" Data

Cells 24 and 25 have a sandy subgrade. The remaining test sections have cohesive subgrades. The analyses of design time data showed that the type of subgrade did not have any effect on "Design Time", design time pavement temperature and design time air temperature. In the case of Cell-24 (3-inch asphalt concrete/4-inch granular base/sandy subgrade), early "Design Time" and lower design time pavement temperature and design time air temperature were observed. It is not because of the difference in thermal properties of sand and cohesive subgrade, but due to the fact that a thin granular layer thickness results in higher stresses in the sandy subgrade (which shows stress hardening behavior), thereby reducing the tensile strains at the bottom of the asphalt concrete layer. The difference in the thermal properties of sand and cohesive subgrade, however, do affect the temperature distribution in the asphalt concrete layer. The thermal gradient observed in the test section with sandy subgrade (Cell-25 : 5-inch full-depth asphalt concrete pavement) was lower than the one observed in the test section with cohesive subgrade (Cell-26 : 6-inch full-depth asphalt concrete pavement). Figure 8.14 shows the temperature profile within the asphalt concrete layer. Thermal gradients within the asphalt concrete layer are shown in Figure 8.15.

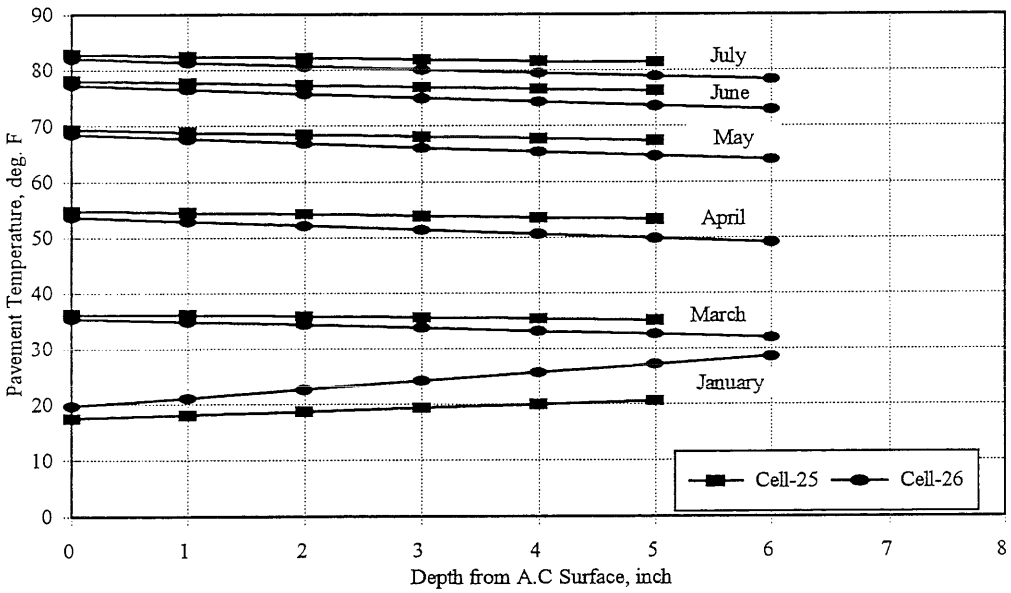

Figure 8.14. Temperature Profile Within Asphalt Concrete Surface

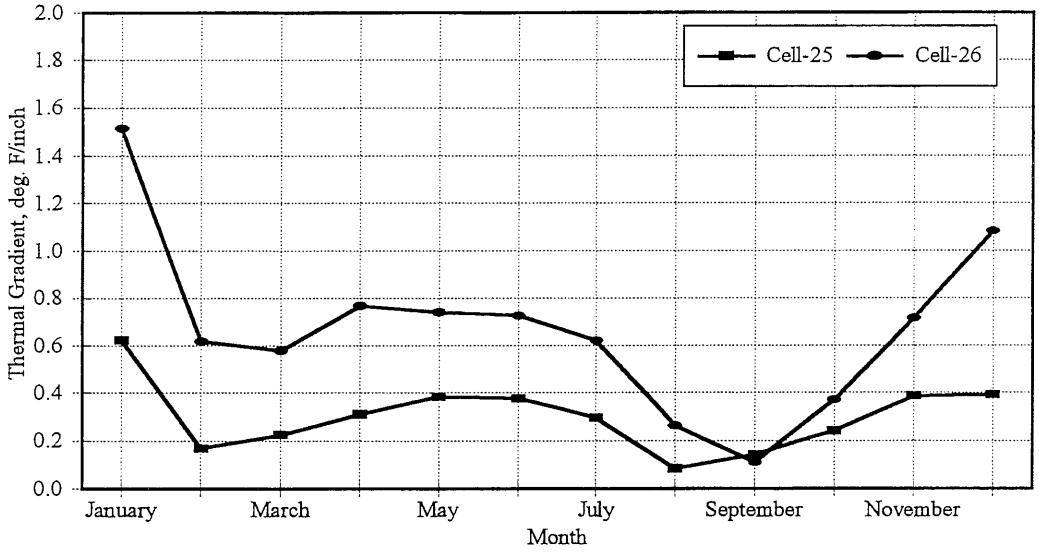

Figure 8.15. Thermal Gradients Within the Asphalt Concrete Layer

8.7 Summary

The three most common modes of distress in flexible pavements are the asphalt concrete fatigue, asphalt concrete rutting, and granular base and subgrade rutting. Asphalt concrete fatigue is a function of asphalt concrete thickness, traffic, and climatic effects on the pavement. A "Design Time" concept is used to characterize the climatic effects on asphalt concrete fatigue. The fatigue life of an asphalt concrete pavement estimated based on "Design Time" asphalt concrete modulus is equal to the fatigue life calculated based on the 12-monthly asphalt concrete modulus inputs. CMS program was used to estimate pavement temperatures as a function of air temperatures. The analysis showed that the "Design Time" is primarily affected by the thickness of asphalt concrete. The granular layer thickness and subgrade type (sand or cohesive) do not have any effect on design time pavement temperature and design time air temperature. Thermal gradients within the asphalt concrete layer were lower in the case of test sections with sand as the subgrade.

The next chapter discusses the effect of subgrade type on pavement structural response and performance.

CHAPTER - IX

"CRITICAL PERIOD" CONCEPT FOR SUBGRADE CHARACTERIZATION

9.1 Introduction

Subgrade support conditions play an important role in pavement thickness design and performance of flexible pavements. The most critical period of pavement support occurs during the spring thaw. When spring thaw occurs, the supporting capacity (strength/modulus) of the subgrade is drastically reduced. This reduces the load distributing quality of granular layers, resting on top of the subgrade, due to the loss of shear strength at the interface. Spring thaw and the accompanying reduced subgrade support can have a significant effect on the behavior and performance of pavement structure. Barenberg [87] showed that the loss in subgrade interface shear strength (because of saturated subgrade-base interface) reduces the resistance to horizontal shear provided to the base, and limits the load distribution capacity.

Low volume roads are typically composed of a granular layer placed on top of a generally fine-grained subgrade. A thin asphalt concrete layer is placed on top of granular layer to provide a wearing surface. Since low volume roads have thin asphalt concrete layer, the pavement behavior is sensitive to the quality of granular base layer and the subgrade support conditions. The magnitude of deviator stress that can be repeatedly applied to the surface of a subgrade from an overlying pavement structure is a function of the strength of the subgrade soil. To limit the accumulation of permanent deformation in the subgrade soil, the subgrade stress ratio (repeated deviator stress/unconfined compressive strength of the soil) should be limited. The recommended subgrade stress ratio (SSR) values to limit subgrade rutting are discussed later in this chapter. The effect of granular base material quality on pavement response and performance was discussed in detail in Chapter-VI. This chapter discusses the effect of subgrade type (sand/cohesive) on the pavement structural response and performance.

9.2 Effect of Subgrade Type on Pavement Structural Response

There are two different type of subgrades in the low volume road loop at the Mn/ROAD project. Test sections LVR-F8 (Cell-24) and LVR-F9 (Cell-25) have a sandy subgrade, and the remaining test sections have cohesive subgrade (AASHTO A-6 soil). The results from laboratory testing on

the specimens of sandy subgrade and cohesive subgrade have been discussed in Chapter-IV and Chapter-V respectively.

The sandy subgrade was characterized as a stress hardening material, and the cohesive subgrade was characterized as the stress softening material. The laboratory tests (triaxial tests) on sand showed that increased moisture content did not have a significant effect on the resilient behavior since the moisture drained freely during the test till the specimen reached an equilibrium moisture content (10.5-percent). The subgrade "breakpoint" modulus, E_{Ri}, characterizes the resilient behavior of cohesive subgrade. The subgrade "breakpoint" modulus values were estimated from the FWD test results using backcalculation algorithms (Chapter-VI). Figures 6.19 and 6.20 show the variation of E_{Ri} with time in the inner lane and outer lane respectively. All the test sections show similar E_{Ri} values. Small difference in moisture content can cause considerable variation in E_{Ri} values (for the Mn/ROAD subgrade, one percent increase in moisture content reduces E_{Ri} by approximately 2.19-ksi [Chapter V, section 5.5]). The E_{Ri} values are lowest during the spring-thaw (values range from 5-7 ksi). The subgrade regains strength after the spring-thaw and during the fall, the E_{Ri} values rise to 10-13 ksi.

FWD deflection D3 (deflection measured at a distance of 36-inch from the center of loading plate) was used to study the effect of seasonal variation in subgrade on pavement structural response. Previous studies have shown that D3 is primarily affected by the subgrade properties and is independent of the pavement section. From results of ILLI-PAVE analyses (Chapter-VII), it was observed that asphalt concrete layer does not contribute to deflection D3. Contribution of granular base layer to deflection D3 is about 2-3 percent. Maximum D3 values were observed during the spring-thaw period. Ratio of deflection D3 and stable subgrade D3 (August 10, 1994) was used to study the effect of spring-thaw on pavement deflection response. Figure 9.1 shows the ratio of D3 and stable subgrade D3 for Cells 24 and 25 (test sections with sandy subgrade). The ratio is lower (0.5-0.7) during the early part of the year since the subgrade is frozen and asphalt concrete stiffnesses are very high. During spring-thaw, the ratio starts increasing and reaches a maximum value of one. Increase in moisture content during spring-thaw did not affect the subgrade support conditions reinforcing the observation made during the repeated load triaxial testing (increase in moisture content did not affect the resilient behavior of sand specimens). Spring time deflections

D3 were similar to the D3 measured during the summer time FWD testing.

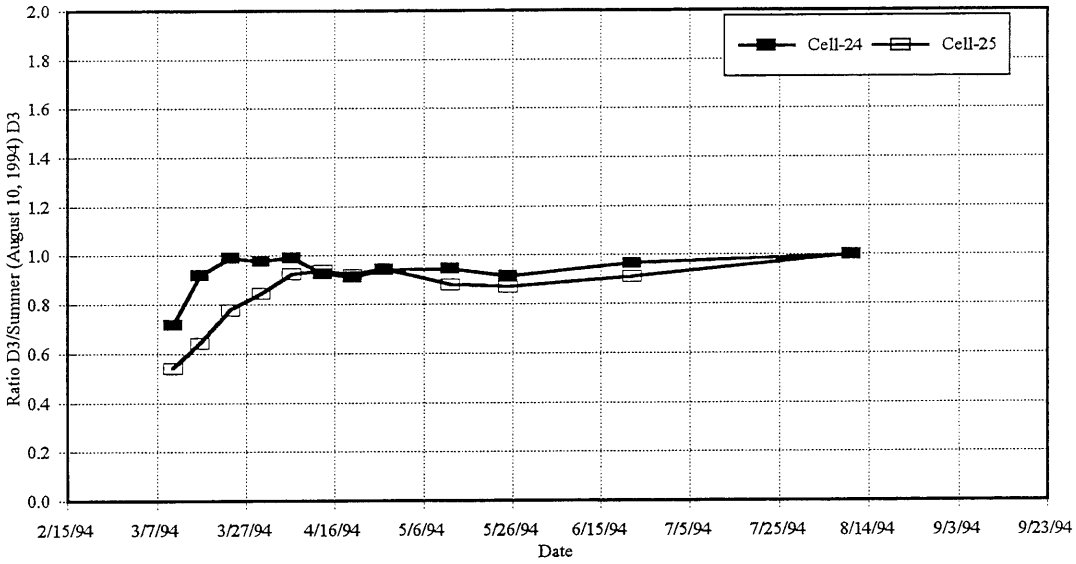

Figure 9.1. Ratio of FWD D3 to Summer Time FWD D3 for Test Sections with Sandy Subgrade

In the case of test sections with cohesive subgrade (Cells 26, 27, 28, 29, 30, 31) the spring-thaw deflection D3 values were 20-60 percent higher than the D3 values measured during summer time FWD testing (Figure 9.2). Cell-26 (6-inch full-depth asphalt concrete pavement) showed 20-percent higher D3 values during spring-thaw compared to the summer D3 values. Cell-27 (3-inch asphalt concrete/11-inch granular base) showed 60-percent increase in the spring-thaw D3 values. For Cells 28, 29, 30 and 31, the spring-thaw D3 values were about 35-40 percent higher than the summer time D3 values. Higher deflection ratios were observed at the same time when the E_{Ri} are at their lowest (as shown in Figures 6.19 & 6.20).

9.3 Effect of Subgrade Type on Pavement Performance

Subgrade rutting is a common form of flexible pavement distress. Subgrade rutting can be controlled by limiting the magnitude of vertical stresses on the subgrade. Lower subgrade stress ratio (SSR) correspond to lower subgrade rutting. Subgrade stress ratio for the test sections were estimated from falling weight deflectometer data using algorithms developed from an extensive ILLI-PAVE database. The algorithms used were as follows:

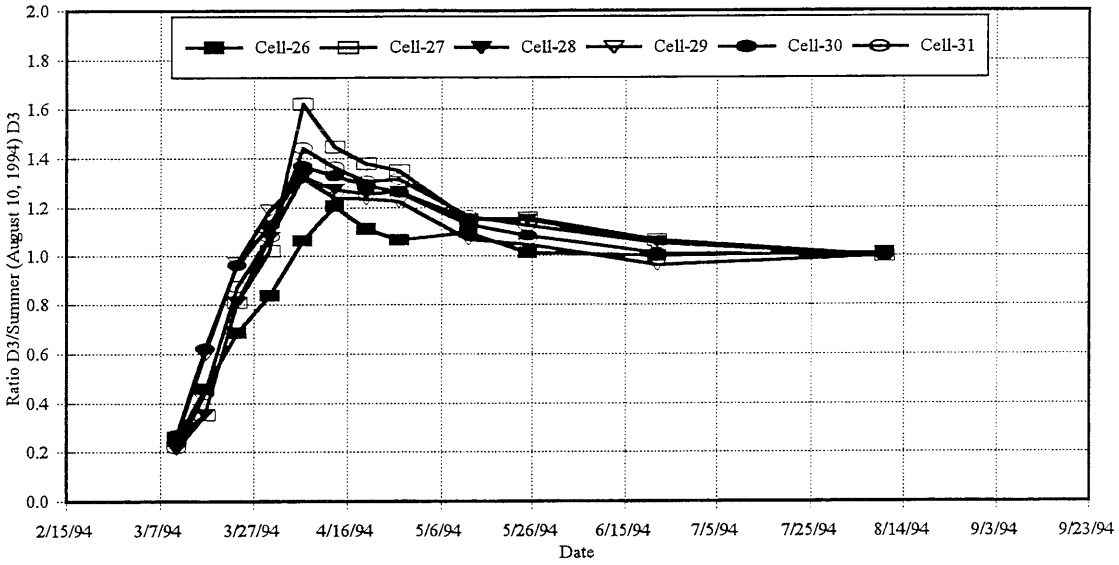

Figure 9.2. Ratio of FWD D3 to Summer Time FWD D3 for Test Sections with Cohesive Subgrade

Conventional Flexible Pavements [70]

$$\text{Log SSR} = 0.3056 + 0.0560*T_{ac} - 0.0222*T_g - 0.0495*(\text{Log}E_{ac})*T_{ac} - 0.4242*\text{Log}\,E_{Ri} \quad \text{.....[9.1]}$$

$R^2 = 0.97$ SEE = 0.061

Full-Depth Asphalt Concrete Pavements [26]

$$\text{Log SSR} = 1.951 - 1.138*\text{Log}\,T_{ac} - 0.515*\text{Log}\,E_{ac} - 0.365*\text{Log}\,E_{Ri} \quad \text{.....[9.2]}$$

$R^2 = 0.978$ SEE = 0.052

Surface Treated Pavements [73]

$$\text{Log SSR} = -0.184 - 0.034*T_g + 0.178 * \text{Log D0} \quad \text{.....[9.3]}$$

$R^2 = 0.93$, SEE = 0.06

where

SSR = Subgrade stress ratio

D0 = Surface deflection at the point of loading, in mils

T_{ac} = Thickness of AC layer, in inches

T_g = Thickness of granular base course, in inches

E_{ac} = Resilient modulus of AC layer, in ksi

E_{Ri} = "breakpoint" resilient modulus of the subgrade, in ksi

Based on the design traffic levels, following subgrade stress ratio values are recommended [72, 76]:

Traffic Design Level	Subgrade Stress Ratio (SSR)
Light (< 20,000 ESALs)	0.75
Medium (< 40,000 ESALs)	0.70
Heavy (< 80,000 ESALs)	0.65

Figures 9.3 through 9.8 show the estimated subgrade stress ratios for test sections on cohesive subgrade.

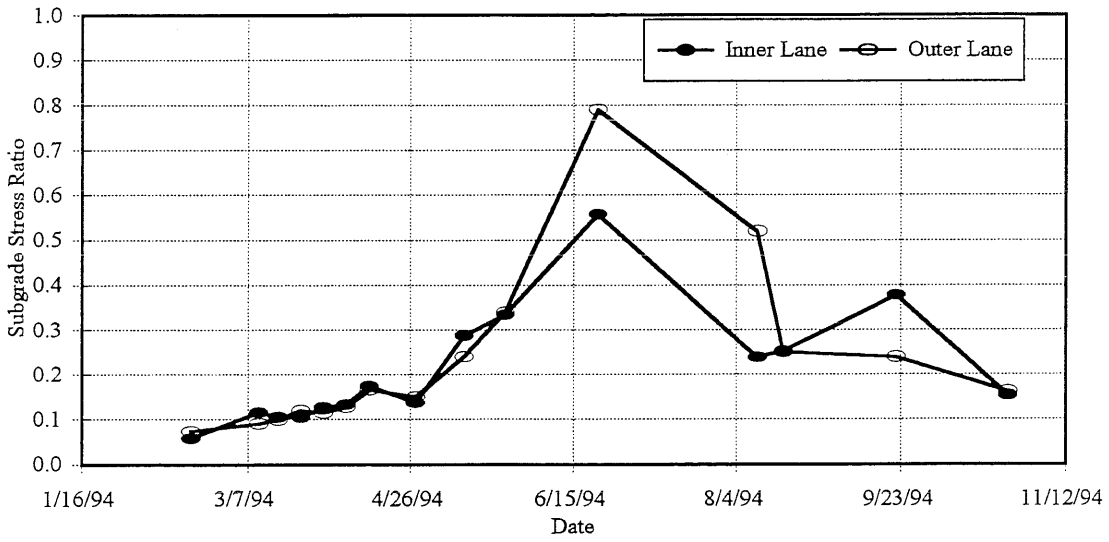

Figure 9.3. Subgrade Stress Ratio for Cell-26

For Cell-26 (6-inch full-depth asphalt concrete pavement), the SSR with time is shown in Figure 9.3. The subgrade stress ratios are within acceptable limits except during summer when values

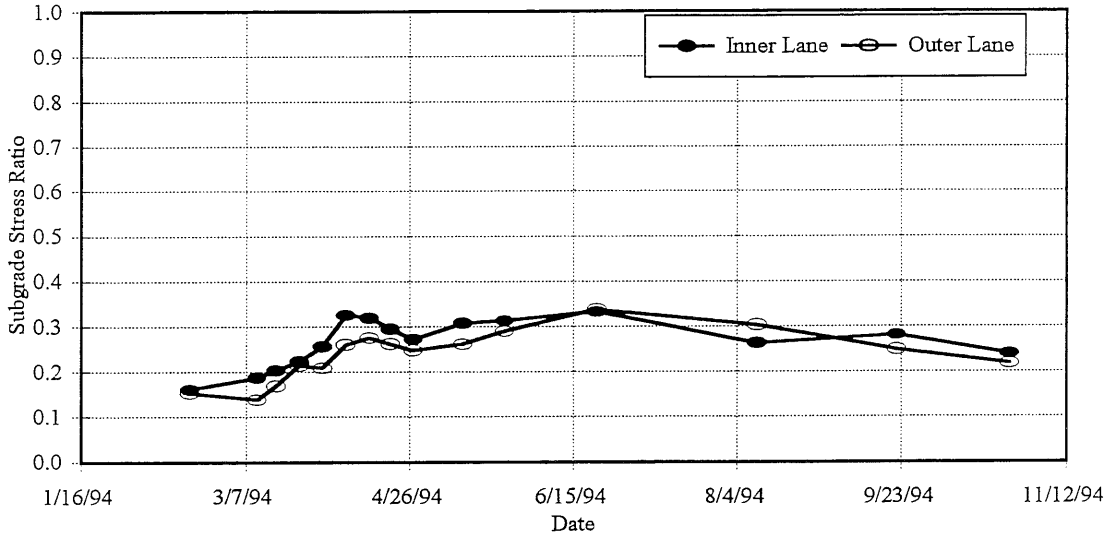

Figure 9.4. Subgrade Stress Ratio for Cell-27

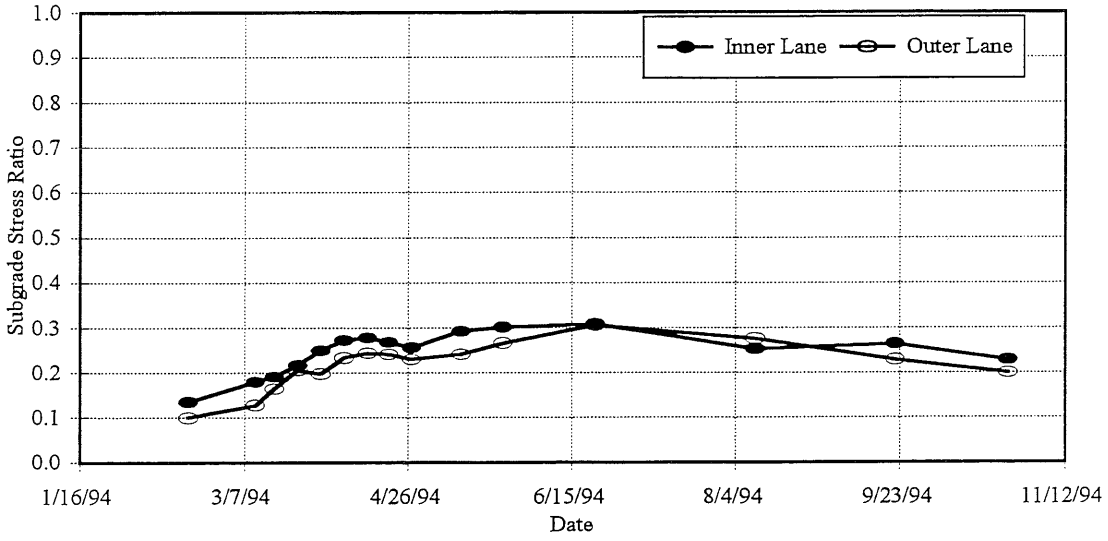

Figure 9.5. Subgrade Stress Ratio for Cell-28

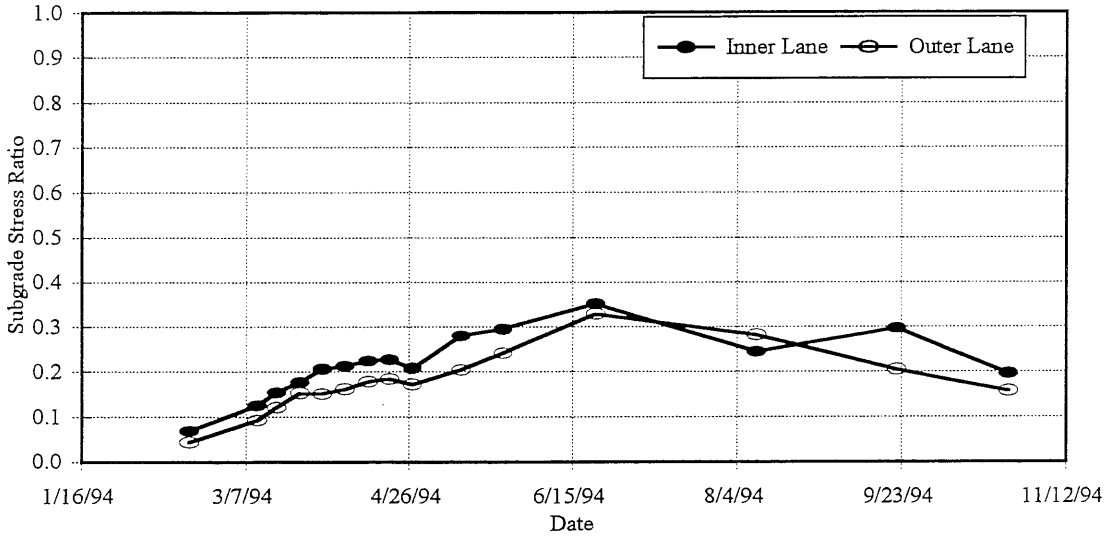

Figure 9.6. Subgrade Stress Ratio for Cell-29

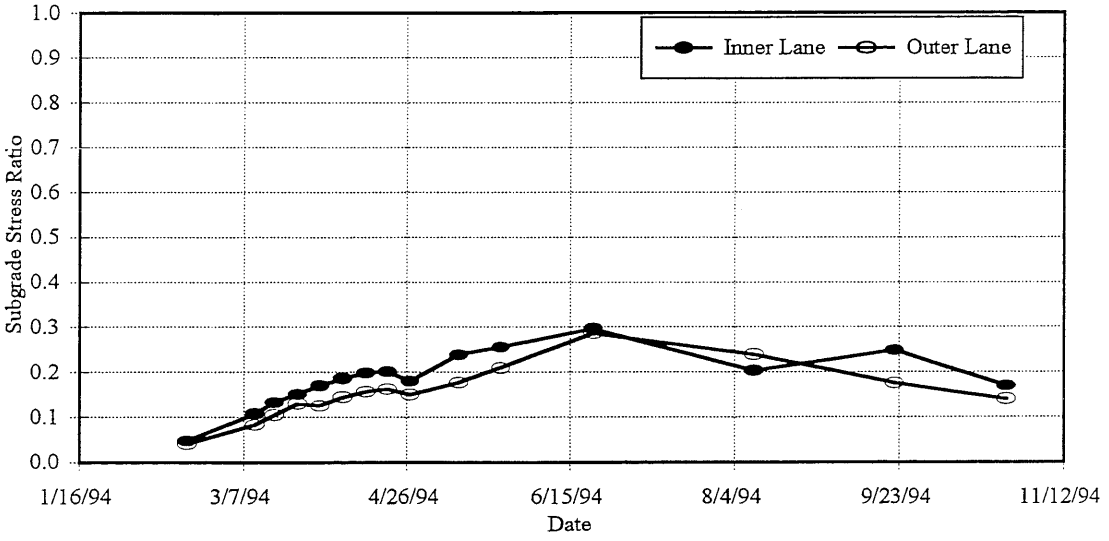

Figure 9.7. Subgrade Stress Ratio for Cell-30

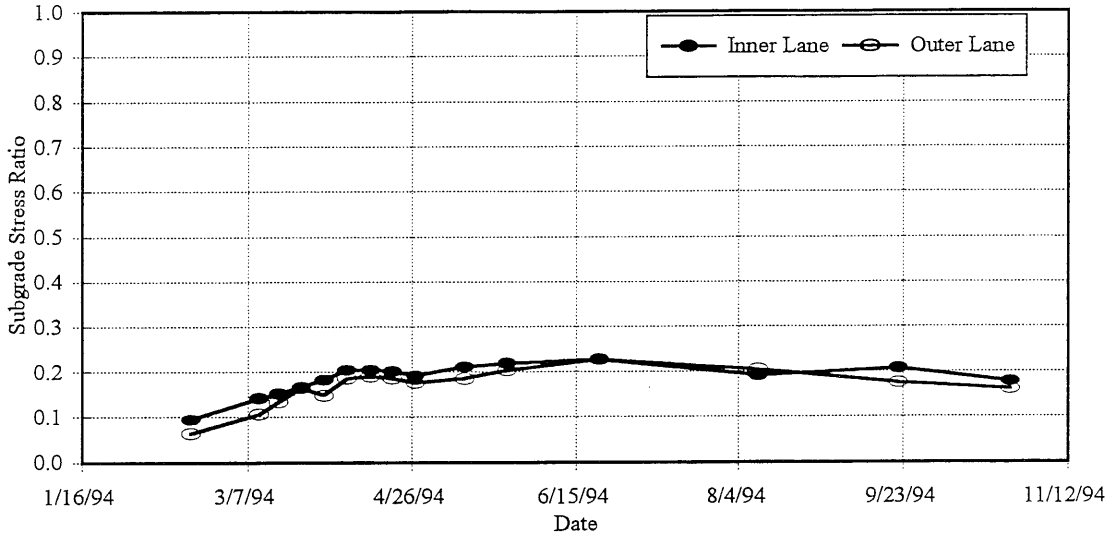

Figure 9.8. Subgrade Stress Ratio for Cell-31

upto 0.8 are observed. For the remaining test sections, the subgrade stress ratios were less than 0.35. Similar behavior was observed in both lanes. During the spring-thaw, the SSR values ranged from 0.2 to 0.35. The subgrade was well protected during the spring-thaw. This reinforces the findings of Chapter-VI that in the conventional flexible pavement test sections (Cells 27 through 31) the rutting is taking place in the granular base layer. Figures 9.9 and 9.10 show the comparison between SSR values for test sections with 3-inch thick asphalt concrete surface and 5-inch thick asphalt concrete surface respectively. Typically, higher SSR values are expected for cohesive subgrade during spring. Previous studies [63, 88, 89] have shown that the resilient behavior of fine-grained cohesive soils is greatly affected by cyclic freeze-thaw action. The studies revealed that substantial increase in resilient deformation (reduced resilient moduli) were caused by the imposition of a small number of freeze-thaw cycles, even though no gross moisture changes were allowed (closed system freeze-thaw). One freeze-thaw cycle is sufficient to drastically reduce the resilient modulus of soil. In this case, highest SSR values were observed during summer. During summer asphalt concrete stiffness is lowest, and the load stresses will increase in the granular base and subgrade. Granular materials exhibit stress hardening behavior. If the granular base has adequate shear strength, the stresses on the top of subgrade are reduced because of the better load distribution capability of granular layer (due to stress hardening) and lower SSR are observed.

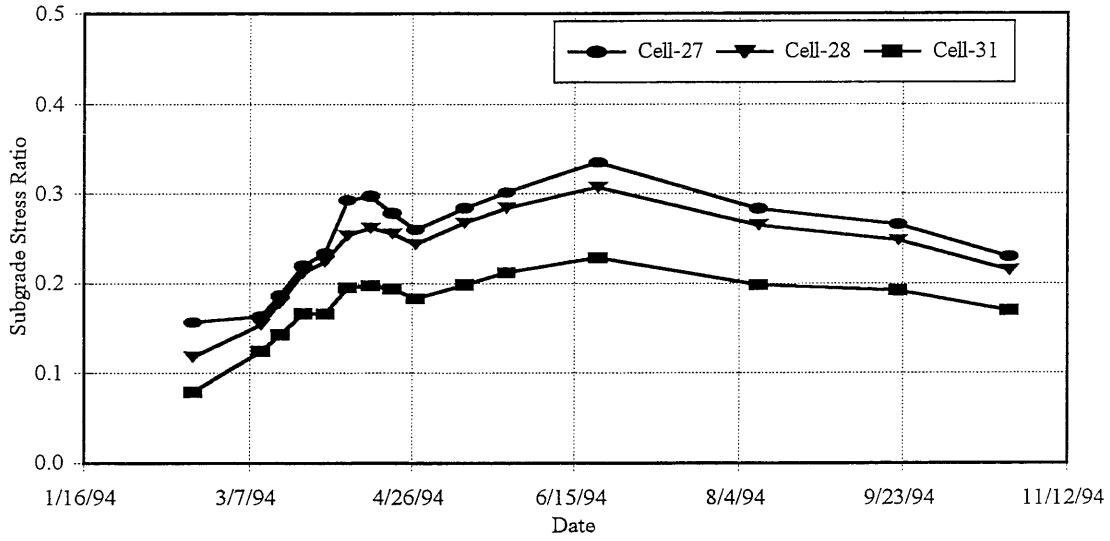

Figure 9.9. Subgrade Stress Ratios for 3-inch Thick Asphalt Concrete Test Sections

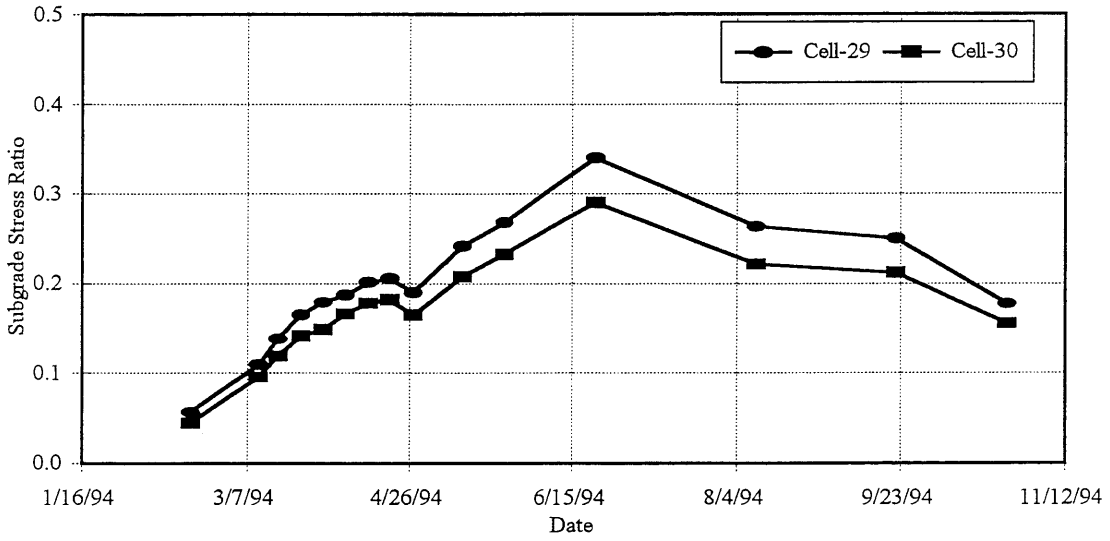

Figure 9.10. Subgrade Stress Ratios for 5-inch Thick Asphalt Concrete Test Sections

However, if the granular base has low shear strength and low stress sensitivity (lower 'n' values in $E_R = K*\theta^n$ model), the granular layer may not stiffen (stress hardening) up and the load

distribution capability of granular layer will be reduced. As a result, the subgrade will be subjected to higher vertical stresses and hence higher SSR values.

Test sections with sand subgrades (Cells 24 and 25) performed better than the test sections on cohesive subgrade. Rutting in Cell-24 (3-inch asphalt concrete/4-inch granular base) is lowest when compared with other test sections with 3-inch thick asphalt concrete surface (Cells 27, 28, 31). Cell-25 (5-inch full-depth asphalt concrete pavement) is performing better than Cell-26 (6-inch full-depth asphalt concrete pavement on cohesive subgrade).

9.4 "Critical Period" Concept for Subgrade Characterization

It has been established that the Mn/ROAD LVR test section rutting occurred in the granular materials. In a flexible pavement, asphalt concrete rutting can be controlled by proper material selection and mix design. Granular base rutting can be controlled by selecting materials with adequate shear strength and low moisture sensitivity. Increasing the asphalt concrete thickness and granular base layer thickness also reduces vertical stresses on the top of subgrade. Stabilization/modification techniques can be employed to improve the shear strength and modulus of subgrade soils.

Proper characterization of subgrade soils becomes very important in the case of low volume roads because of the presence of thin asphalt concrete surfaces. Subgrade soils can be characterized by means of laboratory testing, non-destructive testing like FWD, and empirical relationships. For Mn/ROAD subgrade soils, extensive FWD and laboratory testing data are available. The analysis of FWD data and results from laboratory triaxial testing program on sand showed that in the case of sandy subgrade, pavement response and performance are not significantly affected by change in moisture conditions. However, in the case of cohesive subgrade, both response and performance are significantly affected by the change in moisture conditions and the freeze-thaw cycling in the subgrade soil. Most critical period of pavement support occurs during the spring thaw. High moisture content reduces the strength of soil and the subgrade "breakpoint" modulus E_{Ri}.

In the Illinois design procedure for local roads and streets [2], the subgrade resilient modulus (E_{Ri}) is used as the input for conventional flexible pavements. A springtime E_{Ri}, which reflects high

moisture content and a thaw-weakened condition, is used for design purposes. Design E_{Ri} values can be obtained from field testing, laboratory testing, or estimated from soil property or strength data. The following is a summary of IDOT procedures [2] to determine preliminary E_{Ri} values which can be later adjusted for moisture:

1. Resilient Modulus Testing

   The E_{Ri} of a soil may be determined by performing repeated unconfined compression testing in the laboratory. Subgrade specimens from insitu soil or laboratory-prepared specimens may be tested. Laboratory-prepared specimens with a range of moisture contents and densities can be tested to simulate the variable conditions found in the field.

2. Falling Weight Deflectometer (FWD) Testing

   Design E_{Ri} values can be backcalculated from FWD data taken from existing pavements. County soil maps can be used to identify the major soil series found in an area. A FWD testing scheme that targets existing typical flexible pavements constructed in the major soil series of the area can be developed using this information. Springtime FWD testing is preferred, but a seasonal adjustment factor may be applied to the backcalculated E_{Ri} if the FWD testing is conducted during other seasons. The average E_{Ri} backcalculated from FWD testing should be used as the design E_{Ri}. Backcalculated E_{Ri} values do not represent a single point location, but reflect the composite influence of a large volume of insitu soil, including different soil horizons.

3. Estimating E_{Ri} from Strength Data

   An E_{Ri} value can be estimated from strength data obtained with a Corps of Engineers hand-held cone penetrometer, or a dynamic cone penetrometer (DCP). Both the Corps of Engineers hand-held cone penetrometer, and the DCP are field testing devices used to rapidly evaluate the insitu strength of fine-grained and granular soils. Data obtained from Corps of Engineers hand held cone and DCP testing can be used to estimate CBR and E_{Ri} through the use of following equations:

$$CBR = CI / 40 \quad \text{.....[9.4]}$$

$$\text{Log } CBR = 0.84 - 1.26 * \text{Log}(PR) \quad \text{.....[9.5]}$$

$$Qu = 4.5 * CBR \quad \text{.....[9.6]}$$

$$E_{Ri} = 0.86 + 0.307 * Qu \quad \text{.....[9.7]}$$

where

CBR	=	California Bearing Ratio
CI	=	Corps of Engineers Cone Index, psi
PR	=	DCP Penetration Rate, inch/blow
Qu	=	Unconfined Compressive Strength, psi
E_{Ri}	=	Subgrade Resilient Modulus, ksi

The E_{Ri} value is adjusted for moisture. An E_{Ri} value can be established with Corps of Engineers cone penetrometer or DCP testing at the project or on existing flexible pavement sections constructed on the same soil series as the roadway being designed. Ideally, such testing should be conducted during the spring time. If the testing is not conducted during the spring, the E_{Ri} value calculated from Equation 9.7 will have to be adjusted for the moisture content.

4. Estimating E_{Ri} from Soil Properties

Design E_{Ri} values can be estimated based on a soil's clay content (< 2 micron) and plasticity index (PI). Including organic carbon as an input slightly improves the E_{Ri} estimate. These values can be obtained from laboratory testing of the project's soil or the County Soil Report. The following equations may be used to predict E_{Ri} at optimum moisture content and 95-percent of AASHTO T-99 maximum dry density:

$$E_{Ri}\,(OPT) = 4.46 + 0.098 * (\%\ Clay) + 0.119 * PI \quad \text{.....[9.8]}$$

$$E_{Ri}\,(OPT) = 6.90 + 0.0064 * (\%\ Clay) + 0.216 * PI - 1.97 * OC \quad \text{.....[9.9]}$$

where

E_{Ri} (OPT)	=	E_{Ri} (ksi) at optimum moisture content and 95% of AASHTO T-99 maximum dry density
% Clay	=	Clay content (< 2 microns), percent

PI	=	Plasticity Index
OC	=	Organic Carbon, percent (OC = organic matter / 1.7)

The E_{Ri} (OPT) estimate should be adjusted to reflect insitu moisture conditions. If the County Soil Report is used to estimate the soil's clay content and PI, the midpoint values of clay content and PI values given should be used.

5. Typical E_{Ri} Values

   If data are not available to estimate E_{Ri} values using the previously discussed methods, Tables 9.1 and 9.2 may be used to estimate typical E_{Ri} values. If the water table and frost penetration levels are known, Table 9.1 may be used to determine typical E_{Ri} values based on AASHTO soil classification system. If the frost penetration and water table levels are not known, Table 9.2 may be used to estimate typical E_{Ri} values. These E_{Ri} values were developed from resilient modulus testing of fine-grained Illinois soils, and represent 95-percent of AASHTO T-99 maximum dry density and moisture contents 2-percent wet of optimum.

The "preliminary E_{Ri}" determined by one of the above procedures (except for the resilient modulus laboratory or FWD methods) should be corrected to reflect the insitu moisture present under springtime conditions (if the test data reflects conditions other than those of a normal spring). If the AASHTO T-99 maximum dry density (MDD), the optimum moisture content (OMC), and the specific gravity of soil solids (Gs) are known, the following equation can be used to calculate the moisture content for a given degree of saturation and 95-percent compaction:

$$MC_{\%SR} = [(65.7/MDD) - (1/Gs)] * [SR] \quad \text{.....[9.10]}$$

where

$MC_{\%SR}$	=	Moisture content for a given degree of saturation, %
MDD	=	AASHTO T-99 maximum dry density, pcf
Gs	=	Specific gravity of soil solids
SR	=	Degree of saturation, %

TABLE 9.1

Average Subgrade "Breakpoint" Modulus Values (ksi) Based on Soil Classification, Water Table Depth, and Freeze-Thaw Conditions

	High Water Table *		Low Water Table **	
AASHTO Soil Class	With Frost Penetration into Subgrade	Without Frost Penetration into Subgrade	With Frost Penetration into Subgrade	Without Frost Penetration into Subgrade
A-4, A-5, A-6	2.0	4.0	3.0	6.0
A-7	2.0	5.0	3.5	7.0

* Water table seasonally within 24-inches of subgrade surface

** Water table seasonally within 72-inches of subgrade surface

TABLE 9.2

Average Subgrade "Breakpoint" Modulus Values (ksi) for various Soil Classifications

Soil Classification	Average Subgrade "Breakpoint" Modulus **, ksi
AASHTO	
A-7-6	9.2
A-7-5	6.3
A-6	5.6
A-4	3.8
A-5*	4.5
USDA Textural Class	
Silty Clay, Clay	9.5
Silty Clay Loam, Clay Loam	7.3
Silt Loam, Loam, Silt	6.2
Sandy Clay *	9.0
Sandy Clay Loam *	7.0

* Estimated

** Moisture adjustment necessary

Note: 95-percent of AASHTO T-99 maximum dry density and moisture contents 2-percent wet of optimum

For "very poorly, poorly, and imperfectly drained" soils, the E_{Ri} estimate should be adjusted to a 100-percent degree of saturation. All other drainage classes should be adjusted to a 90-percent degree of saturation. The drainage classification for a soil series can be found in the County Soil Report. Once the moisture content for the required degree of saturation is calculated, the field moisture adjustment and design E_{Ri} can be calculated as follows:

$$FMA = MC_{\%SR} - OMC \quad \text{.....[9.11]}$$

$$\text{Design } E_{Ri} = E_{Ri}(OPT) - [(FMA)*(MAF)] \quad \text{.....[9.12]}$$

where

FMA	=	Field moisture adjustment, %
$MC_{\%SR}$	=	Moisture content for a given degree of saturation, %
OMC	=	Optimum moisture content, %
Design E_{Ri}	=	E_{Ri} for flexible pavement design, corrected for insitu moisture conditions, ksi
$E_{Ri}(OPT)$	=	E_{Ri} at OMC and 95-percent MDD, ksi
MAF	=	Moisture adjustment factor, E_{Ri} decrease per 1-percent moisture increase, ksi / %

Moisture adjustment factors are selected based on USDA soil textural classification as follows:

E_{Ri} Moisture Adjustment Factors Based on USDA Textural Classification

USDA Textural Classification	E_{Ri}(OPT) Decrease / 1% Moisture Increase, ksi/%
Clay, Silty Clay, Loam, Clay Loam, Sandy Clay*, Sandy Clay Loam*	0.7
Silt Loam, Sandy Loam	1.5
Loam, Silt	2.1

* Estimated

A design E_{Ri} of 2-ksi is the lowest allowable design E_{Ri}. If the design E_{Ri} value calculated from Equation 9.12 is less than 2-ksi or does not reasonably compare with historical data for the soil series, other means for determining design E_{Ri} should be investigated.

Equation 9.8 was used to predict the E_{Ri} values for the Mn/ROAD cohesive subgrade soils using the percent clay and plasticity index (Tables 5.1 and 5.2). The E_{Ri} values obtained from the equation are at optimum moisture content. Figure 9.11 shows comparison between the measured (from laboratory testing) and predicted E_{Ri} values.

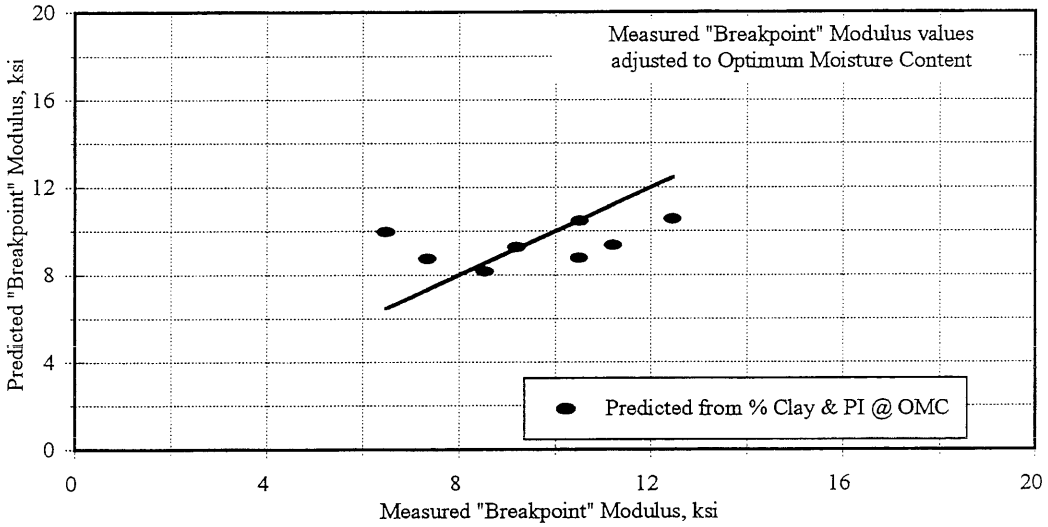

Figure 9.11. Comparison Between Measured and Predicted Subgrade "Breakpoint" Modulus Values

The measured E_{Ri} values were adjusted to optimum moisture content (18-percent) using equation 5.4 which states that for every one percent increase in moisture content, the E_{Ri} value reduces by 2.19-ksi. The E_{Ri} values ranged from 6-ksi to 12-ksi. The difference between the measured and predicted E_{Ri} values is about 1-2 ksi. FWD test results were used to backcalculate the E_{Ri} values (discussed in detail in Chapter-VI and Chapter-VII). The backcalculated modulus values during summer (when moisture content is near optimum) ranged from 8-ksi to 12-ksi (Figure 6.20). In midwest region, subgrade soils are mostly at optimum moisture content (OMC) or wet of OMC.

9.5 Summary

The subgrade significantly affects low volume road pavement structural response and performance. In the Mn/ROAD test sections, sandy and cohesive subgrades were used. The test sections with sandy subgrade showed little or no change in pavement structural response due to changes in

moisture conditions in the subgrade (during spring-thaw). For test sections with cohesive subgrade, the effects of moisture changes during spring on the pavement structural response were significant. Substantial decrease in resilient modulus of fine-grained soils take place by imposition of a small number of freeze-thaw cycles, even though no gross moisture changes are allowed (closed system freeze-thaw). One freeze-thaw cycle is sufficient to drastically reduce the resilient modulus of soil. However, the subgrade stress ratios were in the desirable range (0.65-0.75) and did not contribute to any significant accumulation of permanent deformation in the subgrade. Proper subgrade characterization is very important for economical design of pavement structure. Once the "critical period" design subgrade modulus is determined, adequate thickness of asphalt concrete and granular base layers should be provided to protect the subgrade. Lower subgrade stress ratios will prevent any significant rutting in the subgrade.

CHAPTER - X

SUMMARY, CONCLUSIONS, AND RECOMMENDATIONS

10.1 Review

In the Illinois Department of Transportation (IDOT) Bureau of Local Roads and Streets mechanistic-empirical design procedure, the design criteria for conventional flexible pavements are asphalt concrete fatigue and subgrade stress. A subgrade stress ratio (SSR) criterion is used to consider subgrade rutting. The governing design criteria for full-depth asphalt concrete pavements is the tensile strain at the bottom of asphalt concrete layer. Reduced strain corresponds to increased fatigue life. Subgrade rutting is controlled by limiting the subgrade stress ratio (deviator stress/unconfined compressive strength) at the asphalt concrete-subgrade interface to an acceptable level. In this study, the Mn/ROAD low-volume road data and information was used to further verify/refine/modify mechanistic-empirical based flexible pavement analysis and design concepts and procedures.

In a typical low-volume road, asphalt concrete layer is thin (1-5 inches). Therefore, the granular base layer and subgrade significantly affect the pavement performance. A comprehensive laboratory testing program was established to determine pertinent engineering properties of the granular bases, subbases, and subgrade sand used in the various low-volume road test sections at Mn/ROAD. Rapid shear tests and repeated loading tests were conducted to determine the shear strength parameters (friction angle "ϕ", and cohesion "c"), resilient modulus (E_R), rutting potential, stress history effects on shear strength, and moisture susceptibility. Dynamic cone penetrometer (DCP) tests were conducted to get an indication about the shear strength (CBR) of the granular materials and subgrade sand. The laboratory test results were correlated to the field performance data.

Effect of granular material quality on pavement deflection response and performance was evaluated. The Mn/ROAD FWD data were analyzed to study the effect of granular material quality on the pavement surface deflection response. Rutting in the test sections was monitored and was related to the shear strength of granular materials.

In Chapter-VII, the field measured pavement responses were compared to the ILLI-PAVE (finite element program) predicted pavement responses. In Chapter-VIII, the effect of climatic conditions on the asphalt concrete fatigue life was studied. Effect of asphalt concrete thickness, granular base thickness, and subgrade type on the "Design Time" was evaluated. In Chapter-IX, effect of subgrade type (sand/cohesive) on the pavement structural response and performance was evaluated.

The following sections summarize the findings from this study and recommend areas for future research.

10.2 Summary

The primary objective of this study was to utilize IDOT mechanistic-empirical procedures and Mn/ROAD low-volume road data and information to further verify/refine/modify IDOT's analysis and design concepts and procedures for low-volume road flexible pavements. The following specific conclusions were made from the study:

1. The results from rapid shear tests and permanent deformation tests show that the rutting potential of a granular material can be characterized from rapid shear test at a confining pressure of 15-psi. The stress-strain curve from the rapid shear test was used to predict the permanent deformation accumulation under the repeated load.

2. Granular materials that achieve at least 90-psi deviator stress at 2-percent axial strain at a confining pressure of 15-psi, display a low rutting potential and can be conditioned at a deviator stress of 45-psi and confining pressure of 15-psi (principal stress ratio $\sigma_1/\sigma_3 = 4$). Materials that do not achieve at least 90-psi deviator stress at 2-percent axial strain at a confining pressure of 15-psi, experience dilatation, become unstable, and undergo rapid accumulation of permanent deformation.

3. The laboratory test results show that rapid shear test data can be utilized to predict and rank the permanent deformation behavior of granular materials in the repeated load triaxial testing. The rapid shear test results reflect the rutting trends observed in the field.

4. Results from repeated load testing were used to develop the parameters for K-θ, UT-Austin and Uzan models for characterizing the resilient modulus. The estimated axial strain and resilient modulus values from the three models are in good agreement with the measured values. Less agreement between the measured and estimated axial strain and resilient modulus values was noted for CL-1Csp (poor quality, very low shear strength material).

5. The laboratory testing on cohesive subgrade was performed at MnDOT. Field samples were collected using Thinwall Shelby Tube and bulk bag samples. Based on the gradation test results and Atterberg limits, the soil was classified as AASHTO A-6 soil.

6. An arithmetic model was used to characterize the stress softening behavior of fine-grained subgrade soils. A correlation between subgrade "breakpoint" modulus and unconfined compressive strength was established. Slopes k_1 and k_2 did not show any significant variation with change in unconfined compressive strength. A reduction of 2.19-ksi in the E_{Ri} value for every 1-percent increase in moisture content was noted.

7. The backcalculated (from FWD tests) asphalt concrete stiffness values were comparable to the stiffness values calculated from the Asphalt Institute equation.

8. The FWD data were analyzed to study the effect of granular material quality on the pavement surface deflection response. The surface deflections were normalized to same asphalt concrete and subgrade stiffness. The analysis showed that there is no significant effect of granular material quality on the pavement deflection response in the case of conventional flexible pavements (asphalt concrete surface and granular base).

9. Because of higher stresses within the granular layer, the granular material quality effects on the pavement surface deflection response of surface treated/aggregate surface pavements are significant.

10. The granular material quality significantly affects the performance of the pavement. The shear strength results obtained from rapid shear tests performed at a confining pressure of 15-

psi reflect the rutting trends observed in the low-volume road test sections at Mn/ROAD project.

11. The granular materials used in Mn/ROAD test sections can be ranked in the order of performance based on the laboratory (rapid shear) tests, South African method (stress based safety factor), and the field performance (rut depth measurements). The rankings of the materials are same from all the three methods except for material CL-6sp in Cell-27, which for some reason experienced higher rutting in the field than expected.

12. Finite element program ILLI-PAVE was used to estimate the pavement responses. Estimate of pavement responses is fairly accurate in the case of pavement cross-sections where the asphalt concrete surface behaves like a structural layer (asphalt concrete thickness $\geq$ 5-inch). In the case of thinner asphalt concrete surfaces, the exact match may not be obtained on the deflections, but the predicted geometry of deflection basin (AREA or AUPP term) was comparable to the measured one.

13. The analysis of field FWD data showed that Area Under Pavement Profile (AUPP) can be used for predicting the strains at the bottom of asphalt concrete layer.

14. A "Design Time" concept can be used to characterize the climatic effects on asphalt concrete fatigue. The fatigue life of an asphalt concrete pavement estimated based on "Design Time" asphalt concrete modulus is equal to the fatigue life calculated based on the 12-monthly asphalt concrete modulus inputs. The "Design Time" is primarily affected by the thickness of asphalt concrete. The granular layer thickness and subgrade type (sand or cohesive) do not have any effect on design time air temperature and design time pavement temperature.

15. Thermal gradients within the asphalt concrete layer were lower in the case of test sections with sand subgrade.

16. The subgrade significantly affects low volume road pavement structural response and performance. The test sections with sandy subgrade showed little or no change in pavement

structural response due to changes in moisture conditions in the subgrade (during spring). For test sections with cohesive subgrade, the effects of moisture changes during spring on the pavement structural response were significant.

17. The subgrade stress ratios were in the desirable range (0.65-0.75) and did not contribute to any significant accumulation of permanent deformation in the subgrade. Once the "critical period" design subgrade modulus is determined, adequate thickness of asphalt concrete and granular base layers should be provided to protect the subgrade. Lower subgrade stress ratios will prevent any significant rutting in the subgrade.

10.3 Conclusions

The IDOT mechanistic-empirical design procedure for low-volume road flexible pavements is adequate. The "Design Time" approach for considering climatic effects on asphalt concrete fatigue is appropriate and adequate. Subgrade rutting is critical for low volume roads. Subgrade Stress Ratio (SSR) is a viable parameter for evaluating subgrade rutting potential. It adequately represents both field and laboratory observed phenomenon. Use of the "Critical Period" (spring-thaw) design subgrade properties (unconfined compressive strength, resilient modulus, SSR) limit rutting in the subgrade. Adequate asphalt concrete and granular layer thickness must be provided to protect the subgrade. However, adequate consideration should be given to the shear strength of granular bases used in LVR pavements. The pavement aggregate layers must posses sufficient shear strength/rutting resistance (for a given asphalt concrete thickness) to minimize rutting within the layer. Setting up a minimum limit on shear strength of granular materials to be used in the pavement will help in preventing dilatation (and subsequent accumulation of permanent deformation). From this study, it was established that granular material that achieve at least 90-psi deviator stress at 2-percent axial strain at a confining pressure of 15-psi in a rapid shear test, will not experience dilatation.

10.4 Recommendations for Future Research

The LVR flexible pavement test sections at Mn/ROAD experienced thermal cracking in the asphalt concrete and rutting in the granular base. Some asphalt concrete fatigue cracking is visible at present. Monitoring of test sections should continue on periodic basis. The availability of field data

will contribute in the calibration of transfer function used for estimating fatigue life of an asphalt concrete layer. Results from FWD tests performed above the sensors (if available at a later stage) should be used to compare measured pavement responses (deformation in the component layers, stresses at the top of the subgrade, etc.) to the ILLI-PAVE predicted responses for validating the structural model.

REFERENCES

[1] "Guide for the Design of Pavement Structures", American Association of State Highway and Transport Officials, 1986.

[2] "Conventional Flexible Pavement Design for Local Agencies", Illinois Department of Transportation, August 1995.

[3] Thompson, M. R., and LaGrow, T. G., "A Proposed Conventional Flexible Pavement Thickness Design Procedure", Civil Engineering Studies, Transportation Engineering Series No. 55, University of Illinois @ Urbana-Champaign, 1988.

[4] "Calibrated Mechanistic Structural Analysis Procedures for Pavements", Phase 1, Final Report, National Cooperative Highway Research Program (NCHRP), Project 1-26, Transportation Research Board, March 1990.

[5] Dempsey, B. J., Herlache, W. A., and Patel, A. J., "Climatic-Materials-Structural Pavement Analysis Program", Transportation Research Record 1095, Transportation Research Board, 1986.

[6] Dempsey, B. J., Herlache, W. A., and Patel, A. J., "Climatic-Materials-Structural ~~Pavement Analysis Program", "Environmental Effects on Pavements - Theory Manual",~~ FHWA/RD-84-115, Vol. 3, FHWA, U.S. Department of Transportation, 1985.

[7] Van der Poel, C., "A General System Describing the Visco-Elastic Properties of Bitumens and its Relation to Routine Test Data", Journal of Applied Chemistry, London, Vol. 4, 1954.

[8] Shahin, M. Y., and McCullough, B. F., "Stiffness History of Asphalt Concrete Surfaces in Roads", Transportation Research Record 466, Transportation Research Board, 1973.

[9] Ullidtz, P., "Pavement Analysis", Developments in Civil Engineering, Vol. 19, Elsevier, 1987.

[10] Heukelom, W., and Klomp, A. J. G., "Road Design and Dynamic Loading", Proceedings, Association of Asphalt Paving Technologists, Vol. 33, 1964.

[11] Francken, L., and Verstraeten, J., "Methods for Predicting Moduli and Fatigue Laws of Bituminous Road Mixes Under Repeated Bending", Transportation Research Record 515, Transportation Research Board, 1974.

[12] Bonnaure, F., Gest, G., Gravois, A., and Uge, "A New Method of Predicting the Stiffness Modulus of Asphalt Paving Mixtures", Proceedings, Association of Asphalt Paving Technologists, Vol. 46, 1977.

[13] "Shell Pavement Design Manual", Shell International Petroleum Co. Limited, London, 1978.

[14] "Research and Development of The Asphalt Institute's Thickness Design Manual (MS-1) Ninth Edition", Research Report No. 82-2, The Asphalt Institute, August 1982.

[15] Miller, J. S., Uzan, J., and Witczak, M. W., "Modification of The Asphalt Institute Bituminous Mix Modulus Predictive Equation", Transportation Research Record 911, Transportation Research Board, 1983.

[16] "Mechanistic Pavement Design", A Supplement to Section 7 of the Illinois DOT Design Manual, Springfield, IL, August 1989.

[17] Hill, H. J., "Early Life Study of the FA 409 Full-Depth Asphalt Concrete Pavement Sections", Ph.D. thesis, Department of Civil Engineering, University of Illinois @ Urbana-Champaign, June 1988.

[18] "Calibrated Mechanistic Structural Analysis Procedures for Pavements", Phase 2, Volume II - Appendices, National Cooperative Highway Research Program (NCHRP), Project 1-26, Transportation Research Board, March 1990.

[19] Von Quintus, H. L. et al., "Asphalt-Aggregate Mixture Analysis System : AAMAS", Report 338, National Cooperative Highway Research Program (NCHRP), Transportation Research Board, March 1991.

[20] Pell, P. S., "Keynote Lecture - Pavement Materials", Sixth International Conference on the Structural Design of Asphalt Pavements, Ann Arbor, MI, 1987.

[21] Finn, F., et al, "Development of Pavement Structural Subsystems", NCHRP Report 291, National Cooperative Highway Research Program, Transportation Research Board, 1986.

[22] Pell, P. S., and Cooper, K. E., "The Effect of Testing and Mix Variables on the Fatigue Performance of Bituminous Materials", Proceedings, The Association of Asphalt Paving Technologists, Vol. 44, 1975.

[23] Epps, J., "Influence of Mixture Variables on the Flexural Fatigue and Tensile Properties of Asphalt Concrete", Ph.D. Dissertation, University of California, Berkeley, 1968.

[24] Thompson, M. R., and Cation, K., "A Proposed Full-Depth Asphalt Concrete Thickness Design Procedure", Civil Engineering Studies, Transportation Engineering Series No. 45, University of Illinois at Urbana-Champaign, 1986.

[25] Thompson, M. R., "ILLI-PAVE Based Full-Depth Asphalt Concrete Pavement Design Procedure", Proceedings, Sixth International Conference on Structural Design of Asphalt Pavements, Ann Arbor, MI, 1987.

[26] Gomez-Achecar, M., and Thompson M. R., "Mechanistic Design Concepts for Full-Depth Asphalt Concrete Pavements", Civil Engineering Studies, Transportation Engineering Series No. 41, University of Illinois at Urbana-Champaign, 1984.

[27] Powell, W. D., et al., "The structural Design of Bituminous Pavements", TRRL Laboratory Report 1132, Transport and Road Research Laboratory, U.K., 1984.

[28] "Asphalt Pavement Design Manual for the U.K.", Mobil Oil Company Ltd., London, 1985.

[29] Verstraeten, J., Veverks, V., and Francken, L., "Rational and Practical Designs of Asphalt Pavements to Avoid Cracking and Rutting", Proceedings, Fifth International Conference on the Structural Design of Asphalt Pavements, 1982.

[30] Ullidtz, P., "Overlay and Stage by Stage Design", Proceedings, Fourth International Conference on Structural Design of Asphalt Pavements, Ann Arbor, MI, 1977.

[31] Robnett, Q. L., and Thompson, M. R., "Interim-Report - Resilient Properties of Subgrade Soils - Phase -1 - Development of Testing Procedure", Transportation Engineering Series No. 5, Illinois Cooperative Highway Research Program Series No. 139, University of Illinois, Urbana, Illinois, May, 1973.

[32] "Test Procedures for Characterizing Dynamic Stress-Strain Properties of Pavement Materials", Special Report 162, Transportation Research Board, 1975.

[33] "Soils Manual for the Design of Asphalt Pavement Structures", MS-10, The Asphalt Institute, 2nd Edition, March, 1978.

[34] "Standard Specifications for Transportation Materials and Methods of Sampling and Testing - Part II", 14th Edition, AASHTO, 1986.

[35] "Standard Specifications for Transportation Materials and Methods of Sampling and Testing - Part II", 15th Edition, AASHTO, 1991.

[36] Hicks, R. G., and Monismith, C. L., "Factors Influencing the Resilient Response of Granular Materials", Transportation Research Record 345, Transportation Research Board, 1971.

[37] Brown, S. F., "Repeated Load Testing of Granular Material", Journal of the Geotechnical Engineering, Vol. 100, No. GT7, ASCE, July, 1974.

[38] Allen, J. J., and Thompson, M. R., "Resilient Response of Granular Materials Subjected to Time Dependent Lateral Stresses", Transportation Research Record 510, Transportation Research Board, 1974.

[39] Knutson, R. M., Thompson, M. R., Mullin, T., and Tayabji, S. D., "Materials Evaluation Study : Ballast and Foundations Research Program", FRA-ORandD -77-02, Federal Railroad Administration, 1977.

[40] Townsend, F. C., "A Review of Factors Affecting Cyclic Triaxial Tests", Dynamic Geotechnical Testing, ASTM STP 654, American Society for Testing and Materials, 1978.

[41] Rada, G., and Witczak, M. W., "Comprehensive Evaluation of Resilient Moduli Results for Granular Materials", Transportation Research Record 810, Transportation Research Board, 1981.

[42] Smith, B. E., and Witczak, M. W., "Equivalent Granular Base Moduli Prediction", Journal of the Transportation Engineering Division, Vol. 107, TE6, ASCE, 1981.

[43] Barksdale, R. D., "Performance of Crushed Stone Base Courses", Transportation Research Record 954, Transportation Research Board, 1984.

[44] Pumphrey, N. D., and Lentz, R. W., "Deformation Analysis of Florida Highway Subgrade Sand Subjected to Repeated Load Triaxial Tests", Transportation Research Record 1089, Transportation Research Board, 1986.

[45] Selig, T. E., and Roner, C. J., "Effects of Particle Characteristics on Behavior of Granular Material", Transportation Research Record 1131, Transportation Research Board, 1987.

[46] Barksdale, R. D., and Itani, S. Y., "Influence of Aggregate Shape on Base Behavior", Transportation Research Record 1227, Transportation Research Board, 1989.

[47] Thompson, M. R., and Smith, K. L., "Repeated Triaxial Characterization of Granular Bases", Transportation Research Record 1278, Transportation Research Board, 1990.

[48] Barksdale, R. D., Itani, S. Y., and Swor, T. E., "Evaluation of Recycled Concrete, Open-Graded Aggregate, and Large Top-Size Aggregate Bases", Transportation Research Record 1345, Transportation Research Board, 1992.

[49] May, R. W., and Witczak, M. W., "Effective Granular Modulus to Model Pavement Responses ", Transportation Research Record 810, Transportation Research Board, 1981.

[50] Uzan, J., "Characterization of Granular Materials", Transportation Research Record 1022, Transportation Research Board, 1985.

[51] Brown, S. F., and Pappin, J. W., "Analysis of Pavements with Granular Bases", Transportation Research Record 810, Transportation Research Board, 1981.

[52] Boyce, J. R., "The Behavior of a Granular Material Under Repeated Load", Ph.D. Thesis, University of Nottingham, Department of Civil Engineering, 1976.

[53] Jouve, P., Martinez, J., Paute, J. L., and Ragneau, E., "Rational Model for Flexible Pavements Deformations", Sixth International Conference on the Structural Design of Asphalt Pavements, Ann Arbor, MI, 1987.

[54] Thom, N. H., "Design of Road Foundations", Ph.D. Thesis, University of Nottingham, Department of Civil Engineering, 1988.

[55] Witczak, M. W., and Uzan, J., "The Universal Airport Pavement Design System", Report I of V : Granular Material Characterization, University of Maryland, Department of Civil Engineering, MD, 1988.

[56] Pezo, R. F., "A General Method of Reporting Resilient Modulus Tests of Soils - A Pavement Engineer's Point of View", Paper No. 93082, 72nd Annual Meeting, Transportation Research Board, Washington D. C., 1993.

[57] Itani, S. Y., "Behavior of Base Materials Containing Large-Sized Particles", Ph.D. Thesis, Georgia Institute of Technology, School of Civil and Environmental Engineering, 1990.

[58] Crockford, W. W., Bendana, L. J., Yang, W. S., Rhee, S. K., and Senadheera, S. P., "Modeling Stress and Strain States in Pavement Structures Incorporating Thick Granular Layers", Final Report, The Texas Transportation Institute, College Station, Texas, 1990.

[59] Li, D., and Selig, E. T., "Evaluation of Resilient Modulus for Fine-Grained Subgrade Soils", Geotechnical Report No. AAR91-392R, Department of Civil Engineering, University of Massachusetts, Amherst, MA, November, 1991.

[60] Boateng-Poku, Y., and Drumm, E. C., "Hyperbolic Model for the Resilient modulus Response of Fine-Grained Soils", Geotechnical Special Publication No. 24, American Society of Civil Engineers, 1989.

[61] Thompson, M. R., and Robnett, Q. L., "Resilient Properties of Subgrade Soils", Transportation Engineering Journal, ASCE, Vol. 105, No. TE1, January, 1979.

[62] Drumm, E. C., Boateng-Poku, Y., and Pierce, T. J., "Estimation of Subgrade Resilient Modulus from Standard Tests", Journal of the Geotechnical Division, ASCE, Vol. 116, No. 5, May, 1990.

[63] Elliott, R. P., and Thornton, S. I., "Simplification of Subgrade Resilient Modulus Testing", Transportation Research Record 1192, Transportation Research Board, 1988.

[64] Monismith, C. L., Ogawa, N., and Freeme, C. R., "Permanent Deformation Characteristics of Subgrade Soils due to Repeated Loading", Transportation Research Record 537, Transportation Research Board, 1975.

[65] Majidzadeh, K., Khedr, S., and Guirguis, H., "Laboratory Verification of a Mechanistic Subgrade Rutting Model", Transportation Research Record 616, Transportation Research Board, 1976.

[66] Majidzadeh, K., Bayomy, F., and Khedr, S., "Rutting Evaluation of Subgrade Soils in Ohio", Transportation Research Record 671, Transportation Research Board, 1978.

[67] Khedr, S. A., "Deformation Characteristics of Granular Base Course In Flexible Pavements", Transportation Research Record 1043, Transportation Research Board, 1985.

[68] Knutson, R. M., and Thompson, M. R., "Permanent Deformation Behavior of Railway Ballast", Transportation Research Record 694, Transportation Research Board, 1978.

[69] Garg, N., and Budiman, J., "Effect of Large Size Aggregates on the Performance of Base Materials for Flexible Pavements", Paper presented at the 73rd Annual Meeting of the Transportation Research Board, January, 1994.

[70] Raymond, G. P., and Bathurst, R. J., "Performance of Large-Scale Model Single Tie/Track System", Transportation Research Record 1131, Transportation Research Board, 1987.

[71] Thompson, M. R., and Nauman, D., "Rutting Rate Analyses of the AASHO Road Test Flexible Pavements", Transportation Research Record 1384, Transportation Research Board, 1993.

[72] Thompson, M. R., "ILLI-PAVE Based Conventional Flexible Pavement Design Procedure", Proceedings, Vol. 1, Seventh International Conference on Asphalt Pavements, Nottingham, U.K., 1992.

[73] Elliott, R. P., and Thompson, M. R., "Mechanistic Design Concepts for Conventional Flexible Pavements", Civil Engineering Studies, Transportation Engineering Series No. 42, University of Illinois @ Urbana-Champaign, 1985.

[74] Raad, L., and Figueroa, J. L., "Load Response of Transportation Support Systems", Transportation Engineering Journal, ASCE, Vol. 106, No. TE 1, January, 1980.

[75] Hoffman, M. S., and Thompson, M. R., "Non-Destructive Testing of Flexible Pavements - Field Testing Program Summary", Civil Engineering Studies, Transportation Engineering Series No. 31, University of Illinois @ Urbana-Champaign, June, 1981.

[76] Thompson, M. R., "ILLI-PAVE Based Thickness Design Concepts and Practices for Surface Treatment Pavements", Proceedings, 4th International Conference on Bearing Capacity of Roads and Airfields, Minneapolis, MN, July, 1994.

[77] Mauer, M. C., and De Beer, M., "Computer Programs to Plot DCP Data - Users Manual", Division of Roads and Transport Technology, Pretoria, July, 1988.

[78] Maser, K. R., "Ground Penetrating Radar Survey of Pavement Thickness on Mn/ROAD Sections", Report Submitted to the Minnesota Department of Transportation, Infrasense Inc., Cambridge, MA, November 30, 1994.

[79] Thompson, M. R., "ILLI-PAVE Based NDT Analysis Procedures", ASTM International Symposium on Non-Destructive Testing of Pavement Structures, ASTM Annual Meeting, Baltimore, MD, June 1988, Published in ASTM STP 1026, 1989.

[80] Stubstad, R. N., Baltzer, S., Lukanen, E. O., and Ertman-Larsen, H. J., "Prediction of AC Mat Temperatures for Routine Load/Deflection Measurements", Proceedings, 4th International Conference on Bearing Capacity of Roads and Airfields, Minneapolis, MN, July, 1994.

[81] Mary Stroup-Gardiner, and Newcomb, D. E., "Investigation of Hot Mix Asphalt Mixtures at Mn/ROAD", Report Number 97-06, Center for Transportation Studies, University of Minnesota, February 1997.

[82] Freund, R. J., and Wilson, W. J., "Statistical Methods", Academic Press, Inc., Harcourt Brace Jovanovich Publishers, 1993.

[83] Khedr, S. A., "Deformation Mechanism in Asphalt Concrete", Journal of Transportation Engineering, ASCE, Volume 112, No. 1, January, 1986.

[84] Theyse, H. L., De Beer, M, and Rust, F. C., "Overview of South African Mechanistic Pavement Design Method", Transportation Research Record 1539, Transportation Research Board, 1996.

[85] Maree, J. H., "Design Parameters for Crushed Stone in Pavements", Master's Thesis, University of Pretoria, South Africa, 1978.

[86] Iwasaki, T., Tatsuoka, F., and Takagi, Y., "Shear Moduli of Sand Under Cyclic Torsional Shear Loading", Soils and Foundations, Vol. 18, No. 1, March 1978.

[87] Barenberg, E. J., "A Structural Design Classification of Pavements Based on an Analysis of Pavement Behavior, Material Properties, and Modes of Failure", Ph.D. thesis, Department of Civil Engineering, University of Illinois @ Urbana-Champaign, October 1965.

[88] Bergan, A. T., and Monismith, C. L., "Characterization of Subgrade Soils in Cold Regions for Pavement Design Purposes", Transportation Research Record 431, Transportation Research Board, 1973.

[89] Robnett, Q. L., and Thompson, M. R., "Effect of Lime Treatment on the Resilient Behavior of Fine-Grained Soils", Transportation Research Record 560, Transportation Research Board, 1976.

APPENDIX-A : Asphalt Concrete Mix Properties

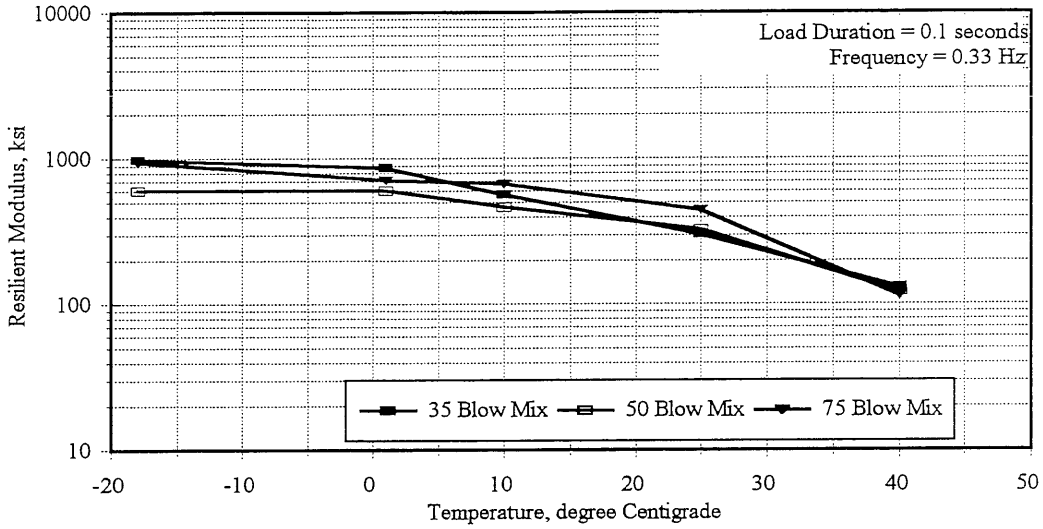

Figure A1. Resilient Modulus-Temperature Relations for Mix Design Materials [81]

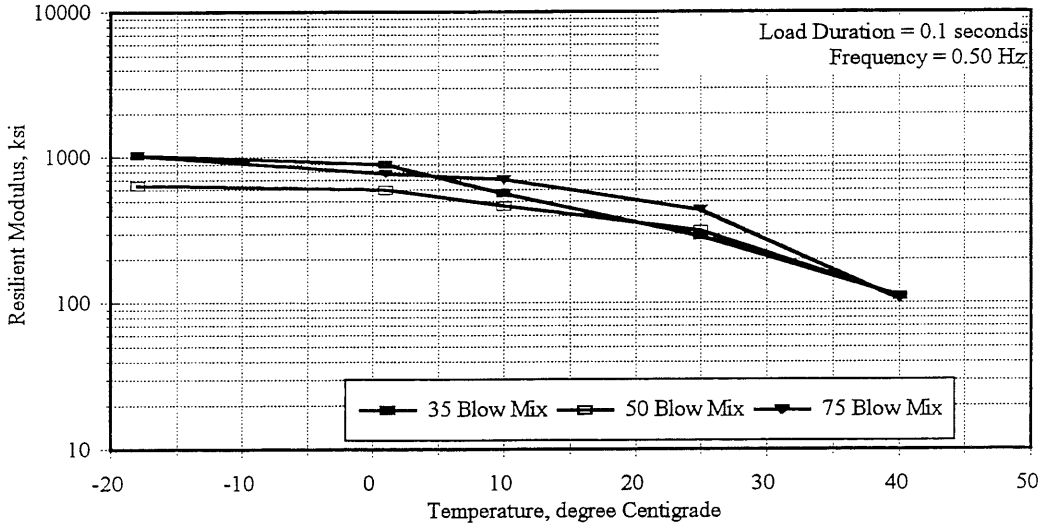

Figure A2. Resilient Modulus-Temperature Relations for Mix Design Materials [81]

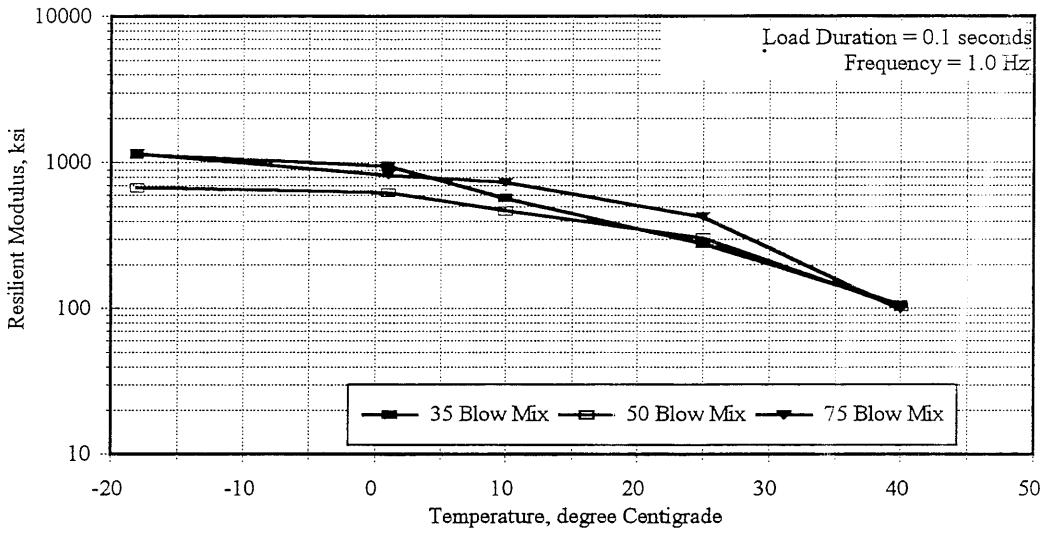

Figure A3. Resilient Modulus-Temperature Relations for Mix Design Materials [81]

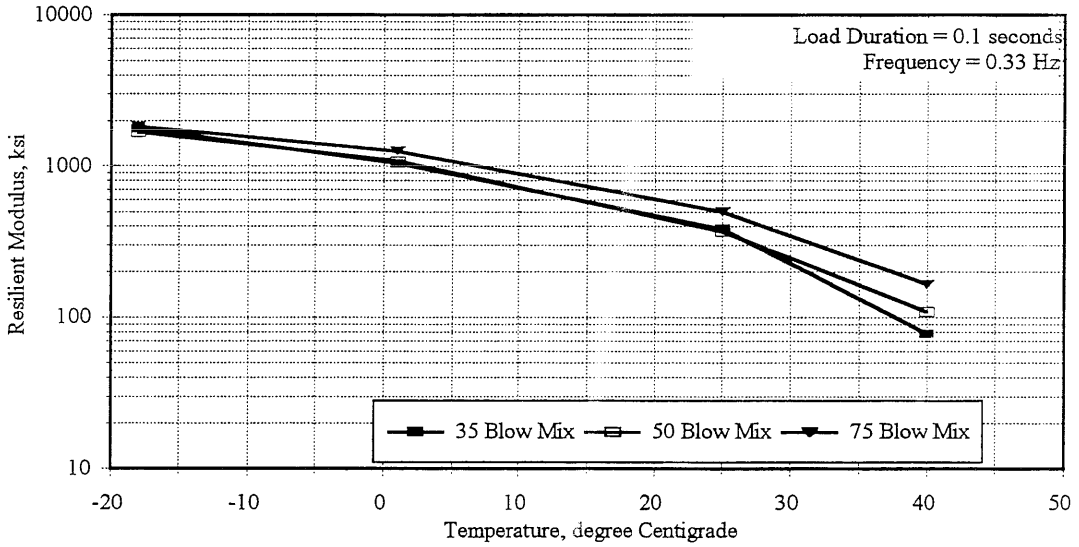

Figure A4. Resilient Modulus-Temperature Relations for Behind-The-Paver Material [81]

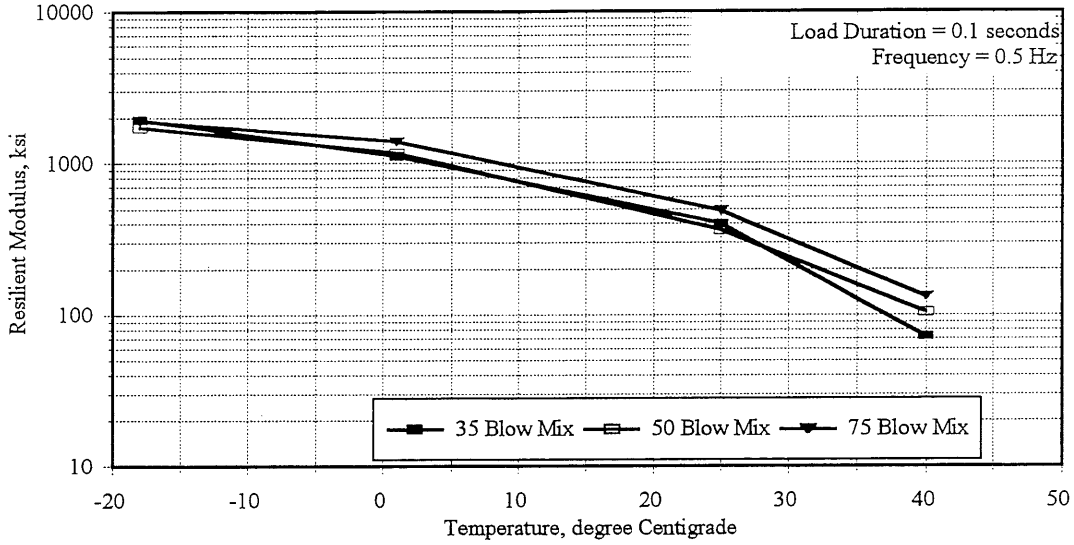

Figure A5. Resilient Modulus-Temperature Relations for Behind-The-Paver Material [81]

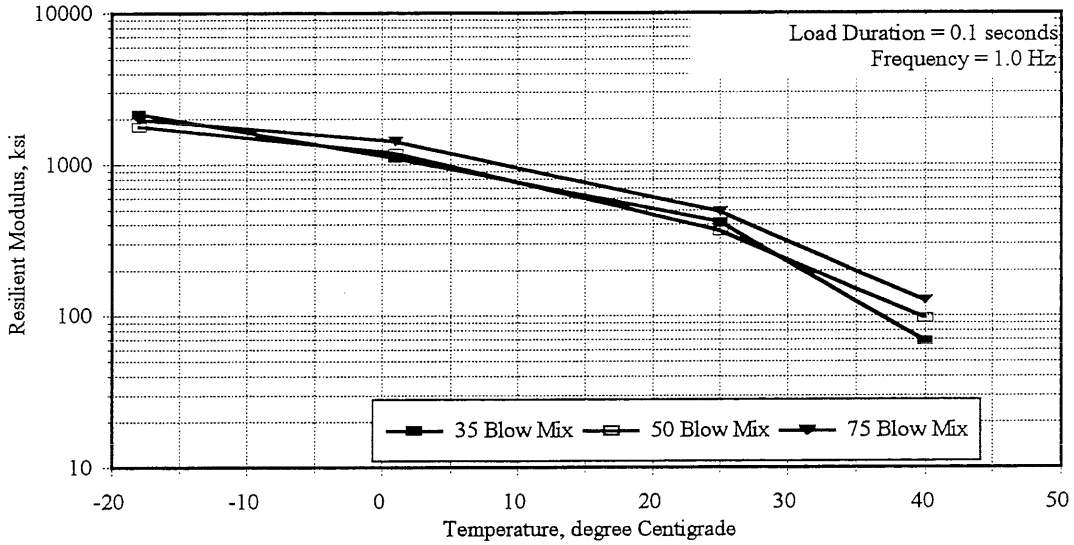

Figure A6. Resilient Modulus-Temperature Relations for Behind-The-Paver Material [81]

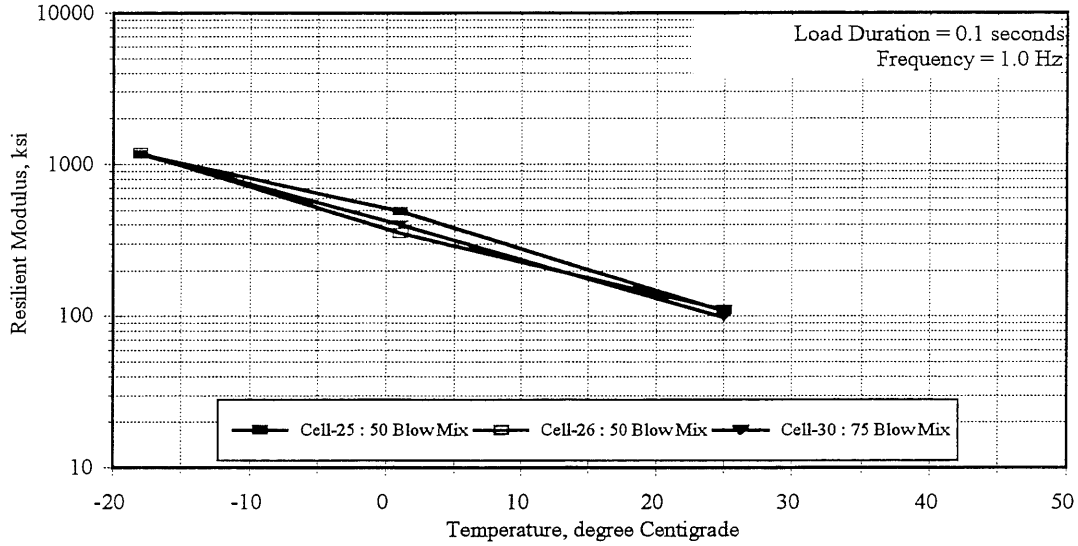

Figure A7. Resilient Modulus-Temperature Relations for Base-1 Cores [81]

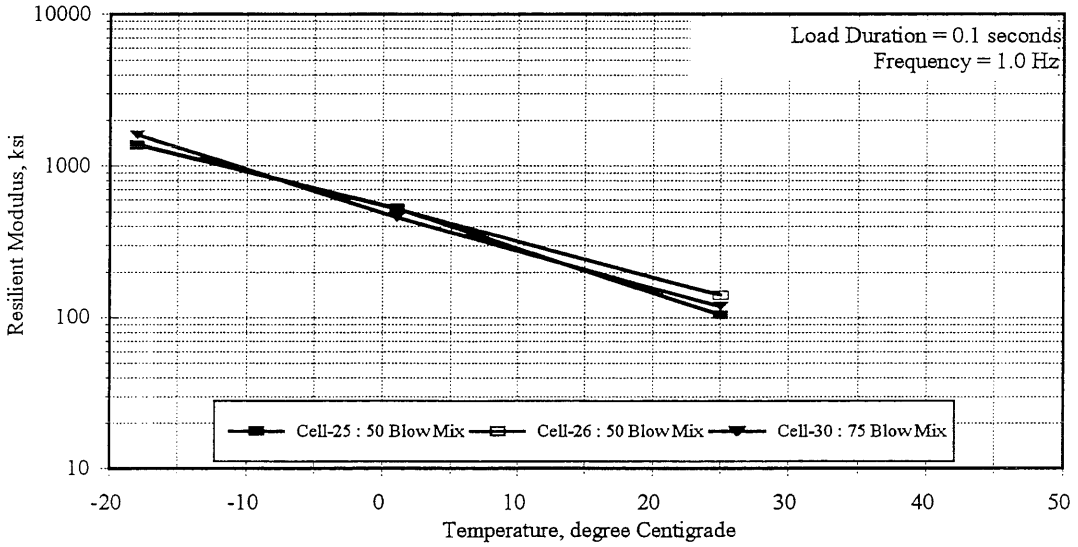

Figure A8. Resilient Modulus-Temperature Relations for Base-2 Cores [81]

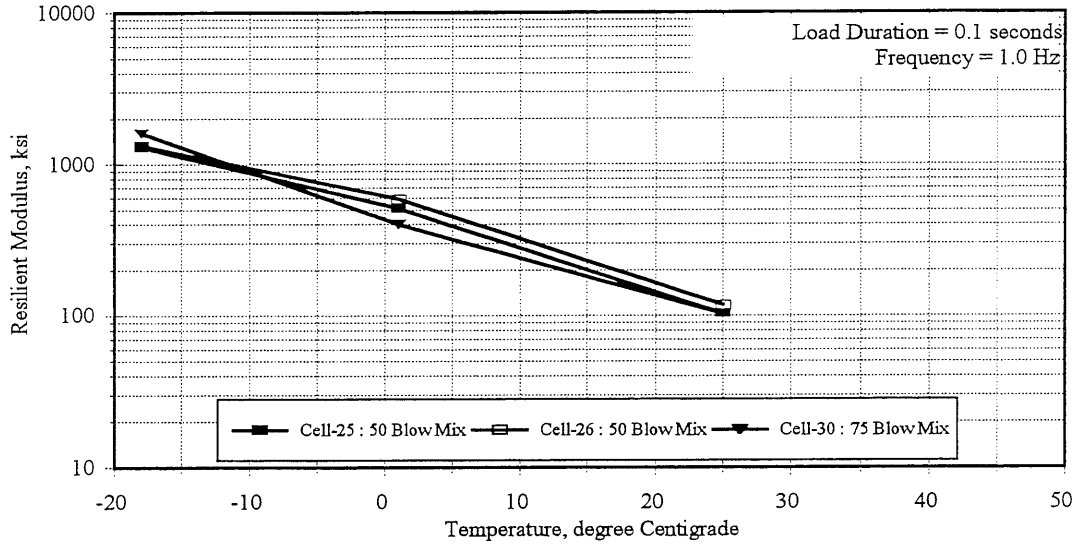

Figure A9. Resilient Modulus-Temperature Relations for Wearing Surface Cores [81]